MECHANISTIC MODELLING OF SEMI-AUTOGENOUS GRINDING

Rodrigo Magalhães de Carvalho

Tese de Doutorado apresentada ao Programa de Pós-graduação em Engenharia Metalúrgica e de Materiais, COPPE, da Universidade Federal do Rio de Janeiro, como parte dos requisitos necessários à obtenção do título de Doutor em Engenharia Metalúrgica e de Materiais.

Orientador: Luís Marcelo Marques Tavares

Rio de Janeiro
Dezembro de 2013

MECHANISTIC MODELLING OF SEMI-AUTOGENOUS GRINDING

Rodrigo Magalhães de Carvalho

TESE SUBMETIDA AO CORPO DOCENTE DO INSTITUTO ALBERTO LUIZ COIMBRA DE PÓS-GRADUAÇÃO E PESQUISA DE ENGENHARIA (COPPE) DA UNIVERSIDADE FEDERAL DO RIO DE JANEIRO COMO PARTE DOS REQUISITOS NECESSÁRIOS PARA A OBTENÇÃO DO GRAU DE DOUTOR EM CIÊNCIAS EM ENGENHARIA METALÚRGICA E DE MATERIAIS.

Examinada por:

_____

Prof. Luís Marcelo Marques Tavares, Ph.D.

_____

Prof. Homero Delboni Jr., Ph.D.

_____

Prof. Jose da Rocha Miranda Pontes, D.Sc.

_____

Prof. Mauricio Leonardo Torem, D.Sc.

_____

Prof. Paulo Laranjeira da Cunha Lage, D.Sc.

RIO DE JANEIRO, RJ - BRASIL

DEZEMBRO DE 2013

Carvalho, Rodrigo Magalhães de

Mechanistic modelling of semi-autogenous grinding/ Rodrigo Magalhães de Carvalho. – Rio de Janeiro: UFRJ/COPPE, 2013.

XXVII, 204 p.: il.; 29,7 cm.

Orientador: Luís Marcelo Marques Tavares

Tese (doutorado) – UFRJ/ COPPE/ Programa de Engenharia Metalúrgica e de Materiais, 2013.

Referências Bibliográficas: p. 187-200.

1. Cominuição. 2. Moagem semi-autógena. 3. Método dos Elementos Discretos. I. Carvalho, Rodrigo Magalhães de. II. Universidade Federal do Rio de Janeiro, COPPE, Programa de Engenharia Metalúrgica e de Materiais. III. Título.

Para minha esposa Lilian.

Resumo da Tese apresentada à COPPE/UFRJ como parte dos requisitos necessários para a obtenção do grau de Doutor em Ciências (D.Sc.)

MECHANISTIC MODELLING OF SEMI-AUTOGENOUS GRINDING

Rodrigo Magalhães de Carvalho

Dezembro/2013

Orientador: Luís Marcelo Marques Tavares

Programa: Engenharia Metalúrgica e de Materiais

O presente trabalho aborda o desenvolvimento da modelagem mecanicista da moagem semi-autógena. Na modelagem mecanicista é feita a combinação de caracterização de minérios e da modelagem da quebra em eventos individuais à simulação de moinhos utilizando o método dos elementos discretos. O trabalho envolveu a avaliação da sensibilidade do modelo à diferentes condições de operação de um moinho, permitindo avaliar efeito de tamanho de bolas, velocidade de rotação e grau de enchimento. O modelo permitiu desenvolver uma metodologia simplificada de análise de moinhos semi-autógenos. Por fim, a proposta final do modelo indica a capacidade de se realizar simulações de moinhos industriais.

Abstract of Thesis presented to COPPE/UFRJ as a partial fulfillment of the requirements for the degree of Doctor of Science (D.Sc.)

MECHANISTIC MODELLING OF SEMI-AUTOGENOUS GRINDING

Rodrigo Magalhães de Carvalho

December/2013

Advisor: Luís Marcelo Marques Tavares

Department: Metallurgical and Materials Engineering

This work describes the development of a mechanistic model of the semi-autogenous grinding. The mechanistic modelling combines ore characterization and the modeling of the breakage in a single impact event to simulate the mill using the discrete element method. The work has involved a sensitivity evaluation of the model to different mill operational conditions, and allowed to evaluate the effect of ball size, rotation speed and mill filling. The model also allowed the development of a simplified analysis methodology to semi-autogenous mills. Finally, the final proposition of the model indicates its capability to be used in industrial scale mill simulations.

Summary

List of Figures

List of Tables

List of Symbols

Latin

A	Maximum t_{10} value for a material subject to breakage
a_a	Parameter of surface breakage model
A_c	Cross sectional area of the steel rod
A_{ij}	Abrasion breakage function king
A^b_{ilk}	Rate of appearance of material in class il in a collision events of class k that caused body breakage
A^s_{ilk}	Rate of appearance of material in class il in a collision events of class k that caused surface breakage
$a_{ijl}(eE,t)$	Surface breakage function in density form
a_j	Distributed abrasion breakage function
A_g	fraction of open area of the discharge rate
a_{HE}	Appearance function from high energy impacts
a_{lr}	Total open area per radial position, lr
a_{LE}	Appearance function from low energy impacts
A_P	Constant in Austin's mill power model
b	Model fitting parameter of t_{10} equation
b'	Model fitting parameter
$b(d,d')$	The distributed form of the breakage function as function of continuous particle size d and d'
$B(d,d')$	Cumulative form of $b(d,d')$
$b(d,d';eE)$	Mass fraction of particles smaller than the size d that are created from the breakage of particles of size d' when submitted to an impact energy eE
$B(d,d';eE)$	Cumulative form of $b(d,d';eE)$
$b_{i,j}$	Fraction of broken material from size class j that appear in size class i
$b_{ijlk}(eE,t)$	Mass fraction of particles in component class l and size class j that appears on size class i when body breakage from collision class k of energy magnitude eE occurs
C	Wave propagation speed on the steel rod
C'	Circulation ratio
c_i	Fraction of material of size class i that returns to the mil
c_n	Normal restitution coefficient
C_g	Characteristic size of the grinding media
C_s	Volumetric fraction of solids in slurry
c_t	Tangential restitution coefficient
d	Particle size
D	Damage
d'	Size of mother particle
d^*	Fitting parameter
d_0	Original particle size (representative size)
d_A	Abrasion model fitting parameter
d_b	Ball diameter
$\overline{d}_b$	Average ball diameter
d_g	Particle size that will always pass through the grate
D^b_{ilk}	Rate of disappearance of material in class il in a collision events of class k that caused body breakage

D_{ilk}^{s}	Rate of disappearance of material in class il in a collision events of class k that caused surface breakage
d_j	Mean particle size of size class j
d_o	Fitting parameter
d_m	Fraction of the charge that reaches the grate per unit of time
D_m	Mill diameter
D_n^*	Amount of damage suffered by particles on the n-th impact cycle is
d_{r_i}	Discharge rate of particles in size class i
e	Fraction of energy in a collision that is captured by a single particle
E	Energy
E_1	Potential energy at the maximum height inside the mill
E^*	Specific energy coordinate as function of E_{max}
E_{50b}	median of the particle fracture energy distribution of the particles that break in the impact
E_{cs}	Specific impact energy
$E_{k,n}$	Specific kinetic energy of the striker (kinetic energy of the striker divided by particle mass) in n-th loading event that is all converted into deformation energy
E_m	Specific energy
$E_{m,\infty}$	Fitting parameter
$E_{m50,j}$	Median specific fracture energy of particles of a size class j
E_{m50u}	Median specific fracture energy of particles that did not suffer body breakage
$E'_{m50,i}$	Median specific fracture energy of particles of a size class j before correction with surface type
E_{max}	Upper truncation parameter of fracture energy distribution
E_{min}	minimum specific impact energy able to break the particle
e_q	The fraction of energy received by each particle contained in the bed
$f(r_q)$	Fraction of particles contained in the q-th ring around the center of contact
$F(t)$	The force time profile
$F(eE, d')$	Breakage probability of a particle of size d' when it receives a amount energy eE in a collision event inside the mill
f_{drops}	Frequency of drops
f_i	Fraction of the feed in size class i
$F_{il}(eE, t)$	Fracture energy distribution of particles in class il at time instant t
$F_{il}^*(E, t)$	distribution of fracture energies of particles in class il that suffered damage
$F_{il}(E, 0)$	Original fracture energy distribution of the ore in class il or $F_{il}(E, t_0)$
$F_{il}^*(E, t)$	fracture energy distribution of particles in class il that underwent damage
$F_{il}(E, t)$	Fracture energy distribution of the particles in class il in the hold-up before the impact cycle
$F_{il}(E, t + \mathrm{d}t)$	Fracture energy distribution of the ore in class il after the collisions in the infinitesimal time frame $\mathrm{d}t$
$F_j(E_m)$	Breakage probability or fracture energy of particles of size class j
f_{mat}	Ore particle property
F_n	Normal force of the contact
f_n^r	Normal repulsive force in the contact
f_n^d	Normal damping force in the contact
$F_{n+1}(E)$	Fracture energy distribution after impact n
F_P	Correction factor for the conical section of the mill
f_s	Fraction of mill filling filled by fine particles

f_{so}	Standard value for f_s
f_t^r	Tangential repulsive force in the contact
f_t^d	Tangential damping force in the contact
F_t	Tangential force of the contact
F_v	Volumetric flow
F_{vo}	Standard flow that is equivalent to a standard fines filling
g	Gravity
$G\ [\ln(E/E_{50})/\sigma_E\ ]$	Breakage probability of particles within a size class which their fracture energy distribution follow the lognormal distribution of median E_{50} and standard deviation of σ_E when they are submitted to collision energy E
$G_{il}(t)$	Fraction of the charge in class il that underwent damage
h	Initial bed height
h_1	Geometric measure
h_2	Geometric measure
$H_{il}(t)$	Fraction of the charge in class that appeared in class il due to breakage
I_i	Inertia momentum of element i
$I_{il}(t)$	Fraction of the charge in class il that was not captured
J_c	Volumetric mill filling
J_s	Volumetric ore filling or fractional hold-up inside the mill
k	Collision class
k_1	Elastic stiffness of the element 1
k_2	Elastic stiffness of the element 2
k_d	Restitution coefficient
K_e	Elastic constant of the contact
K_g	Geometric constant of the contact
k_{il}	Fractional mass loss rate due to abrasion in a collision
$k_{i1..i4}$	Constants for the breakage rate
K_i^{imp}	Model calibration constant
k_j^2	Constants of grate discharge model
k_{media}	Stiffness coefficient of grinding media
k_n	Number of impacts received by the particle
k_n^1	Constants of grate discharge model
k_p	Stiffness coefficient of particles
K_P	Constant in Austin's mill power model
k_r	Stiffness coefficient
K_R	Rate of change in the diameter
k_{steel}	Stiffness coefficient of steel
L	Length of the cylindrical section of the mil between the liners
L_{EFF}	Effective grinding length
L_i	Length of the surface between the cones
lr	Index of grate opening radial position
L_t	Length of conical sector
M	Ore hold-up in the mill
m_b	Ball mass
M_b	Mass of particles contained in bed layout
m_g	Size fraction of the smallest particle considered as grinding media
m_i	Mass captured in a collision
M_i	Mass of element i in DEM
$m_{ilk}(E)$	Mass of particle in class il that are captured in a collision of energy E
m_p	Particle mass
$\bar{m}_{p,j}$	Average mass of particles in size class j

n	Index number
n_c	Number of concentric shells
N_{balls}	Number of ball size classes
$N_{cap,i}$	Number of particles in size class i that are captured in a collision
$n_{cap,q}$	Number of particles captured in the ring q
n_g	Parameter for the grate discharge condition
n_i	Exponent of breakage function
n_i	Unitary vector
N_k	Total number of collision pairs
N_m	Empirical factor
N_{ore}	Number of ore size classes
N_{rev}	Number of different liner materials
P_{80}	Size where 80 % of particles are smaller
$P(d)$	Cumulative passing on the size d
$p(e)$	Energy split function among captured particles in a collision
$p(e_q)$	Mass fraction of particles contained in the bed that receive a fraction e_q of the collision energy
$p(E)$	Probability density function of the impact energies in the mill
P^{imp}	Term of impact split
P_{cylinder}	Mill power due to the cylindrical section of the mill
P_{DEM}	Mill net power calculated from DEM simulation
P_{G}	Gross power
p_i	Fraction of the product in size class i
$p_k(e)$	Energy split function among captured particles in a collision of class k
P_M	Mill power
P_{NL}	No load power
Q	is the slurry discharge flow rate
$Q_{il}(t)$	Fraction of material il in the charge that entered the mill in time step $\mathrm{d}t$
r	Radial position
R	Effective contact radius
r_1	Geometric measure
r_2	Geometric measure
r_{50}	Parameter of the energy split model
r_c	Radius of capture of a monolayer particle bed
r_{cone}	Radius of the conical section of a distance L_c from the cylindrical section
r_e	Contact radius due to the elastic deformation zone
r_g	Contact radius due to the particle height
r_{d1}	Radius of element 1 in the contact
r_{d2}	Radius of element 2 in the contact
r_i^{imp}	Frequency of breakage impacts of particles in size i
r_i	Radial position of the internal surface of the mill
R_i	Knots of the breakage rate function
r_m	Radius of the mil between the liners
r_q	Number of particles captured in each individual ring
R_s	Specific rate of particle mass loss
$s(P)_i$	Specific breakage rate from the collisions of the balls against the pebbles
$s(S)_i$	Specific rate of self-breakage of the pebbles
$s(d)$	Selection function
S_1	Specific breakage of reference size class 1
S_{20}	Median size of the top 20% of the charge
s_i^b	Volume of all steel balls in size class i

s_i^p	Volume of all particles contained in size class i
s_j	specific breakage rate of the ore in size class j
t	Time
t_c	Time which the particle suffered its primary fracture
T_i	Resulting torque in element i
t_{HE}	t values from high energy impacts
t_{LE}	t values from low energy impacts
t_n	Percentage of passing material on the screen aperture equivalent to the original particle size divided by the index number n
v_0	Impact velocity
v_a	Parameter of surface breakage model
V_r	Tangential velocity of a particle in the radial position r
$W^{in}(t)$	Mass flowrate into the mill
$W^{out}(t)$	Mass flowrate out of the mill
$w_{il}(t)$	Mass fraction of particles in size class i and component l on the mill charge in time t
$w_{il}^{in}(t)$	Mass fraction of particles in size class i and component l on the mill feed stream in time t
$w_{il}^{out}(t)$	Mass fraction of particles in size class i and component l on the mill product stream in time t
w_j	Fraction of the *hold-up* in size class i
w_n	Weight function
x_{COM}	The horizontal center of mass of the mill
x_i	Horizontal position coordinate of the particle i
x_n	Energy coordinates
y	Integration variable in t_n model
Y	Young's modulus
Y^*	Function of Young's modulus

Greek

α_n	Parameter of the appearance function model
α_r	Parameter of the energy split model
Γ^{imp}	Specific rate of impact generation
β	Particle shape factor
β_n	Parameter of the appearance function model
γ	Damage parameter
γ_r	Mean radial position of the grate openings
$\dot{\delta}_n$	Normal deformation rate
δ_n	Normal deformation
$\dot{\delta}_t$	Tangential deformation rate
δ_t	Tangential deformation
Δ	Maximum deformation of the particle bed during impact
η	Resistance coefficient
θ	Fitting parameter
θ_s	Angular displacement of the shoulder position of the charge
θ_t	Displacement of the charge toe position

θ_{tp}	Angular displacement of the slurry toe position
ϑ_c	Deformation at the fracture
ϑ_n	Maximum deformation achieved during the n-th loading event
λ_A	Abrasion model fitting parameter
λ_r	Depth of the pulp lifters expressed as a fraction of diameter
Λ	Selection function parameter
μ	Selection function parameter
μ_s	Static friction coefficient
μ_r	Rolling friction coefficient
$\Xi(\vartheta)$	Load displacement profile
ρ	Specific gravity
ρ_c	Charge density – ore plus balls and water
σ_∞	Fitting parameter
σ_j^2	Variance of the distribution of fracture energies
τ	Average residence time
υ	Poisson's ratio
v_j	Linear velocity of element j
v_{ij}	Relative velocity at the contact point
φ	Fitting parameter
φ_c	Percentage of mill critical speed
$\emptyset$	Parameter of Austin's breakage function
ω_j	Angular velocity of element j
ω_k	Frequency of collisions of class k
ω_m	Mill speed
χ	Maximum tangential deformation before the slips occurs

Nomenclature

AG	Autogenous grinding
CFD	Computational fluid dynamics
DEM	Discrete element method
DWT	Drop weight test
EGL	Effective grinding length
HPGR	High pressure grinding rolls
ILC	Impact Load Cell
JKMRC	Julius Kruttschnitt Mineral Research Centre
LTM	Laboratório de Tecnologia Mineral
PBM	Population balance model
PEPT	Particle emission positron tracking
PET	Positron emission tomography
RBT	Rotary breakage tester
ROM	Run-of-mine
SAG	Semi-autogenous grinding
SPH	Smooth particles hydrodynamics
SPI	Sag power index test
UCM	Unified comminution model
UFRJ	Universidade Federal do Rio de Janeiro
VCM	Virtual comminution machine

I. Introduction

Tumbling mills are tubular shaped equipment that are widely used in the minerals industry. Its main purpose is to break solid particles until they reach the size required to liberate the valuable minerals. Particle fragmentation occurs due to the axial rotation of the cylinder, whose its internal surface is able to rise the elements in the charge (ore particles and steel balls grinding media). The particle size reduction process is a highly energy intensive process, as many authors claim that the power consumption of all comminution processes are about 3 % of all electricity generated in Earth (Schoenert, 1986, La Nauze and Temos, 2002 and Fuerstenau and Abouzeid, 2002).

Autogenous (AG) and semi-autogenous (SAG) mills are tumbling mills in which grinding media includes coarse ore particles. In the specific case of autogenous mills, the grinding media are formed exclusively by ore particles.

In mineral processing, the increase in production capacity of existing plants and the reduce of the ramp-up in new operations are both majors goals. However, there is a growing number of operations in which engineers have not been able or faced difficulties in making their plants reach their designed capacity in recent years (Weerasekara *et al.,* 2013).

The design of a grinding circuit that includes AG or SAG mills requires a number of standardized bench tests with the ore. Then empirical correlations take the results from these tests to estimate the performance of the circuit. This is possible only if there is information available from, for example, other existing industrial mills grinding ores with similar properties of the ore of interest.

Even though several process simulators in the market are able to provide useful information to design engineers and plant operators, the mathematical models that are contained inside mineral processing plant simulators are not generally fully predictive, having to rely heavily on data from ore testing in pilot or even industrial-scale plants. As such, risk reduction in the design may only be reached from a costly test campaign.

The current models (Austin *et al*., 1986, Leung *et al.*, 1987) and process simulators (JKSimMet, UsimPac, ModSim) can answer a number of questions. They allow to predict with great confidence the mill power, help us select the liner design to minimize charge projection and the performance of an industrial mill if provided good data from pilot scale tests.

However, in case of projects at greenfield stage or those that will process ore with unusual/uncommon behavior, it may be risky to use the traditional tools because they fail to answer questions such as:

- Will the autogenous mill circuit work for a certain type of ore?
- Will the ore produce enough autogenous grinding media?
- How will the mill respond to blending of different ore with different breakage properties (hard/soft)?
- Will particles of critical size accumulate in the mill?
- What is the optimum ball load on SAG grinding?
- How will the mill respond to changes and disturbances on ore grindability?
- How will the grinding performance change as liner wears?

To overcome these limitations more advance modelling capabilities are required. The constant development of the Discrete Element Method (DEM) application for tumbling mills, which started in 1992 with the work of Mishra and Rajamani (1992), now allows simulation of charge motion in large scale mills. However, the simulation of charge motion alone does not answer the questions posted above.

The development of mechanistic models to describe particle breakage is a step further from the traditional models. Such mechanistic modeling approach aims at filling the void that exists between particle breakage characterization to the use of information obtained from DEM simulations, and then descriptions of mill transport to predict mill performance.

Although a number of researches have proposed distinct ways to structure their DEM-based models of comminution, the modelling approach developed by the researchers at the Laboratório de Tecnologia Mineral (LTM) from Universidade Federal do Rio de Janeiro (UFRJ) has been recognized as one which combines richness of detail and simplicity in formulation. As such, it figures as one of the leading approaches in the field in advanced modeling in comminution.

The mechanistic approach used in the UFRJ model has been previously validated on the application for ball mills (Tavares and Carvalho, 2010). Ball mills are, in a way, simpler to model and describe quantitatively using the mechanistic model than AG and SAG mills because the grinding environment is not significantly influenced by ore properties.

The UFRJ model uses the concept of breakage probability and fracture energy. Based on this information and on a model proposed by Tavares and King (2002), the modeling approach is capable of describing particle weakening due to unsuccessful impact events. In other approaches, such as UCM (Powell, 2006) and HFS (Herbst, 2004), this is either not addressed at all or its description requires the particle population to be described with averaged properties or, alternatively, particles to be tracked individually, which is computationally demanding. The UFRJ model overcomes this by the use of distribution of properties among particles of similar basic properties such as size classes.

This thesis presents the development of the mechanistic model of comminution applied to mills in which ore particles have a role as grinding media, such as autogenous and semi-autogenous mills. The requirements of the mechanistic models are:

- To overcome the limitations of the equations and mathematic models currently used on mill design and optimization;
- To decouple the contribution of material and equipment in product generation process;
- To describe each one of the breakage mechanisms that occurs in tumbling mills;
- To describe mechanistically the effect of mill design and operation variables in grinding.

This thesis is structured in ten chapters. After the introduction and aim of the work, presented in Chapters I and II, the literature in the field is reviewed in Chapters III-VI, including the original mechanistic model description in Chapter VI. Chapter VII presents the experimental procedures used to generated data to feed the model. Chapter VIII presents the DEM simulations conducted for the several mills. Chapter IX presents the model framework proposed and the model validation and results of application. Chapter X finishes the thesis with the conclusions.

II. Objective

The objective of this thesis is to establish the foundations of the mechanistic model applied to semi-autogenous mills.

III. Comminution and particle breakage

In this chapter, a review on the main comminution processes is presented. The particle breakage fundamentals are reviewed, covering both the traditional characterization and the more recent ore breakage methods from the last decade. Then, the fundamentals of particle breakage that form the basis for the construction of the mechanistic model are analyzed.

III.1 Comminution overview

Comminution is a process which particulate material is subjected to size reduction due to the application of energy, either by the application of explosives or by the use of crushing and grinding processes. The main goal of comminution in the minerals industry is the release of the valuable ore minerals from the gangue.

Grinding is carried out to reduce the size of the particles in the product in such a way that ensures the optimization of mineral processing for the particular ore. If the ore is not ground fine enough it will result in a coarser and insufficiently liberated product that may cause the downstream processes to be unable to generate product within the desirable grade (Wills and Napier-Munn, 2006). Another situation is the one in which the ore is over ground. In this case, the valuable component may be fully liberated from the gangue but the particle sizes may be finer than required for an optimal performance of the concentration processes, resulting in losses of metal to waste. In addition to that, in these conditions there will be a waste of energy during the grinding process.

Several types of equipment are used in comminution. Each one of them have peculiarities regarding the force application mechanisms to the ore particles as illustrated in Figure III-1.

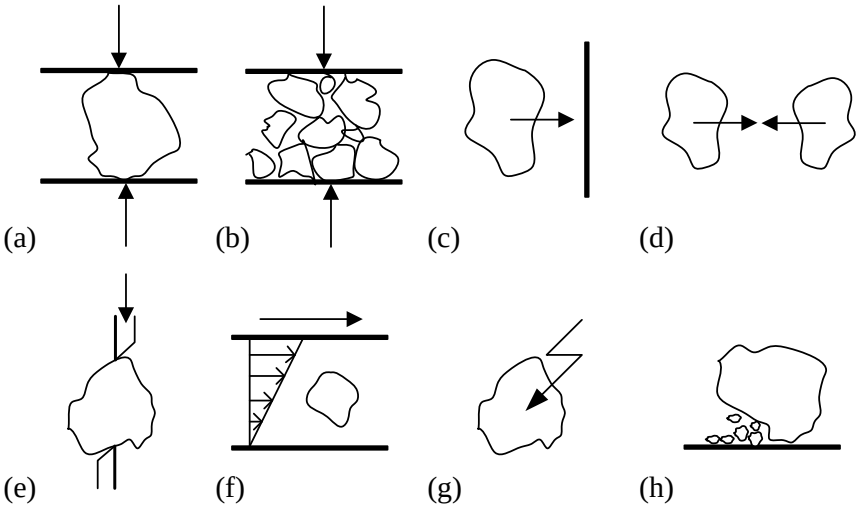

Figure III-1 Stress application methods in comminution equipment: load application directly to individual particles (a) or a particle bed (b) between two solid surfaces; particle projection against a solid surface (c) or against other particles (d); use of cutting equipment (e); application of shear (f); application of non-mechanical energy such as microwave, electrical shocks, heat, plasma (g) and surface breakage due to abrasion (h) - modified from Rumpf (1990)

Equipment used to promote particle size reduction of materials use different stress application mechanisms to cause particle breakage. When particles have coarse sizes, the energy needed to fracture each individual particle is typically higher, however the stresses and the energy per unit mass or volume, or specific energy, is lower. As particle sizes become finer, the specific energy (per mass unit), as well as the stresses required for breakage, increase rapidly. This explains the use of different comminution equipment depending on the size of the particles to be comminuted and the desired particle product size.

Most of the processes used in size reduction in the minerals industry use tumbling mills. These mills can be of several types: ball, rod, autogenous (AG) or semi-autogenous (SAG). The grinding action occurs due to the movement of the grinding media, which can be balls, rods, pebbles or non-spherical commercial media such as the Cylpebs. This movement results in collisions, which promote breakage of the particles due to either body or surface breakage.

Crushing is the first comminution stage after the rock blasting and is usually carried in a number of stages, reducing particle size in such a way that the ore may be fed to

downstream grinding circuits. In the crushing circuit, particle sizes can be as coarse as 100 cm, which is the case of the primary crushing feed stream, going to sizes as fine as 10 mm in the top size of the tertiary crushing product.

Grinding circuits that can be fed with particles up to 300 mm in size are used to reduce particle size to a few dozen micrometers. The product size specification depends on the type of ore and the aim of the operation, maximizing the ore recovery through the use, when needed, of concentration processes after the grinding stage.

Regarding tumbling mills, some definitions should be introduced. One of them is the critical speed of a mill, which is the rotation speed which makes the grinding load (usually balls) initiate a centrifugal movement adjacent to mill walls, and are not projected in the middle of the charge. From the force balance between the gravity and the centrifugal force acting in these charge elements, the critical speed in rotations per minute can be written as,

$$\text{Critical speed} = \frac{42.2}{\sqrt{D_m - d_b}} \qquad \text{III-1}$$

where D_m is mill internal diameter and d_b is the maximum diameter of the grinding media particles, both expressed in meters. It is common to refer to the mill operation speed as function of the parameter named fraction of critical speed, φ_c (Austin and Concha, 1994).

III.2 Ore characterization

The most commonly used way to describe a population of particles, ore sample or a mass stream in a process circuit is on the particle size. The particle size distribution is commonly used to characterize an ore sample or it may be used as a result from another characterization technique correlating the outcome of a bench scale grinding tests, such as the Bond grindability test (Bond, 1949).

In order to determine the distribution of particle sizes contained in any given stream, the most widely used technique is screening. The particles in the sample are disposed on a series of screens of decreasing square openings. The particles retained in each screen are weighted and the fraction of the original sample on each screen is logged, resulting in a table such as the one presented on Table III-1. Typically, the series

of sieves used obey the geometric progression with a $\sqrt{2}$ ratio. Other size analysis techniques can be used such as sedimentation, X-ray scattering, cyclo-classification (elutriation), machine vision and others, which are particularly useful outside the range of sizes in which sieving is the most convenient alternative.

Table III-1 Example of size analysis

Screen opening (mm)	Representative particle size (mm)	Retained mass (kg)	% retained on screen	% cumulative passing
203.2	-	0.00	0.00	100.00
152.4	176.0	0.00	0.00	100.00
127.0	139.1	51.96	11.47	88.53
101.6	113.6	61.97	13.68	74.85
76.2	88.0	94.90	20.95	53.90
50.8	62.2	126.89	28.01	25.89
25.4	35.9	58.94	13.01	12.88
12.7	18.0	19.98	4.41	8.47
9.5	11.0	6.70	1.48	6.99
6.4	7.8	8.02	1.77	5.22
3.18	4.49	5.57	1.23	3.99
2.36	2.74	2.08	0.46	3.53
1.70	2.00	1.63	0.36	3.17
1.18	1.42	1.54	0.34	2.83
0.850	1.001	1.45	0.32	2.51
0.600	0.714	1.36	0.30	2.21
0.425	0.505	1.27	0.28	1.93
0.300	0.357	1.22	0.27	1.66
0.212	0.252	1.13	0.25	1.41
0.150	0.178	1.00	0.22	1.19
0.106	0.126	0.86	0.19	1.00
0.075	0.089	0.72	0.16	0.84
0.053	0.063	0.68	0.15	0.69
0.038	0.045	0.50	0.11	0.58
Sink	0.019	2.63	0.58	-

On Table III-1 the first column represents the opening sizes of each screen, the second column shows the representative size of particles that are coarser than the equivalent screen opening. The representative size is obtained by the geometric mean between the screen opening in which the particles were retained and the upper screen

opening in which the particles passed through. A common way to display particle size distributions is by curves of the cumulative passing percentage on each screen as the example on Figure III-2.

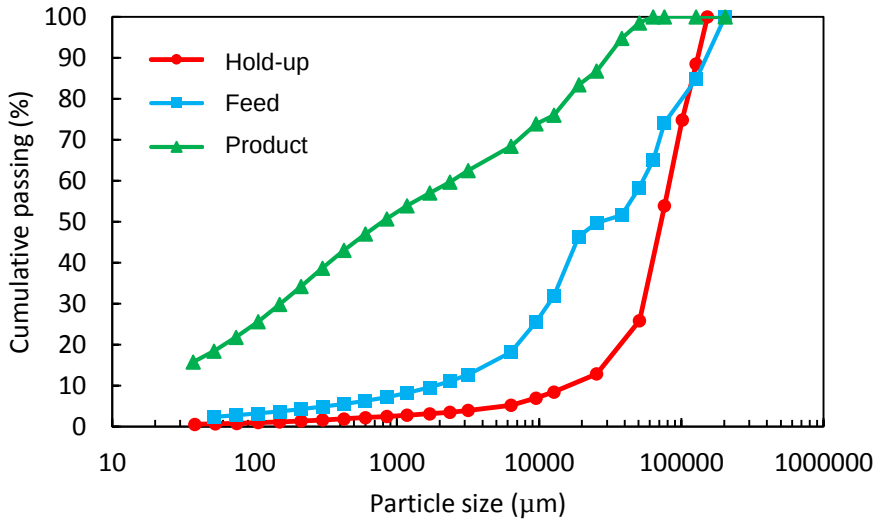

Figure III-2 Example of size analysis showing data from mill feed, mill hold-up and the product of a Pilot Scale SAG mill

Throughout the 20th century a large number of methods have been used for ore characterization for comminution. Tests may be classified in those that attempt to emulate the performance of a particularly crushing and milling equipment and those that attempt to describe particle breakage mechanisms (Tavares, 2007).

Recently, Verret *et al.* (2011) showed a review about the several test procedures used on the design and optimization of SAG mills. Today, it is recognized that pilot plant tests are those who give the most valuable information in respect of ore strength to the autogenous and semi-autogenous grinding. Even though the pilot scale tests require a huge amount of ore, they cover practically the same particle size range as in the industrial operational. However, many commercially available tests usually done from drill-core samples, give quick estimates about the performance of mills.

Table III-2 presents the work done by Verret *et al.* (2011) comparing the comercially available tests as function of the mill size, particle size and amount of sample required. As each type of test covers a different size range resulting in divergences on which is the best methodology to design and optimize SAG mills. While bench scale tests

require less samples, the results produce errors of an order of 20%. On the other hand, pilot-scale tests give a better estimative but are very costly. It is known that small differences on the value of the Bond Work index may result in large discrepancies on the specific energy consumption of an industrial mill and, even though there may be large differences on the specific energy consumption, the particle size distribution of the product may be very similar (Digre, 1989). Usually pilot scale tests required to the design of AG and SAG mills demand more than one hundred tons of the sample (Loveday, 2004).

Figure III-3 shows the particle size range covered by the tests used to characterize the ore for AG mill application and compares to the usual range of particloes processed on AG mills. The pilot plant test is the methodology that covers almost the entire size range of the industrial mill.

Table III-2 List of standardized ore characterization tests and their requirements (Verret *et al*., 2011)

Grinding test	Mill diameter (m)	Top size (mm)	Bottom size (mm)	Sample amount (kg)	Sample consumed (kg)	Type of test	Steady state	Use of database
Bond low-energy Impact	N/D	76,2	N/D	25	10	Individual particles	No	Yes
Media competency	1,83	165	N/D	750	300	Batch	No	Yes
MacPherson Autogenous	0,46	32	1,18	175	100	Continuous	Yes	Yes
JK Drop-weight	N/D	63	N/D	75	25	Individual particles	No	Yes
SMC Test	N/D	31,5	N/D	20	5	Individual particles	No	Yes
JK RBT	0,45	53	N/D	75	15	Individual particles	No	Yes
SAGDesign	0,49	38,1	1,7	10	8	Batch	No	Yes
SPI	0,305	38,1	1,7	10	2	Batch	No	Yes
AG Pilot Plant	1,75	200	Several	>50000	>50000	Continuous	Yes	Yes
Lab-scale HPGR	0,26	12,7	3,35	400	360	Locked-cycle	Yes	Yes
SPT	N/D	19,1	3,35	10	7	Locked-cycle	Yes	Yes
HPGR Pilot Plant	0,9	50	Several	>2000	>2000	Continuous	Yes	Yes
Bond Rod Mill	0,305	12,7	Several	15	10	Locked-cycle	Yes	Yes
Bond Ball Mill	0,305	3,35	1,18	10	5	Locked-cycle	Yes	Yes
Modified Bond	0,305	3,35	0,149	2	1,2	Batch	Yes	Yes

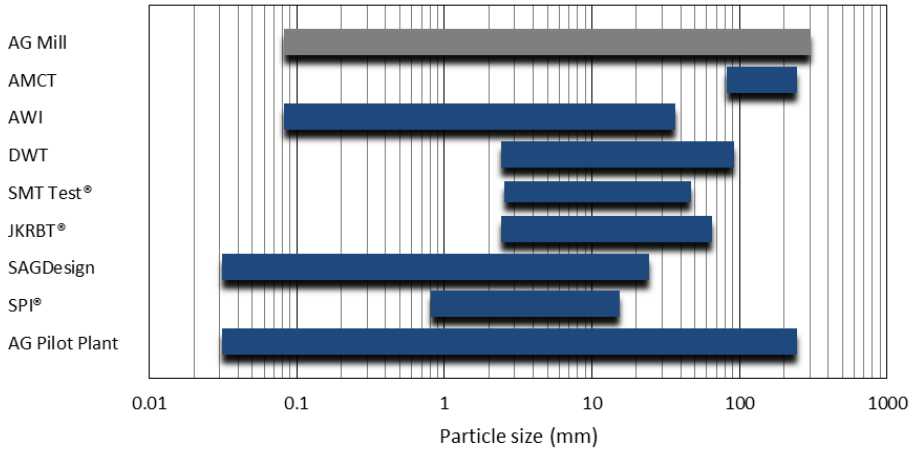

Figure III-3 Particle size range on each of the standard ore characterization tests for AG and SAG applications (Verret *et al.,* 2011)

These breakage tests commonly used are inadequate as they are dependent on the equipment used to break the particles. That being said the traditional tests go against the idea of decoupling the effect of ore and the environment that is one of the main features of the mechanistic approach (Powell and Weerasekara, 2010).

III.3 Particle breakage

Ideally, ore characterization should consist of conducting bench scale tests to characterize ore breakage under conditions that are similar to those found in the mills, covering the size range from very coarse particles to finer ones. Then, with the aid of mathematical models the prediction of the ore behavior in the industrial scale machine would be possible. This idealized situation requires the availability of appropriate models and the understanding of particle breakage. As Powell and Weerasekara (2010) claim, updated breakage characterization techniques are required to simulate the breakage modes found on comminution machines. This agrees with the research vision from UFRJ group lead by Tavares (Tavares, 2009). The authors recognize the damage effect when particles suffer different types of impact and the need for the development of a model that describes all breakage modes such as: volumetric breakage of individual particles and particle beds, surface breakage and abrasion as well as their cumulative effect. The

contribution of each particle breakage mechanism and their characterization tests and models is analyzed on the following sub-topics.

III.3.1 Single particle breakage

Particle breakage may be defined as an energy application event to a solid particle that causes mass loss of the original particle and generates daughter particles or fragments as shown on Figure III-4.

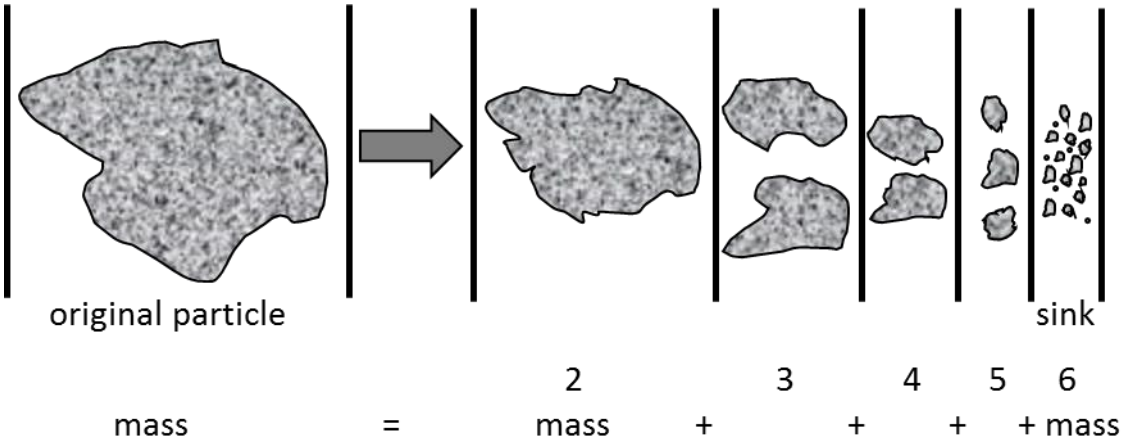

Figure III-4 Example of the breakage of the mother particle generating the progeny particles that fit in finer size classes (Austin and Concha, 1994)

Besides that, breakage of a particle may or may not occur depending on the mode of energy application. Each ore particle has unique characteristics such as shape, size, surface area, mineralogical composition and internal structure. The need to understand how particles behave when they are subjected to energy application has been an important research topic identified by many authors such as King (2001), Austin and Concha (1994) and others.

Due to these characteristics, in the beginning of the 1990s, Professor R. Peter King from Utah Comminution Center conducted the research involving the breakage of the individual particles and brought the attention to the importance of the microscale approach for the particle breakage processes. Studies carried in the University of Utah showed that a particle population have an intrinsic variability in their response to fracture (Tavares, 1997). As such, even within particles of the same ore, particle size class and composition, one can find particles that have widely variable strengths, with some being

easy to break and particles that are much tougher. This variability is generally attributed to a number of factors that may exert a significant influence on comminution processes (King, 2001). Indeed, the lack of ability to deal with particle strength variability is one of the weakest points of the traditional populational balance model (PBM) applied to comminution because the traditional PBM deals with the average properties of the material (ore particles), which are discussed in section IV.2. For instance, the limitations exhibited by the traditional PBM could be overcome with the inclusion of the variability of the ore particle properties. However, it is necessary to understand how the energy needed to break a particle is characterized.

The microscale characterization of the fracture of individual particles required the development of a new device that was able to measure the strength of each particle, when they are subjected to the conditions that are similar to those found on mills and crushers. This device, named Impact Load Cell (ILC) was developed in Utah Comminution Center (Weichert and Herbst, 1986). It consists of a long steel rod equipped with strain gauges, and photo-diode and laser system. The ILC allowed the study of fundamental properties of ore particles such as the strength (King and Bourgeois, 1993; Tavares and King, 1998). Figure III-5 shows the Impact Load Cell and its data acquisition equipment.

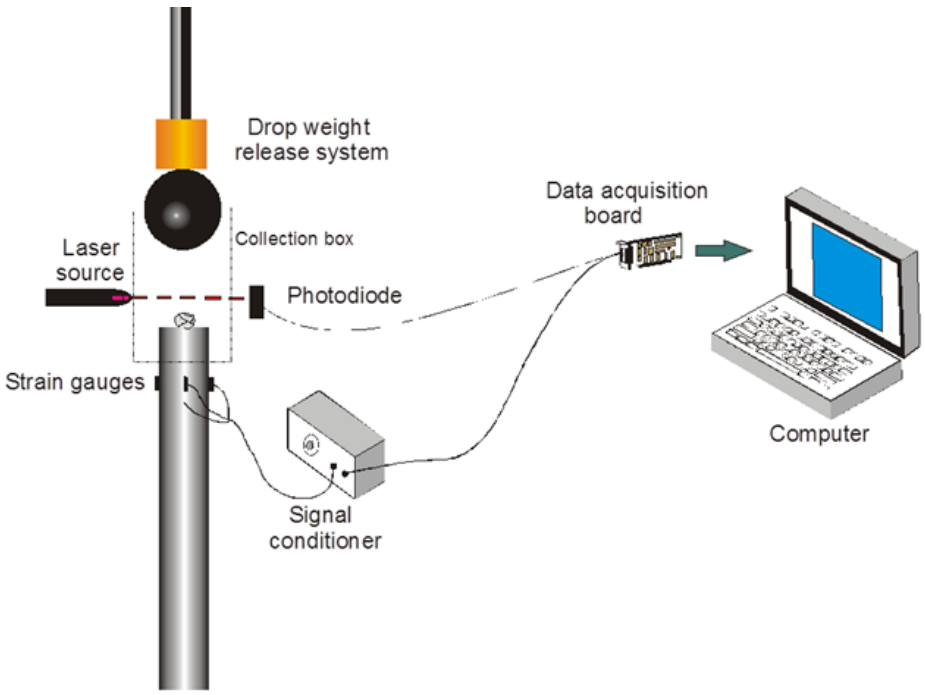

Figure III-5 Scheme of the Impact Load Cell (Tavares, 2007)

In the Impact Load Cell, particles contained in a given size range are submitted individually to the impact of a falling weight, usually a steel ball. The impact makes the strain wave propagate down the steel rod. The strain gauges installed on the steel rod detect the wave and the data acquisition system generates the force-time profile as shown in Figure III-6. The force time profile is then transformed into the specific particle fracture energy, which is calculated from Equation III-2.

$$E = \frac{1}{m_p}\left[v_0 \int_0^{t_c} F(t)dt + g\int_0^{t_c} F(t)tdt - \frac{1}{2m_b}\left(\int_0^{t_c} F(t)dt\right)^2 - \frac{1}{\rho A_c C}\int_0^{t_c} F^2(t)dt \right] \quad \text{III-2}$$

In this equation, t_c is the time which the particle suffered the primary fracture, m_p is the particle mass, m_b is the ball mass,v_0 is the impact velocity, g is the acceleration due to gravity, A is the cross sectional area of the steel rod, ρ is the specific gravity and C is the wave propagation speed on the steel rod (Tavares, 2007, Tavares and King, 1998, Tavares and King, 2004).

Typical force-time profiles are shown in Figure III-6, which demonstrate (Tavares and King, 1998) that the variability in the results is significant. Particles in the same size range show different force time profiles which result in variability on the measure of their strengths.

The characterization of a single material using the ILC requires dozens of fracture energy measurement tests, or the so-called, fracture energy tests. The fracture energy of each individual particle is calculated from its force-time profile. Figure III-7 shows the compiled result of the characterization of copper ore particles within different size classes. Figure III-8 shows a single result from the impact load cell test on one hundred limestone particles in the size range 4.5-3.75 mm. The distribution of the values of the particle fracture energies for a given sample and size could be modelled by a number of analytical equations. Tavares and King (1998) demonstrated that the lognormal distribution could be successfully used to describe it, given by

$$F_j(E_m) = \frac{1}{2}\left[1 + \mathrm{erf}\left(\frac{\ln E_m - \ln E_{m50,j}}{\sqrt{2\sigma_j^2}}\right)\right] \qquad \text{III-3}$$

where $E_{m50,j}$ is the median of the distribution, σ_j^2 is the distribution variance and E_m is the specific energy.

$E_{m50,j}$ is the median specific fracture energy of particles of a size class j. This parameter indicates the specific energy required to break 50% of the particles in the size class j in a single impact event. E_m is expressed in terms of specific energy which is the ratio between the energy (E) and the average mass of particles of the size class j, which for irregular shaped particles may be described using the III-4,

$$\bar{m}_{p,i} = \beta \rho d_i^3 \qquad \text{III-4}$$

in which, β is the shape factor and usually sits around 0.62 for ores such as copper or iron ore.

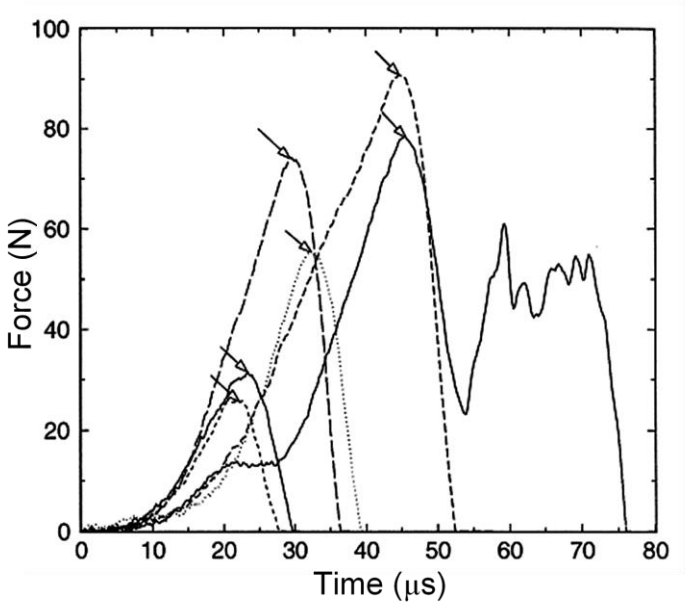

Figure III-6 Force time profiles of 1.00-1.18 mm quartz particles impacted by a steel ball weighting 0.0283 kg at the speed of 1.16 m/s. The arrows shows the time instant which the fracture happened (Tavares and King, 1998)

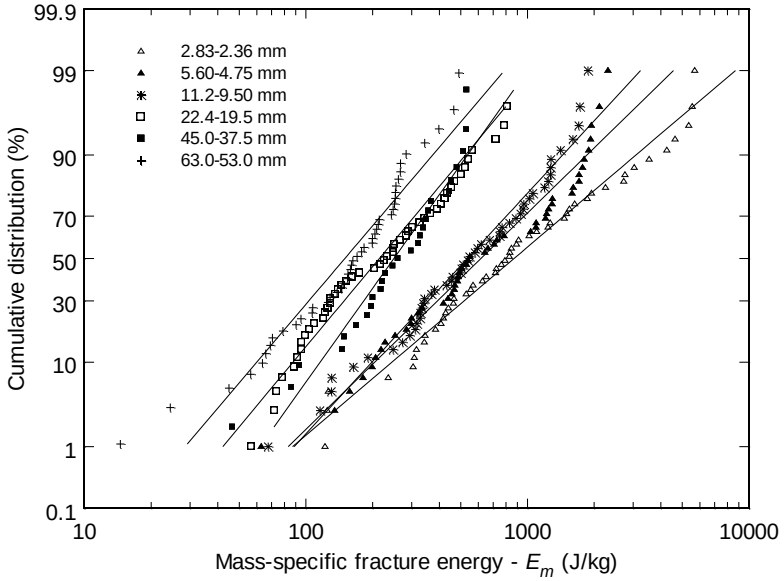

Figure III-7 Fracture energies distribution for a copper ore. Each symbol represents a single impact test conducted on an individual particle. The lines are the lognormal fit using Equation III-3

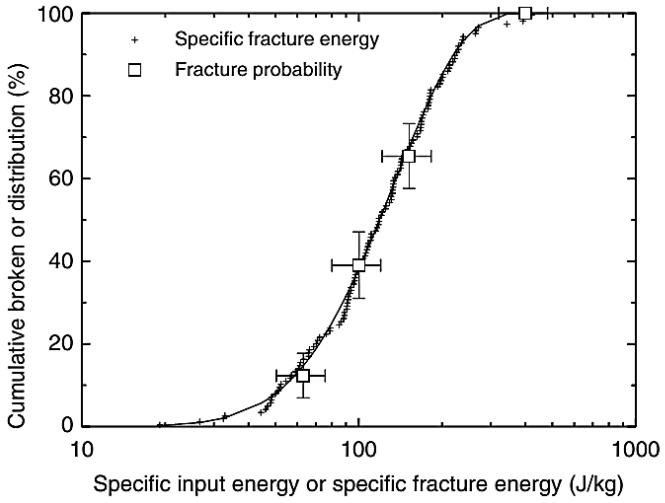

Figure III-8 Distribution of fracture energies of 4.75 x 4.00 mm limestone particles (Tavares, 2007)

The distribution of particle strengths could also be modeled with the upper truncated version of the lognormal equation, in this case, the Equation III-3 turns into,

$$F_j(E_m) = \frac{1}{2}\left[1 + \mathrm{erf}\left(\frac{\ln E^* - \ln E_{m50,j}}{\sqrt{2\sigma_j^2}}\right)\right] \quad \text{III-5}$$

which,

$$E^* = \frac{(E_{max}E_m)}{(E_{max} - E_m)} \quad \text{III-6}$$

Figure III-7 also shows that fracture energies distributions can significantly increase with particle size. They are usually determined by testing particles contained in narrow size classes, using the $\sqrt[4]{2}$ series of sieves. Usually for finer sizes, the fracture energy is higher, and this effect is illustrated in Figure III-9. Tavares (2007) proposed a function to describe the effect of the particle size on the value of the median specific fracture energy $\left(E'_{m50,i}\right)$. This function has three parameters that must be fit from data, being given by

$$E'_{m50,i} = E_{m,\infty}\left[1 + \left(\frac{d_o}{d_i}\right)^{\varphi}\right] \quad \text{III-7}$$

In some cases the variance of the fracture energy distribution may also vary with the particle size, in this case, a similar Equation has been proposed to account for this effect (Carvalho and Tavares, 2013),

$$\sigma_i = \sigma_\infty\left[1 + \left(\frac{d^*}{d_i}\right)^{\theta}\right] \quad \text{III-8}$$

where $E_{m,\infty}$, d_o, d^*, σ_∞, θ and φ are fitting parameters.

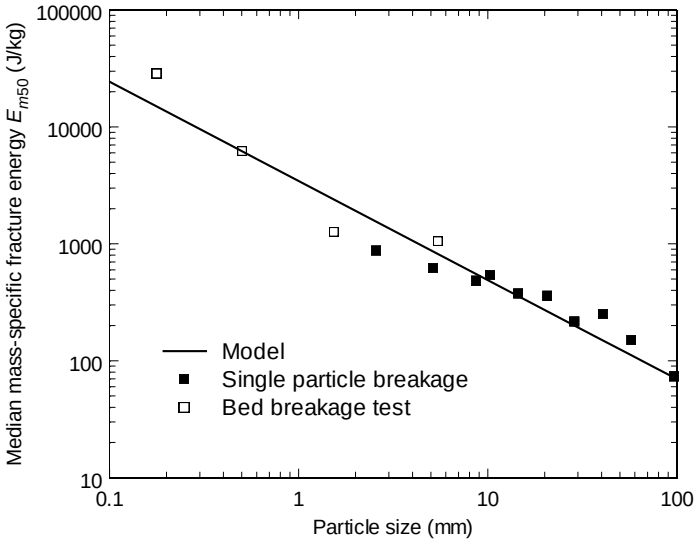

Figure III-9 Median specific particle fracture energy as function of the particle size for a copper ore. The line is the model fit and the filed squares are the data calculated from fracture energy tests

When measuring the specific particle fracture energy using the impact load cell the particles are positioned on the top of the steel rod and receive impact from a falling steel ball. Tavares (2004) proposed a correction for the surface type involved in the collision event based on the elastic constants of the elements in contact, on the basis of Hertz contact theory. The correction parameters must be applied to the value of the median specific particle fracture energy $E'_{m50,j}$ in order to compensate the measured fracture energy when the collision involves elements other than ore against steel surface. The correction equation is,

$$E_{m50,i} = E'_{m50,i}\left(\frac{k_{steel}}{k_{steel}+k_p}\right)\left(\frac{k_{media}+k_p}{k_{media}}\right) \qquad \text{III-9}$$

in which k_{steel}, k_{media} and k_p are the stiffness coefficient for the steel, the impact media and the particle, respectively. These coefficients are calculated from the ratio between the Young's modulus and the complement of the squared Poisson ratio (Johnson, 1985). The stiffness value commonly used for the steel ball is $k_{steel} = 236\ \mathrm{GPa}$.

The breakage function, or appearance function, is of great importance to the quantification of the breakage product of materials in comminution processes. The breakage function is the function that describes how the mass is distributed among the

fragments generated on a single event of particle breakage (primary fracture) and it is represented usually on its cumulative form (Figure III-10). The distributed form of the breakage function $b(d, d)$, represents the fraction of the product of the primary breakage from a particle of size d' which falls into the size d. In comminution processes, the product generated may be calculated from the successive application of the breakage function. It is possible to describe comminution as a process that may be mathematically modelled by considering a succession of individual impacts that result in a product. This concept may be applied to several mathematical models of breakage processes.

Several apparatus and tests have been constructed and proposed to determine the ore breakage function, the simplest of them being the Drop Weight Test (DWT) (Napier-Munn *et al.*, 1996). In this test, particles suffer impacts individually by a weight (flat anvil or spherical grinding media) from a known height. Then, the fragments from all impacts are collected and a size distribution analysis proceeds. Figure III-11 shows a scheme of the Drop Weight Test.

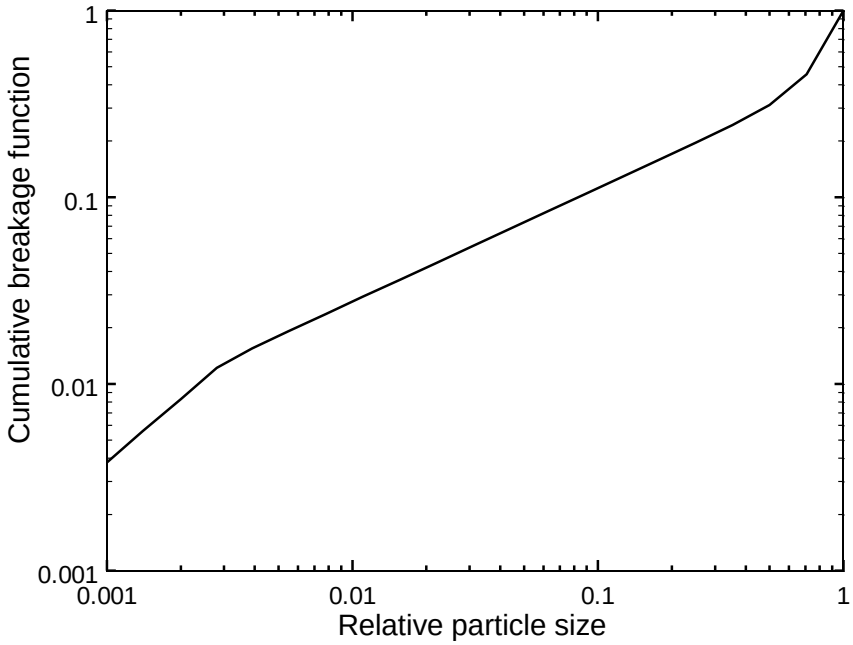

Figure III-10 Typical example of a breakage function

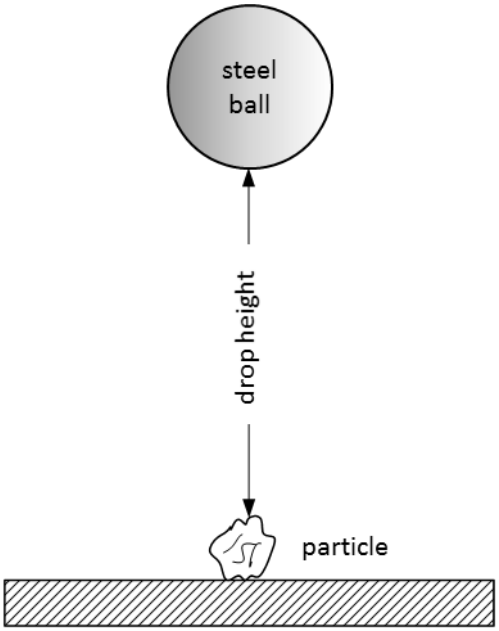

Figure III-11 Scheme of the *Drop Weight Test* (King, 2001)

By varying the drop height, it is possible to apply different impact energies to the particles. This allows a correlation between breakage degree and applied energy. The breakage degree will be higher for higher impact energies (King, 2001). Also, according to King, many attempts have been done to model the shape of the cumulative breakage function $B(d, d')$ for each type of breakage, no theoretical model has been established to reproduce the outcomes of single impact breakage. However, some empirical models predict these types of breakages with a good level of confidence.

One of the most accepted empirical particle breakage models is the one proposed by Austin (1984). It is based on the hypothesis that two distinctive populations of daughter particles composes the breakage fragments, as the example shown on Figure III-12.

Each of these populations has a functional form of the type,

$$B(d, d') \propto \left(\frac{d}{d'}\right)^{n_i} \qquad \text{III-10}$$

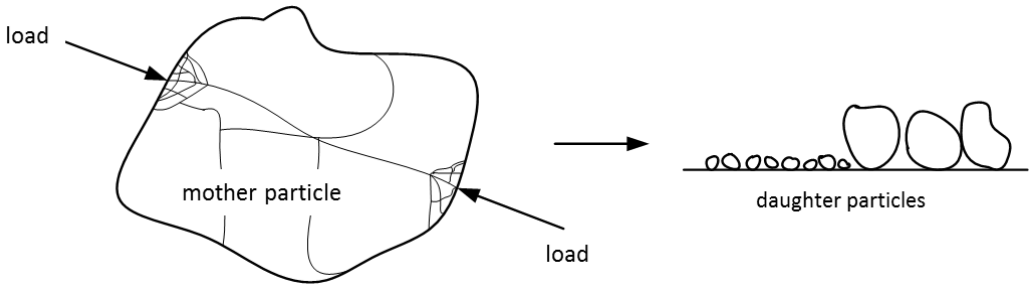

Figure III-12 Fine particles generation from cleavage of a single original particle (King, 2001)

The different values of parameter n_i may correspond to the stresses that cause fracture by impact or by compressive forces at the stress application points. The cumulative breakage function may be described as,

$$B(d, d') = \emptyset \left(\frac{d}{d'}\right)^{n_1} + (1 - \emptyset)\left(\frac{d}{d'}\right)^{n_2} \quad \text{III-11}$$

The first term in Equation III-11 describes the amount of the fine fraction generated from the breakage and $\emptyset$ is the fraction of the breakage products that contributes to the fine fraction. This breakage function model is used in Austin phenomenological model approach (Austin and Concha, 1994). This breakage model is mostly used in the methodologies that are based on batch grinding tests and it does not have any correlation to the energy level applied on the particles.

Another type of empirical models are those that correlates breakage with the energy input. The analysis of data from individual particle breakage tests suggest that an increase in energy input results in an increased generation of fine particles. An example is shown in Figure III-13, which presents the particle size distribution from a single particle drop weight test at three different impact energies.

Each breakage product size distribution may be parameterized as a function of the so-called t_n parameters (Narayanan and Whiten, 1988). The t_n parameters are the percentage passing on the screen aperture equivalent to the original particle size divided by the index number n so that,

$$t_n = P\left(\frac{d_0}{n}\right) \qquad \text{III-12}$$

where d_0 is the original particle size (representative size) and $P(d)$ is the cumulative passing on the size d.

The most important of the t_n parameters is t_{10} which refers to the percentage of material generated after breakage that is smaller than one tenth of the original particle size. When analyzing the t_{10} value from a particle size distribution generated from the breakage of other particles, it is possible to determine the degree of breakage the original particle suffered. A method of correlating the impact energy applied to particles E_{cs} to the amount of breakage generated consists of using the t_{10} parameter. Figure III-14 shows the experimental data as t_{10} as a function of E_{cs} for the size distributions displayed in Figure III-13 (Napier-Munn *et al.*, 1996). This relationship may be fitted using an exponential function of the type,

$$t_{10} = A\left(1 - e^{-bE_{cs}}\right) \qquad \text{III-13}$$

where A and b are model fitting parameter and vary as function of the ore. The $A * b$ value is widely used as the ore characterization parameter that indicate the amenability to breakage and has been used as an auxiliary indicators when designing comminution circuits. A low $A * b$ suggest that the ore is hard to break.

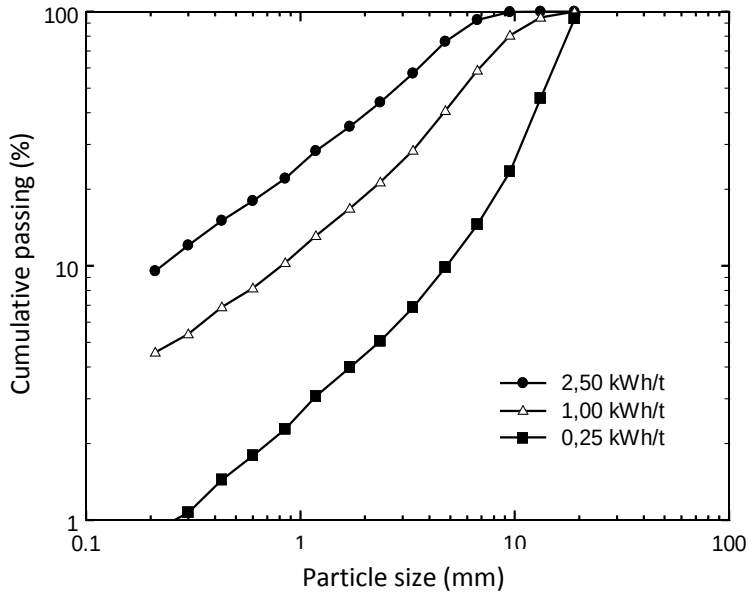

Figure III-13 Drop Weight Test product size distributions from a copper ore at original size of 22.4-19.2 mm impacted at different energy levels

The t_{10} versus E relationship describes the effect of the energy input on breakage, on the other hand it does not allow the calculation of the entire breakage function. Thus, a correlation was proposed among the t_{10} and the other t_n parameters to describe the entire size distribution at these specific (d_0/n) size coordinates. It is possible to represent the same particle size distributions of Figure III-13 in the form of the graph t_{10} versus t_n, as shown in Figure III-15 (Napier-Munn *et al.,* 1996).

It is common to use a set of polynomials such as cubic splines to interpolate the data from the t_{10} versus t_n (t_{10} - t_n) curve (Napier-Munn *et al.,* 1996). This is a very useful technique and it is implemented on JKSimMet® (JKSimMet, 2003) process simulator. The interpolation data set is named appearance function and is usually tabulated as a list of corresponding t_n values at selected t_{10} coordinates as shown in Table III-3.

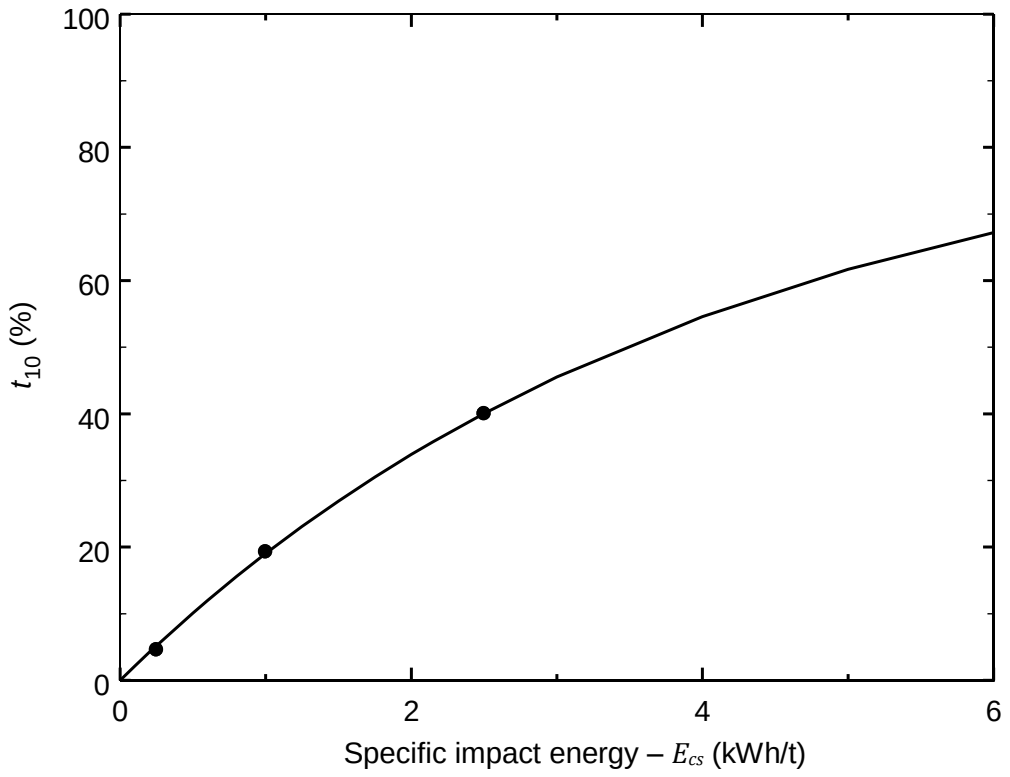

Figure III-14 Relationship between t_{10} and the specific impact energy E_{cs} used on the breakage of copper ore particles in the Drop Weight test. Dots are the experimental results (Figure III-13) and the line is the data calculated from the fitted model $A = 87$ and $b = 0.247$ (Equation III-13)

Table III-3 Appearance function for the copper ore of Figure III-13

t_{10}	Relative to initial particle size				
	t_2	t_4	t_{25}	t_{50}	t_{75}
	Cumulative passing (%)				
10	92.4	78.5	56.6	24.7	5.2
20	98.6	95.9	85.0	47.8	10.4
30	99.8	99.4	95.7	66.1	15.9
50	100.0	100.0	99.8	89.0	27.9

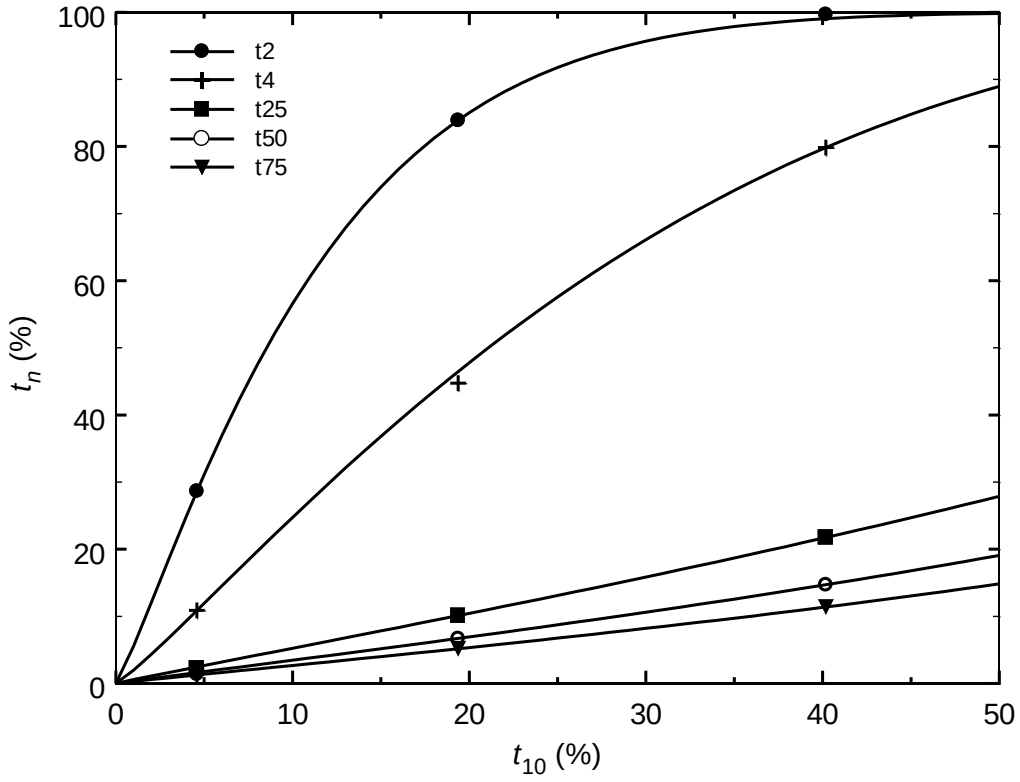

Figure III-15 t_{10} versus t_n for the DWT result presented in Figure III-13 (dots) and fitting using cubic splines (solid lines)

Each vertical line, traced from a certain t_{10} value allows the reconstruction of the full particle size distribution, expressed in terms of the cumulative percentage passing.

Several impact breakage experiments can be conducted for a selected ore in order to populate the appearance function and then having each t_{10} - t_n curve fitted.

In traditional population balance modeling of mills, breakage is usually considered as being the event in which the original particle leaves its size class (Austin *et al.,* 1984). However, in the mechanistic microscale modelling, a particle is considered broken when it loses at least 10 % of its original mass, even when it stays on its original size class (but its fragments are of smaller sizes). This definition is required to keep the consistency with the breakage definition used on the fracture energy tests on the Impact Load Cell (ILC) (Tavares and King, 1998). Thus, it is possible that a particle suffers breakage but still remains on its original size.

The individual impact tests have been clearly showing that the breakage function is determined as a function of the energy available to break a particle (energy input). The higher the energy input, the finer the breakage product. This mainly occurs due to successive breakage events of the original particle and its fragments until the total input energy is dissipated.

The correlation between the applied energy and the degree of breakage has been characterized by the t_{10} - E_{cs} relationship as presented on Equation III-13. However, it is known that this relationship varies with particle size. Some attempts to model this behavior were made to formulate a single equation that accounts for this effect, such as the empirical equation proposed by Kojovic *et al.* (2010), by modifying the original t_{10} equation into (Equation III-13),

$$t_{10} = A\{1 - \exp[-f_{mat} d_0 k_n (E_{cs} - E_{min})]\} \qquad \text{III-14}$$

where, A (%) represents the maximum t_{10} value for a material subject to breakage, f_{mat} is an ore particle property, d_0 is the original particle size and k_n is the number of impacts received by the particle, E_{cs} is the specific impact energy and E_{min} is the minimum specific impact energy able to break the particle. This model also takes into account the damage accumulation effect, but this will be discussed later.

On the other hand, Tavares (2009) proposed to incorporate the effect of fracture energy, which varies as a function of particle size in the t_{10}-input energy relationship. The breakage function of a material is now characterized not only by the impact energy

applied to the particles but also by the median of the fracture energy distribution from particles that break in the impact event. Thus, Equation III-13 becomes,

$$t_{10} = A\left[1 - \exp\left(-b'\frac{E_m}{E_{50b}}\right)\right] \qquad \text{III-15}$$

In this equation, the parameters A and b' are functions of the ore and are determined by fitting the t_{10} equation using particle fracture data from several size classes. E_{50b} is the median of the particle fracture energy distribution of the particles that break in the impact which is equivalent to E_{m50} when all particles break.

The result is Equation III-15 that describes the relationship between the applied energy and the fragments distribution, also including the effect of particle size as shown in Figure III-16.

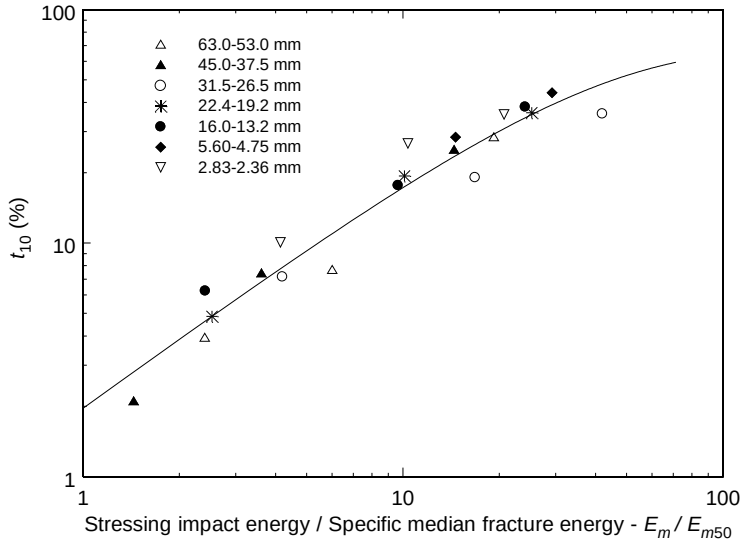

Figure III-16 Measured t_{10}values from DWT of a copper ore as function of the ratio of applied energy over the median of the fracture energy distribution of the broken particles (Carvalho and Tavares, 2011)

III.3.2 Surface breakage

There are situations when the energy applied to a particle is not sufficiently high to cause body breakage (either catastrophic or by cleavage) or that applied energy is mostly resulting from shear stresses. This breakage mode, which includes particle abrasion and chipping has significant importance on the performance of AG and SAG

mills. Surface breakage of particles, with generation of very fine powder results in the mass loss of the original particle, which becomes progressively rounded. As observed by Loveday and Naidoo (1997), the relative mass loss of particles tumbled in a pilot scale mill was constant after an initial rounding process for particles between the range of 20 to 80 mm.

Loveday (2004) proposed some tests in AG and SAG mills to calculate particle mass loss rate. These batch tests were conducted on mills with different diameters (0.6, 1.2 and 1.8 m). Water flow was used to carry the material smaller than 13 mm out of the mill and to allow monitoring of fine particles production per rock mass unit in the mill. This definition was then used to model the steady state operation of a 12 m diameter SAG mill using pilot-plant data.

Loveday and Naidoo (1997) observed that there is an initial rapid rounding of the particles in 0.6 m mill tests. From this point on a slow, continuous, and predictable process of removal of fine particles occurs. The authors proposed a model for the specific rate of particle mass loss R_s,

$$R_s = -\frac{dm_p}{dt}\frac{1}{m_p} \qquad \text{III-16}$$

This definition does not predict the size distribution of the surface breakage products and it is slightly different from the equation used on traditional population balance models. The focus of this equation is on rock cores generating fragments that are small enough (3 to 19 mm) to be removed from the test mill. The authors found that the rock abrasion rate, per unit mass, remains relatively constant with particle size (20 to 180 mm) and it is given by,

$$R_s = \left(-3K_R d^2 \frac{\mathrm{d}d}{\mathrm{d}t}\right)\frac{1}{K_R d^3} = \frac{3}{d}K_R \qquad \text{III-17}$$

where K_R is the rate of change in the diameter, which increases linearly with rock size.

Powell and Weerasekara (2010) have also observed from pilot scale SAG tests that the rate of fines generated from abrasion is higher at the beginning of the tests and it tends to decrease linearly with time. At the beginning, the shapes of the particles were mostly irregular, evidencing chipping, which they have called angular abrasion. However,

after 25 minutes of the batch test they observed a constant wear rate, at which time particles were mostly rounded in shape.

Given the irregular surface of the particles at the beginning of grinding, the initial surface breakage produces slightly coarser products (chipping fragments) and the original particle becomes rounded due to chipping, and fragments generated become smaller. King (2001) names these particles as abrasion fragments. The distribution of fragments can be described in as cumulative function,

$$A_{ij} = 1 \qquad d_i \geq d_A$$
$$A_{ij} = \left(\frac{d_i}{d_A}\right)^{\lambda_A} \qquad d_i \geq d_A \qquad \text{III-18}$$

where d_A e λ_A are material parameters. King (2001) proposes that the surface breakage distribution may be considered independent of the original particle size, so the cumulative form A_{ij} becomes A_j, while in its distributed form it is $a_j = A_j - A_{j-1}$.

III.3.3 Particle damage

Inside a comminution machine, particles are subjected to repeated stress application events (or impacts). These impacts are often of lower magnitude than needed to cause breakage of the particle in the first stressing event.

In order to describe particle breakage due to repeated impacts quantitatively it is needed to properly identify the dominant mechanisms. Essentially, according to (Vervoorn and Austin, 1990) there are at least two reasons why a particle may not fracture on the first impact, but only after a number of stress application events. Tavares and King (2002) showed that the mechanism based on the pre-existing crack propagation is probably the reason for the particle breakage after repeated impacts as the example shown on Figure III-17. In this case, even though breakage does not occur the particles suffer internal changes in the structure and become weaker, thus requiring a lower energy magnitude to cause breakage. These changes are associated to the fact that some of the energy in the impact event was used in internal crack propagation, affecting the internal structure of the particle, resulting in a weaker particle (Tavares and King, 2002).

Based on these ideas, Tavares and King (2002) proposed the application of damage mechanics theory to particle breakage. Damage mechanics is a field of solid mechanics that evolved significantly in the last decades due to its capacity to describe situations in which the fracture mechanics formulation became too complex or formulations are unavailable.

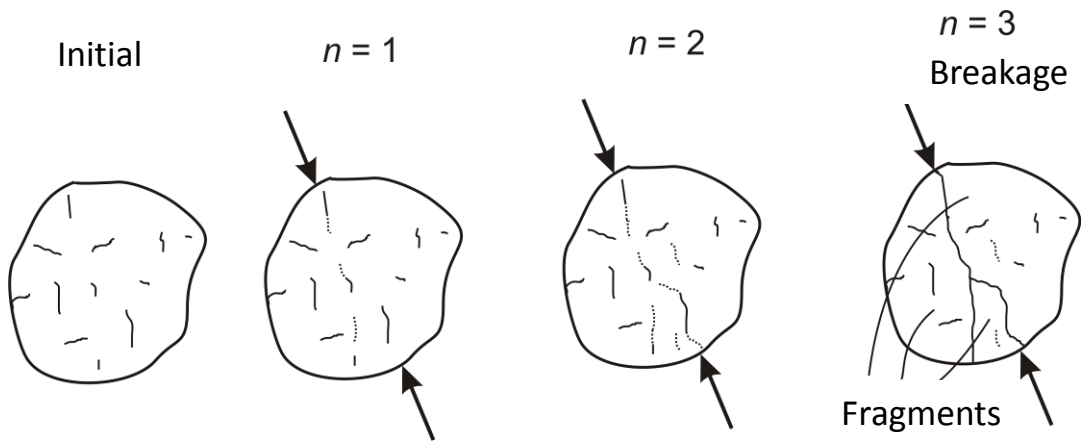

Figure III-17 Illustration of particle weakening due to damage accumulation of a particle subject to repeated impacts (Tavares, 2009)

The mathematical model developed by Tavares (1997) is one of the core features of the mechanistic approach from LTM/UFRJ and it is based on the Hertz contact theory and damage mechanics, resulting in a simple final form as shown by Equations III-24 and III-25. The energy expressed as absorbed stress by one particle subjected to load can be calculated by the direct integration of the load displacement profile $\Xi(\vartheta)$, and dividing the result from the particle mass m_p,

$$E_{k,n} = \frac{1}{m_p} \int_0^{\vartheta_n} \Xi \mathrm{d}\vartheta \qquad \text{III-19}$$

If it is assumed that all the energy applied to a spherically shaped particle, corresponding to the kinetic energy of the striker, is effectively converted into deformation energy – without energy losses to the plain surface under the particle – then (Tavares, 2009),

$$E_{k,n} = \frac{1}{m_p}\int_0^{\vartheta_n} \frac{k_r\sqrt{d}}{3}\left[1-\left(\frac{\vartheta}{\vartheta_c}\right)\right]\vartheta^{3/2}\,d\vartheta \qquad \text{III-20}$$

where ϑ_c the deformation at the fracture, after solving Equation III-20 and defining D_n^* as,

$$D_n^* = \left(\frac{\vartheta_n}{\vartheta_c}\right)^{\gamma} \qquad \text{III-21}$$

which ϑ_n is the maximum deformation achieved during the n-th loading event and d is particle diameter, and recognizing that the particle stiffness before the loading event n is $k_{r,n-1}$, then Equation III-20 becomes,

$$E_{k,n} = \frac{2}{15}\left(\frac{2\gamma+5-5D_n^*}{2\gamma+5}\right)\frac{k_{r,n-1}\vartheta_n^{5/2}d^{1/2}}{m_p} \qquad \text{III-22}$$

which $E_{k,n}$ is the specific kinetic energy of the striker (kinetic energy of the striker divided by particle mass) in n-th loading event that is all converted into deformation energy.

The specific energy required to shatter the particle, which is called particle specific fracture energy, can be calculated by replacing $D_n^* = 1$ and $\vartheta_n = \vartheta_c$ in Equation III-22, which gives,

$$E_{n-1} = \frac{4\gamma}{15(2\gamma+5)}\frac{k_{r,n-1}\vartheta_n^{5/2}d^{1/2}}{m_p} \qquad \text{III-23}$$

By assuming that the Equation III-21 remains valid under several impacts, and replacing Equation III-23 into Equation III-22, it is possible to establish the relationship between the specific fracture energy and the impact energy in successive impacts as

$$E_n = E_{n-1}(1-D_n^*) \qquad \text{III-24}$$

Rearranging Equations III-22 and III-24 and replacing in Equation III-21, the amount of damage suffered by particles on the n-th impact cycle is,

$$D_n^* = \left[\frac{2\gamma}{2\gamma + 5 - 5D_n^*}\frac{E_{k,n}}{E_{n-1}}\right]^{\frac{2\gamma}{5}} \quad \text{III-25}$$

This model does not require working directly with the force-deformation curves of each particle. As such, this simplifies the modelling effort in a way that there is only a single parameter to be fitted or estimated per ore type, which is γ, called the damage parameter. Equations III-24 and III-25 should be solved iterativelly by any numerical method, and the convergence of D_n^* is usually achieved within a few iterations.

Damage parameter characterization

The characterization of the damage parameter may be carried out conveniently by fitting the model to data from repeated impact tests, besides the initial fracture energy distribution of the ore. As such, the damage parameter can only be estimated if fracture energy distribution data is available prior to testing.

As previously mentioned in section III.3.1, results of fragmentation tests on the Impact Load Cell can be used. The direct integration of the force-deformation profiles to the point of fracture gives the energy required to cause primary fracture of the particle. Alternatively, the distribution of particle fracture energies may be estimated on the basis of the breakage probability distributions. This later may be estimated by subjecting a large number of particles to impact, one by one, and then finding the ratio between the proportion broken and the total number of particles that are impacted as a function of impact energy (Tavares, 2009).

In practice what happens when the entire population of particles that have a distribution of fracture energies is subjected to sequential impacts of known magnitude is represented in Figure III-18. The figure depicts four impact events. Initially, there is the distribution of particle fracture energies of the original material contained in a given size range. After all particles are subjected to the first impact of magnitude $E_{k,1}$, a part of the population, which has fracture energies below $E_{k,1}$, break and disappear from the distribution while the particles that do not break undergo weakening and damage, which is calculated using Equations III-24 and III-25.

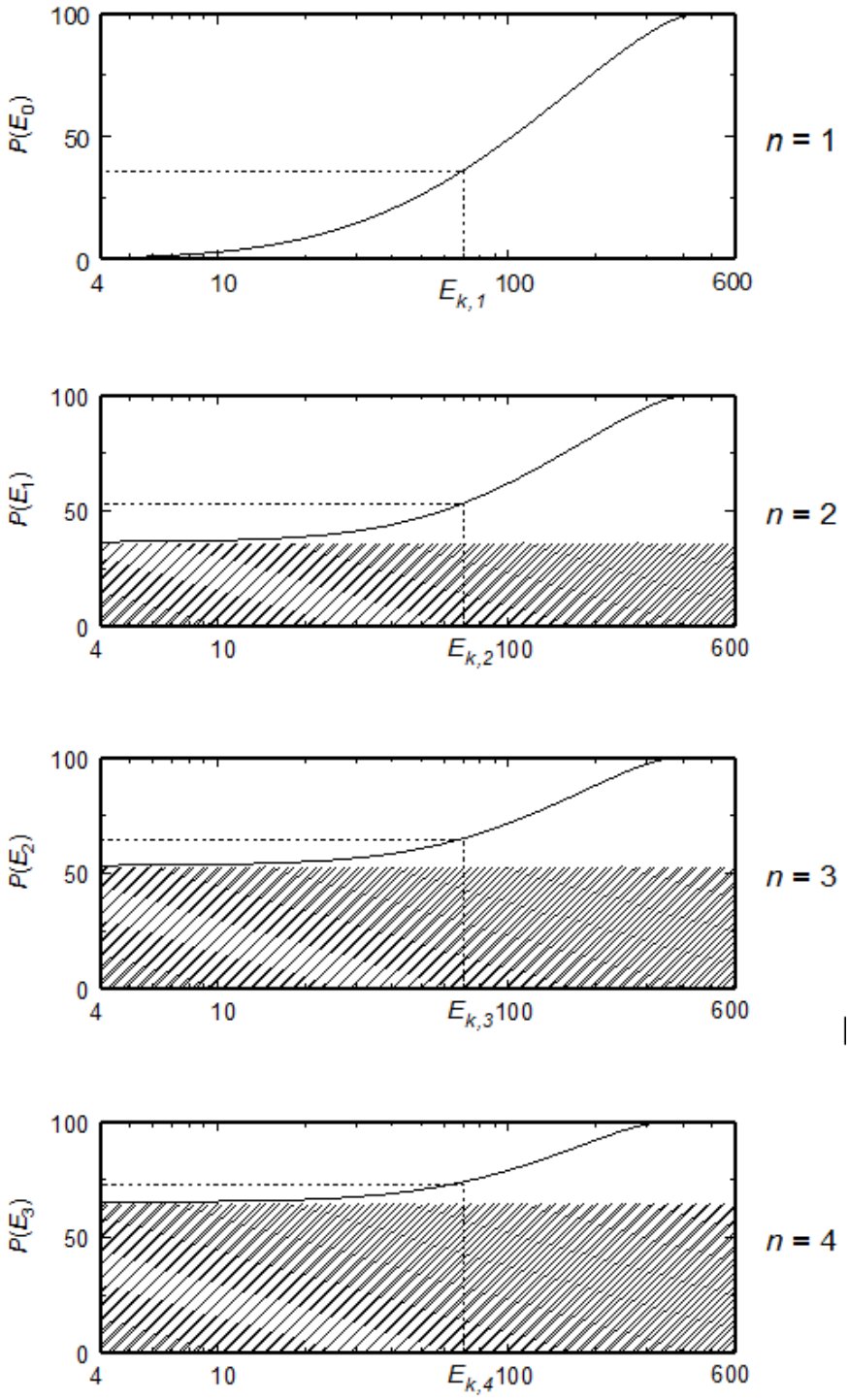

Figure III-18 Simulation of three sequential loading events using $\gamma = 3.3$, from fracture energy data of Figure III-8 and impact energy $E_{k,n} = 70.6$ J/kg which is constant in all simulated events (Tavares and Carvalho, 2007)

From the distribution of breakage probabilities, repeated impact tests were conducted. In this test, particles were subjected individually to an impact, from the drop of a weight onto a flat surface at a specified energy level. This is done in such a way that impacts are repeated until the particle breaks. The impacts are repeated and the number of impacts required to break each particle is recorded. The proportion of broken particles for each number of impacts at any given energy level is noted. Figure III-19 presents a typical result of such test as well as fitting of the model, given an optimal damage parameter (γ).

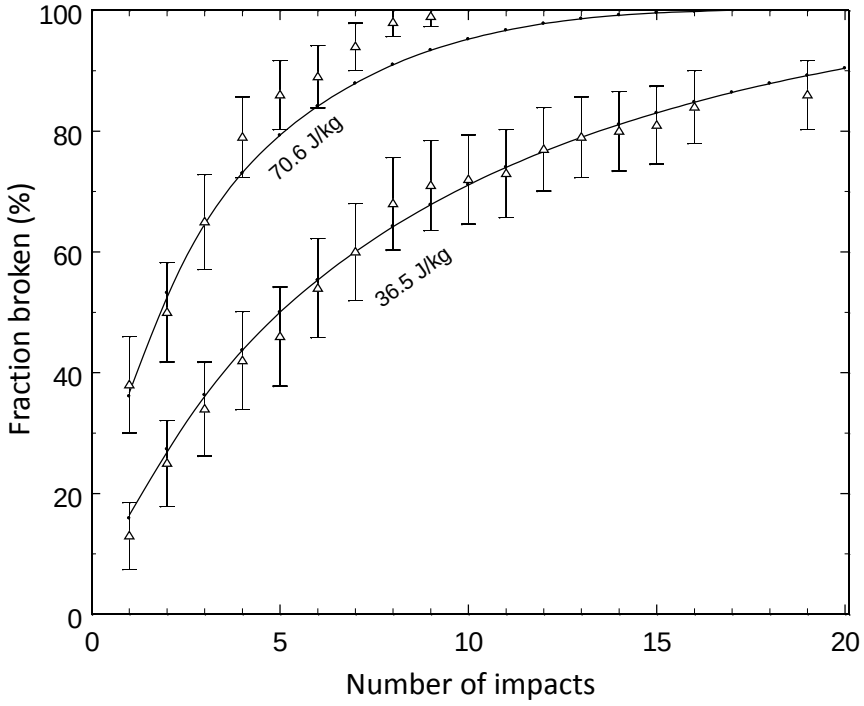

Figure III-19 Measured cumulative percent broken (symbols) bauxite particles contained in the range of 45 x 37.5 mm compared to fitted (points) results after repeated impacts at two energy levels. The solid line connects the fitted values for $\gamma = 3.3$ (Tavares, 2009)

The application of the model requires simultaneous solution of Equations III-24 and III-25. Given that D_n^* is implicit in Equation III-25, an iterative procedure is used which typically converges in less than 10 iterations from an initial guess of $D_n^* = 0$. When the fracture energy of the particle at stage n is smaller than the stressing energy, all of it will be absorbed and the particle breaks. As a result of the impact, which fractured a part of the particle population given by $F_n(E_k)$, the distribution of fracture energies after the impact is then given by

$$F_{n+1}(E_{n+1}) = \frac{F_n(E_{n+1}) - F_n(E_k)}{1 - F_n(E_k)} \quad \text{III-26}$$

An equivalent and more convenient procedure to use the model is by calculating the distribution of fracture energies after an n-th stressing event, being given by

$$F_{n+1}(E) = \frac{F_n[E/(1 - D^*)] - F_n(E_k)}{1 - F_n(E_k)} \quad \text{III-27}$$

where,

$$D^* = \left[\frac{2\gamma(1 - D^*)}{(2\gamma - 5D^* + 5)}\frac{E_k}{E}\right]^{\frac{2\gamma}{5}} \quad \text{III-28}$$

where E is the fracture energy of the particle that remained unbroken after the n-th impact. Equation III-28 should be solved using an efficient numerical procedure. Figure III-20 illustrates the procedure, showing the procedure for the traditional method (left) as well as the reverse approach (right).

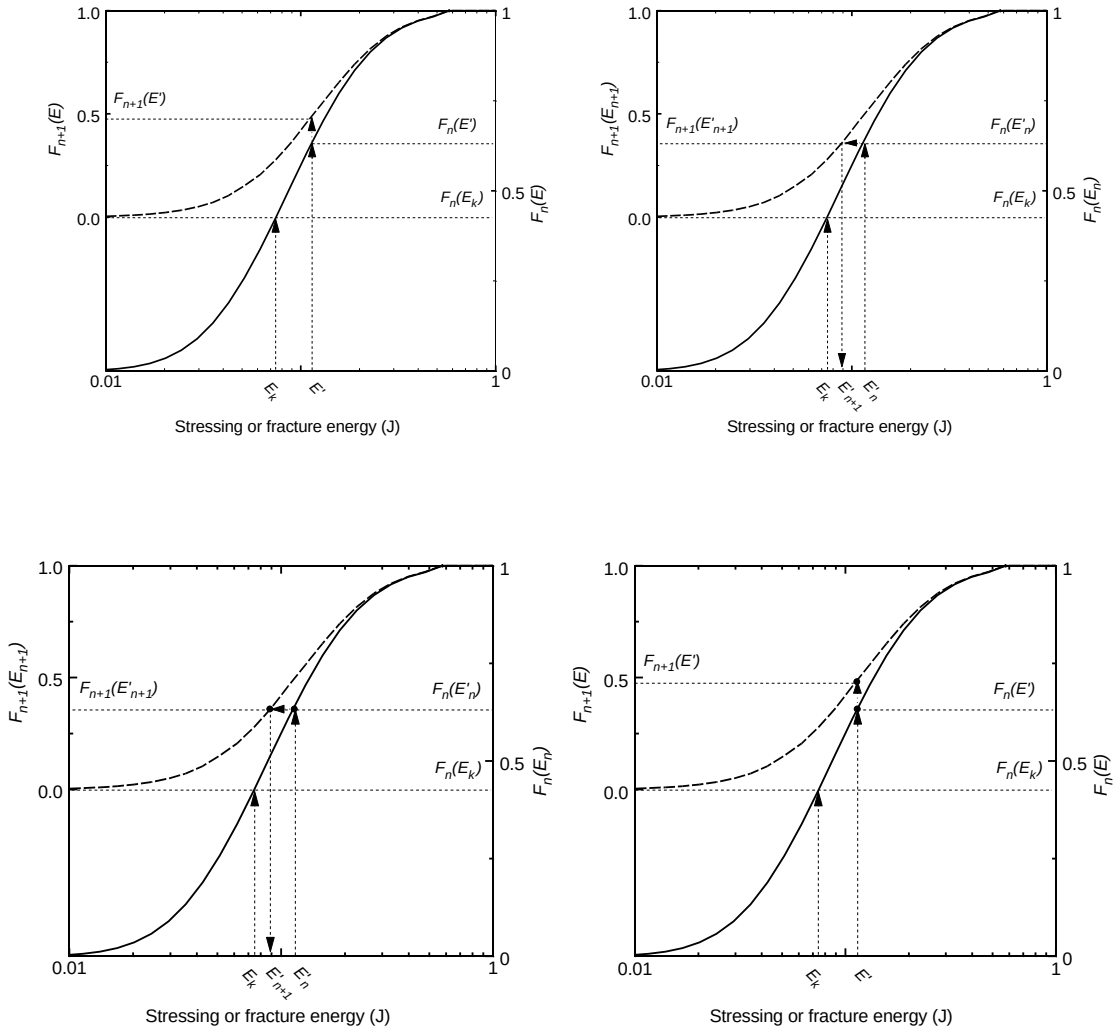

Figure III-20 Two methods of calculating the fracture energy distribution of the particle population after the damage event

IV. Autogenous and semi-autogenous mill

In autogenous mills coarse ore particles act as grinding media, being called autogenous grinding media. Breakage of the particles occurs due to the fall of the grinding media onto the particle bed inside the mill and by the abrasion and attrition mechanisms caused by the circular movement of the particles. Figure IV-1 illustrates the mill charge extracted from a pilot scale test with a copper ore.

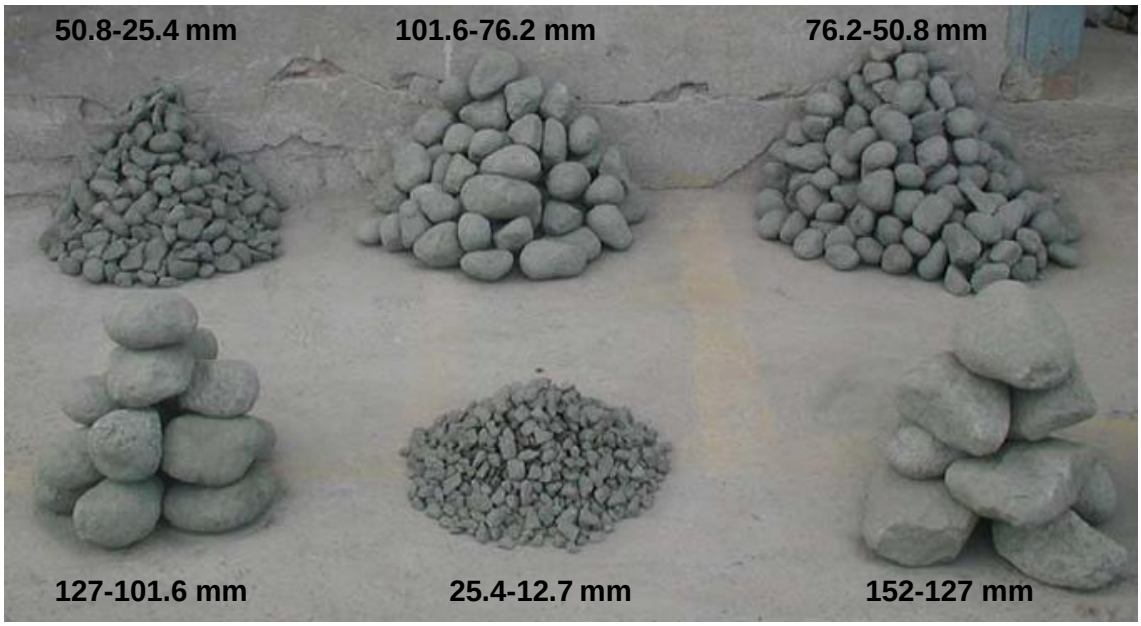

Figure IV-1 Particles extracted from the charge of a pilot scale SAG mill

In semi-autogenous mills the steel grinding media along with the autogenous grinding media are responsible for the breakage of the ore particles. The use of steel grinding media becomes important when the coarser ore particles are too tough and do not break due to the self-breakage. As such, the steel balls provide the impact energy required for these particles to break, preventing them from accumulating in the mill and then ensuring the continuity of the operation. Given that, the cost of replacing the broken and worn out steel ball is significant in this type of mill. The addition of steel grinding media also becomes important when the ore is too soft to generate proper autogenous grinding media.

The number of autogenous and semi-autogenous mills in comminution circuits increased significantly in the last two decades. An interesting study has been carried out

along the SAG Conferences that occurs every 5 years (Jones Jr and Fresko, 2011). It is a survey among autogenous and semi-autogenous mill operators. The work lists parameters such as diameter, length, effective grinding length, number of mills, installed power, type of motor, manufacturer, type of operation (dry or wet), ore, location and year of commissioning.

The autogenous and semi-autogenous mills are able to process a wide variety of ore types, being the most widely used in grinding gold ore (30%), iron (26%) and copper (25%), which together, correspond to 81% of total mill power installed in the world (Figure IV-2). The installed power in mills used to grind other ores, such as Zinc, Nickel and Platinum is also displayed.

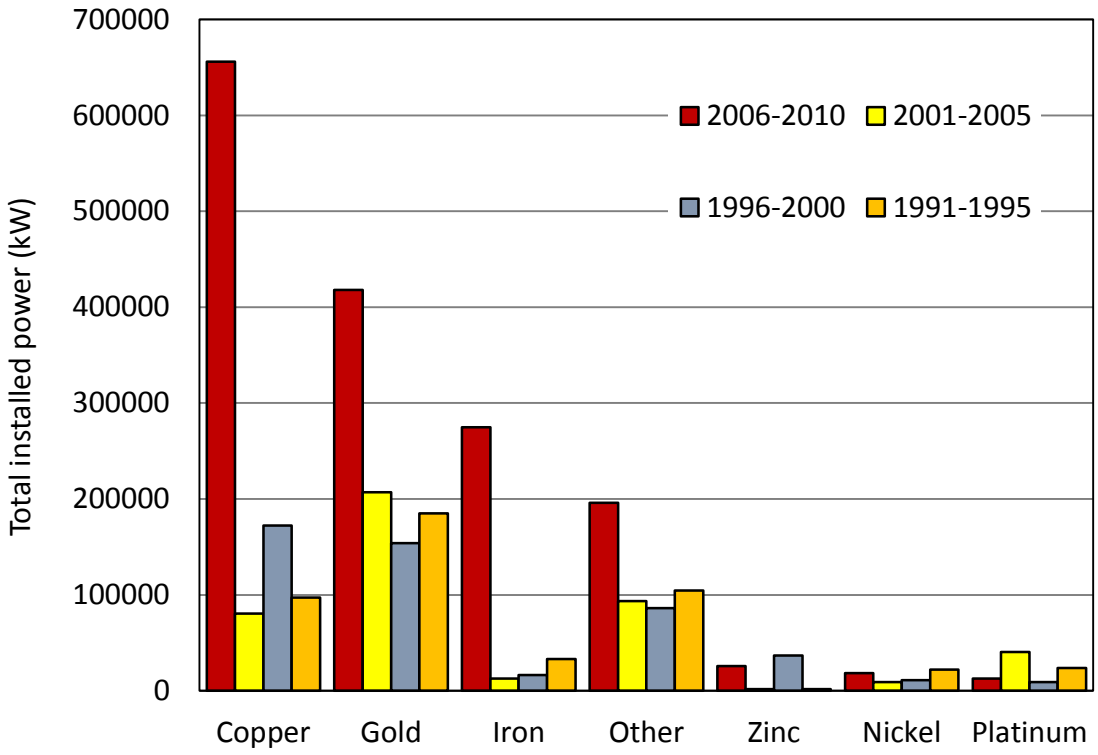

Figure IV-2 Total installed power per ore type as in 2010 (Jones Jr and Fresko, 2011)

Assessing the installed capacity of AG/SAG mills over time, it becomes evident that in the beginning of the 21st century there was a significant increase, which followed the recovery of growth in the minerals industry all over the world. Figure IV-3 illustrates this evolution through the analysis of the installed capacity of new mills, as well as the

cumulative in the world. Another important set of data published by Jones Jr. (2006) is the number of AG/SAG that have been sold every year since 1955 (Figure IV-4).

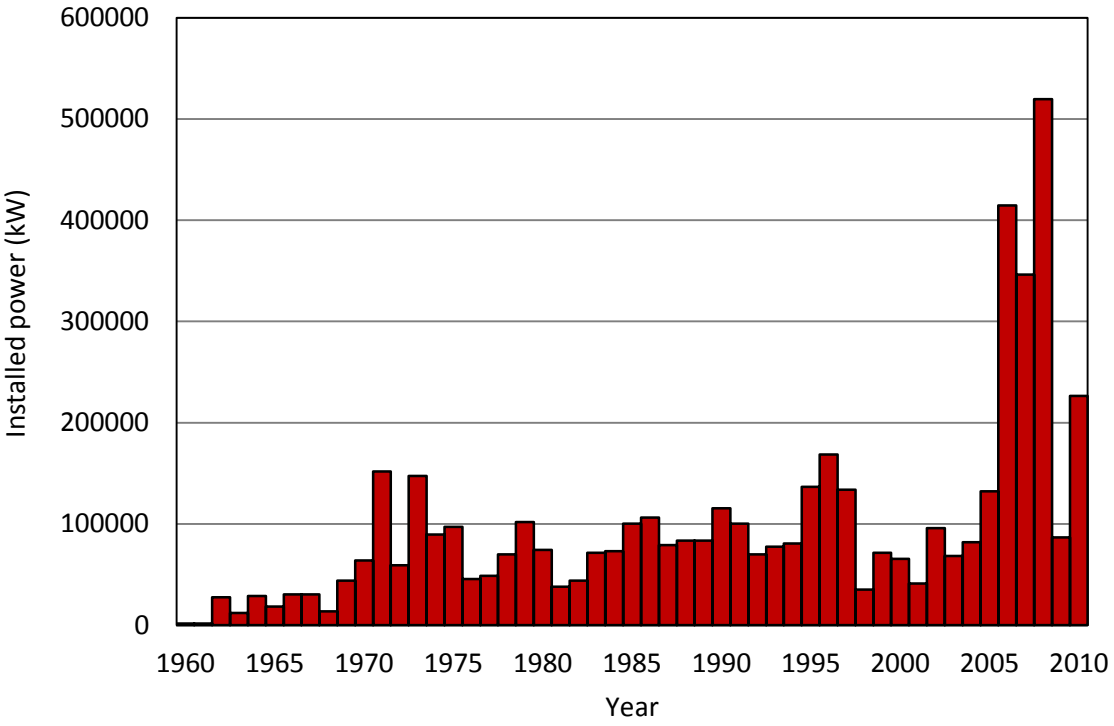

Figure IV-3 Installed power in mills sold in the last 50 years (Jones Jr and Fresko, 2011)

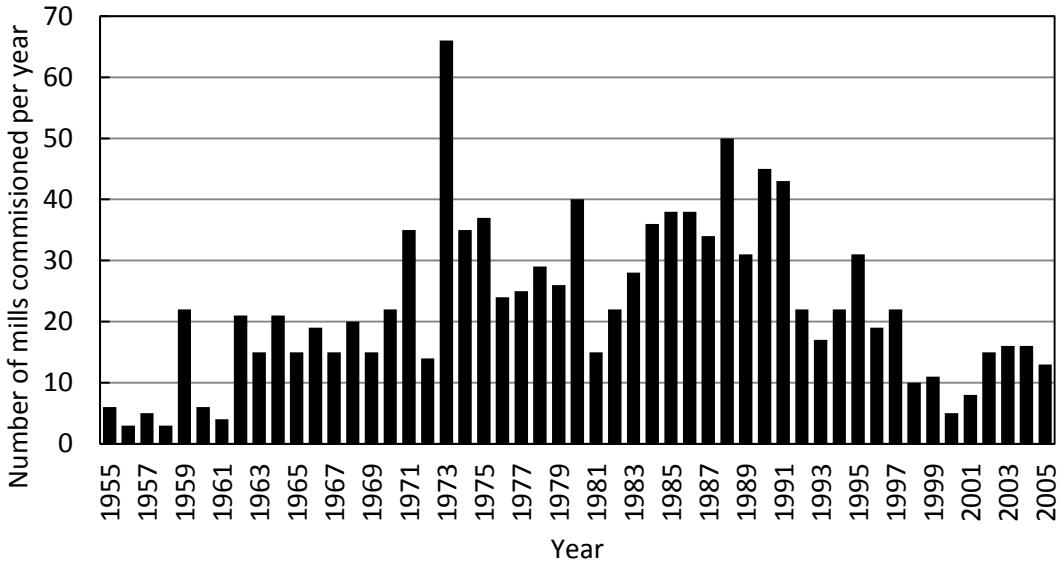

Figure IV-4 Number of AG and SAG mills commissioned per year (Jones Jr and Fresko, 2011)

The underlying mismatch between Figures II-7 and II-8 is due to the fact that, although the number of new mills comercialized has not increased markedly in recent years, their power and capacity has. This is because of the significantly larger mill diameters and powers that became the standard in recent years in the minerals industry. In Brazil, the largest SAG mill installed is at Sossego Mine from Vale, with 26,000 hp, which was commissioned in 2003.

Due to the ability to receive coarser particles and produce finer product, AG and SAG mills can replace both secondary and tertiary crushing and primary grinding stages. In some cases it can even replace the final grinding stage in an ore processing plant.

The use of autogenous and semi-autogenous mills in comminution circuits depends on the type of ore that is processed and sometimes even on the country of origin. For instance, South African run-of-mine (ROM) mills, which are low aspect ratio SAG mills, are operated with a higher ball filling.

One parameter that defines the geometry of the mill is the aspect ratio, which is the ratio between the diameter and the length of the mill. These mills often have a high aspect ratio, with large diameters. In this case, they are sometimes denominated as “pancake-shaped” mills, with values of 1.5 to 3 for the aspect ratio. Also, these mills can be built with an aspect ratio close to 1, or even with the aspect ratio lower than 1 such as the traditional geometry found on ball mills.

AG and SAG mills may have a conical or flat shape at the sides of the cylindrical section. In the first case, the charge level (balls and ore) inside the grinding chamber defines the effective grinding length or EGL (Figure IV-5). This EGL number, as many authors recommend (Jones Jr., 2006), should be given when reporting the parameters of AG/SAG mills as long as other dimensions such as diameter and length. To ensure data coherence, they suggest that the reports should contain internal mill dimensions, internal length between liner and between lifters, or, EGL. An example given by Jones Jr is a 32 ft x 15 ft, which is equivalent to 13.5 ft of EGL.

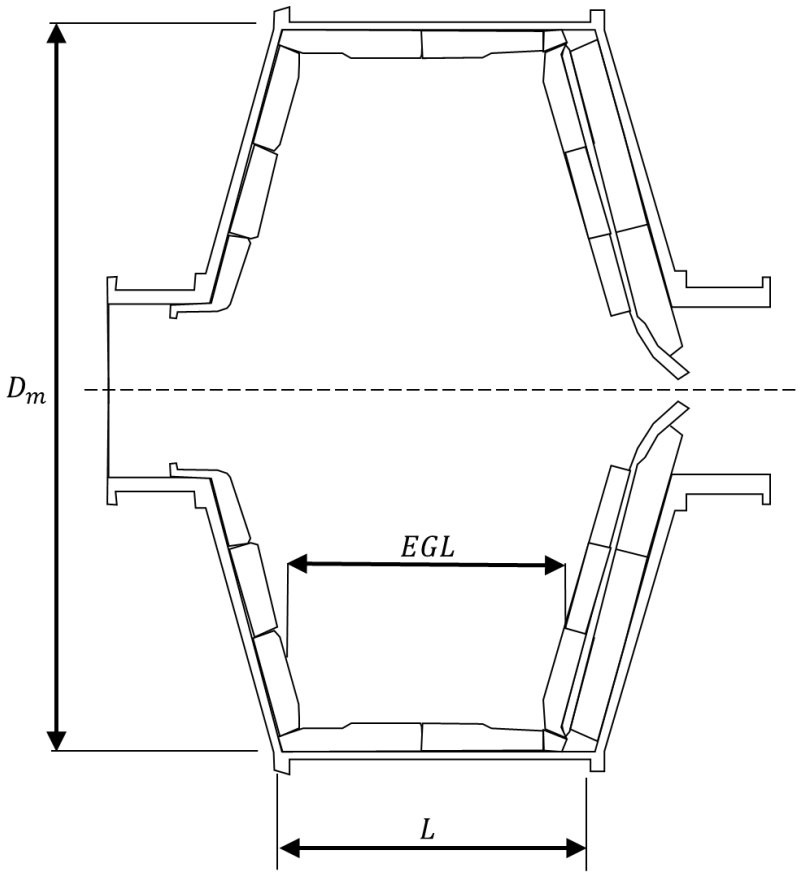

Figure IV-5 AG and SAG mill profile showing EGL measurement (Wills and Napier-Munn, 2006)

A variation of the semi-autogenous mills is the so-called ROM (run-of-mine) mill or South African mill (Powell and Mainza, 2006). These mills have low aspect ratio, with ball charges that can go up to 35 % of the grinding chamber volume. The particle size distribution of the ore fed to the mill is coarser as the name says, being fed with run of mine material, although often from underground operations.

High aspect ratio semi-autogenous mills has been used in a majority of cases on the processing of highly competent, or hard to break, gold and copper ores. The operation of these mills represents a significant challenge. The main predominant phenomena in this process: particle breakage and material transport, need a deeper understanding and better mathematical models to predict the performance of these machines.

Besides the aspect ratio, AG and SAG mills have a number of other important constructive aspects, which are:

- Discharge grate
- Pulp lifter
- Liner configuration
- Lifter bars
- Pebble ports

In ball mills, once the operation conditions has been defined through the control of rotation speed of the mill, ball charge and slurry solids concentration, the energy transfer from the grinding environment to ore particles is not significantly influenced by the ore characteristics. On the other hand, in autogenous and semi-autogenous mills the energetic regime of the grinding environment depends significantly on the properties of the ore particles that act as autogenous grinding media. These particles should be ideally strong enough to act as grinding media and then contribute to the breakage of the smaller particles and, at the same time, be susceptible to self-breakage, to breakage by the impact of the steel grinding media or even by attrition or abrasion when they are moving among the mill charge (Gupta and Yan, 2006).

In autogenous mills, the impacts of higher magnitude occur in the middle of the charge, closer to the mill base, while for semi-autogenous mills these impacts occur closer to the charge surface. The addition of steel grinding media significantly increases the processing capacity of the semi-autogenous mills. However, this capacity increase has a direct relationship in the operation costs due to higher replacement costs of the balls and the increase in the mill power consumption (Djordjevic *et al.,* 2006).

Autogenous and semi-autogenous mills are usually operated in closed circuit, with the mill discharge being classified using a trommel and/or a vibrating screen. The circulating load is usually lower than the one found in ball mill circuits. Usually the trommel oversize is fed to a crusher, whose task is to break the pebbles into smaller particles to be fed again to the mill (Fuerstenau and Han, 2003). The circuits that contain the pebble crushing stage are called SABC circuit and an example is showed on Figure IV-6. Also, autogenous and semi-autogenous mills operate in wet mode in almost all grinding circuits, but in very few applications, such as for iron ores, they can also operate in dry mode (Jones Jr., 2006).

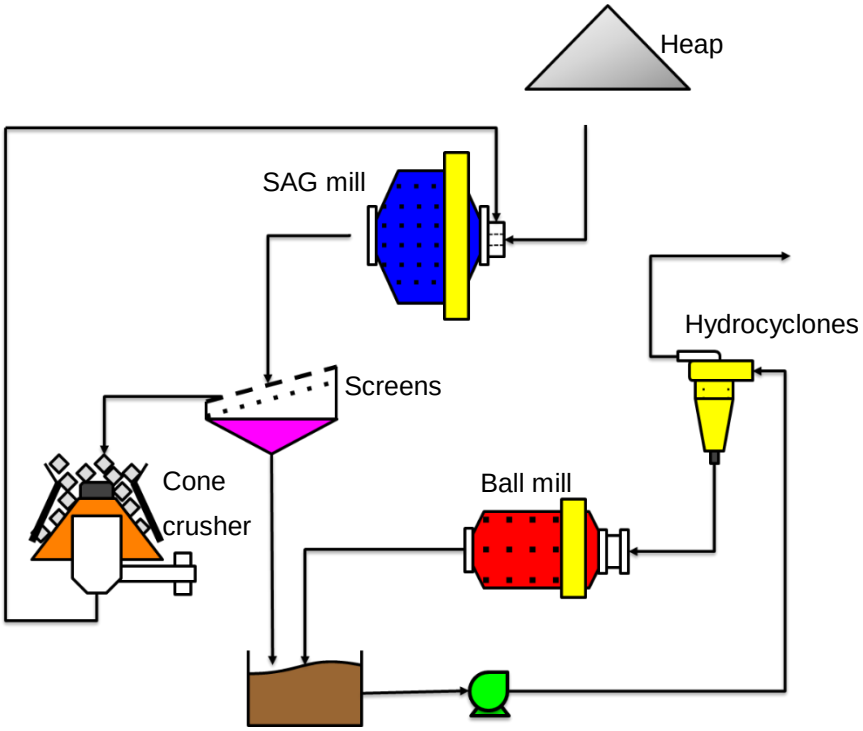

Figure IV-6 Typical SABC grinding circuit (Bergerman *et al.*, 2009)

IV.1.1 Transport in AG and SAG mills

The time spent by the ore inside the mills is an important parameter and it affects the quality of the product directly. It has been a great challenge to understand this part of the grinding process and develop better mathematical models. The flow of material, slurry and particles, plays a major role and can be split in two different behaviors. The first one is the centrifugal movement of the charge and the second is the flow through the discharge grate and pulp lifters.

The resistance to the slurry flow in tumbling mills is mainly caused by the grinding charge. Further resistance is caused by the discharge grate whose performance is function of the open area and the openings position. The discharge rate is directly dependant on the size and number of openings. The larger their number, the lower the hold-up will be. For high load volumes or mill fillings, the discharge rate is less affected by open area. When the empty spaces in the middle of the charge become saturated, a pool of slurry is formed. The grinding media has a major role in the ore hold-up constitution, which places between the intertices and is influenced by mill speed and feed rate (Latchireddi and Morrell, 2003).

In a recent study, Powell (2011) evaluated the performance of a large number of industrial mills and concluded that the pulp flow in AG and SAG mills is not affected by open area of the discharge grate, excluding the pebble ports. Figure IV-7 shows the charge motion profile for a SAG mill based on the work of Powell (2011). In this case, it displays a slurry pool region. The pulp inside the mill fills the charge volume and forms the pool region near the toe region. As most of high-energy impacts occur at this region, the size reduction due to breakage is reduced as the descending particles fall into the pool instead of hitting the charge toe. In the middle of the charge there is a high level of attrition between the material layers that rise into the shoulder. This movement corresponds to the production of fine particles. The makeup of the pool causes the dilution of the pulp that reduces the pulp viscosity and reduces mill efficiency. In addition to this, the pool flow along the mill carries the particles in suspension directly to the discharge. Another effect is mill power reduction: pooling causes the center of mass displacement towards the mill center as it is placed on the opposite side of the charge (Powell and Valery, 2006).

One of the factors that affects the appearance of the slurry pool is the particle size distribution of the charge. The movement of the pulp through the mill may completely change depending on the hold-up particle size. Powell and Valery (2006) say that the reason for this is the residence time of the named sand particles, which are particles within the size range of 1 mm to 10 mm. The authors also report the case of an autogenous mill with 6 meters in diameter, which was operating with a slurry pool. In this case, by increasing the amount of coarser particles in the feed, the mill power reached a peak indicating the disappearance of the slurry pool and the increase in the efficiency.

Morrison and Cleary (2008) claim that a fraction of the comminution energy is spent in the pulp region of tumbling mills. Viscosity effects that are caused by the amount of fine ore particles (below 37 μm) may lock the coarser particles on the pulp surface thus facilitating their selection to breakage.

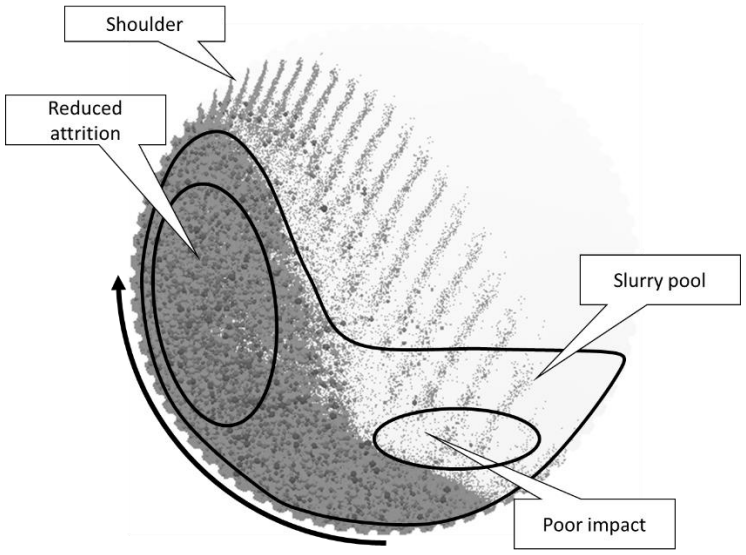

Figure IV-7 Axial scheme of a SAG mill showing some of the regions as defined by Latchireddi and Morrell (2006), including the slurry pool region

In a pilot scale mill equipped with single grate discharge the maximum discharge rate can be twice as high as that observed in mills with discharge grate and pulp lifters for the same pulp hold-up in the mill, as reported by Latchireddi and Morrell (2003). Also, Powell and Valery (2006) report that there is an ineficiency in pulp lifters systems. The pulp lifters are an important component of grate dischage mills which are used in autogenous and semi-autogenous mills, as well as some ball mills. Regarding mill speed, the discharge rate reaches peak performance as mill speed increases, although at over 80% of critical speed, the mills equipped with pulp lifters show a decrease in discharge performance (Latchireddi and Morrell, 2003).

The purpose of pulp lifters is to allow the slurry to be transported through the grate openings to the discharge trunnion. However, the action of pulp lifting causes the so called flow back, which is the return of the pulp to the interior of the mill. Usually, the impact of the flowback in SAG circuits may not be significant. However this phenomenon can be noticed when the mill is operated in closed circuit with hydrocyclones or fine screens, so that a large amount of pulp goes through the mill. Figure IV-8 shows a scheme that represents the different mechanisms that influence slurry transport through AG/SAG mills (Condori and Powell, 2006). In order to evaluate the possibility to increase the performance of pulp lifters Latchireddi and Morrell (2006) have studied the pulp flow in mills equipped with twin-chamber pulp lifters.

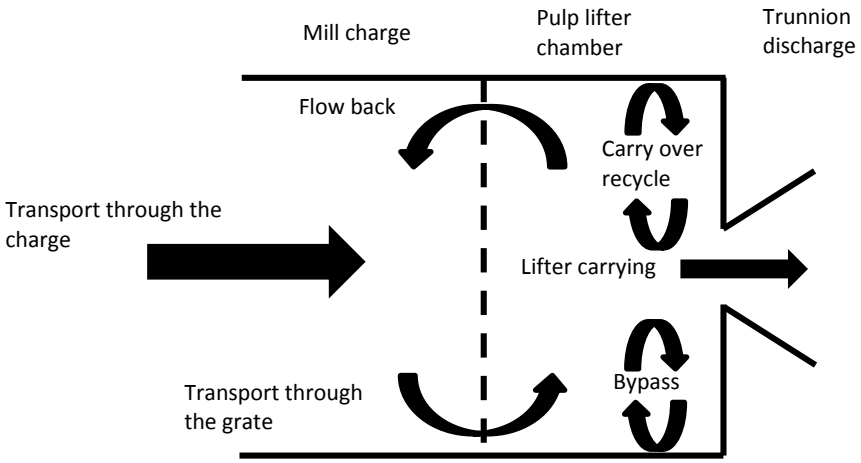

Figure IV-8 Aspects of pulp transport in AG/SAG mills, adapted from (Condori and Powell, 2006)

For autogenous mills equipped only with grate discharge without pulp lifters Latchireddi and Morrell (2003) have observed that the mill hold-up increases directly with feed rate and mill speed. This trend with speed may be related to the reduction in charge porosity. The range of variables studied was from 2 to 12% of open area, from 10 to 40 mm of grate opening and from 40 to 100 mm of pebble ports.

IV.1.2 Power in tumbling mills

A good estimation of the mill power is of great importance on the design of grinding circuits, because mill power is an important design outcome when opting for AG and SAG mills. In the majority of cases, the choice of the circuit or process is directly related to the operational cost.

Many studies have been published that propose methodologies and equations that aim at predicting the power required in AG and SAG mills. For autogenous mills operating in dry mode Macpherson and Turner (1980) proposed a simple equation that is a function of diameter and mill length,

$$P_M = 0.992 L D_m^{2.8} \rho_c \qquad \text{IV-1}$$

where L is mill length and D_m is mill diameter, with both expressed in meters and ρ_c is charge density – ore plus balls and water - in t/m³. The power is then given in kW.

The energy efficiency of the mills will be higher in large diameter mills as stated by Morrison and Morrell (1997). Austin and Concha (1994) have proposed an equation that may be used for both low and high aspect mills. They assumed that mill power is given by the sum of the power required by the cylindrical section and the conical section at the feed and discharge ends. As such, the power consumption of AG and SAG mills could be calculated by

$$P_M = K_P D_m^{2.5} L \varphi_c \left(1 - \frac{0.1}{2^{9-10\varphi_c}}\right) \rho_c J_c (1 - A_P J_c)(1 + F_P) \qquad \text{IV-2}$$

in which A_P and K_P are constants, J_c is the fraction of the cylindrical section of the mill that is filled by the charge and $(1 + F_P)$ is a correction factor for the conical section of the mill.

The value of F_P is given by the expression, which is valid for $J_c < 0.45$,

$$F_P = \frac{0.046}{J_c(1 - A_P J_c)} \left(\frac{\frac{h_1}{L}}{\left(1 - \frac{d_1}{2r_1}\right)} \left[\left(\frac{1.25 \frac{r_1}{D_m}}{0.5 - J_c} \right)^{0,1} - \left(\frac{0.5 - J_c}{1.25 \frac{r_1}{D_m}} \right)^4 \right] + \frac{\frac{h_2}{L}}{\left(1 - \frac{d_2}{2r_2}\right)} \left[\left(\frac{1.25 \frac{r_2}{D_m}}{0.5 - J_c} \right)^{0,1} - \left(\frac{0.5 - J_c}{1.25 \frac{r_2}{D_m}} \right)^4 \right] \right) \qquad \text{IV-3}$$

Figure IV-9 illustrates a scheme of a conical end shaped SAG mill containing the variables used on Equation IV-3. It is recognized that Austin's model is valid for mill fillings from 25% to 30% and can be used confidently once mill dimensions are known.

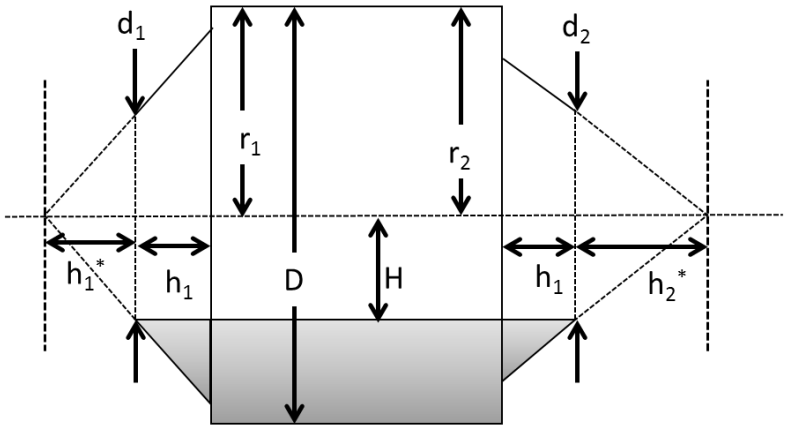

Figure IV-9 Dimensions for a conical end shaped SAG mill (Austin and Concha, 1994)

One alternative to Austin's power model is the one proposed by Morrell (1996). His model uses information from the mass of particles and the amount and slurry inside mills to predict charge volume, density and position. A representative scheme of charge position is shown in Figure IV-10. Morrell assumes that the fraction of the charge composed of slurry occupies the interstices between the grinding media, but this interstitial filling is not homogeneous, being lower close towards the shoulder and extends to the charge toe. This situation occurs in all ball mills equipped with overflow discharge (no grates) and ends up consuming less power when compared to mills equipped with discharge grate. A lower power consumption is also observed in AG/SAG mills that receive high feed rates, resulting in overload of the discharge system (pulp lifters).

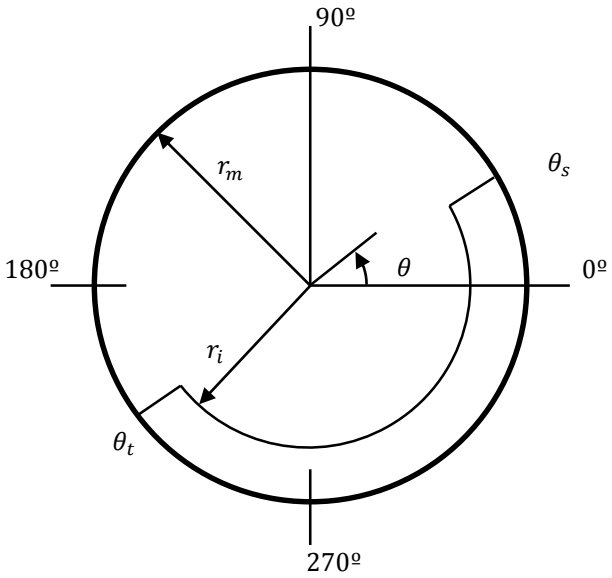

Figure IV-10 Mill charge scheme according to Morrell (1996)

Morrell has proposed an energetic approach, assuming that power is the rate at which the potential and kinetic energy are transferred to the charge. The cylindrical and conical sections are also treated separately, allowing a more accurate prediction of the power given the equations

$$P_{\text{cylinder}} = \int_{r_i}^{r_m} V_r L r g \rho_c (\sin\theta_s - \sin\theta_t) + \rho_p (\sin\theta_s - \sin\theta_{tp}) \mathrm{d}r \qquad \text{IV-4}$$

and,

$$P_{\text{cone}} = \int_{0}^{L_i} \int_{r_i}^{r_{cone}} V_r L r g \rho_c (\sin\theta_s - \sin\theta_t) + \rho_p (\sin\theta_s - \sin\theta_{tp}) \mathrm{d}r \mathrm{d}L_c \qquad \text{IV-5}$$

where L_c is the length of conical sector, L_i is the length of the surface between the cones, L is the length of the cylindrical section of the mill between the liners, P_{cone} and $P_{cylinder}$ are the power required to move the charge (net power), in kW, r is the radial position, r_i is the radial position of the internal surface of the mill, r_m is the radius of the mill between the liners. r_{cone} is the radius of the conical section of a distance L_c from the cylindrical section, V_r is the tangential velocity of a particle in the radial position r, θ_s is the angular displacement of the shoulder position of the charge, θ_t is the displacement of the charge toe position, θ_{tp} is the angular displacement of the slurry toe position, ρ_c is the grinding media charge density (balls and rocks) e ρ_p is the pulp density.

The variation in the angles (θ_t, θ_s) and the tangential speed of particles were empirically modelled from lab scale results. The final form of Morrell's model is

$$P_{\text{NET}} = K D^{2,5} L_{\text{EFF}} \rho_c J_c \left[\frac{5.97\varphi_c - 4.43\varphi_c^2 - 0.985 - J_c}{(5.97\varphi_c - 4.43\varphi_c^2 - 0.985)^2}\right] \varphi_c \times \left[1 - (1 - 0.954 + 0.135 J_c) \mathrm{e}^{-19.12(0.954 - 0.135 J_c - \varphi_c)}\right] \qquad \text{IV-6}$$

in which L_{EFF} is the effective grinding length (EGL).

Morrell also defines the no load power of the mill which has to summed to the net power of the mill to obtain the gross power. The no load power equation is given by

$$P_{\text{NL}} = 1{,}68 D_m^{2,05} [\varphi_c (0{,}667 L_{\text{t}} + L)]^{0,82} \qquad \text{IV-7}$$

Finally, the gross power of the mill is

$$P_{\text{G}} = P_{\text{NL}} + P_{\text{NET}} \qquad \text{IV-8}$$

IV.1.3 AG and SAG circuit layout

In the past, comminution circuits were often composed of primary, secondary and tertiary crushing stages followed by single or double grinding stages of rod and/or ball mills depending on the type of ore processed. However with the use of semi-autogenous grinding, which is a mill that is able to receive coarse feed distribution and generate products that are similar in size as those from ball milling, there was an opportunity to replace crushing and ball mill stages by a single SAG mill. Consequently, flowsheets could now be designed that overcome the complexities of crushing and grinding circuits, even though the SAG circuits are more sensitive to disturbances on the ore properties. Figure IV-11 shows an example of that. The image on top is a traditional circuit (two crushing stages and two stage grinding) while the bottom image a single SAG circuit replaced the crushing stages and the primary grinding (Rosario, 2010).

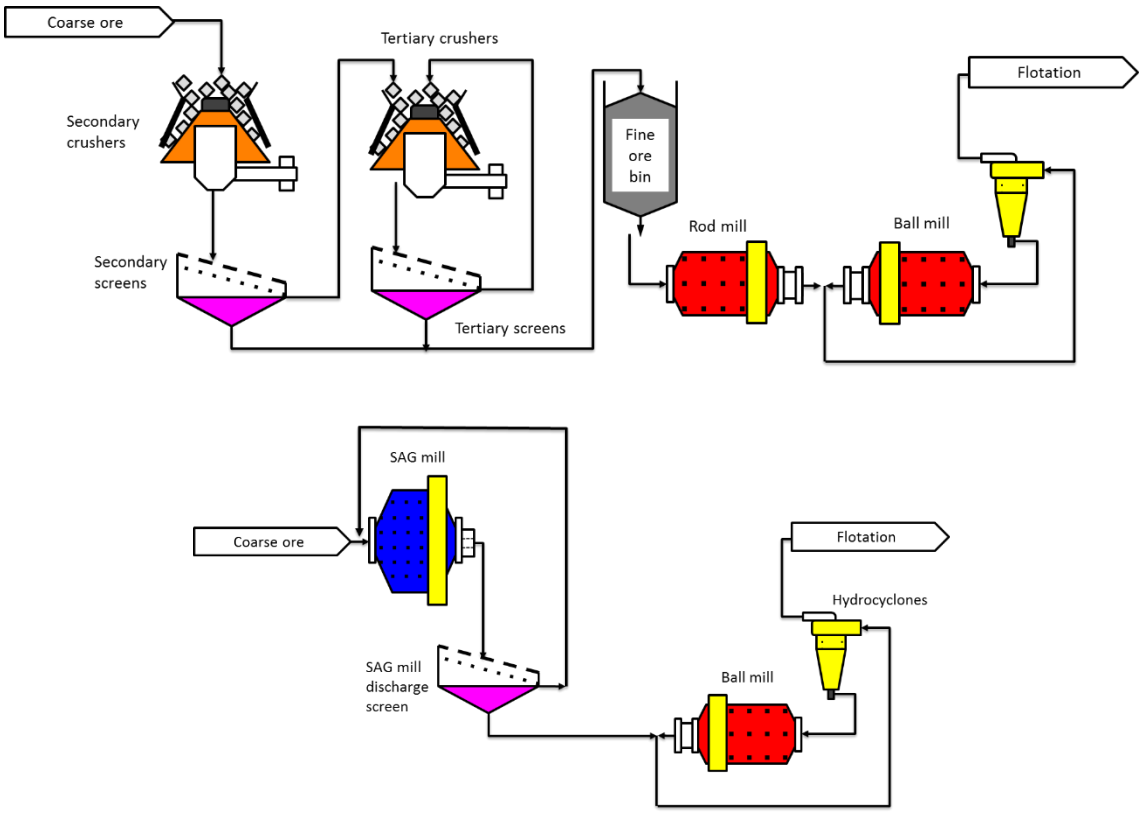

Figure IV-11 Circuit flowsheets showing the replacement of crushing and grinding stages (top) by a single SAG unit (bottom) (Rosario, 2010)

As mentioned at the beginning of this chapter another typical circuit layout is the case when the AG or SAG mill discharge is classified and the recycle stream goes to a

pebble crusher to be fed again to the mill. This layout is called SABC circuit. This becomes necessary when the breakage rates of the critical sized particles are low, which would result in accumulation of material in the mill and its discharge through the pebble ports. These particles are fed to a crusher, usually a cone crusher, with the crusher product returning to the mill. An example of operation with this circuit layout is the Sossego copper ore processing plant in Brazil (Figure IV-6). Due to the high competence of the ore it was required to open the grate to allow the mill to properly discharge the pebbles at the high feed rate required on that circuit (Bergerman *et al.,* 2009).

Another layout possibility is the SABC layout on open mode. In this case there is a bypass on the recycle that allows a fraction of the particles to avoid the pebble crusher stage. This allows the operator to select the best mode of operation depending on the run of mine ore characteristics. In this case, pebble crushing may be active only when needed. Rosario (2010) gives an example of a plant that has this capability and processes a highly variable ore, containing zones of friable ore and other zones with highly competent ore.

A limiting factor in large SAG mills that operate in open circuit is the discharge rate of the pebbles. It is possible to achieve great increases in the feed rate by operating at the highest possible discharge rate of pebbles, but in most of the cases, the open area of these mills does not exceed 10 %.

In the last few years, another layout has been proposed (Rosario, 2010) that includes the high-pressure grinding rolls (HPGR) to crush the pebbles. In this case, as HPGRs reach high reduction ratios, the product of the pebble breakage may not be fed back to the SAG mill, but rather directly to the downstream ball grinding circuit. An example is shown in Figure IV-12. As reported by Sepulveda (2008) the reverse circuit – with previous classification – can be advantageous when the feed contains more than 30 % of fines in the target P_{80} of the circuit.

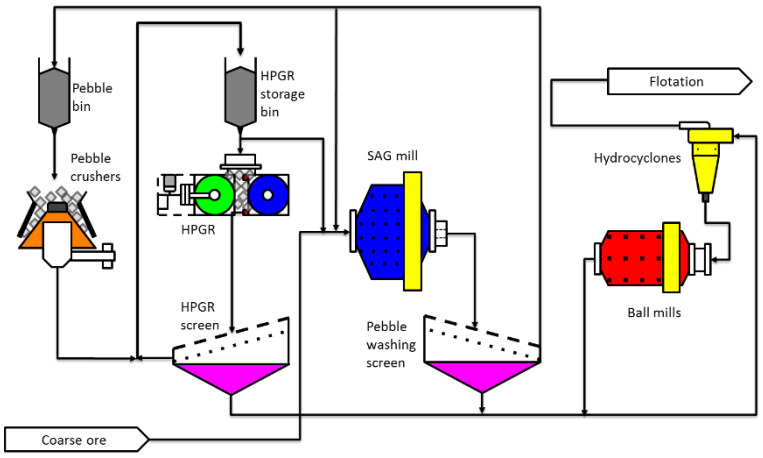

Figure IV-12 SAG circuit example containing pebble crushing in High Pressure Grinding Rolls (Rosario, 2010)

IV.1.4 Grinding dynamics in AG and SAG mills

The SAG mill is generally recognized as a very complex system that shows a number of nonlinear behaviors, with disturbances that include high rates of changes when compared to the response time of the entire plant to the commands or manipulated variables (Amestica *et al.,* 1996). Grinding suffers from the cyclic behavior of the charge, the erratic discharge of the product, the high recirculation rates and the occurrence of non-planned stops (Mishra, 2003).

The evaluation of the performance of a SAG mill in industry can be a very tricky task due to the fact that operators do not want to have their plant disturbed even if it is operating far from the optimum grinding condition. With that in mind Powell and Mainza (2006) have developed a technique to allow the comprehension and the operational mapping of the AG and SAG mills which is the called grindcurves. The authors introduce the concept called mill signature, in which each mill has its own signature as a function of operational conditions, design and ore characteristics. A way to determine this mill signature is by measuring its response to operational changes. The named grindcurve are then generated by combining mill responses to each gradual change in its conditions. In order to evaluate the grinding circuit performance, some comments have to be made regarding the measured variables.

One marker in the product particle size distributions can be used when there is no quick direct access to the complete particle size distribution such as the results obtained with the use of laser size analysis equipment.

A full crash-stop of the pilot or industrial mill is required in order to analyze the slurry charge. Both ore and water feed streams are halted. In ball mills, it is necessary to wait for the slurry solids to settle before measuring the depth of the solids. This measure is related to the ball filling level. The ideal scenario is the one in which the amount of solids is such that it covers the ball level surface. If the solids are only found below the level of the balls, the mill is considered “underloaded” with slurry, with the opposite situation occurring when the ore covers the balls the mill, which is considered overloaded. Also, in AG/SAG mills the slurry level should be right below the level of the charge to maximize fine grinding. However, in this case there is the chance of slurry pool formation which has to be avoided.

The authors say the optimum solids concentration does not depend on other process parameters – except for the case when the mill suffers with discharge limitations. For mills producing the final product of the circuit, as ball mills and single stage SAG, there is a single point of transition in the solids concentration that correlates to the maximum breakage rate. This point is observed evaluating the slurry discharge flow situation, which vary from laminar, of high viscosity to turbulent as function of solids concentration. In mills operating in open circuit configuration, it is easier to reach the maximum capacity by reducing solids concentration than maximizing the breakage rates by changing operating parameters.

Instant samples – the goal is to collect complete information from the process in diverse operational conditions. This allows identification of the throughput, power and product size peaks. The single point size analysis technique is used to check the stability of the product and then the sampling of the important streams is done.

Powell and Mainza (2006) provide evidence for the difficulties in establishing standards for tests in SAG mills. They comment that in many cases these mills are operating more on standard conditions (filling, speed, solids concentration) than in design criteria. Still, there is a trend of keeping the operation based on historical data and neglect continuum changes in the process, such as, changes in ore type, ball charge, liner profile and others. Therefore, many circuits are operating outside their optimal conditions.

The construction of the grind curve may be tricky, as the increase in the feed rate to the circuit may produce pseudo-steady and unstable states. It is known that in order to reach new steady-state conditions, it is required to make only small and constant increases in the feed rate. Figure IV-13 shows examples of grind curves generated for two SAG mills. On the abscissa there is the mill filling, the left ordinate shows the power consumption in kW and the right ordinate shows the throughput in tons per hour and the hold-up mass of the mill. The authors have been successfully using the grindcurve technique and they recommend that no evaluation of mill performance should be made without the generation of the grindcurve for the range of the operation conditions of the circuit.

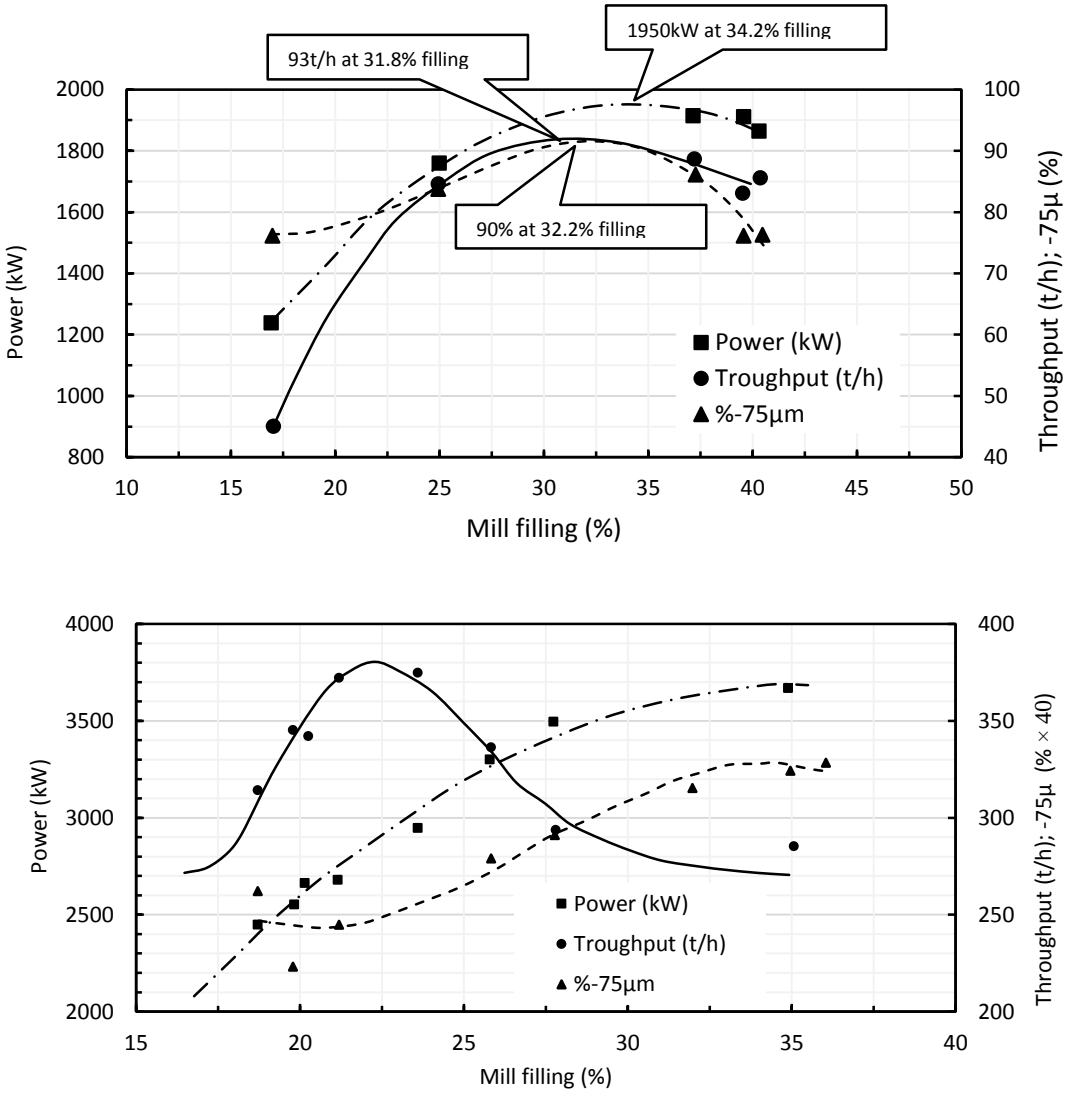

Figure IV-13 Examples of grindcurves for two SAG mills (Powell and Mainza, 2006)

IV.2 Traditional modelling approach

Over the years, many mathematical approaches have been proposed to describe the grinding process that occurs in AG and SAG mills. Among the main models, the works of Austin (Austin *et al.,* 1986) and the model of Leung (Leung *et al.,* 1987) deserve greater attention. Both have been the basis for a great number of more recent models proposed by King (2001), Morrell *et al.,* (1996), Delboni Jr. and Morrell (1996) and Amestica *et al.* (1996). The sections that follow describe these approaches in some detail.

IV.2.1 Austin's model

Austin's modelling approach (Austin *et al.,* 1987 e Austin *et al.,* 1986) follow the phenomenological way of steady state comminution modelling. In the 1980s his research group conducted extensive experimental work to understand the breakage mechanisms on autogenous and semi-autogenous mills. Alongside that was the modelling of ball mills, in which it was recognized that the traditional population balance approach was unable to describe the breakage rates of coarser particles in these mills.

His model is based on the assumption of first order breakage rates also used in modeling ball mills, with the additional mathematical description of the self-breakage and superficial breakage. The general equation can be described as

$$Fp_i = Ff_i + W\sum_{j=1}^{i-1} b_{i,j}s_j w_j - Ws_i w_i \qquad \text{IV-9}$$

which can also be rearranged as

$$p_i = f_i + \tau\sum_{\substack{j=1 \\ i>1}}^{i-1} b_{i,j}s_j w_j - \tau s_i w_i \qquad \text{IV-10}$$

where p_i is the fraction of the product in size class i, f_i is fraction of the feed in size class i, s_i is the specific breakage rate of the ore in size class i, $b_{i,j}$ is the fraction of broken material from size class j that appears in size class i, w_i is the fraction of the *hold-up* in

size class i and τ is the average residence time. F represents the mass flowrates of both feed and product and M is the ore hold-up in the mill.

The mill modeled as a perfect mixing grinding region coupled with an internal classification stage is shown on Figure IV-14. The classification effect caused by the discharge grate is modelled by the insertion of an internal recycle effect, described by the circulation ratio C'. This way, as $F' = (1 + C')F$, the apparent feed of the mill is,

$$(1 + C')Ff_i' = Ff_i + F(1 + C')w_i c_i \qquad \text{IV-11}$$

where c_i is the fraction of material of size class i that returns to the mill. The circulation ratio C' is given by

$$C' = \frac{\sum_i F(1 + C')w_i c_i}{\sum_i F(1 + C')w_i(1 - c_i)} = \frac{\sum_i w_i c_i}{\sum_i w_i(1 - c_i)} \qquad \text{IV-12}$$

or,

$$1 + C' = \frac{1}{\sum_i w_i(1 - c_i)} \qquad \text{IV-13}$$

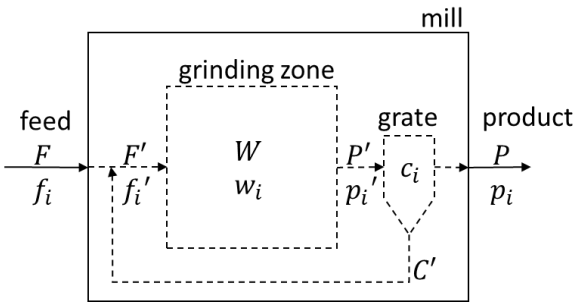

Figure IV-14 Illustration of the mill model with internal classification (Austin and Concha, 1994)

The final version of the mill with internal classification is obtained by replacing Equation IV-14 into Equation IV-10 and assuming $w_i = p_i'$,

$$w_i = \frac{f_i + \tau \sum_{j=1}^{i-1} b_{i,j} s_j w_j}{\tau s_i + (1 + C')(1 - c_i)} \qquad \text{IV-14}$$

According to Austin *et al.* (1987), the hold-up of particles smaller than the mill grate opening depends on the flow properties of the slurry through the mill. As such, in order to make the model properly account for this effect, the discharge or particle retention should be described. Based on this observation, Austin proposed an empirical relationship for the transport given by,

$$\frac{f_s}{f_{so}} = \left(\frac{F_v}{F_{vo}}\right)^{N_m} \qquad \text{IV-15}$$

where f_s is the fraction of mill filling that is filled by fines (particles smaller than the grate opening). F_v is the volumetric flow and N_m is a empirical factor. The holdup of fines may be defined as

$$f_s = \left(\frac{W}{\rho_s V_m C_s}\right)\sum_{n}^{i_g} w_k \qquad \text{IV-16}$$

in which C_s is the volumetric fraction of solids in slurry, V_m is the internal volume of the mill, n is the index of sink class, ρ_s is the specific gravity of the solid and i_g is the size class related to the grate opening. The value of F_{vo} refers to a standard flow that is equivalent to a standard fines filling. Based on pilot plant data, Austin *et al.* (1987) have proposed an empirical relationship that correlates F_{vo} to mill dimensions,

$$F_{vo} = k_m \varphi_c A_g D_m^{3,5} \frac{L}{D_m} \qquad \text{IV-17}$$

in which φ_c is the fraction of the critical speed of the mill and A_g is the fraction of open area of the discharge rate. Equations IV-14, IV-15 and IV-16 should be solved simultaneously to obtain,

$$\tau = \left(\frac{W}{F_{vo}\rho_s C_s}\right)\left(\frac{f_{so} C_s \rho_s V_m}{W \sum_{k=n}^{i_g} w_k}\right)^{1/N_m} \qquad \text{IV-18}$$

Given the values of s_i there is a single value of τ that satisfies Equations IV-14 and IV-18.

Austin's model depends on the knowledge of transport parameters (F_{vo} and f_{so}) from pilot or industrial scale mills to calibrate the value of N_m parameter. This

dependence on real data is common to the group of phenomenological models and also appears on Leung's approach.

Probably the major contribution of Austin's model is the addition of sub models to describe particle breakage due to the mechanisms of abrasion and self-breakage. He considers the mass lost by abrasion as obeying a constant rate and the rate of abrasion may vary with particle size. Austin proposed that breakage either resulted from fracture, self-breakage due to autogenous impacts or by impacts from grinding media. All these composed a single selection function and an average breakage function.

In AG and SAG mills, particles situated in the critical range have lower breakage rates and tend to accumulate in the mill. The selection function model is composed of the sum of a few functions, each of them representing a breakage phenomenon that occurs in these mills, as illustrated in Figure IV-15. Region 1 shows the increase on the breakage rate with the increase in particle size. This happens because the coarser particles are more amenable to being captured by the grinding media. As the particle size increases, there is a maximum breakage rate and from this point on breakage rates decrease. Austin and Concha (1994) associate this effect to the lower probability of the coarser particles receiving effective impacts. The breakage rate of this region is considered non-first order because the breakage is a mix of shattering due to high energy impacts and chipping due to the low energy impacts. In section 3, the breakage rate begins to rise again due to the self-breakage of the coarse particles and their collisions against the balls.

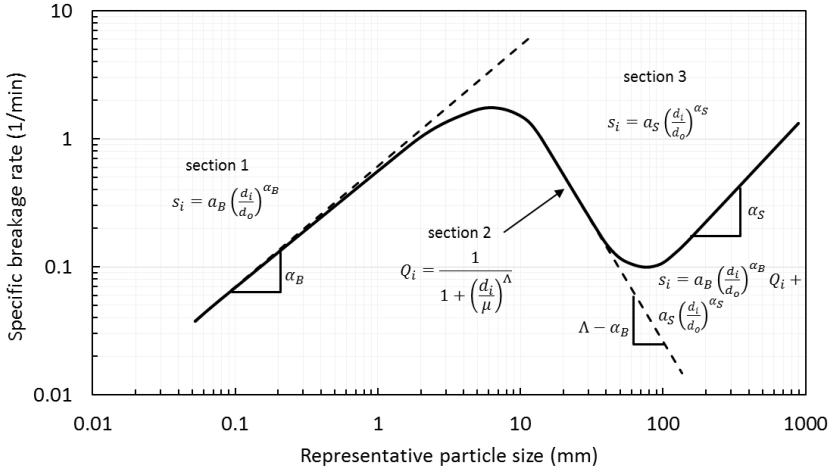

Figure IV-15 Selection function of a semi-autogenous mill and Austin's model equations (Austin *et al.*, 1987)

Austin defines the breakage rate in the self-breakage zone as the sum of the selection function of each phenomena resulting in: $s_i = s(B)_i + s(P)_i + s(S)_i$, in which $s(P)_i$ is the specific breakage rate from the collisions of the balls against the pebbles and $s(S)_i$ is the specific rate of self breakage of the pebbles. The breakage rates of particles in section 1 of Figure IV-15 may be calculated from batch grinding results which gives input to a set of scale-up equations as function of operational and design parameters.

King (King, 2001) has proposed an alternative approach for the calculation of the breakage rates while kept the other sub models the same as in Austin's model. King says that particles with size below 10 millimeters have a very low breakage probability by self-breakage mechanism so their contribution to the specific breakage rate of the material in a SAG mill can be neglected. As such, King proposed a new equation for the estimation of the selection function of ores in SAG mills given by

$$s(d) = \frac{s_1 d^{\alpha}}{1 + \left(\frac{d}{\mu}\right)^{\Lambda}} + f \times \mathrm{G}\left[\frac{\ln\left(\frac{E}{E_{50}}\right)}{\sigma_E}\right] \qquad \text{IV-19}$$

The conceptual model proposed by King was the first model to include the concept of particle fracture energy distribution and breakage probability. The expression $G\ [\ln (E/E_{50})/\sigma_E\ ]$ refers to the breakage probability of particles within a size class which their fracture energy distribution follow the lognormal distribution of median E_{50} and standard deviation of σ_E when they are submitted to collision energy E. The collision energy is estimated – for the particles that suffers self-breakage – by the equation,

$$E = f_{drops}\, g D_m \qquad \text{IV-20}$$

and assuming that each coarse particle suffers only one drop per mill revolution, the frequency of drops (f_{drops}) is described by,

$$f_{drops} = \frac{0.705\varphi_c}{\sqrt{D_m}} \qquad \text{IV-21}$$

in which g is the acceleration due to gravity and D_m is the mill diameter. This model, however, has not yet been validated for industrial mills.

IV.2.2 Leung's model

Leung's model (Leung *et al.,* 1987) correlated particle breakage inside the mill with the average energy applied to the particles using information from individual particle breakage obtained in the laboratory. The model also requires mass transport equations through the mill. Although it is not used extensively today, it is the basis to models that are currently used which take advantage of Leung's model robustness. Based on the perfect mixing model in a similar way that Austin considered (Equation IV-10), it is possible to write the mass balance equation per size classes as,

$$0 = Ff_i - Fp_i + M\sum_{j=1}^{i} s_j w_j b_{ij} - Ms_i w_i \qquad \text{IV-22}$$

where,

$$Fp_i = d_{r_i} Ms_i \qquad \text{IV-23}$$

and Ff_i is the feed mass flow of particles in size class i, Fp_i is the product mass flow of particles in size class i, s_i is the breakage rate of particles in size class i, Mw_i is the mass of particles in size class i in the mill hold-up, d_{r_i} is the discharge rate of particles in size class i and b_{ij} is the breakage distribution function or appearance function. Equation IV-22 represents the mass balance in each size class i.

Leung´s model describes particle breakage as result of the action of two mechanisms. The first is the breakage due to high energy impacts while the second is the abrasion generated by low energy impacts. The energy transferred by the autogenous grinding media is considered to be an average value which is function of mill diameter. It considers the average size of the top 20% of the charge that corresponds to,

$$S_{20} = (P_{100} * P_{98} * P_{96} \dots P_{80})^{\frac{1}{11}} \qquad \text{IV-24}$$

where $P_{100}, P_{98}, \dots, P_{80}$ are the particle sizes corresponding to the equivalent cumulative percentages 100, 98, etc., and the potential energy in J at the maximum height inside the mill is,

$$E_1 = \frac{4}{3}\pi(S_{20})^3 \rho g D_m \qquad \text{IV-25}$$

where ρ is the ore density in kg/m³, g is gravity acceleration in m/s² and D_m is the mill diameter in meters.

In the case of SAG mills, Equation IV-24 should also take into account the presence of balls. This is made by converting the ball size distribution into an equivalent mass of pebbles. The result is then integrated into the charge size distribution and finally the parameter S_{20} is calculated from this corrected distribution. To describe the energy level associated to finer particles, Leung used an hypothesis from Austin and Concha (1994), which assumes the energy applied to a particle of size d (specific comminution energy– E_{cs}) follows the proportionality relation,

$$E_{\mathrm{cs}}(x) \propto \frac{1}{d^{1,5}} \qquad \text{IV-26}$$

Leung's model uses an empirical model to calculate the breakage due to low energy impacts. The results come from laboratory scale tumbling tests as presented in section III.3.2. The appearance function generated from the tumbling tests is then combined with the appearance function from impact tests resulting in

$$b = \frac{t_{LE} b_{LE} + t_{HE} b_{HE}}{t_{LE} + t_{HE}} \qquad \text{IV-27}$$

in which b_{LE} and b_{HE} are the appearance functions from low and high energy impacts while t_{LE} and t_{HE} are the t_n values from low and high energy impacts. Leung's model is completed with empirical relationships for the mass transport and the internal classification due to discharge grate. The model is schematically represented in Figure IV-16.

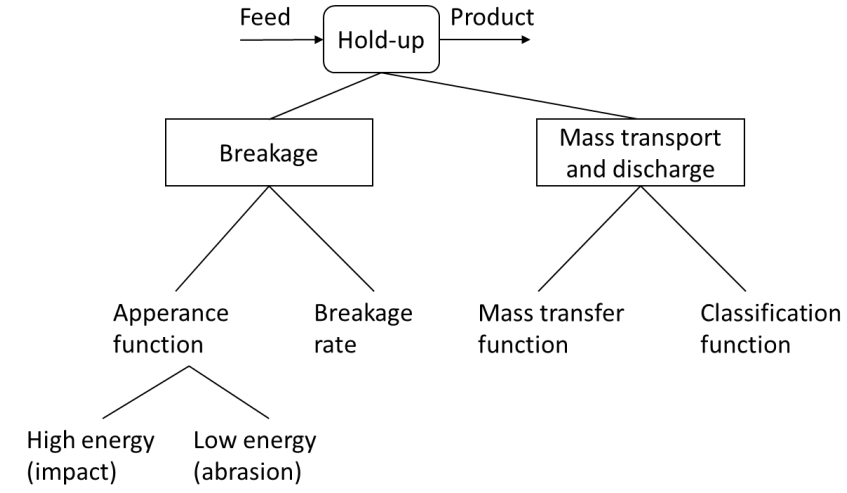

Figure IV-16 Leung's model structure (Leung *et al.,* 1987)

The breakage rate model uses a spline interpolation of five knots defined at specific particle sizes. The standard knots are presented on Figure IV-17.

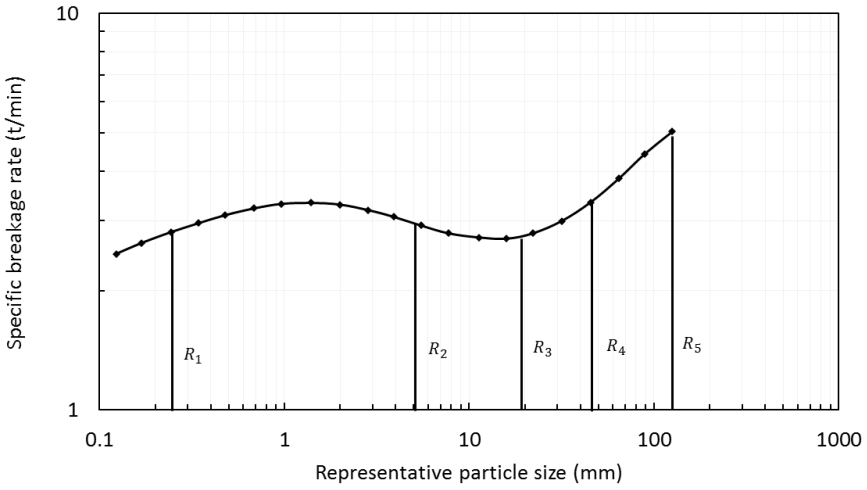

Figure IV-17 Breakage rates calculated from Leung's model (Leung *et al.,*1987) and the particle size equivalent to the cubic spline knots

The model in its original form does not predict the effect of variables such as the mill speed on the ore breakage rate. The influence of mill diameter appears on the calculation of the average input energy applied on coarse particles in the charge as reported in Equation IV-25. The internal classification by the discharge grate was modelled using a simple classification function D_r given by

$$D_r = 1 \qquad d < d_m$$
$$D_r = \frac{\ln(d) - \ln(d_g)}{\ln(d_m) - \ln(d_g)} \qquad d_g > d > d_m \qquad \text{IV-28}$$

where d is the particle size that will always pass through the grate, that is, the size of particle below which will all be carried by the slurry and have fluid-like behavior, and d_g is the grate opening which defines the maximum size of a particle that can be discharged through the grate. The definition of the discharge rate comes from the rearrangement of Equation IV-23 to explicit the discharge function dr_i which can be calculated from

$$dr_i = d_m D_r \qquad \text{IV-29}$$

in which d_m is the fraction of the charge that reaches the grate per unit of time and D_r is the classification function given by Equation IV-28. Figure IV-18 presents the graphical representation of the classification function based on pilot scale SAG mill data, with the dashed lines representing the sizes d_g and d_m.

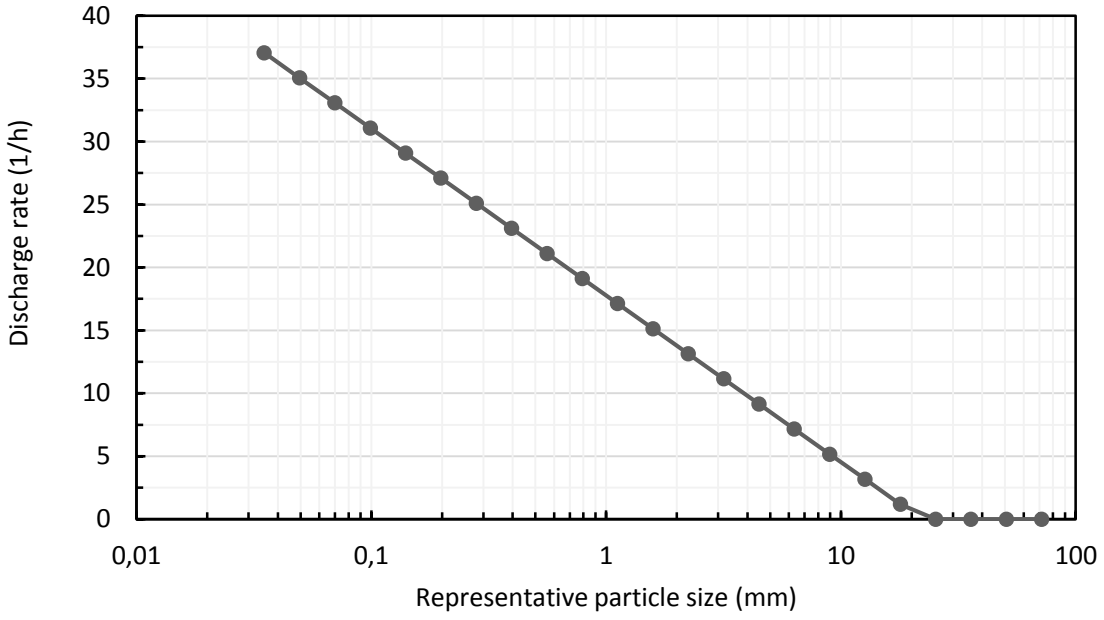

Figure IV-18 Discharge rate calculated from pilot scale SAG mill data

The mass transport equation follows Austin's approach considering the amount of particles in the charge that are smaller than the grate opening is directly proportional to a power relation of the feed rate. Leung suggests values for the correlation resulting in,

$$f_s = 0{,}37F_v^{0,37} \qquad \text{IV-30}$$

The use of this model is limited to mill with to 9 meters of diameter and required breakage rates previously calibrated from pilot scale mill (up to 2 meter in diameter) data. The weakness of this model is the lack of sensitivity to operational conditions such as solids concentration, grate open area, liner design, mill speed and rheology properties of the slurry (JKSimMet, 2003).

To overcome the weakness of Leung's model, Morrel *et al.* (1996) have focused on the modelling of mills larger than 9 meters in diameter. The use of such large diameter mills was a trend at that time in Australia. The authors reported that several surveys were conducted in a number of circuits operating over a range of conditions. Their work focused on correlating the database of pilot plant data to large-scale mills. They used the traditional Leung's model as a basis but proposed small modifications to it. For the coarse size range, the authors defend that impact breakage and abrasion are the major mechanisms due to cataracting motion of the charge. In other words, high breakage rates for the coarse particles translates into higher throughput. Moreover, for low rotation speeds, abrasion breakage would dominate breakage. The ball size directly affects the breakage of the coarse particles and the coarser the balls the smaller the frequency of the impacts, which result in the appearance of a valley region in the selection function to be more steep than when using balls of smaller sizes. In summary Morrell´s updated model (Morrell, 2004) uses different equations to estimate the mass flow and slurry discharge. The model was validated using data from twenty-one industrial circuits containing AG or SAG mills.

Equation IV-31 describes how the discharge rate changes as a function of particle sizes. The slurry transport outside of the mill can be described using the discharge equation, rearranging and making dr_i explicit. Usually one assumes that particles below a size d_m are carried over by the water directly to the discharge grate. From the value of d_m the discharge rate decreases until the maximum particle size that can be discharged, which is equivalent to the pebble ports opening.

$$d_m = \frac{\sum_m Fp_i}{\sum_m Ms_i} \qquad \text{IV-31}$$

in which the sums of the numerator and denominator are the slurry discharge and hold-up respectively.

To estimate the value of d_m, Morrell suggests an empirical model, which was later modified by Latchireddi and Morrell (2003) to also consider the effect of discharge grate and pulp lifter design. The result is the general equation

$$J_s = \eta \gamma_r^{n_1} A_g^{n_2} {J_t}^{n_3} {\varphi_c}^{n_4} Q^{n_5} D^{n_6} \quad \text{IV-32}$$

in which J_s is the fractional hold-up inside the mill, A_g is the fraction of open area, J_c is the fractional volume of grinding media (including autogenous grinding media) and φ_c is the fraction of critical speed. Q is the slurry discharge flow rate, γ_r is the mean radial position of the grate openings, η is a resistance coefficient that varies depending on the type of slurry flow (through the mill or through the slurry pool) and n_1 to n_6 are model parameters. The value of γ_r can be calculated by,

$$\gamma = \frac{\sum r_{lr} a_{lr}}{r_m \sum a_{lr}} \quad \text{IV-33}$$

where a_{lr} is the total open area per radial position, lr and r_m is the internal radius of the mill. The model parameters n_1 to n_6 are functions of the pulp lifters and according to Latchireddi and Morrell (2003), can be modelled by,

$$n_n = n_g - k_n^1 \exp\left(-k_j^2 \lambda_r\right) \quad \text{IV-34}$$

where n_g is a parameter for the grate discharge condition, k_n^1 and k_j^2 are constants and λ_r is the depth of the pulp lifters expressed as a fraction of diameter. For an industrial scale mill the discharge flow can be estimated by combining Equations IV-31 and IV-32 in

$$d_m = \frac{Q}{J_s} \quad \text{IV-35}$$

So the Equation IV-32 is used to first predict J_s for a given flow rate Q. These two parameters are then used on Equation IV-35 to predict d_m.

The requirement of having pilot scale data in order to use the SAG model lead the authors to look for a way to somehow predict the breakage rates as function of the operation parameters. The authors have then established an empirical equation for the calculation of the breakage rates at the standard knots of the spline function. The knots of the cubic spline can be estimated according to the equation

$$\mathrm{Ln}(R_i) = k_{i1} + k_{i2} J_b \bar{d}_b + k_{i3} \omega_m + k_{i4}(J_c) \qquad \text{IV-36}$$

where R_i are the knots of the breakage rate function and $i = 1..5$. J_b is the ball filling, J_c is the total mill filling, $\bar{d}_b$ is the average ball size, ω_m is the mill speed and $k_{i1..i4}$ are constants for the breakage rate. Due to the access to a very large industrial data base, it was possible to back calculate the values of the constants $k_{i1..i4}$ and, with that, Morrell (2004) successfully predicted the performance of 21 mills (19 industrial scale) regarding the effects of changes in ball charge, ball sizes, total hold-up and mill speed. However, the values of the optimum parameters are not open to public access.

One weakness of Morrell's approach is the definition of the energetic level to be applied to the particles, as it uses the same of Leung's assumptions. His simplified approach makes that part of the breakage effect to be transferred to the fitting parameters from pilot and industrial scale mills. In practice, this makes the dependence on real world plant data even higher in order to properly use his model to predict industrial performance.

The model developed by Delboni Jr. and Morrell (1996) aimed to overcome the limitation on the energy input calculation on Leung's model by correlating the breakage rate and the energy input to the charge movement, in terms of charge composition: ore particles, balls, water and size distribution. It was meant to result in a model that would not require parameter fitting. According to the authors, the breakage frequency could even be back-calculated from particle size distribution online, being then independent of operational conditions.

The mathematical model used to predict charge movement was based on previous work by Morrell (Morrell,1996), which was originally developed for power prediction. The model assumes that mill charge is composed of concentric layers and the slip of these layers cause the shear effect that is responsible for the attrition mechanisms of the particles, while breakage by impact occurs due to the fall of the particles and grinding media in charge toe. Delboni's model deals with the grinding charge as contactors and they are responsible for the energy applied towards breakage on each mechanism. The model calculates the frequency of breakage events from mill charge rotation and sliding rates in the mill. Delboni Jr and Morrell (2002) correlated the frequency of breakage events to the surface area of the grinding media. The model is solved iteratively, considering pseudo-steady-states of the charge. The energy regime is recalculated after

each iteration, as it is sensitive to the changes in the mill hold-up. The impact frequency model proposed is,

$$r_i^{imp} = \Gamma^{imp} P_i^{imp} K_i^{imp} \qquad \text{IV-37}$$

where r_i^{imp} is the frequency of breakage impacts of particles in size i, Γ^{imp} is the specific rate of impact generation, P^{imp} is the term of impact split and K_i^{imp} is a model calibration constant.

The total number of impacts was derived from Morrell's model, and it deals with the particle size distribution which are part of the grinding charge. The specific rate of impact generation is defined as the mean frequencies in which the grinding media particles reach the toe region of the mill. The expression that allows this estimation is given by

$$\Gamma^{imp} = \frac{\sum_i^{n_c} N_s^{imp}}{\left[\frac{\sum_i^{m_g}\left(s_i^p + s_i^b\right)}{\frac{C_g^3 \pi}{6}}\right]} \qquad \text{IV-38}$$

where N_s^{imp} is the number of collisions per unit of time in the concentric s, n_C is the number of concentric shells, s_i^p is the volume of all particles contained in size class i, s_i^b is the volume of all steel balls in size class i, m_g is the size fraction of the smallest particle considered as grinding media and C_g is the characteristic size of the grinding media.

V. Discrete element method

The evolution of phenomenological models has reached the point whereby more detailed information with respect to descriptions of the energy transfer regime to the ore particles inside tumbling mills was required in order to gain deeper insights into the performance of mills and also to improve the predictability of models. In fact, it is important that the characterization of the breakage environment be made with the greatest fidelity to reality, not only in terms of particle movement but also energetically.

This chapter gives an overview of the discrete element method, describing the different applications to tumbling mill simulation and briefly presenting alternative techniques to DEM.

V.1 Overview

The year 1979 represented the first application of a mathematical model that was capable of describing the movement of particulate material. Developed by Cundall and Strack (1979), the model originally aimed at describing the motion of soil particles in geomechanics. The first application of the so-called Discrete Element Method in the minerals industry happened a few years later when it was used in the simulation of grinding media motion in ball mills (Mishra and Rajamani, 1992).

In the past, the only way to estimate the energy transfer regime inside a tumbling mill was through the description of the force balance between the particles and the mill liners. However, this method could associate only the possible maximum energy that particles could reach when falling as function of their masses, mill filling and speed. An example of that is the model proposed by Powell and Nurick (1996). In fact, these researchers have demonstrated that classic applications of modeling erroneously assumed that only one major collision per mill revolution took place.

The capability to simulate complex physical systems that exist in comminution machines has been increasing with the evolution of DEM techniques and the computational power (Weerasekara and Powell, 2010).

Modeling the elastic properties of granular material has been the aim of study since the pioneering work of Mindlin in the 1950s (Mindlin, 1949). Since then, many authors have implemented in three dimensions DEM simulation of the grinding media in rotating

drums. The most common approach considers the solid particles to be able to overlap and collision forces resulting from the relative normal and tangential velocities. Usually, in the mill simulation the linear spring-dashpot model is chosen to describe particle collision dynamics. Recently, the rapid advance in computational power has made it possible to make use of a more accurate contact model, which is the Hertz-Mindlin model that is available in commercial software such as EDEM® (Dem Solutions Ltd., 2010).

The model is based on Hertz contact theory and utilizes the linear elasticity model of continuum environment to calculate the normal force of two perfectly elastic spheres in contact, neglecting attraction effects. Hertz has showed that two spherical particles of radius r_1 and r_2 in contact interact with applied normal force given by,

$$F_n = f_n^r + f_n^d = -k_r \left\| \delta_n^{1/2} \right\| \delta_n - \left(k_d \left\| \delta_n^{1/4} \right\| \right) \dot{\delta}_n \qquad \text{V-1}$$

The stiffness constant k_r is given by,

$$k_r = \frac{4}{3} Y^* \sqrt{R^*} \qquad \text{V-2}$$

and the restitution constant,

$$k_d = c_n \left(6 m_i Y^* \sqrt{R} \right)^{\frac{1}{2}} \qquad \text{V-3}$$

In these equations, c_n is the normal restitution coefficient and Y^* depends on Young's modulus Y

$$Y^* = \frac{Y}{2(1 - \upsilon^2)} \qquad \text{V-4}$$

on Poisson´s ratio υ, and the effective radius R is,

$$\frac{1}{R} = \frac{1}{r_{d1}} + \frac{1}{r_{d2}} \qquad \text{V-5}$$

The normal deformation rate, defined by $\dot{\delta}_n = \left(\mathrm{v}_{ij} \cdot \mathrm{n}_i \right) \mathrm{n}_i$, is function of relative velocity v_{ij} at the contact point,

$$\mathrm{v}_{ij} = \left(\mathrm{v}_j - \mathrm{v}_i\right) + \left[\omega_j \left\| r_{dj} \right\| \mathrm{n}_j - \omega_j \| r_{di} \| \mathrm{n}_i\right] \quad \text{V-6}$$

where n_i is the unitary vector that has its origin from particle center i respectively in direction to the contact point with the other particle involved in the contact (particle i) and vice versa. In the case of spheres submitted to an angular load, the tangential contact force is calculated by Mindlin's model (1949). As in the case of normal force, the tangential force applied to the particle t is the sum of the repulsion and damping terms, as

$$F_t = f_t^r + f_t^d \quad \text{V-7}$$

The repulsive force is calculated by,

$$f_t^r = \mu_s \| f_n^r \| \left[1 - \left(1 - \frac{\left\| \delta_t \right\|}{\chi}\right)^{\frac{3}{2}}\right] \left(\frac{\delta_t}{\left\| \delta_t \right\|}\right) \quad \text{V-8}$$

where μ_s is coefficient of static friction and,

$$\chi = \mu_s \frac{2 - v}{(2 - 2v)\left\| \delta_n \right\|} \quad \text{V-9}$$

is the maximum tangential deformation before slip occurs. In order to satisfy Coulomb friction law, this force is limited to $\mu_s f_n^r$, which results in the relation, $0 \leq \left\| \delta_t \right\| \leq \chi$

The restitution force is proportional to the tangential deformation rate at the contact point, $\dot{\delta}_t$,

$$f_t^d = -c_t \left(6 m_i \mu_s \| f_n^r \| \frac{\sqrt{1 - \frac{\|\delta_t\|}{\chi}}}{\chi}\right)^{\frac{1}{2}} \dot{\delta}_t \quad \text{V-10}$$

where c_t is the tangential restitution coefficient and the tangential deformation rate is,

$$\dot{\delta}_t = \mathrm{v}_{ij} - \left(\mathrm{v}_{ij} \cdot \mathrm{n}_i\right)\mathrm{n}_i \quad \text{V-11}$$

The acting torque on particle i when it collides against a particle j, may be modeled by the product of the force acting on the particle and its radius. According to Zhou *et al.* (1999), the resulting torque can be defined as the rolling friction torque, given by:

$$T_i = -\mu_r \| f_n^r \| \frac{\omega_i}{\|\omega_i\|} \qquad \text{V-12}$$

where μ_r is the rolling friction coefficient.

The contact force model requires the information from both particle restitution and friction coefficient. These parameters are particle material dependent and measuring or determining their values may be a difficult task. This limitation comes from the natural variability on physical properties of the material that constitute the simulated particles, which in case of mills may be the grinding media and the liners.

The calculation algorithm of the DEM is simple and can be described in three main stages:

- A search mesh is used to periodically build a list of interactions regarding the particle neighborhood. The limit-objects appear as virtual particles. Using only particle pairs near the neighborhoods list, reduces the calculation of the force to a single operation $\aleph(N_t)$, being N_t the total number of particles.
- The collision forces on each of the particles and limit-objects are evaluated by the use of the neighborhoods list and the contact model. The result then becomes the new reference state for the next iteration.
- All forces on each of the objects and particles are summed and the following equations of motion are integrated:

$$m_i \frac{\mathrm{d}v_i}{\mathrm{d}t} = \sum (F_{n_i} + F_{t_i}) + g \qquad \text{V-13}$$

$$I_i \frac{\mathrm{d}\omega_i}{\mathrm{d}t} = \sum T_i \qquad \text{V-14}$$

In these equations m_i and I_i refers the mass and inertia momentum of a particle i and $\mathrm{v}_i = (v_{i,x}, v_{i,y}, v_{i,z})$ and $\omega_i = (\omega_{i,x}, \omega_{i,y}, \omega_{i,z})$ are their linear and angular velocities.

In the case of solids particle simulation in DEM the gravitational force must by summed to the total contact forces that act on the particles.

On the other hand, in the case of breakage prediction, DEM shows disadvantages that limit its application as a complete tool to predict comminution processes. Apart from demanding a high computational power to the calculation, the parameters used in the model require calibration as in the case of restitution and friction coefficients (Powell and Morrison, 2007). The calibration of these parameters has to be carried out empirically. As such it may present a challenge and exert great influence on the final result on the application of the tool. The proper calibration of the contact parameters in DEM is of vital importance when utilizing the method as a quantitative tool to characterize the mechanical environment inside comminution machines. For mill simulations Cleary says that an average particle overlap of 0.1 and 0.5% are expected, and require spring stiffness of the order of 10^7 N/m in 2-D simulations and 10^6 N/m in three dimensional simulations (Cleary, 2001).

One application of the DEM as an investigation tool is the study by Khanal *et al*. (2007), who investigated the behavior of the particles when stressed in a bed. They defined the bed breakage as being the breakage of a number of particles in a single time instant, and done usually by compressive loads such as the ones found on HPGR and crushers. They observed that particles positioned close to the walls break differently than those located closer to the center of the bed and that the increase in bed height reduces the energy absorption because a fraction of the applied energy will be used in particle repositioning and material blocks move out of the stress zone. The authors have modeled particles as a cluster of particles bonded with a cohesion force. The simulations were carried out in 2-D environment using PFC2D (Itasca Consulting Group Inc., 1999).

DEM can be coupled to other simulation techniques; one such example is the work carried out by Bagherzadeh *et al.* (2011). In their work they have simulated particle breakage by a combination of DEM to build a particle composed by solid sub particles, with finite element method (FEM) to describe crack propagation on the mother particle. Their aim was the prediction of particle behavior on rock dams, that is, the type of dams built from rock fragments. In the simulations, DEM provides contact information among all system particles, obtaining data such as stresses and loading conditions. This information was used to feed the FEM simulation that analyses each particle individually and determines if breakage will occur. In case of breakage, the crack will propagate in a straight line, generating two daughter particles. These particles would replace the mother

particle in DEM for the next iteration. They have carried out simulations in two dimensions and nothing was mentioned about the effect of repeated stressing events.

In mill simulations, the work published by Cleary *et al.* (2006) stands out. They used smoothed particles hydrodynamics (SPH) coupled with DEM to simulate the motion and discharge of the slurry in a pilot scale SAG mill. Jayasundara *et al.* (2010) described coupling of DEM to computational fluid dynamics (CFD) to predict flow behavior in a stirred mill as function of operational conditions. The coupling works on the following way: DEM generates information such as position and velocities of individual particles on each time step. An algorithm analyzed the porosity based on DEM outputs and the drag force in a calculation cell. Then CFD model utilizes this data to calculate the fluid flow field from which the drag forces acting on particles is calculated. The resulting drag forces are incorporated into DEM to calculate particle motion on the next time step. They have also carried out DEM experiments by changing mill filling and have observed that the collision frequency is higher and the energy magnitude is lower for higher fillings.

On another work, Jayasundara *et al.* (2010) compared the flow modelling on IsaMills® from CFD-DEM coupling simulations with experimental results obtained from particle emission positron tracking (PEPT). In CFD-DEM coupling, fluid properties such as velocity field, distribution of particle speeds, radial acceleration and power consumption were analysed at steady state with a macroscopic viewpoint. A DEM code was developed by the research group of the University of New South Wales, while the CFD code used was CFX® (Ansys Inc.). The parameters from DEM simulations used by the authors are given on Table V-3.

Cleary and Hoyer (2000) have validated DEM simulations of centrifugal mills against experiments which were recorded using a high speed camera. The experiments were carried out in the 1980s by Hoyer and provided a wide range of operational conditions to be validated in DEM. The authors cite that the inclusion of particle shape in the DEM modeling would require greater computational power. In their work, the simulations were done in two dimensions and the particles were modelled as discs or super-quadric shapes. They mentioned that particles with shape factor of 20:1 required 2.2 to 2.5 times higher computational cost than circular shaped particles. The authors defined the rolling friction as the force that causes a pool ball to stop.

Table V-1 shows the results obtained by the authors correlating the specific power to the spring stiffness used in the simulation and the maximum particle overlap. In DEM

simulations the spring stiffness is chosen to be less than the real value of Young's modulus of the material. Usually, k = 2x10^6 gives good accuracy in many industrial applications but in the case of centrifugal mills the high acting forces produce an overlap of 3.6%, with peaks of 55% which is more than half the particle radius. This resulted in an error of 9% on power consumption prediction. The value of 2x10^8 produced good results as obtained for higher values in the spring stiffness.

Table V-1 Parameters evaluated by Cleary and Hoyer (2000) and their effect on the mill power

Spring stiffness N/m	Specific power	% difference to reference	Average overlap (%)	Maximum overlap (%)
2x10^6	0.2732	9.0	3.6	55
2x10^7	0.2647	5.6	0.6	15
2x10^8	0.2544	1.5	0.11	3.5
2x10^9	0.2527	0.8	0.017	0.9
2x10^{10}	0.2507	-	0.003	0.25

V.2 Applications to tumbling mills

A direct application of DEM to tumbling mills is in the prediction of the impact point of the grinding charge, minimizing the wear or the degradation of the lifters and liners (Mishra, 2003). According to Mishra (2003), DEM also provides a prediction of power consumption in ball mills, autogenous and semi-autogenous mills with an error of less than 10%.

The traditional PBM-based models do not allow the analysis of elementary processes involved on particle breakage, such as the effect of contact geometries and other factors related to the grinding environment. Mishra (2003) suggests that being a numerical tool, DEM has been offering a qualitative understanding of the effect of operational and design variables of mills regarding the dynamic behavior of the charge. Mishra (2003) identified the type of applications of EDEM to tumbling mills, which are:

- Charge motion analysis
- Power consumption analysis
- Lifter design
- Lifter wear
- Microscale breakage modelling

The main set of information extracted from DEM simulations of tumbling mills is the collision energy spectrum. Currently there are two types of collision information that can be captured from DEM simulations: one is by the normal and tangential energy loss calculated from the spring-dashpot model and the second is from the kinetic energy of the particle immediately after the collision event. Powell *et al*. (2008) have compared these two methods of obtaining the collision energy spectrum. They comment that the difference is significant and there is no general agreement among the researchers about which one is valid when simulating mills. However, it is important to be consistent to the breakage model that is used the predict breakage.

A typical simulation of a section of an industrial mill that contains thousands of particles generates an enormous amount of data, reaching some dozens of gigabytes of information. From this data, one should extract the collision information of the particles and compile the data in a proper and compatible way to the comminution models. Powell and Weerasekara (2010) suggest a way to post-process the collision energy data. The binning method or clustering places each collision energy in equally log-scale spaced energy intervals. The energy coordinates proposed follow the relationship,

$$x_n = \frac{x_{n-1}}{2^{16}} \qquad \text{V-15}$$

being x_n the n-th level of energy. The appropriate clustering of collision energies is of great importance as it can change the aspect of the collision energy spectrum (Weerasekara and Powell, 2010). In order to log the collision energies the authors tracked particle velocities and their contacts. In the case of the Unified Comminution Model (UCM) the authors have also considered necessary to track the collision history of each individual particle in the simulation for later application of the damage model proposed by JKMRC researches. It is worth noting that one of the differences between the Unified Comminution Model proposed by Powell and Weerasekara (2010) and the mechanistic modelling approach proposed by the UFRJ group (Carvalho, 2009) is the interpretation of how particle populations respond to repeated collision events.

In their work, Weerasekara and Powell (2010) simulated a pilot scale SAG mill operating at 75% of its critical speed, with power consumption of 9.44 kW. The internal mill diameter is 1,696 mm, length of 575 mm and equipped with 11 lifter bars of 50 mm x 50 mm. They started with a base particle size distribution for the hold-up with d_{80} close to 120 mm. From the base case, they simulated two additional mills with 3 meters and 6

meters in diameter and two more particle size distributions for the hold-up. The parameters used on their simulations are listed on Table V-3.

Some issues are worth mentioning in respect to the effect of mill size on the distribution of collision energies in the work of Weerasekara and Powell (2010). With an increase from 1.6 m to 3 m in mill diameter, they observed that particles finer than 11 mm suffered an increase in their collision energies. However, in a mill with 6 meters in diameter these energies suffered a considerable reduction. For particles coarser than 43 mm, the collision energies were higher in larger diameters and particles in the size range of 15 to 30 mm showed a peak on their collision energies in the 3 meters diameter mill. It was found that the larger mill diameter allowed the impacts to reach a high energy level, but this ends-up narrowing the collision energy distribution at different particle sizes. From these observations, they concluded that the effect on the particle size distribution has a great influence on mill power and the way it is distributed among the charge. The toe region receives the highest impact energies, while in the center of the charge shear, impact energies dominate.

A typical method to validating DEM mill simulations is by comparing the power calculated from simulation to the power measured in a real mill. Dong and Moys (2002) conducted experiments where they recorded the trajectories of a single ball as a function of different contact parameters. The authors used a single ball in a mill equipped with a single lifter operating at a range of values in respect to the critical speed. In order to track the ball they used stroboscopic photography, reaching measurement errors smaller than 1.2 mm. They then simulated the mill using DEM in two dimensions with the aid of the software Millsoft® (Rajamani *et al.,* 2000) which is dedicated to tumbling mills. The parameters used are listed on Table V-3. They have found a set of contact parameters that matched the power measured. However, the comparison to measured power is just a single point in DEM validation, being impossible to guarantee that it represents the optimum solution. Indeed, there is a chance that many different combinations of parameters would result in the same mill power but with no garantee in reproducing the real-life behavior of the particles.

One of the most important questions that arise when simulating mills with DEM technique is the definition of the smallest particle size. This includes ore particles and steel balls that have to be present in the simulation. According to Cleary (2001), 20 mm particles may be considered as the minimum size in simulations involving AG and SAG mils. In his work, the effect of the lower truncation on particle size distribution was

evaluated by changing the minimum size from 1 mm to 10 mm in a 5 meter in diameter ball mill. The simulations showed no significant effect on mill power. In addition to that, the researcher simulated a 10-meter diameter and 4 meter long SAG mill. This mill was equipped with 72 lifter bars with a face angle of 5 degrees. Mill filling was 30 % and the speed was 75 % of the critical speed. The maximum ore particle size was 250 mm and the balls were within the range of 50 to 200 mm. The full mill simulation required the use of 281 thousand particles.

Even though DEM can provide the power consumption due to the charge motion, this power does not include the effect of slurry movement in the charge or the mechanical losses in the motor or couplings. Thus, it is expected that mill power obtained from DEM simulations will be systematically lower in respect to the measurements taken in real mills. The power consumption can be calculated by the integration of all energy losses in terms of normal and shear components of all collisions (Cleary, 2001).

The advances in computational power allowed DEM simulations to be carried out using 3-D models, previously done in a 2-D environment. This allowed the simulation of slices of even full size complete mills. However in the same mill operating at the same conditions there are differences in the results given by each type of simulation, 2-D, 3-D slice or full 3-D. Cleary *et al.,* (2003) assessed the effect of each type of simulation considering four types of approaches and compared the results to photography of real mill experiments.

In order to simulate this complex system, such as the grinding environment in tumbling mills, some degree of simplification has to be used. However, many of these simplification or assumptions has not been propertly tested, evaluated or validated. As part of the effort to widen the application of DEM, Cleary *et al.,* (2003) validated charge motion simulations of a 600 mm diameter SAG mill by comparing the toe and shoulder positions, as well as the power consumption of the experiments against the values obtained from DEM. The mill had an internal diameter of 592 mm and 200 mm in length, being a 1:10 scale of the Alcoa SAG mill from Pinjarra (Australia). In the 2-D simulation of this mill 2,800 to 4,500 particles were required. According to Cleary *et al.* (2003) the size of the 3-D slice models depends on the slice length. For instance for a 100 mm slice, four times the maximum particle diameter, the total number of particles varied between 85,000 and 111,000 for this mill. The full 3-D simulation, required 170,000 to 221,000 particles.

The analysis of the full 3-D simulations reproduced the experimental results very well (Cleary *et al.,* 2003). The 3-D slice gave different results of those from full 3-D, emphasizing the wall effect only described in the full 3-D model. For longer mills, the wall effect is relatively reduced, as the motion profile changes in the axial direction. One of the conclusions from Cleary *et al.,* (2003) is that the DEM calculated power should not be higher than the power measured. When comparing DEM power to the values obtained from Morrell's Equation, there was a good correlation with the 3-D slice simulation in DEM.

Besides having measurement errors, which makes the results a more difficult to analyze, Powell and Weerasekara (2010) attempted to parametrize the collision energy spectra as a funcion of the simulated particle size. This is an interesting approach, since after the DEM simulation is properly validated and calibrated, it would be possible, in principle, to describe the mechanical environment inside SAG mills with minimum use of computing power.

The effect of changes on mill liner profile was modeled in DEM. Powell *et al.* (2011) modeled the effect of liner wear on the SAG performance. The authors used a 3-D slice simulation of a full size SAG mill and the mill geometry was obtained by 3-D scanning of a real mill.

Morrison and Cleary (2004) used DEM to model ore breakage in a pilot scale SAG mill. The researchers analyzed the collision history of each representative particle, attempting to understand which simulation generated information that were useful for breakage prediction on this mill type. In the simulated mill, 90% of the charge was composed of particles coarser than 6 mm, representing a total number of particles from 250,000 to 450,000. The mill used was 1.8 x 0.6 m Hardinge type and an industrial scale SAG (11 meters in diameter). Table V-2 presents some of the mill parameters simulated.

Morrison and Cleary (2004) say that after a few revolutions a particle in this type of mill is not able to accumulate sufficient damage in order to suffer body breakage. They consider that the breakage (mass loss) occurs due only to abrasion effect. This contradicts the damage model proposed by Tavares (1997), which predicts this effect as the result of the impacts. However, the authors do not consider either the ore charge variability in which particles contained in narrow size classes present different energy requirements in order to break. Indeed, within the particle population there may exist some weaker particles that are more amenable to be broken. As such, this explains what

is seen in reality when, for instance, 200 mm ore particles may break catastrophically in real pilot scale mills.

Table V-2 Characteristics of the mill simulated by Morrison and Cleary (2004)

Number of particles	425,000	Mill filling	39%	Ball filling	5%	16 lifters on feed cone
Mill speed	24 rpm	% critical speed	76%	Ore top size	122 mm	8 lifters on discharge end
Bottom size	6 mm (90% of charge)	Mill dimensions	1.8x0.6m	16 lifters	10º face angle	

Powell and Weerasekara (2010) listed a series of conclusions related to DEM simulations of mills:

- Collision events should be logged and individually allocated to breakage modelling; this is dramatically different from using cumulated energy to the particles
- An improved understanding of the normal and tangential components of the impact in breakage is required
- The dashpot energy is not used when a particle suffers fracture. In fact only a tenth of the energy is absorbed when the breakage occurs.
- The ability of dealing with material conditioning is required (wear, rounding, weakening)
- A technique to compute the energy loss on fine particles (named sub-DEM) is needed
- In the presence of fines as a dry or slurry bed, the energy absorbed by coarser particles is considerably lower than the one simulated by DEM.

Recently, Morrison and Cleary (2010) proposed a model to estimate fine particle breakage by the grinding media in a small diameter ball mill using DEM. The motivation is that many researchers use DEM to simulate grinding media motion or even motion of the coarse particles that act as grinding media in AG/SAG mills. However, when dealing

with fine particles (sub-DEM) the DEM simulations becomes harder, requiring greater computing power. As such, the authors presented a new DEM code that allowed the simulation of fine particle to interact with the grinding media in a periodic slice of a ball mill. They claimed they could estimate the breakage rates of the particles directly from DEM simulations as they would be only function of the effective collisions between ore particles and grinding media.

They simulated breakage of ore particles with sizes ranging from 2.80 to 1.18 mm. The ball filling was 24 %, equivalent to 157 steel balls of 27 mm diameter. They simulated several levels of voids filling, from 50 % to 150 % reporting that the average particle overlap was lower than 0.25 % of the radius of the finest particle size. The acceptable total overlap will be reduced with the reduction in the particle size. As such, for a relativelly small model containing aproximatelly 500,000 particles, the simulation time may be very long. They also claimed that the simulation reached a steady condition after 1.5 seconds of simulations, or, a single mill revolution. Regarding the simulation results, they observed that the distribution of ore particles is heterogeneous with ore particles compacted near the centre of the charge and at the shoulder while on toe region there were few fine particles. For the case of lower powder filling the fine particles presented enough mobility to flow between the charge. The powder particles concentrates in certain regions of the mill fully filling the space between the balls while other regions, near the charge toe, become less populated by the powder. The simulation results showed that for low powder filling, the power concentrates near the shoulder of the charge and the particles that fall into the toe are the ones elevated by the lifters, resulting in streams of powder that almost reach the top of the mill. For powder fillings near 100 %, which is close to the operational practice in industrial mills, the fines fill almost all the voids contained in the charge in movement, being less concentrated near the toe region. The lowest energy consumption corresponded to 50 % of powder filling and grew almost linearly until reaching the value of 37 W for 150 % powder filling.

Table V-3 List of parameters used in DEM simulations

							Friction coefficient								
Authors	Equipment	Materials	Density (kg/m^3)	Young's modulus (N/m^2)	Shear modulus (GPa)	Poisson ratio	Sliding	Rolling	Static	Restitution	Spring stiffness (N/m)	Normal stiffness (N/m)	Shear stiffness (N/m)	Number of particles	Particle size (mm)
Jayasundara *et al*. (2010)	Stirred mill	Glass beads	2,500	$2.0x10^7$		0.29	0.3				-			N/D	3
Jayasundara *et al*. (2010)	Isa Mill	Glass and ceramic beads	2,500 3,700	$2.0x10^7$		0.29	0.1 (part/part) 0.3 (part/liner)			0.7 0.5				112,000 168,600 224,800	
Morrison and Cleary (2010)	Ball mill	Steel balls						-	0.5	0.8 (ball/ball) 0.5 (ball/ore) 0.3 (ore/ore)	$2.0x10^6$			500,000	
Ramos *et al.* (2011)	Ball mill	Iron ore	3,800		0.1	0.25		0.2 (ore/ore)	0.35 (ore/ore)	0.51 (ore/ore)					
		Steel balls	7,800		70	0.30		0.36 (ore/ball) 0.2 (ball/ball)	0.39 (ore/ball) 0.01 (ball/ball)	0.35 (ore/ball) 0.70 (ball/ball)					
Djordjevic (2005)	Pilot AG/SAG mills	Ore	2,500				0.4					$4x10^5$	$3x10^5$		10-80
Djordjevic *et al.* (2006)		Ore Steel balls	2,650 7,800		10 150	0.25 0.30	0.5 0.15								
Dong and Moys (2002)	Ball mills	Steel balls							0.75 (ball/ball) 0.375 to 0.750 (ball/liner)	0.2 (ball/ball) 0.05 a 0.6 (ball/liner)		$4x10^5$	$3x10^5$		
Weerasekara and Powell (2010)	SAG mills	Ore Steel balls	2,680 7,800		1.0 200	0.30 0.29		0.01 (ball/ball) 0.01 (ball/min) 0.01 (min/min)	0.3 (ball/ball) 0.3 (ball/ore) 0.3 (min/min)	0.3 (ball/ball) 0.3 (ball/ore) 0.2 (ore/ore)					

Recent work at LTM consisted of grinding experiments conducted on a 30 cm x 30 cm mill, where the power filling level varied from 60 to 140 %. The measured power consumption showed little variation and the lowest powder filling corresponded to the highest power consumption. This experimental evidence contradicts the results of Morrison and Cleary (2010) indicating that DEM simulation outputs have to be investigated very carefully.

In another work, published by Djordjevic (2005), the goal was to compare the power consumption when the charge is characterized by different particle size distributions, while keeping the total mass and the mill speed constant. The author used the PFC3D DEM code and the mill simulated had 0.98 m of internal diameter and was equipped with nine square (5 cm) lifter bars. The charge of the mill was composed of spherical particles with 10 and 80 mm diameters. The material parameters are listed on Table V-3.

Djordjevic (2005) showed that it is possible to truncate the size distribution of the charge by avoiding the use of fine particles by transferring their equivalent mass to the immediately superior size. The resulting errors on power calculation were 2.4 % by truncating the distribution on 40 mm. When comparing the error of the experimental measurement, which was around 10 %, the value was considered acceptable. However, the truncation on coarser particles (60mm) presented an error close to 10 %.

V.3 Alternative techniques to measure charge motion and collision energies

The positron emission particle tracking technique or its acronym PEPT is of great importance in order to provide insights and information to better understand particle motion inside mills. It was developed in 1997 (Parker *et al.,* 1997) and was recently implemented on the University of Cape Town. The technique is a variant of the positron emission tomography (PET) and can be considered as a powerful tool that provides information that may allow the development of more rigorous mathematical models. In addition to that, it has been used to answer questions related to slurry transport in mills and also to validate simulation results obtained using the discrete element method. However, the technique has a series of limitations such as scale; it is limited to laboratory scale mills due to the size of the camera. It deals with a radioactive environment, limiting

the transfer to other research centers. The capacity of simultaneous particle tracking is also a limitation in terms of quantity and size. In their work, Govender *et al*. (2010) claimed that it was possible to track ore particles from 1 mm, 2 mm and 4 mm as a function of the operational conditions in a laboratory scale ball mill. From PEPT experiments, it was observed that mill charge cycles approximately 1.7 times on each revolution of the mill and this number is a function of the mill filling and speed (Govender and Powell (2006).

Another interesting technique is the use of instrumented grinding media such as the one developed by Martins *et al.* (2008). They have built and instrumented a ball that is able to measure physical variables on the aggressive environment that is the interior of a ball mill. The development of the iBall was possible with the great advance on the electronic field, since some of the components required to build the machine became commercially available only recently. The ball is a data acquisition system inserted into a protector shell. Sensors such as 3-axis accelerometers, tri-axial strain gauges and a temperature sensor compose the ball. It is possible to calculate several physical variables as a function of time, including the rotational kinetic energy, the applied net momentum, the applied net force and the angular momentum.

VI. Mechanistic modelling

The mechanistic model of comminution considers modelling the breakage of the ore particles using theories that are more fundamental. While the traditional phenomenological population balance based models do not decouple the contributions of the machines from the ore used to calibrate the model parameters. For instance, data gathered to model a ball mill could not be used to simulate a SAG mill. The mechanistic models require information of the ore breakage in an independent form. As Morrell and Delboni Jr. (2005) identified the need for a more detailed energy transfer model in order to allow the proper prediction of the AG and SAG mill performance; some approaches arise combining information from advanced computation techniques such as the Discrete Element Method. The advance of the DEM simulations of comminution processes allowed the development of more robust mechanistic models.

Some attempts have been made to counter the limitation of the phenomenological models. Cho (1987) carried out drop weight tests where a population of particles were displaced in a bed configuration. He tried to correlate the breakage to the energy application that occurs in each collision between grinding media inside mills. He noticed that some particles in the bed remained unbroken after being hit, indicating that among the population there would be some weaker particles. He proposed the use of some kind of distribution of particle strengths to model his breakage tests properly but he faced computational limitations at that time as DEM simulations were not available.

Höfler and Herbst (1990) overcame this limitation by estimating the collision energy spectra by back calculation from input and output data from their model, which was based on collision energies. In this way they have successfully predicted the product size distribution in a 25 cm ball mill. However, soon later Mishra carried out the first DEM simulation of a mill as discussed in Chapter V.

A good mechanistic model of a mill is one that given a collision event it can predict what the mode of breakage (surface, damage or body breakage) will be. In other words, what the progeny size distribution will be as function of the contact properties and ore breakage properties if a breakage event occurs.

This chapter reviews some of the mechanistic model approaches. Then it focuses on the UFRJ mechanistic model for ball mills and the particle interaction model.

VI.1 Overview

With the aim of decoupling the contributions of material and the mechanical environment in mill, King and Bourgeois (1993) proposed a conceptual model for ball mills that describes the grinding environment using the impact/collision energy spectrum obtained using the DEM. In their formulation, the breakage distribution function of the mill is described by

$$b(d,d') = M\int_0^\infty b(d,d';eE)p(E)\mathrm{d}E \qquad \text{VI-1}$$

where, $p(E)$ is the probability density function of the impact energies in the mill, $b(d,d';eE)$ is the mass fraction of particles smaller than the size d that are created from the breakage of particles of size d' when submitted to an impact energy E. King and Bourgeois (1993) estimated the impact energy absorbed by the particles in the bed (parameter e) from a single particle fracture model.

King (2001) has proposed a model that now considers not only the impact energy spectra but also the distribution of fracture energy of the particles. From the energy-specific breakage function obtained from breakage of individual particles as function of the energy input, the average cumulative breakage function would be given by,

$$B(d,d') = \int_0^\infty\int_0^1 B(d,d';eE)\,F(eE,d')p(e)p(E)\mathrm{d}e\mathrm{d}E \qquad \text{VI-2}$$

where $F(eE,d')$ is the breakage probability of a particle of size d' when it receives a amount energy eE in a collision event inside the mill and $B(d,d';eE)$ is the breakage function that results from a single collision event of resulting in the absorbed energy eE. $p(E)$ is the density distribution for the collision energies in the mill (collision energy spectrum) and e is the fraction of energy in that collision that is captured by a single particle. $p(e)$ is a function that describes how the energy is split among the captured particles. It is worth noting that King has recognized the importance of describing breakage based on the energy applied to a single particle as he inserted the energy split term $p(e)$ into the model.

In order to illustrate the application of the microscale approach proposed by King, it is assumed a hypothetical comminution machine in which the feed material contains particles classified in a narrow size fraction (mono size distribution) and the distribution of fracture energies of this particle population is given by Equation III-3. Moreover, in this hypothetical machine, in each breakage cycle all the particles in the population receive a specific collision energy of 100 J/kg. According to the distribution of fracture energies of the particles, nearly half of the population would break, and the remaining ones would be those with fracture energies above 100 J/kg that, would not suffer changes on their fracture energies. During the following impact cycle at the same energy level, these particles would remain intact. Since this is not observed in reality, the model does not describe properly how the particle population evolves during grinding.

The conceptual model proposed by King showed promise in spite of its limitations. The requirement of descriptions on how the energy is split among the particles positioned on the bed, which is required by the model, adds another degree of complexity to the model, since this is not known. Also, in analogy to some of its predecessors, the model is also based on particle properties that do not evolve during grinding, which has been illustrated above to provide unrealistic descriptions in grinding. Finally, the model in the form it was originally proposed has not been validated or used by other researchers.

Another model that followed the mechanistic approach is the unified comminution model (UCM) proposed by Powell (2006). He presented the framework of the model which also aims at decoupling the contributions from the machine to the contributions of the ore in the generation of fragments from breakage (Powell and Weerasekara, 2010). The vision of the UCM is to bring all comminution models to a common base. The first idea arose in 2006 and since then the authors have developed it further, while recognizing the many challenges associated to the high complexity of the systems. The UCM is divided in main sub-areas: mechanical environment, transport, particle energy transfer, damage modes and breakage, and the breakage test techniques.

The concept of the UCM was tested in 2010 (Powell and Weerasekara, 2010), for the case of a pilot scale SAG mill. DEM simulations indicated a large number of impacts (30 to 80 %) of negligible energetic magnitude – below 10^{-6} kWh/t (0.0036 J/kg). These impacts were recognized as just a DEM artifact because in fact these very low energy collisions are not related to media motion. This value of 0.0036 J/kg is equivalent to dropping a particle from a height of 0.36 mm, which is known to be an insufficient value to break or even cause physical changes in the particle (Powell and Morrison, 2006).

The authors have also assumed that the breakage function of particles that do not break does not change as a function of the number of impacts received, or in other words, with the damage accumulation on the particles. This observation has been previously confirmed by the work of Tavares (2009). In respect to abrasion, the authors have identified that the surface breakage rates are reduced as the particles become more rounded.

Another attempt to develop a mechanistic description of grinding is the work done by Morrison and Cleary (2008), having called it the Virtual Comminution Machine (VCM). Their vision states that VCM would allow the design of a machine entirely by CAD (Computer Aided Design) modeling. The machine design would be detailed enough that would be possible to predict its virtual operation, in which case the VCM task would be, simulating size reduction of the ore. The key outcomes of the model would be the size distribution of the product, the power consumption, the degree of wear and even the load on equipment components.

The whole idea behind the VCM concept is to allow the design of more energy efficient equipment without going through or saving time from real world prototyping. The authors defend that VCM should be able to correlate each collision level inside a comminution machine to the level of particle breakage. It is recognized, however, that this task is challenging.

An approach that has the potential to overcome many, if not all the limitations presented by the previous approaches is the one developed at the Laboratório de Tecnologia Mineral from COPPE, at Universidade Federal do Rio de Janeiro, called UFRJ approach or UFRJ mechanistic model. The work proposed a mechanistic modeling approach based on population balance model and some of the formulations proposed by King (Carvalho and Tavares, 2009; Carvalho, 2009). The model decouples the dominant mechanisms on comminution processes. Information from collision energy spectrum given by DEM or any other technique is used to build the model. The variability of particle breakage properties is considered, being characterized by the use of the fracture energy distribution or breakage probability. The general formulation of the model considers also that particle properties change with time: for instance, particles become weaker due to repeated impacts, which is described by the damage model proposed by Tavares and King (2002). The rational basis of the model provides the conditions for it to be, in principle, fully predictive, with the potential to become an excellent tool with

application not only on optimization of comminution processes but also on the design of mills and circuits.

As part of the Masters of Science dissertation of the author (Carvalho, 2009), the formulation of the model was proposed. Also the conceptual description of size reduction in a number of systems, from those in which breakage is unwanted, such as degradation during handling and transport of materials, to a preliminary formulation of comminution in autogenous mills. However, at that moment, the equation proposed was based on a number of hypotheses that limited the application of the model to the ball mill case.

A general scheme of the principles of the UFRJ mechanistic model established in 2009 work is illustrated in Figure VI-1. A general look at this model reveals similarities to UCM from Powell and VCM from Morrison and Cleary, particularly in its view of decoupling the contributions from machine and ore. The model has inputs from fundamental ore breakage properties, which combined its capacity of decoupling machine from ore contributions, puts it in good standing when comparison to traditional population balance models.

As mentioned, the mechanical environment inside comminution machines is characterized by the collision energy spectrum, which gives the input on how the energy dissipated in the charge is applied to the particles to be grounded. As discussed previously, in most grinding processes the collision energy spectrum can be estimated using the discrete element method. In the case of material handling and transport the collision energies may be estimated using analytical equations. For instance in a transfer chute, where particles are dropped from a given height the simple product of acceleration due to gravity and the height gives the specific particle collision energy.

The model also requires that mixing and transport characteristics be informed, as for example, if the mill can be considered as a perfect mixer with or without internal classification, and also how mass is discharged (mass transfer relationship). For the sake of simplicity, the mechanistic model proposed considered the ball mill as a perfect mixing reactor. Although the approach could be extended to other cases such as plug flow regime, by considering a distribution of residence times in the case of continuous mills or even time/space-discrete collision events in the case of material handling (Tavares and Carvalho, 2012) and some crushers such as the vertical shaft impact crusher (Cunha *et al.,* 2013).

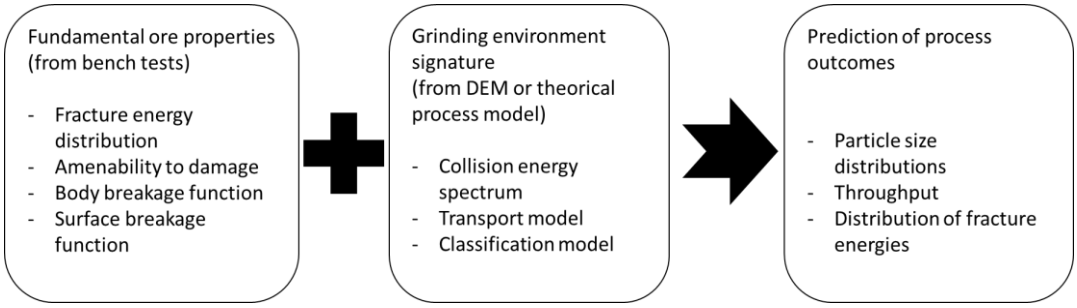

Figure VI-1 Framework of the UFRJ mechanistic model as proposed in 2009 (Carvalho, 2009)

The population balance model discretized in particle size classes is the base of the mechanistic model approach. This first simplification is not important since it keeps the modeling approach consistent to the current methodology of measuring particle sizes, which is sieving. The model is also formulated in a way that allows accounting for composition or mineralogical class. Thus, it is possible to model processes that involve the differential breakage of distinct minerals that compose an ore. An example is the case of iron ore which is composed of iron minerals which typically present comparatively low strength (low fracture energies/high breakage probability) and silicate minerals such as quartz which present higher strength. As such, when subjected to comparative impact energies, different breakage products could be obtained. This may become a challenge when the mill operates in closed circuit, since the tougher unbroken particles would return from the classifier and return to the mill, so that the recycle stream will present a different composition from the fresh feed. This type of situation, however, cannot be tackled with the use of traditional PBM formulations.

VI.2 Ball milling

The UFRJ mechanistic model deals with each collision individually, and requires information of the type of collision: grinding media against ore particle, autogenous collision, particle-particle or particle-liner as showed on Figure VI-2.

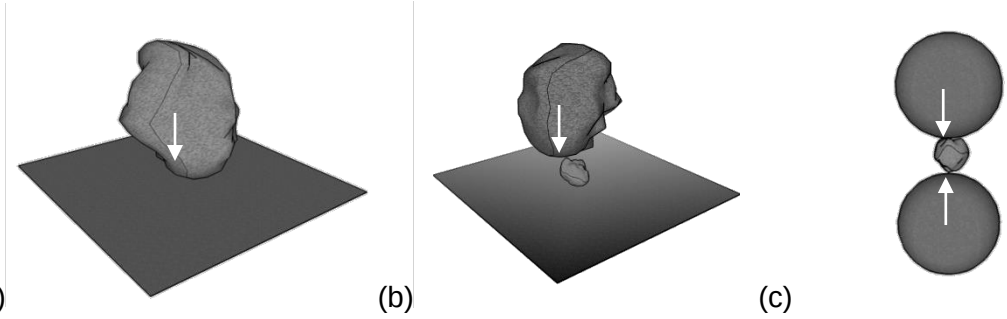

Figure VI-2 Examples of impact modes (a) particle-liner (b) particle-particle and (c) ball-particle-ball.

The collisions are considered to be always of binary type, the simplest case is showed on Figure VI-2a where a particle collides against mill liner. In both Figure VI-2 b and c, the major elements of the collision (rock particle (b) and two balls (c)) hit captures a smaller ore particle. The ore mass captured by these collision is given by a particle interaction model which development is discussed in section VI.3.

The general equation assumes the process as a perfect mixing reactor such that the material properties (particle size distribution, mineralogical composition, fracture energies, etc.) are equally distributed throughout the reactor. Thus, the equation can be written for a continuous and dynamic process as,

$$\frac{d[w_{il}(t)M(t)]}{dt} = w_{il}^{in}(t)W^{in}(t) + \sum_{k} \omega_k\left[-D_{ilk}^{b}(t) - D_{ilk}^{s}(t) + A_{ilk}^{b}(t) + A_{ilk}^{s}(t)\right] - w_{il}^{out}(t)W^{out}(t) \qquad \text{VI-3}$$

where $w_{il}^{in}(t)$, $w_{il}(t)$, $w_{il}^{out}(t)$ are the mass fractions of particles in size class i and component l on the feed stream, the mill charge and the product stream. $W^{in}(t)$ and $W^{out}(t)$ are the feed and discharge rates, ω_k is the frequency of the collision events of the k-th class inside mill and the terms $D_{ilk}(t)$ e $A_{ilk}(t)$ are the rates of disappearance and appearance of material respectively. The superscripts b and s refer to the body breakage and the surface breakage of the material, respectively.

One of the key factors is the modelling of the breakage of the particles that cannot appear on DEM simulations due to computational restrictions, the fine particles or the

named sub-DEM particles. This can be tackled by assuming that in each collision between the elements of the DEM simulations a fraction of the energy loss contributes to the breakage of the sub-DEM particles. As such, the model requires the assumption that given a collision event, one or more particles of the entire population can be captured. The energy transferred by each impact event is then split among the captured particles that may or not break, depending on their fracture energy distribution and on the amount of energy received individually.

The particle breakage model incorporated in the UFRJ model for a ball mill is based on ball-on-ball collisions, assuming that between balls a given volume of particles will be captured. Depending on the collision energy and the ore properties, the collision may result in different breakage mechanisms. Figure VI-3 presents the calculation algorithm for a collision between two grinding media elements.

Figure VI-3 shows that, in a collision event, a fraction of particles may be captured and thus be eligible to break. If a particle is captured and fractures, suffering body breakage, it may or may not leave its original size class, the term that responds for this effect is the term b_{ii} of the breakage function of particles in size class i. The particles that are captured in a collision and that do not break due to the impact, may lose a fraction of their mass, suffering surface breakage due to abrasion/chipping mechanisms, according to the rate k_{ij}.

The rates of appearance and disappearance are calculated from each size class i, ore class l and collision class k. For body breakage these rates are defined as,

$$D_{ilk}^{b}(t) = w_{il}(t) \int_{0}^{\infty} m_{ilk}(E) p_k(E) \int_{0}^{1} [1 - b_{iilk}(eE, t)] F_{il}(eE, t) p_k(e) \mathrm{d}e \mathrm{d}E \qquad \text{VI-4}$$

$$A_{ilk}^{b}(t) = \sum_{j=1}^{i-1} w_{jl}(t) \int_{0}^{\infty} m_{jlk}(E) p_k(E) \int_{0}^{1} \left[b_{ijlk}(eE, t)\right] F_{jl}(eE, t)\, p_k(e) \mathrm{d}e \mathrm{d}E \qquad \text{VI-5}$$

In the appearance and disappearance terms, $p_k(E)$ is the density distribution of collision energies E in class k in the mill. m_{ilk} is the mass of the particles in size class i that are captured in each collision event related to collision class k. Finally, $p_k(e)$ is the energy split function among the captured particles. The particle interaction model, which is the relationship between the captured particles and the energy split, will be discussed in section VI.3.

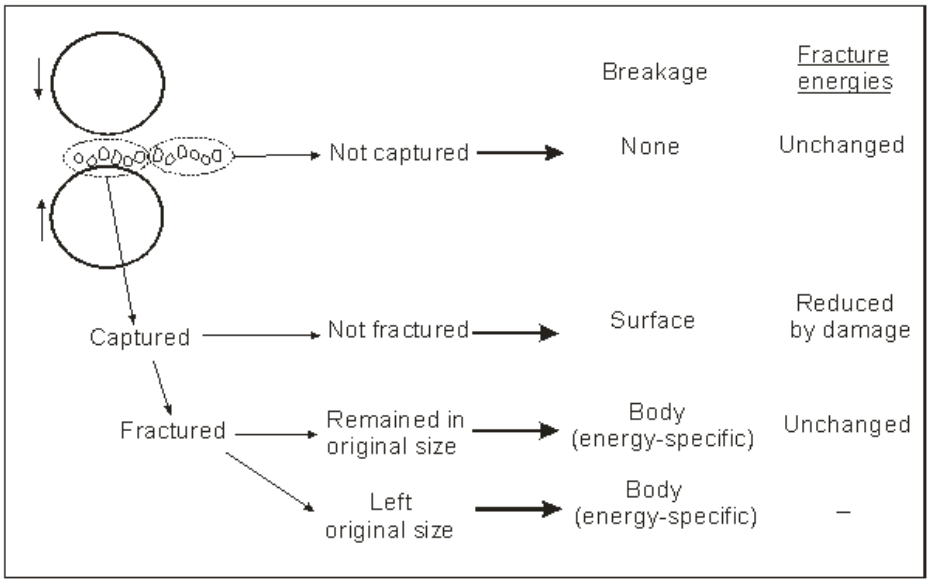

Figure VI-3 Collision event modelling scheme

$b_{ijlk}(eE,t)$ is the mass fraction of particles in component class l in size class j that appears on size class i when body breakage from collision class k of energy magnitude eE occurs. $F_{il}(eE,t)$ is the fracture energy distribution of particles in size class i of ore class l at time instant t. Thus, $F_{il}(eE,t)$ is the fraction of particles in class il that break when subjected to collision energy eE. The terms describing surface breakage due to abrasion mechanisms may be written as,

$$D_{ilk}^{S}(t) = w_{il}(t)\kappa_{il}\int_{0}^{\infty} m_{ik}(E)p_k(E)\int_{0}^{1}[1-F_{il}(eE,t)]p_k(e)\mathrm{d}e\mathrm{d}E \qquad \text{VI-6}$$

$$A_{ilk}^{S}(t) = \sum_{j=1}^{i-1} w_{jl}(t)\kappa_{il}\int_{0}^{\infty} m_{jk}(E)p_k(E)\int_{0}^{1} a_{ijl}(eE,t)\left[1-F_{jl}(eE,t)\right]p_k(e)\mathrm{d}e\mathrm{d}E \qquad \text{VI-7}$$

where $a_{ijl}(eE,t)$ is the abrasion breakage function in density form and κ_{il} is the fractional mass loss rate due to abrasion.

As discussed in section III.3, it is assumed that ore particles within a narrow size class present different fracture energies or breakage probabilities. In addition, when particles are generated from breakage of coarser particles, the fracture energy distribution of the new particles (in the same size class) obey the same lognormal behavior characteristic from the ore.

In order to illustrate the application of a time step iteration of the UFRJ mechanistic model in a ball mill, let us consider the following example: after the impact cycle, the new distribution of fracture energies of ore particles in class il should be calculated. This is carried out by a mass balance computing the amount of particles il that have different fracture energy distributions. For instance, particles that are fed to the mill and the ones that are originated from breakage, have the original fracture energy distribution of the ore in that class, $F_{il}(E, t_0)$ or $F_{il}(E, 0)$. Another material fraction is the amount of particles that underwent damage, in which their fracture energy distribution is defined as $F_{il}^{*}(E, t)$. The last fraction is the fracture energy distribution of the particles in the mill hold-up before the impact cycle $F_{il}(E, t)$ and $F_{il}(E, t + \mathrm{d}t)$ is the fracture energy distribution after the collisions in the infinitesimal time frame $\mathrm{d}t$, or, in other words, at the time $t + \mathrm{d}t$. Figure IV-4 shows this example where the top three distributions are $F_{il}(E, t_0)$, $F_{il}(E, t)$ and $F_{il}^{*}(E, t)$ respectively, which following the energy convolution equation, results in the distribution of fracture energies after the time step $F_{il}(E, t + \mathrm{d}t)$.

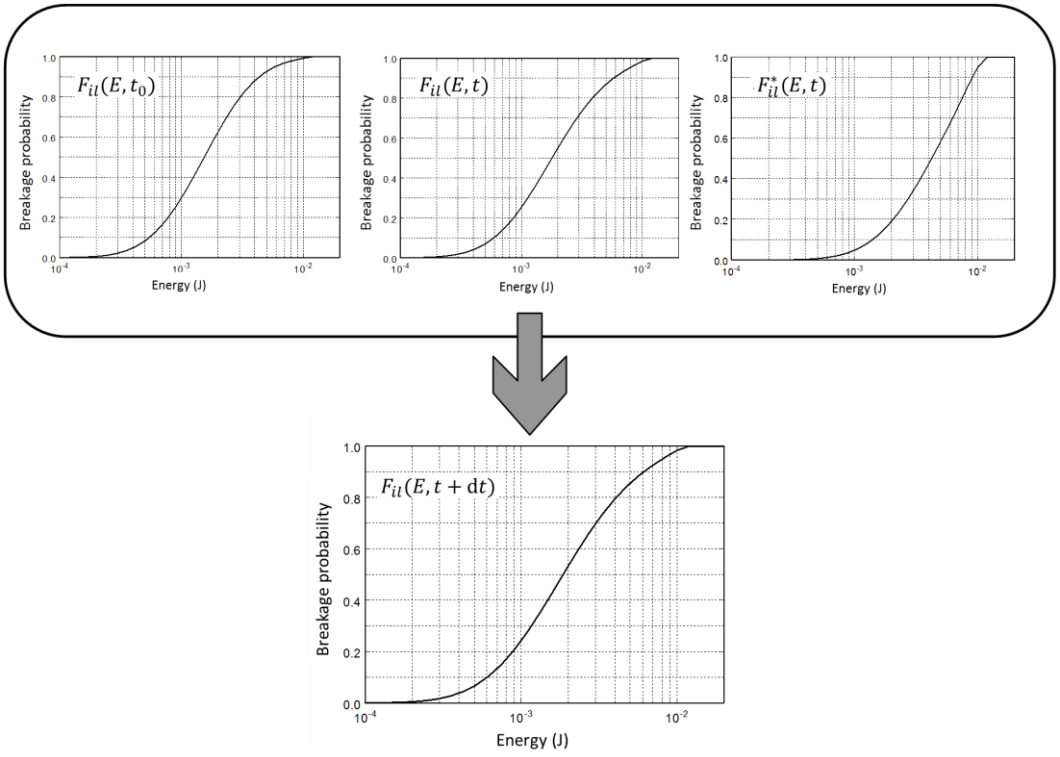

Figure VI-4 Illustration of the fracture energies convolution procedure

Thus, complementing the main UFRJ model equation that describes the mass balance in each size and component class (Equation VI-3), there is the expression

$$F_{il}(E, t + \mathrm{d}t) = \frac{G_{il}(t)F_{il}^{*}(E, t + \mathrm{d}t) + \big(H_{il}(t) + Q_{il}(t)\big)F_{il}(E, t_0) + I_{il}(t)F_{il}(E, t)}{G_{il}(t) + I_{il}(t) + H_{il}(t) + Q_{il}(t)} \quad \text{VI-8}$$

which may be called the “energy convolution equation” where the original fracture energy distribution of the material in class il is characterized by a log-normal distribution as presented in section III.3.1. Considering now the size and component class il, the distribution of fracture energies of the feed material (Equation III-3) may be rewritten as,

$$F_{il}(E, 0) = \frac{1}{2}\left[1 + erf\left(\frac{lnE^{*} - lnE_{m50,il}}{\sqrt{2\sigma_{il}^{2}}}\right)\right] \quad \text{VI-9}$$

where,

$$E^{*} = \frac{E_{max,il}E}{E_{max,il} - E} \quad \text{VI-10}$$

and the equation that correlates the dependency of the median fracture energy ($E_{m50,il}$), adapted from Equation III-7, to ore properties is,

$$E_{m50,il} = E_{\infty,l}\left[1 + \left(\frac{d_{0,l}}{d_i}\right)^{\phi_l}\right]\bar{m}_{p,il} \quad \text{VI-11}$$

while the standard deviation in Equation VI-9 as function of particle size is given by Equation III-8.

The distribution fracture energies of the mill contents in class il, given by $F_{il}(E, t)$, may also be considered as the distribution of fracture energies of the material that has not suffered collisions in the time interval $\mathrm{d}t$ and $F_{il}^{*}(E, t)$ is distribution of fracture energies of particles that suffered impact but did not break, thus received damage, given by,

$$F_{il}^{*}(E, t+\mathrm{d}t) = \frac{\int_0^{E_{il}^{*}} p_k(\varepsilon) \int_0^1 \left[\frac{F_{il}\left(\frac{E}{1-D}, t\right) - F_{il}(e\varepsilon, t)}{1 - F_{il}(e\varepsilon, t)} \right] p_k(e)\mathrm{d}e\mathrm{d}\varepsilon}{\int_0^{E_{il}^{*}} p_k(\varepsilon)\mathrm{d}\varepsilon} \qquad \text{VI-12}$$

The equation above may be obtained from integrating the solution of the combined damage equation (Equations III-27 and III-28) in all energy coordinates in the collision energy spectrum. The damage model equation (Equation III-28) may be rewritten as,

$$D = \left[\frac{2\gamma_l(1-D)}{(2\gamma_l - 5D + 5)} \frac{e\varepsilon}{E} \right]^{\frac{2\gamma_l}{5}} \qquad \text{VI-13}$$

where E_{il}^{*} is the maximum fracture energy of the particles in class il which is equal to $E_{max,il}$ in $t = 0$. As comminution progresses, the equality $F_{il}\ (E_{il}^{*}) = 1$ is kept. The system of differential equations should be solved simultaneously to the energy convolution equations for each class il. The terms of the energy convolution are defined by

$$\frac{dG_{il}(t)}{dt} = \sum_k \frac{\omega_k}{M(t)} w_{il}(t)(1-\kappa_{il}) \int_0^{\infty} m_i(E) p_k(E) \int_0^1 [1 - F_{il}(eE_k, t)] p_k(e) dedE \qquad \text{VI-14}$$

is the rate of change in the particles that were damaged and remained in class il, and

$$\frac{dH_{il}(t)}{dt} = \sum_k \frac{\omega_k}{M(t)} \left[\sum_{j=1}^{i} w_{jl}(t) \int_0^{\infty} m_j(E) p_k(E) \int_0^1 b_{ijlk}(eE, t) F_{jl}(eE, t) p_k(e) dedE + A_{ilk}^{S}(t) \right] \qquad \text{VI-15}$$

which is the rate of change of the material that appeared due to breakage (body and surface) from coarser or equal size then the class il.

$$\frac{dI_{il}(t)}{dt} = \frac{w_{il}(t)}{M(t)}\left(\frac{M(t)}{dt} - \sum_k \omega_k \int_0^\infty m_{il}(E)p_k(E)dE\right) \quad \text{VI-16}$$

which is the rate of change of the material fraction that were not captured and the rate of material in class il that enters the process is

$$\frac{dQ_{il}(t)}{dt} = \frac{w_{il}^{in}(t)W^{in}(t)}{M(t)} \quad \text{VI-17}$$

Even though the model was not completed at that moment (Carvalho, 2009; Tavares and Carvalho, 2009), it generated very good results, which demonstrated that it was capturing several important microprocesses that influence mill performance.

Some key assumptions in the model were:

- Breakage results only from the normal component of the collisions
- The batch mill is perfectly mixed
- Particles are involved in each collision in the mill
- The fracture strength of a particle is the same if it was produced as a progeny of a low-energy or a high-energy stressing event
- Given the energy distribution function used, it is also assumed that the collision energy is equally split by particles present in the active breakage zone
- Surface breakage mechanisms, namely chipping, abrasion and attrition may all be described by a first-order process, with a single rate constant.

One of the first demonstrations of the capabilities of the UFRJ mechanistic model was in predicting non-first order rates for coarse particles that are usually found on laboratory-scale ball batch ball mills. The model was able to predict the disappearance of coarse particles in ball mills at rates that differed from first order with good agreement with experiments. It was also able to produce fair to good descriptions of breakage rates of particles in intermediate to finer size ranges, although it was not the aim of that work. Indeed, simulations demonstrated that, in the case of finer sizes the contributions of particle damage and abrasion were negligible, so that breakage was almost entirely due to body fracture, yielding approximately first-order rates. On the other hand, simulations

of grinding coarser particles showed significant deviations from first-order breakage kinetics, with contributions of abrasion, which demonstrate that particle damage should be taken into account in predicting particle breakage in these sizes, otherwise simulations resulted in predictions that were not consistent with empirical observations. Figure VI-5 and Figure VI-6 present some results, which plot the mass remaining in the top size along with the elapsed time from mono size batch grinding tests done in a 30 cm x 30 cm laboratory batch ball mill. Balls were of 25 mm in diameter, mill filling was 30 %, and the mill was operating at 67 % of the critical speed.

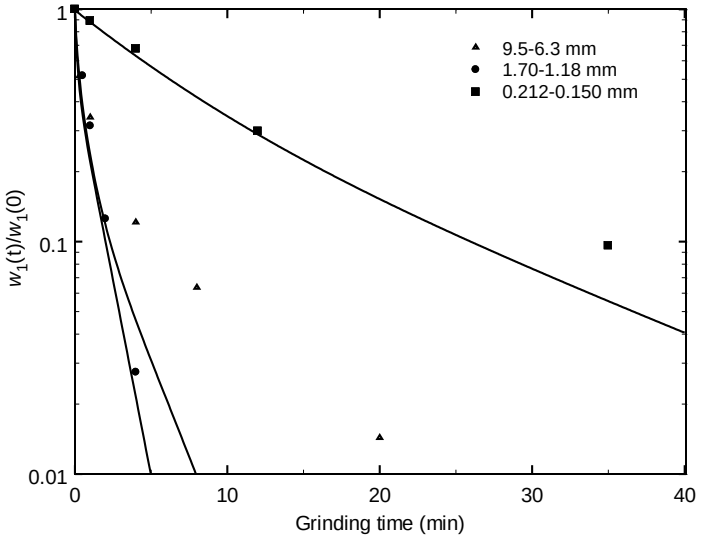

Figure VI-5 Comparison between experimental disappearance plots and simulations using the mechanistic model for selected sizes of limestone. Dots are the experimental measurements and the lines model prediction

A comparison is made from the simulation results of the Master of Science dissertation published in the 2011 paper (Carvalho and Tavares, 2011). Figure VI-7 shows a comparison between the distribution of fracture energies and the collision energy spectra of the material that generated the results presented in Figure VI-6. The magnitude of the collision energies in the mill is not sufficiently high to break coarser particles (coarser than 6.3 mm) immediately. As the experimental data shows that these particles actually disappear after a certain time, the simulation indicates there is a certain level of damage that makes the particles weaker, thus moving the distribution of fracture energies to the left, until the moment when a fraction of the population starts to break.

This leads into the non-first order behavior observed on the experimental disappearance plots.

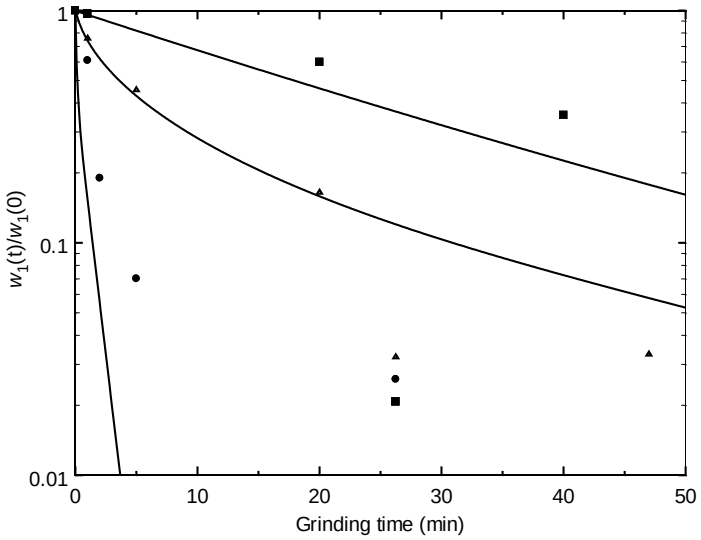

Figure VI-6 Comparison between experimental disappearance plots and simulations using the mechanistic model for selected sizes of granulite. Dots are the experimental measurements and the lines model prediction

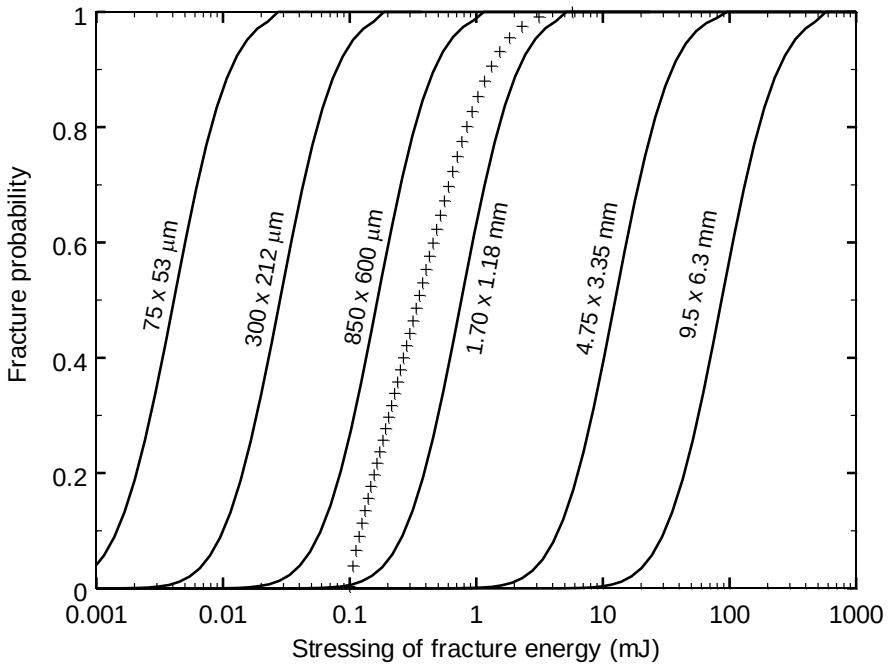

Figure VI-7 Comparison showing the distribution of fracture energies of copper ore at different size ranges (solid lines) to the collision energy spectra (crosses) of the 30 cm batch mill

In addition to these preliminary simulations, the authors also proposed a modification on the damage model equation in order to make it more computationally efficient. This change is only worthwhile in the context of applying the UFRJ model since it provides a more efficient solution in modeling of the repeated impact events (Equations III-24 and III-25). As described in Tavares and King (2002), and on section III.3.3, after being individually impacted with collision energy E_k, all particles contained in a sample will have their fracture energy reduced according to Equation III-24.

The evolution of the fracture energies of the particles that remain in top size was tracked on the simulations of Figure VI-5. The is displayed in Figure VI-8, which shows that initially, the population of particles in the top size has a median fracture energy of around 100 mJ. Ss grinding progresses the relative proportion of tougher particles increase, given their lower probability of fracture, while some weaker particles are generated, given the progressive effect of damage from unsuccessful breakage events. After 5 minutes of grinding the median fracture energy of the survived particles is approximately 150 mJ. This shows that the model is able to account for a well-known effect on grinding circuits, which is the fact that the recycle streams are, on average, usually harder to break than the fresh feed to a mill (Tavares and King, 1998).

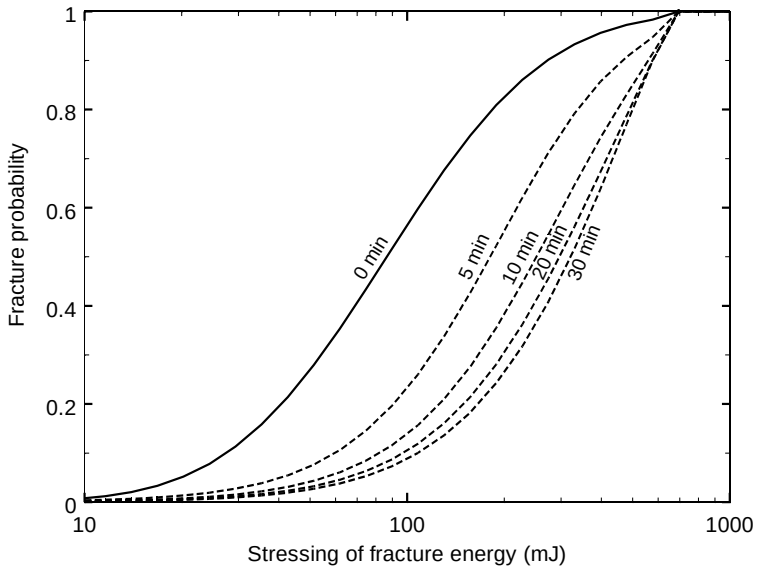

Figure VI-8 Evolution of distribution of fracture energies of particles that remained in the top size from batch grinding of granulite (9.5-6.3 mm)

VI.3 Particle interaction model

A mechanistic description of a comminution process requires the understanding of the micro processes that dominate breakage. In order to make use of the DEM collision information to predict breakage of the ore particles that are not present explicitly in the DEM simulations (sub-DEM particles) there is a need for an estimation of the total mass of the particles captured and also on how the collision energy is split among the captured population.

The mass captured and the energy split models are pieces of the puzzle to predict how the particles that are “invisible” in DEM (sub-DEM particles) respond to an energy input. The combination of these two models can be defined as the particle interaction model and it is continuously improved to more robust models describing quantitatively effects such as the grinding media size, energy input, size of particles in the bed (Barrios *et al.,* 2012).

The mechanistic modeling as proposed in 2009 used simpler assumptions to facilitate the testing of the model. The results obtained during the development indicated its great potential, which became evident from results shown in Figures VI-5 and VI-6. The assumptions regarding particle interaction considered in the simulations were:

- The collisions available from the balls are distributed on the ore charge based on the mass fraction on each particle size
- Particles captured on a single ball-ball event have the same probability to be exposed to a collision event
- Collision energy is equally distributed among the captured particles
- Particle capture occurs as if they were distributed on a monolayer bed

The suite of mathematical expressions that estimate the mass capture and the energy split is defined as particle interaction model. The preliminary results generated as the outcomes of the original development of the mechanistic model (Carvalho, 2009) used a simplified approach. The number of particles captured in a collision event was estimated as a function of ball and particle size

$$N_{cap,i} = 1 + a(d_b/d_i)^b \qquad \text{VI-18}$$

The parameters in Equation VI-18 were $a = 0.0021$ and $b = 1.7$, yielding, for instance, $N_{cap} = 1$ for 8 mm particles and $N_{cap} = 47$ for particles measuring 63 μm. Then, the mass of material captured for each particle size class in the collision could be calculated by multiplying the number of particles in the size by the average mass of a particle of class i ($\overline{m}_{p,i}$), giving

$$m_i = N_{cap,i}\overline{m}_{p,i} \qquad \text{VI-19}$$

In an early work, Bourgeois (1993) recognized that particles positioned between colliding grinding media absorb different proportions of the stressing energy, according to their radial position in the bed. On the original formulation of the mechanistic model (Carvalho, 2009), for the case of relatively coarse particles, it was reasonable to assume that the collision energy splits equally among particles positioned within the active zone of breakage in a mill. In this case, the energy distribution function may be given by the Dirac delta type function, given by

$$p(e) = \delta\left(e - 1/N_{cap,i}\right) \qquad \text{VI-20}$$

As presented in section VI.2, although the simulation outcomes were good, describing the non-first order effects on the breakage rates of the coarse particles as observed on the literature, simulations described only qualitatively the experimental results. In order to improve simulations it was identified that the simplifying assumptions had to be revised, leading to an improved and detailed particle interaction model. In order to fill this gap, a detailed experimental study was conducted by Barrios (2010), which lead to a model of particle interaction that was later published (Barrios *et al.,* 2011). The idea of that work was to improve the particle interaction model by studing breakage of ore particles positioned on bed. One of the key observations from Barrios particle interaction model is that in the collisions inside a mill particle may be captured between: two grinding media, grinding media and mill liners, so all these contacts have to be described accordingly. Also on a single layer particle bed, there are a certain number of particle rings that might be captured in any collision event. This is shown on Figure VI-9, where the darker particles are those positioned closer to the center in the monolayer.

Assuming that when particles are stressed in a bed they are arranged according to a dense hexagonal packing, then the number of particles captured as a function of radius could be estimated by

$$N_{cap,i} = \frac{1}{4} + \frac{3}{4}\left(\frac{2r_c}{d_i}\right)^2 \qquad \text{for } r_c \geq \frac{d_i}{2}$$

VI-21

$$N_{cap,i} = 1 \qquad \text{for } r_c < \frac{d_i}{2}$$

where r_c is the radius of capture of the bed of particles, d_i is the mean size of the particles caught by the grinding media, estimated from the geometric mean of sieves containing the narrow size fraction.

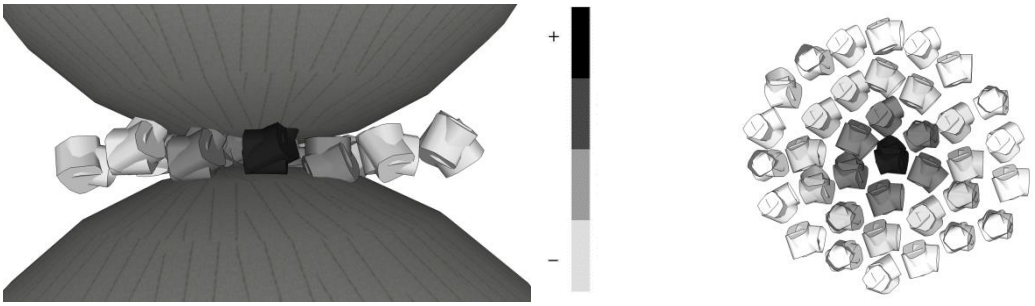

Figure VI-9 Graphical representation of grinding media impact on a monolayer particle bed (Barrios *et al.,* 2011)

The aim of the mass capture model is to estimate, when in a monolayer bed subject to impact loading, how many rings or number of particles of a certain size that would be captured. The next question to be answered is how the energy is split among these captured particles. One should note that there are important differences between stressing of a single particle and of particle beds. Whereas in stressing a single particle the amount of energy that is applied is known, in a bed of particles it is usually impossible to know with confidence the proportion of the stressing energy that particles positioned in different parts of the bed actually receive. In addition, in the case of a bed, a source of inefficiency is associated to the fact that part of the stressing energy is wasted in rearranging particles within the bed and as internal friction (Barrios *et al*., 2011). In stressing beds under unconfined conditions, an additional source of uncertainty is associated to the fact that most material contained in the bed will be ejected and escape from being stressed during the nipping phase, whereas under confined conditions only a rearrangement of particles will occur.

The experimental work required the use of an interesting method to estimate the radius range of particles captured by the falling ball. The particles were positioned on top of a carbon paper, so that after the collisions the particles hit by the ball left marks on the paper. By varying particle size, ball size, impact energy and ore type, Barrios covered a range of variables that are known to influence the capture radius. The final form of the model to predict the capture radius is a result which combines the contributions of the radius, r_e, of the elastic deformation zone and the contact radius, r_g, due to the geometry effect such as particle height. The total capture radius is then given by,

$$r_c = r_e + r_g \qquad \text{VI-22}$$

The radius of the elastic deformation zone resulting from the collision of two bodies is given by Hertz contact theory as (Johnson, 1985)

$$r_e = \left(\frac{15E}{16K_e}\right)^{1/5} K_g^{2/5} \qquad \text{VI-23}$$

where K_g is the geometric constant of the contact, given by

$$K_g = \frac{r_{c1}r_{c2}}{r_{c1}+r_{c2}} \qquad \text{VI-24}$$

and the elastic constant of the contact is given by (Tavares and King, 2004)

$$K_e = \frac{k_1 k_2}{k_1 + k_2} \qquad \text{VI-25}$$

where r_c and k are the radius of curvature and the elastic stiffness of each of the bodies in contact, respectively.

Whenever particles are present, it is necessary to account for the fact that the radius of the zone in which particles are captured increases due to the influence of their height and to the degree of penetration of the striker in the bed during breakage:

$$r_g = \sqrt{\left(\frac{d_b}{2}\right)^2 - \left[\frac{d_b}{2} - h\left(\frac{\Delta}{h}\right)\right]^2} \qquad \text{VI-26}$$

in which Δ is the maximum deformation of the bed during impact. In the case of a monolayer bed, the initial bed height (h) may be considered equal to d_i, although it is

certainly influenced by particle shape. The ratio Δ/h is defined as the maximum relative deformation of the bed and can be fitted to experimental data with the application of the mechanistic model.

$$\frac{\Delta}{h} = a_c \left[1 - \exp\left(-b_c \left(\frac{E}{E_{50b,i}}\right)^c\right)\right] \qquad \text{VI-27}$$

in which a_c, b_c and c are constants that must be fit to data. It accounts for the fact that the greater the magnitude of the impact energy, the higher the maximum relative deformation of the bed. It also considers that, the smaller the median material- and size-specific fracture energy of the particles being nipped, the greater the relative deformation. Data from impacts involving different ball diameters, particle sizes and materials (copper ore and limestone) were fit to Equation IV-28.resulting in the constants $a_c = 0.3621$, $b_c = 0.1517$, and $c = 0.4125$, which were found to be reasonably valid for both materials and all size ranges studied (Barrios, 2011).

By simply using the particle interaction model equations it is possible to calculated the number of particles captured in collisions of balls of different sizes at different impact energies (0.1 and 1.0 J) as shown on Figure VI-10.

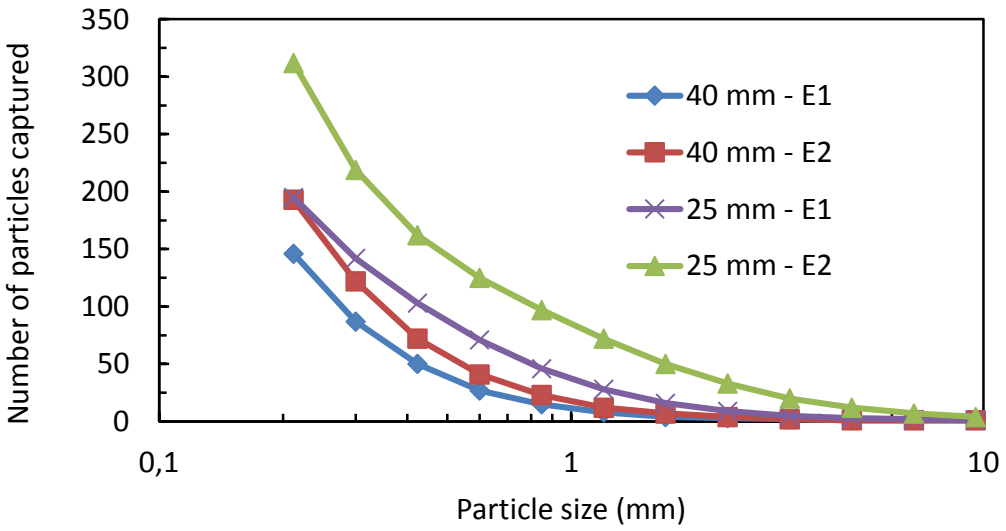

Figure VI-10 Effect of ball size and particle size in the monolayer bed in the number of captured particles for a copper ore for two different impact energies (E1 = 0.1 J and E2 = 1.0 J)

An important feature of the present model is its amenability to extrapolation, given that it provides a detailed description of the influence of the most relevant variables, which include particle size, impact geometry, impact energy and the material-specific particle fracture energy. This is particularly advantageous regarding its application in predicting breakage for modeling grinding mills (Carvalho and Tavares, 2009) given the widely different impact energies, ball diameters and particle sizes that may be found within the comminution environment.

The second part of the model is the energy split relationship. The equal partition among the particles approach has often proven to overestimate breakage (Barrios *et al.,* 2011). Bourgeois (1993) has suggested from his experiments that whenever a falling ball hits particles in a bed, particles in the center would undergo more intense breakage than those located at the vicinity. Therefore, a more appropriate description of the energy split was proposed in the work of Barrios *et al.* (2011). The authors proposed that energy split is estimated assuming an empirical monotonically decreasing continuous function $F(r)$, which depends on the distance from the center of collision r, given by

$$F(r) = \exp\left[-0.693\left(\frac{r}{r_{50}}\right)^{\alpha_r}\right] \qquad \text{VI-28}$$

where α_r and r_{50} are model fitting parameters.

Then they discretized the bed in *n* radial rings from the center (*r* = 0) to the border of the contact disc ($r = r_c$) with the values $r =$ 0, 1, 2, … n, giving 0, r_1, … r_{n+1}. As a result, the number of particles captured in each individual ring *q* may be calculated assuming that spherical particles of radius r are arranged from a central position as the particle arrangement displayed on Figure VI-9

$$n_{cap,q} = \frac{3}{d^2}\left(r_{q+1}^2 - r_q^2\right) \qquad \text{VI-29}$$

One assumption had to be made: if the mass M_b of material contained in the bed is smaller than the mass of material estimated to be captured in the bed, m_i (Equation IV-19), owing to the fact that some of the outer bed rings may be absent, then the actual radius of capture r_c' may be calculated by

$$r_c' = d\left[\frac{1}{3}\left(\frac{M_b}{\overline{m}} - \frac{1}{2}\right)\right]^{1/2} \quad \text{VI-30}$$

Further, whenever $r_q > r_c'$, then $n_{cap,q}$= 0.

Particles contained in the q-th ring around the center of contact will receive a proportion of the collision energy from the ball, given by

$$f(r_q) = \frac{F(r_q)}{\sum_{l=1}^{n}[F(r_l)]} \quad \text{VI-31}$$

which ensures that $\sum_{l=1}^{n} f(r_l) = 1$. The fraction of energy received by each particle contained in the bed may be calculated by

$$e_q = \frac{f(r_q)}{n_{cap,q}} \quad \text{VI-32}$$

The mass fraction of particles contained in the bed that receive this fraction of the energy may then be calculated by

$$p(e_q) = \frac{n_{cap,q}}{N_{cap}} \quad \text{VI-33}$$

The validity of the model was demonstrated as the simulation of bed breakage predicted the experimental results obtained by Bourgeois (1993). These results can be found elsewhere (Barrios *et al.*, 2011)

VII. Experimental

Data used in this thesis for model development included results obtained from several physical experiments that were conducted previously and that were part of the LTM material database, as well as during the course of this thesis. The tests included those that dealt with the characterization of breakage response of individual particles, yielding the breakage function, the distribution of fracture energies and the damage accumulation characteristics. In addition, a number of grinding experiments have been done, including laboratory scale ball milling in LTM, pilot scale semi-autogenous and autogenous grinding on external facilities. This chapter will briefly describe the procedures adopted and the outcomes of each test used.

VII.1 Materials and characterization tests

Research conducted at Laboratório de Tecnologia Mineral has generated an extensive database containing particle breakage test results for a variety of rocks and ores. Data from selected ores has been used in the present work, which include:

- Measurement of the distribution of particle fracture energies, using the Impact Load Cell
- Measurement of the amenability to fracture under repeated low-energy impacts, using the impact load cell
- Measurement of the energy-specific single-particle breakage function, using the drop weight test
- Measurement of the self-breakage characteristics, using drop shatter tests;
- Measurement of the rate of generation of fines by surface breakage (abrasion) using the JK abrasion mill
- Batch grinding tests.

Some of the characterization tests follow procedures that have become standard in industry worldwide such as the Drop Weight Test (Napier-Munn *et al.,* 1996) while others follow internal standards at LTM, including measurements of particle fracture energies and batch ball mill grinding tests.

Several criteria were used for selecting the ores that were used on the present work. The first was related to the availability of sample for conducting the tests. Second, the availability of data from industrial or pilot plant scale grinding tests was desirable. There was a total of six ore samples that were selected: a copper ore, two limestone samples, two iron ores and one granulite.

Breakage characterization started with standard Drop Weight Tests on single particles in order to obtain information from the single-particle breakage function of these ores. The general procedure adopted in the test is described on Napier-Munn *et al.* (1996). Samples of one hundred particles were subjected to impacts at each energy level in the present work. Each particle is broken individually and after each impact, the fragments are collected. The result is a single size distribution describing the breakage product of the collective of the sample. The particle size distribution characterizes the t_{10}parameters related to the impact energies. From at least three values of t_{10}at different impact energies, the values of the A and b parameters were fitted to Equation III-13. A summary of the parameters obtained for all six ores is presented on Table VII-1.

For each ore sample the particle sizes tested were: 63-53 mm, 45-37.5 mm, 22.5-31.5 mm, 22.4-19 mm and 16-13.2 mm. The specific impact energies were, approximately, 360 J/kg, 900 J/kg, 1,800 J/kg, 3,600 J/kg, 9,000 J/kg and 18,000 J/kg. At least three impact energies were used for each particle size. As the standard DWT does not require testing particles contained in sizes below 13.2 mm, some additional tests were conducted on particles in the size ranges of 2.83-2.36 mm and 5.6-4.75 mm.

Table VII-1 Full list of material parameters used on the simulations in this thesis

	Copper ore	Granite	Limestone #1	Limestone #2	Iron ore #1	Iron ore #2
E_∞ (J/kg)	60.0	130.7	7.0	150.0	44.9	16.8
d_o (mm)	400	1.1	100	0.79	4.3	20.1
$\emptyset$ (-)	0.45	1.99	0.80	1.30	1.28	0.84
σ_∞	0.40	0.90	0.39	0.30	0.46	0.40
σ_0 (mm)	1	0.173	10.47	1	1	1
σ^*	0	1.65	0.08	0	0	0
$\alpha_{1.2}/\beta_{1.2}$	0.51/11.95	0.43/10.26	0.19/7.78	0.08/8.76	0.98/5.99	1.78/22.03
$\alpha_{1.5}/\beta_{1.5}$	1.07/13.87	0.92/10.74	0.56/7.51	0.56/7.48	1.01/5.01	2.45/20.67
α_2/β_2	1.01/8.09	1.31/9.15	0.78/5.55	1.31/7.57	1.36/3.80	1.53/8.26
α_4/β_4	1.08/3.03	1.18/2.97	1.12/3.01	1.21/3.03	1.22/2.17	1.50/3.64
α_{25}/β_{25}	1.01/0.53	0.93/0.49	1.17/0.54	0.98/0.50	0.95/0.67	0.82/0.42
α_{50}/β_{50}	1.03/0.36	0.92/0.39	1.43/0.40	0.98/0.31	0.89/0.48	0.76/0.24
α_{75}/β_{75}	1.03/0.30	0.90/0.31	1.92/0.42	0.95/0.22	0.92/0.41	0.70/0.16
γ	5.0	5.4	5.4	5.0	3.0	5.0
ρ (g/cm³)	2.93	2.79	2.71	2.98	4.35	2.8
β (-)	0.62	0.64	0.60	0.62	0.62	0.62
A (%)	67.7	47.5	53.3	63.4	60.4	44.2
b' (-)	0.029	0.027	0.033	0.033	0.051	0.029
t_a (%)	6.7	6.7	1.6	5.0	1.6	0.2
d_A (mm)	0.25	0.25	0.21	0.21	0.21	0.30
λ (-)	0.3	0.3	0.3	0.3	0.3	0.3

From the DWT results, the table of t_{10} versus t_n can also be extracted. The procedure described on section III.3.1 to extract the values of t_ns from the product size distributions was applied. In order to provide a more detailed description of the particle size distribution of sizes immediately below the original particle size, the values of $t_{1.2}$ and $t_{1.5}$ were used in addition to the standard value of t_2, t_4, t_{25}, t_{50} and t_{75}. Figure VII-1 shows the values of t_ns plotted against the t_{10} from each drop weight test for Limestone #1. The complete list of parameters can be found on papers published by the LTM research group (Tavares and Neves, 2008; Barrios *et al.,* 2011).

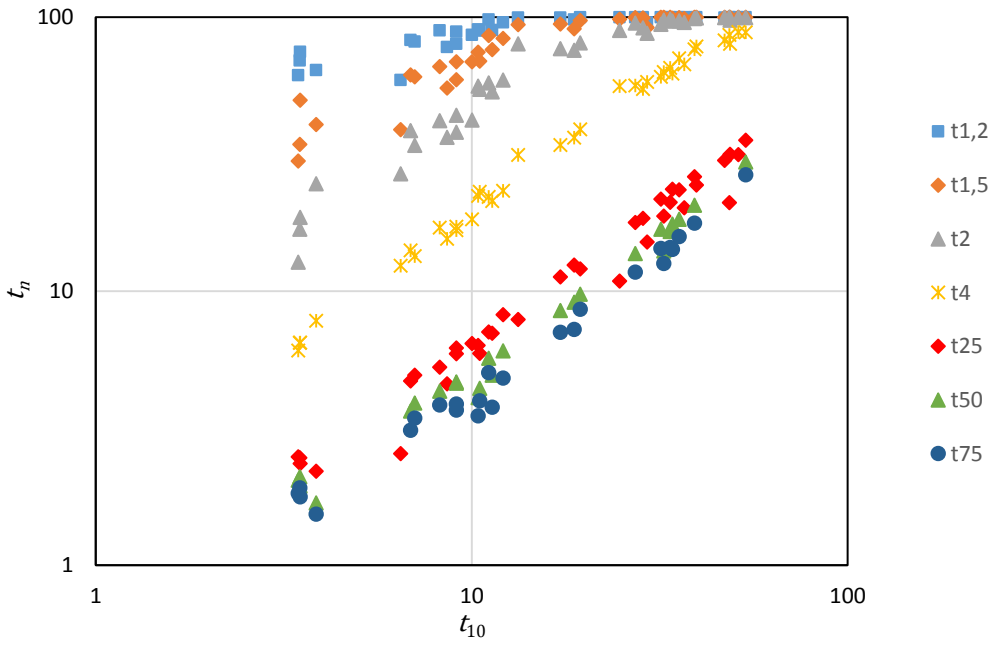

Figure VII-1 t_{10} versus t_ns plot of DWT results for the Limestone #1

Fracture energy measurements were carried out using the Impact Load Cell (Figure III-5) and required usually 50 particles for each mono-sized sample per ore. Sizes fractions tested were: 63-53 mm, 45-37.5 mm, 22.4-19.5 mm, 11.2-9.50 mm, 5.60-4.75 mm and 2.83-2.36 mm. Results for the copper ore expressed on terms of the median mass-specific fracture energy are shown on Figure VII-2. The full test procedure is explained in details in Tavares (2007). Also, the combination of results from drop weight tests and impact load cell allows the estimation of the b' parameter of Equation III-15. Figure VII-3 shows the t_{10} plot from the application of Equation III-15 for the different ores used on simulations in this Thesis. The maximum value of t_{10} ranges from 44 % (iron ore #2) to 67 % (copper ore). Breakage of iron ore #1 results in higher t_{10} values for a given ratio of impact energy/fracture energy.

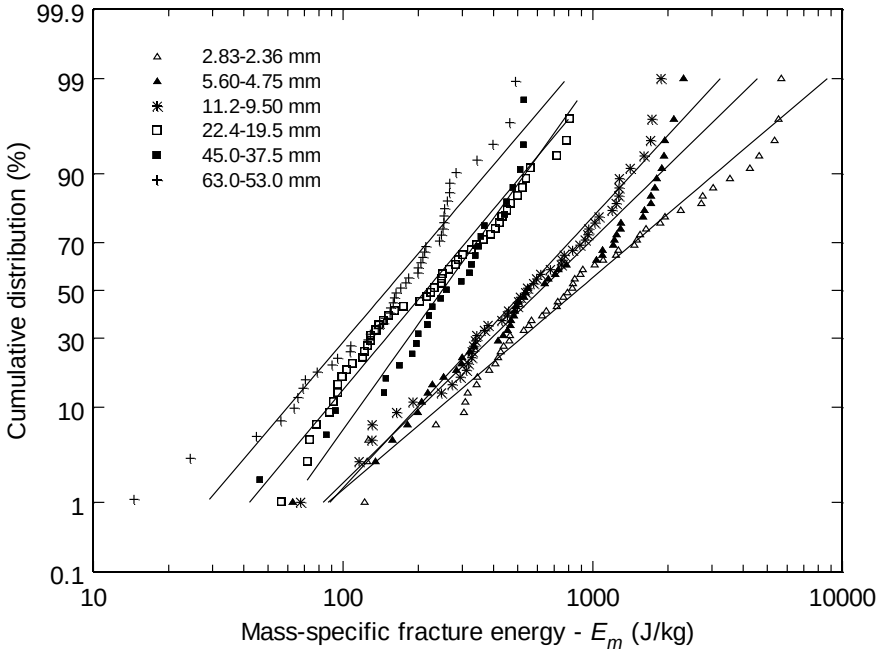

Figure VII-2 Results from fracture energy measurements of copper ore

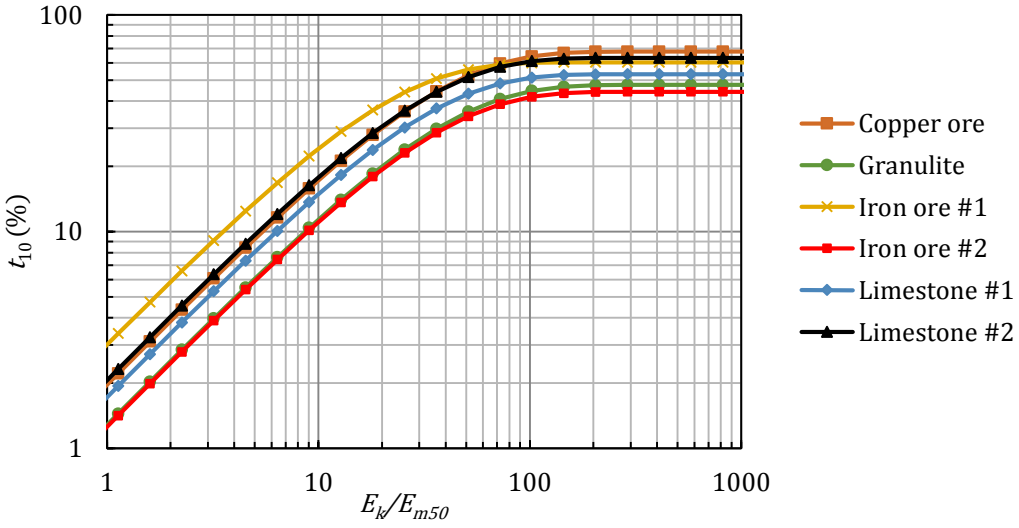

Figure VII-3 Modelled t_{10} energy ratio relationship for the different ores used in this Thesis

In order to characterize the mass loss due to low energy impacts the standard JKMRC abrasion test (Napier-Munn, 1996) was used. In these tests, samples of 3 kg of

55-38 mm are ground for 10 minutes in a 30 x 30 cm mill equipped with four 10 mm lifter bars rotating at 53 rpm (70% of critical speed). The final product is removed from the mill and sieved on a $\sqrt{2}$ series of screens. The result is given by the t_a number which is 1/10th of the percentage passing the size of 4.5 mm, which is the t_{10}. The values of t_a for the selected ores are listed on Table VII-1.

Repeated impact tests were carried out using the same Impact Load Cell used in particle fracture energy measurements, with the difference that the absorbed energy was not recorded. IT was used at least one hundred particles per test contained in a preselected size fractions for the ore sample in question. Size fractions used in the present work were 45-37.5 mm, 22-19.2 mm and 11.2-9.5 mm. Three impact energy levels were used for each particle size: 360 J/kg, 180 J/kg and 90 J/kg. In this test, particles were individually submitted to impact by a falling steel ball and have their mass recorded after each collision, repeating the impact procedure for each particle. Whenever the particle mass is smaller than 10 % of its mass at before the impact it is considered broken. The result can be plotted as the number of broken particles as a function of number of impacts, as shown in cumulative form in Figure VII-4. The damage parameter was then calculated from the simulation of the repeated impacts experiments using the model described on section III.3.3. As such, the damage parameter is fitted in order to minimize the sum of squares between the experimental results and the model.

In order to characterize the amenability of coarse particles to break when they are submitted to free fall inside the mill the self-breakage tests were conducted. The test consisted in dropping a single particle repeatedly from a certain height on to a steel plate firmly fixed on the floor. Drop heights chosen were 2 meters, 4 meters and 8.4 meters. Particle size ranges were 125-75 mm and 75-53 mm. The mass and size of each particle was tracked after each impact. This allowed the calculation of the average mass loss per impact cycle, which was useful to estimate the abrasion or surface breakage rate. Also, the impact number which the particle was broken or lost 10 % of its initial mass was also logged. Results from tests on 125-75 mm copper ore particles are presented on Figure VII-4.

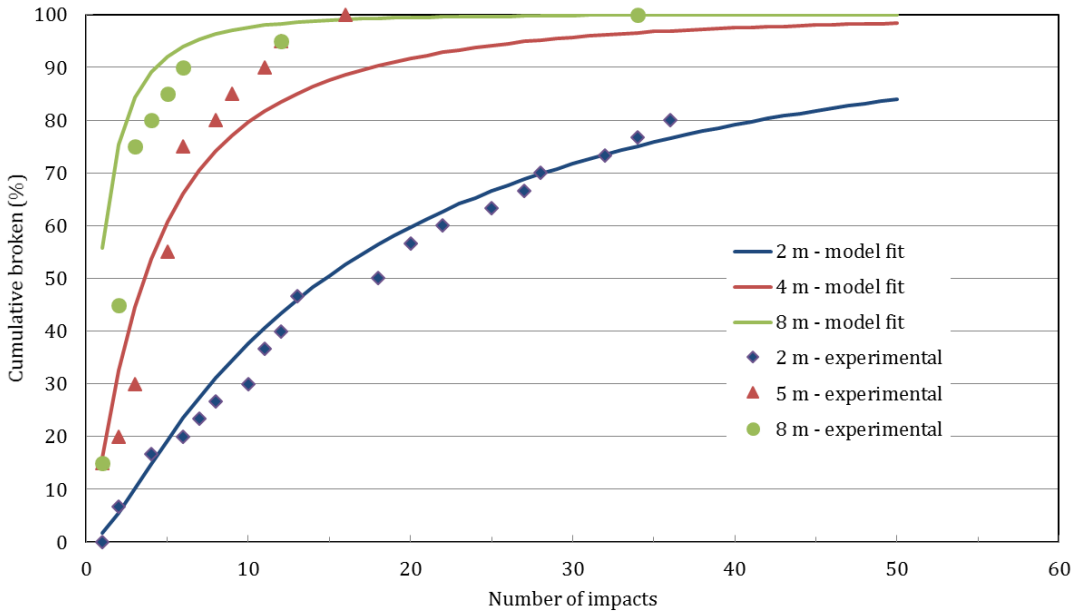

Figure VII-4 Typical result of the self breakage test of 125-63 mm copper ore particles comparing experimental measures with the model fitted through the damage parameter estimation

Batch grinding tests were conducted on a laboratory scale mill measuring 30.5 cm of length and 30.5 cm of diameter. The mill was equipped with four lifter bars of 27 mm width, 7 mm height and 30.5 cm length. The samples selected for the tests were classified on narrow size ranges: 9.5-6.3 mm, 4.75-3.35 mm, 3.35-2.35 mm, 1.70-1.18 mm, 0.85-0.60 mm, 0.425-0.300 mm and 0.212-150 mm. Ball filling was kept at 30 %, which is equal to 29.8 kg of steel balls. Ball sizes were 25 mm in diameter. Powder filling was calculated to be 100 %. Mill speed was fixed at 54 rpm, corresponding to 67.5 % of critical speed.

The test procedure consisted of first filling the mill with alternate layers of balls and powder (Figure VII-5), then grinding for a short period of time (usually 30 seconds). The mill contents were then dumped on a tray equipped with a coarse screen on top to separate the balls from the ore sample (Figure VII-6). A representative sample of the ore particles was then subjected to sieving and then fed back to the mill to be ground again. Usually the grinding times chosen were 30 seconds, 2 minutes, 8 minutes and 20 minutes.

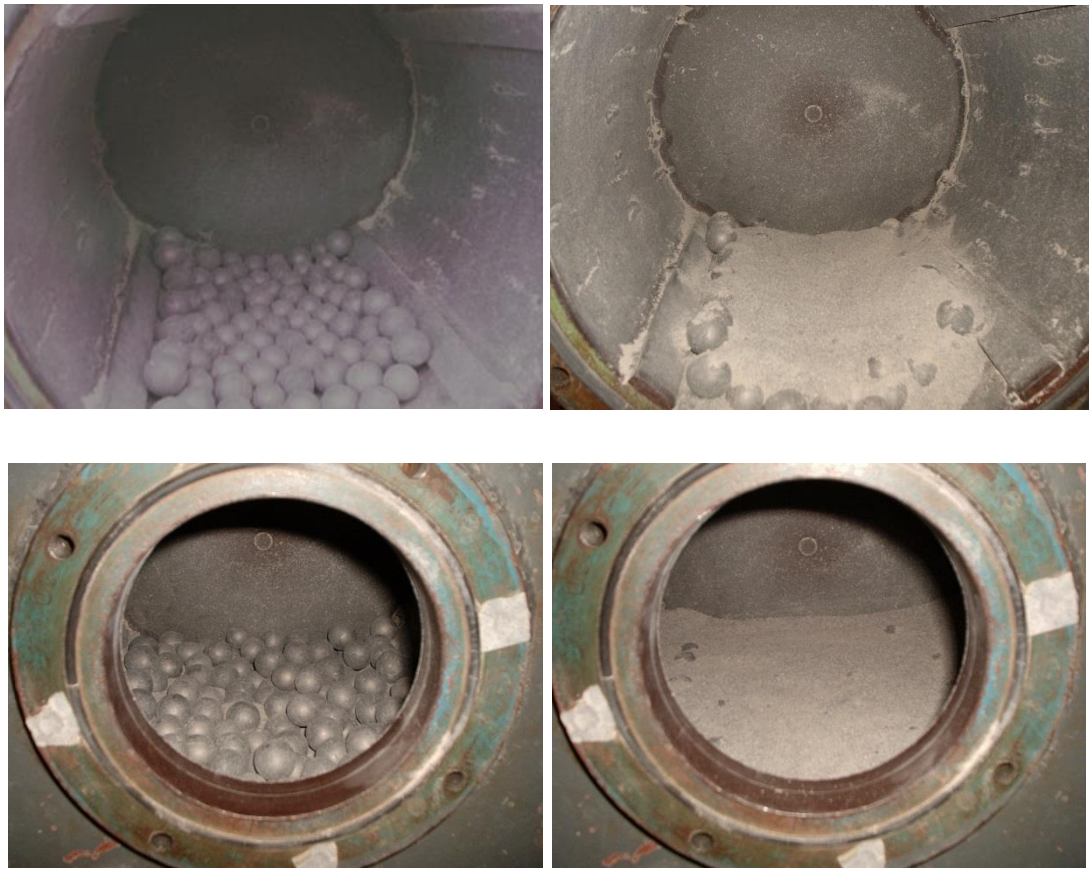

Figure VII-5 Sequential steps of the batch mill loading procedure

Figure VII-6 Charge dumping procedure after each grinding time

Another set of batch grinding tests were available to use as basis for modelling to provide information on the breakage of coarse particles, caused either by ball impacts or self-breakage. The procedure was similar to the batch ball mill test described previously

though the mill and particle sizes were different. The mill used was a 62 cm in diameter mill equipped with 20 squared lifter bars of 5 x 5 mm in width and height and the mill length is 31.4 mm. A three dimensional representation of the mill is presented on Figure VII-7. The size fractions tested were 76.2-50.8 mm, 50.8-38.1 mm, 38.1-25.4 mm, 25.4-19.0 mm and 19.0-12.7 mm. The ball filling was 10 %, resulting in 44 kg of 63 mm steel balls. The ore filling was 15 %, which was equivalent to 26.4 kg of ore particles. The total mill filling was 25% and the speed was 42.6 rpm or 57.72 % of critical speed. The disappearance plot for each mono-size test is presented on Figure VII-8.

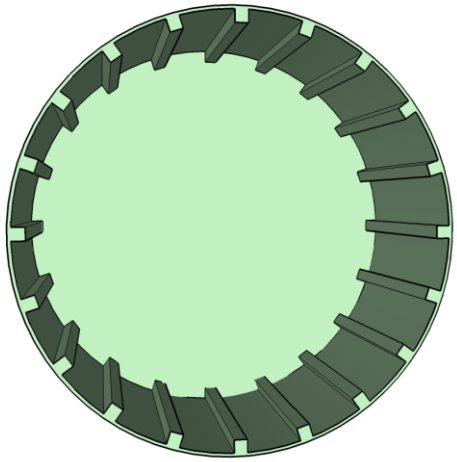

Figure VII-7 Internals of the 60 cm diameter mill used for SAG batch grinding tests

These typical results suggest that, for all sizes, there is some degree of breakage occurring during the first minutes of grinding. This is noticed by the steep decrease in the percentage remaining in the original classes. Then, for the coarser particles, the remaining fraction evolves following a first order trend. This happens because all the weak particles in the population have already been broken and the mass loss is caused by the abrasion of the tough particles. For fine particles, the energy provided by the balls is high enough to guarantee that they will break the remaining particles, this effect among to the damage and weakening of these particles keeps the breakage rates almost constant during the grinding.

A set of data from pilot scale semi-autogenous grinding tests was available to test the model. This data were obtained from a series of tests conducted in a 1.8 diameter

SAG mill, equipped with sixteen belly lifters and eight lifters on the discharge grate and on the feed end cone (Figure VII-9). The mill discharge has grate openings of 12.5 mm and the discharge grate was, for the selected test, equipped with pebble ports measuring 2.5 inches (63 mm) (Figure VII-10). A trommel, that is, a rotating cylindrical screen, was attached to the mill discharge end to retain the coarse particles (pebbles) and steel ball scats. The trommel undersize was then fed to a screw classifier. In selected tests, the coarse product of the classifier was sent back to the mill, thus closing the grinding circuit. The mill was installed on top of a set of load cells, which after proper calibration provides the total mass of the hold-up (ore particles) with an accuracy of 1 kg. Each test consisted on feeding the mill with fresh material until the ore load reached a target value, which was previously calculated based on the desired ore filling. Depending on the ore competence, the fresh feed rate required changes in order to maintain the mill filling constant at the target value. The fresh feed was transferred to the belt that fed the mill using wheel barrels, and the mass on each wheel barrel was strictly controlled by collecting the right amount of mass of ore particles of certain sizes from stockpiles containing particle of the required size range. Once the grinding circuit operation reached steady state the samples were collected from the discharge streams. The mill was then crash stopped and its contents were removed and sieved in order to estimate the hold-up size distribution.

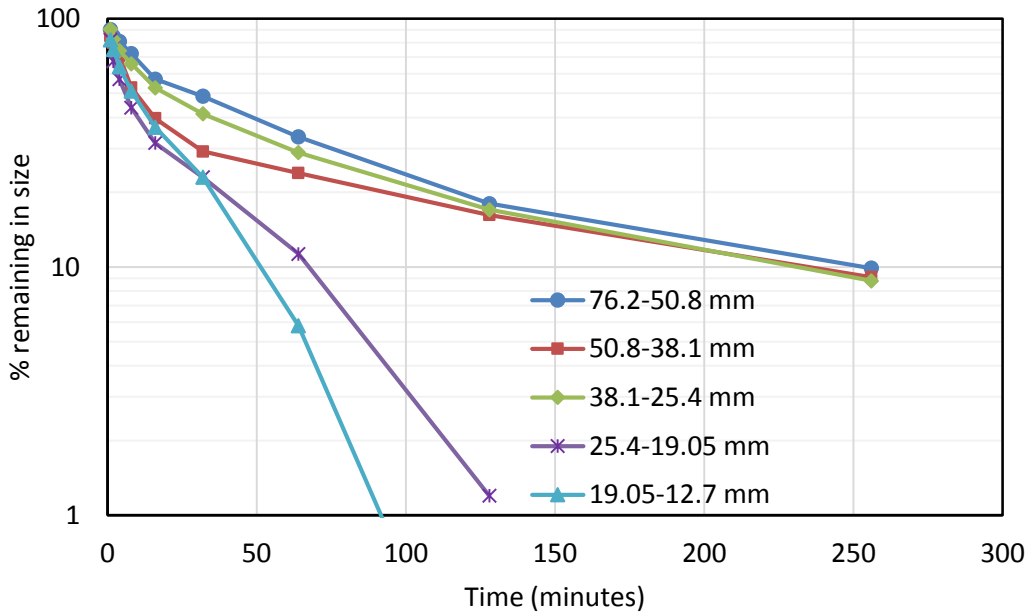

Figure VII-8 Disappearance plots of the 60 cm SAG batch grinding tests

Figure VII-9 Pilot scale 1.8 m SAG mill

Figure VII-10 Worn-out part of the discharge showing the grate openings and the square shaped pebble ports measuring of 2.5 inches (63 mm)

Eleven tests were conducted, which covered the following range of operation parameters:

- Ball top size: 4” (101 mm) to 5” (125 mm)
- Mill speed: 72 to 76% of critical speed
- Mill filling: 24 to 26%
- Ball filling: 0 to 15%
- Solids concentration inside the mill: 72 to 80% (w/w)

For each of these tests the following data was available:

- particle size distribution of fresh feed, mill contents and mill discharge streams,
- solids concentration in the different streams,
- power draw.

The particle size distributions of the mill feed for all eleven cases are shown on Figure VII-11, which demonstrates that most of them follow the same trend. The outliers are: case 06 which shows a finer feed, and cases 05 and 07 which shows a coarser mill feed. These cases will be discussed later among the simulations results. The products of the mill for all the cases are displayed on Figure VII-12, which shows the same trend, and case 05 being the outlier as it is a coarser particle size distribution. The particle size distribution of the ore contents for each test is presented in Figure VII-13. The range of variation of the particle size distributions of the hold-up is significant and its effect on the grinding energy environment will be analyzed in the context of DEM simulations of the charge motion.

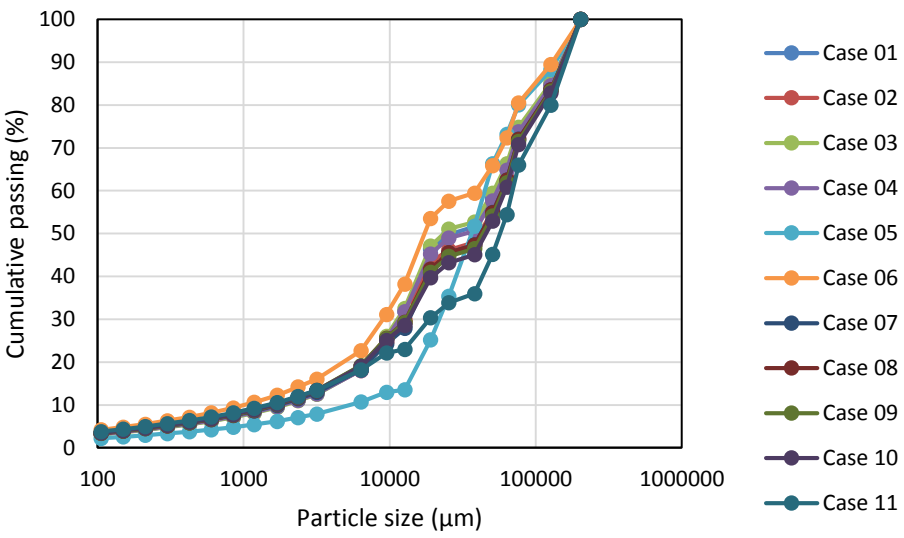

Figure VII-11 SAG mill feed size distribution for the pilot plant tests

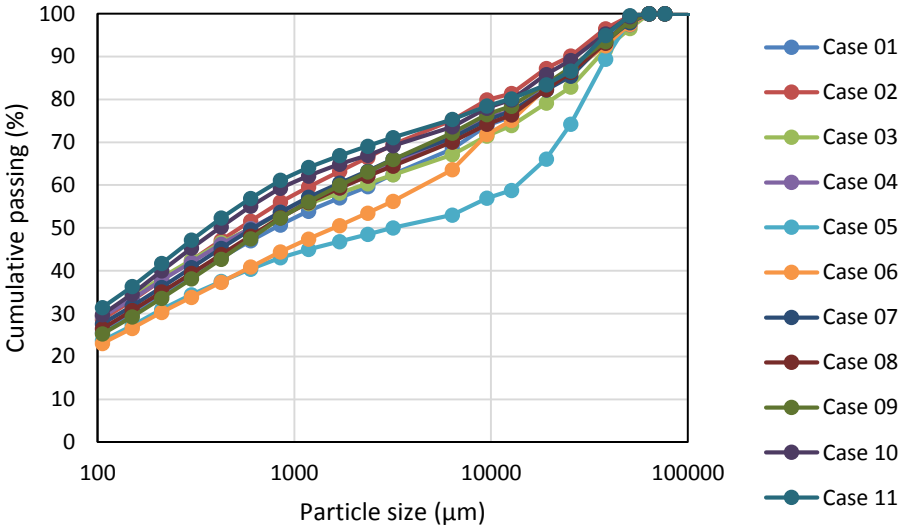

Figure VII-12 SAG mill discharge size distribution for the pilot plant tests

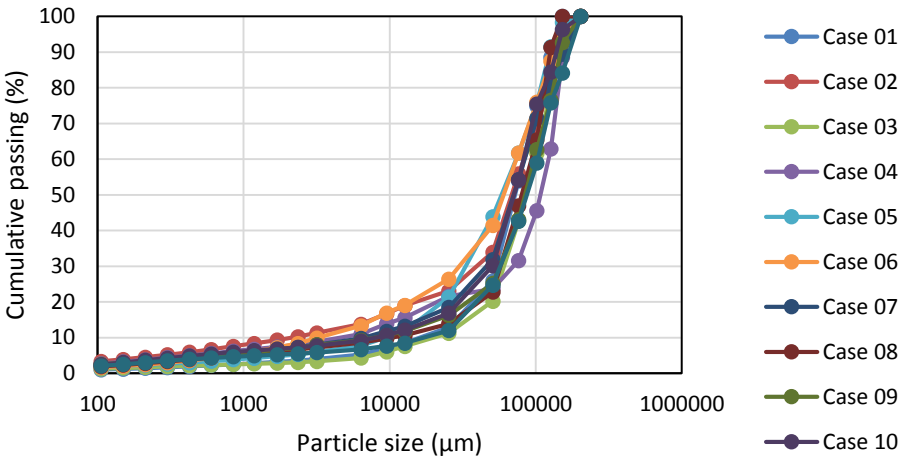

Figure VII-13 SAG mill ore charge size distribution in the pilot plant tests

The mill geometry was modeled into 3-D CAD using Sketchup® (Trimble, 2012) in order to provide detailed enough information for DEM simulations. Details of the mill are shown in Figure VII-14 and Figure VII-15.

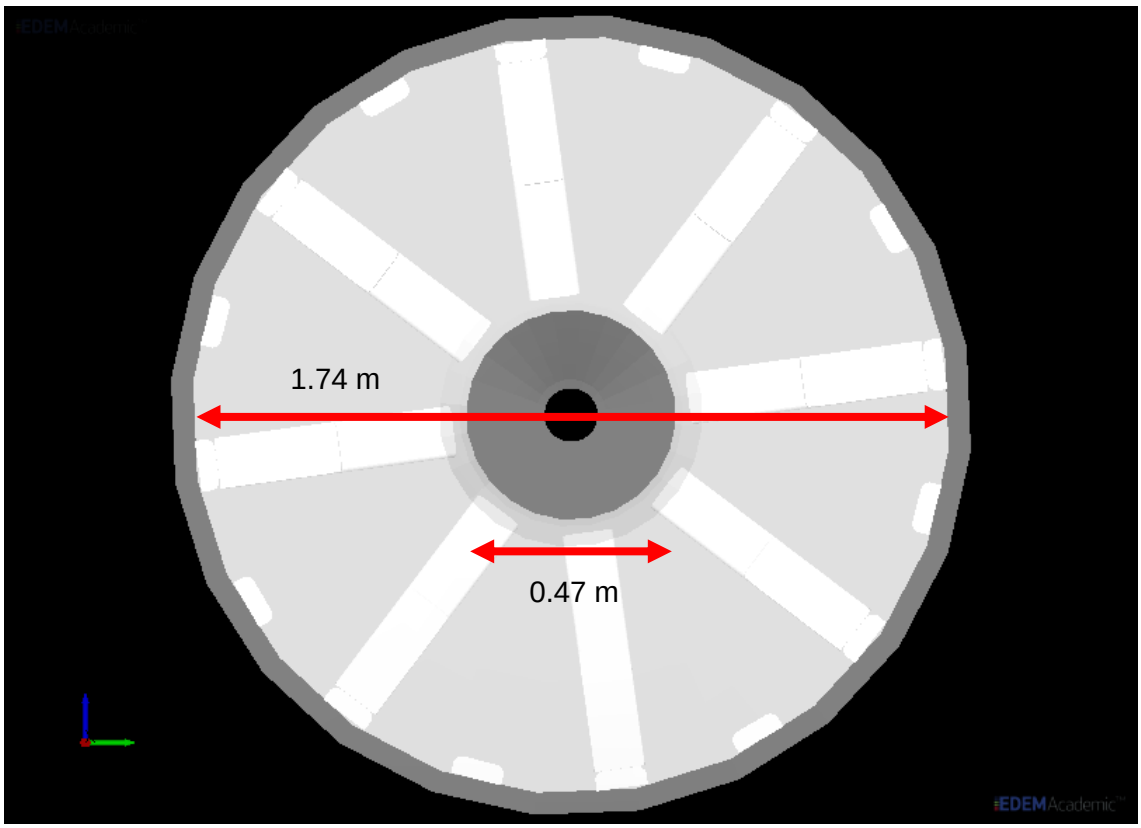

Figure VII-14 Mill section slice (internal diameter is 1.74 and feed opening is 0.47 m in diameter)

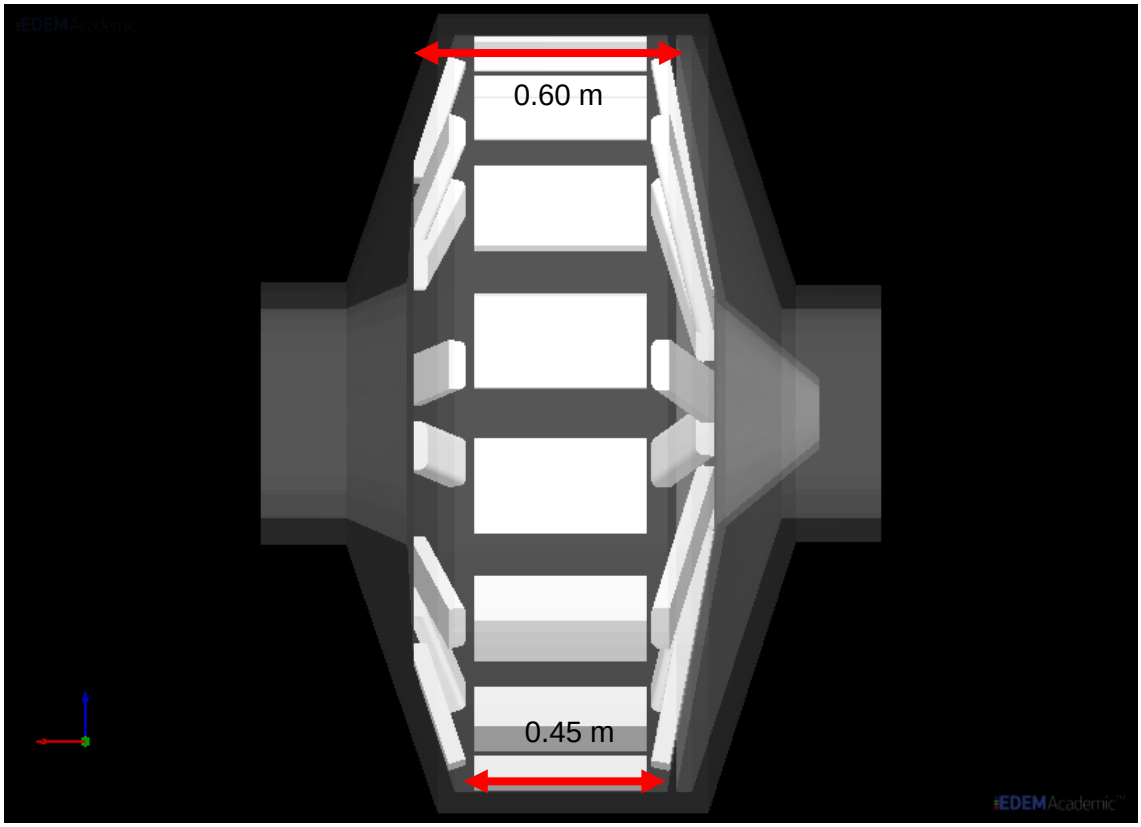

Figure VII-15 Internal structure of the mill showing the conical section profile

VII.2 Parameter calibration for DEM simulations

A number of experiments were carried out in order to estimate the values of the parameters used in DEM simulation that could more appropriately reproduce the material behavior inside the mill. One of the experiments conducted is a bench scale repose angle test (Figure VII-16), in which a certain amount of particles are placed inside an empty cylinder and the result is the angle formed by the particles after quickly pulling up the cylinder, as depicted in Figure VII-17. This test aims at estimating the friction coefficient of contacts among ore particles and ore particles against the steel surface. In the latter case, the platform for the repose angle is a steel plate. In order to demonstrate the validity of the set of parameters chosen, tumbling tests were conducted on the 30.5 cm x 30.5 cm mill equipped with four lifter bars. This mill is the same used in the batch grinding tests. In this case, the front lid of the mill was replaced by an acrylic lid, which allows observing the mill contents while the mill is in motion. Experiments were recorded using a standard point-and-shoot camera (Kodak) at a recording speed of 30 frames per second. Although it did not allow identifying the individual particles inside mill, it allowed

visualizing the cloud of particles representing their movement and general positions. The optimal set of parameters estimated is listed on Table VII-2 (Carvalho and Tavares, 2011).

Figure VII-16 Repose angle test to determine friction coefficients between ore particles

Figure VII-17 Result of the repose angle experiment with 9.5-6.3 mm particles of iron ore

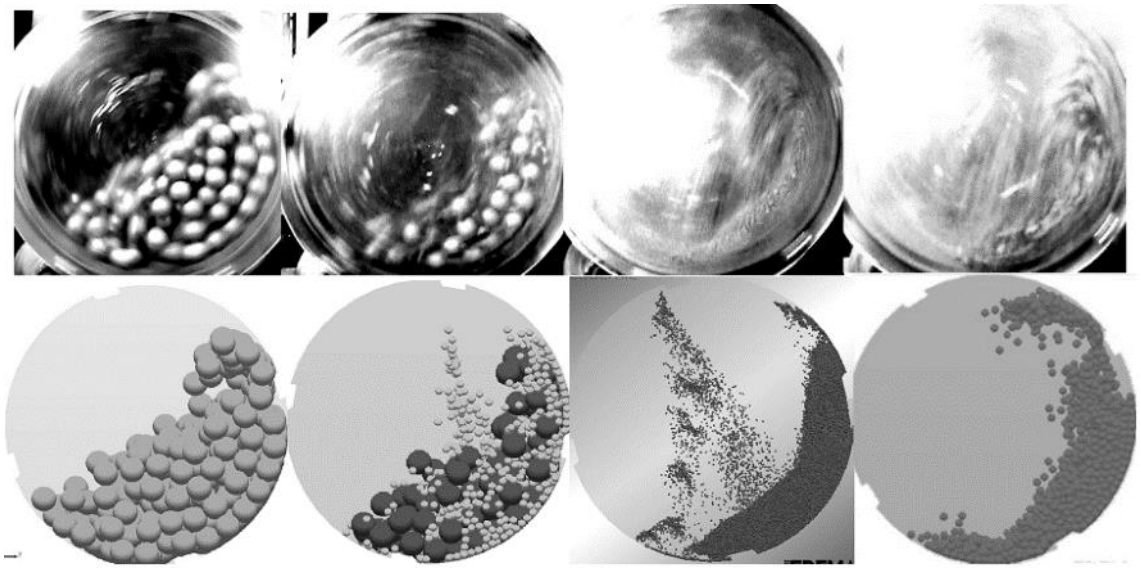

Figure VII-18 Comparison between the experiments and the validated DEM simulations for different mill fillings (Ramos *et al.*, 2011)

Table VII-2 Set of DEM parameters for the simulations in this work (Carvalho and Tavares, 2011)

Parameter	Steel (balls and liner)		Particles (copper ore)
Poisson´s ratio	0.30		0.25
Shear modulus (GPa)	70		0.1
Density (kg/m³)	7800		2930
Contact	Restitution coefficient	Static friction coefficient	Rolling friction coefficient
Ball-ball / Ball-liner	0.70	0.20	0.01
Particle-particle (ore)	0.51	0.35	0.20
Particle-ball / Particle-liner	0.35	0.39	0.36

VIII. DEM Simulations

The software used to run DEM Simulations was EDEM, which has been updated to newer versions during the last four years. This software is provided by Dem Solutions Ltd., (2010) and allows quick construction of the simulation. Once the contact model parameters have been calibrated the DEM simulations provides good visual representation of the charge motion. However, to process and understand its quantitative outcomes represents a challenging task.

As shown in Chapter V, the contact models available to use DEM simulations of tumbling show very similar behavior (Table V-3). For the case of tumbling mills, in which the particles placed inside DEM environment are the grinding media, being steel balls and coarse ore particles, the Hertz-Mindlin no-slip model (Mindlin, 1949) is applicable.

This chapter describes the data extraction and post-processing of the outcomes from DEM simulations. Also, it reports the results from DEM simulations of all the mills simulated in this Thesis.

VIII.1 Data collection

The myriad of data generated form a DEM simulation of a tumbling mill needs to be treated properly. In order to facilitate data extraction and reduce some of the repeated analysis stages, a computational tool was developed. The type of information generated that are useful when analyzing the mill performance are:

- Positioning of the particles as function of time
- Number/frequency of collisions
- Magnitude of the collisions
- Type of elements involved in collisions
- Power draw
- Particle velocities.

The way EDEM handles the data from simulation is by tracking the positions of the particles, their speeds and rotational vectors. The software saves instant information of these parameters for each element in the simulation at pre-defined time steps. These

time saving steps went from 0.1 seconds to 0.01 seconds depending on the size of the simulation. For example, for longer simulations the saving time interval was increased to 0.1 seconds in order to save disk space. As stated by Powell *et al.* (2008), the data generation from DEM simulations can reach the size of several gigabytes.

For all the DEM simulations of mills performed in this thesis, the data extraction to analysis was made after the charge motion reached a pseudo-steady state. This is checked by observing the fluctuations on the center of mass of the mill. Usually, it takes a few revolutions to stabilize the charge, but due to the chaotic behavior of the elements inside the mill, a level of fluctuations is expected as it is observed on the power draw of ball mills from laboratory to industrial scale.

In addition to the particle data (position, speed, rotation) recorded in the simulations the collision data is also recorded. EDEM is able to store the data of each individual collision that occurred during the simulations. The energy is dissipated due to both components of the contact force (normal and tangential). As such, EDEM stores the data of the normal energy loss and the tangential energy loss of the collision, the spatial coordinates of the collision, the time instant of collision start and the duration of the contact that generates the collision. In addition, the identity numbers of the elements involved in the collision (particles and/or geometry elements) are also stored.

The data extraction code should correlate to the final use of the data. For instance, the simplest case of extracting the data from DEM simulation is the calculation of the mill power by using the center of mass of the charge. In order to do this, the mass and spatial coordinates of the particle elements on each time instant saved are required.

The simplest case is of a laboratory scale ball mill, in which the balls have the same diameter, or that are defined as within same size class. In this case, the DEM data treatment involves extracting the collision data and, separating the collision by type of contact involved which, in this case means two different collision classes: balls-balls and balls-liner. The 3-D geometry of this mill and a snapshot of the simulation in EDEM are shown in Figure VIII-1.

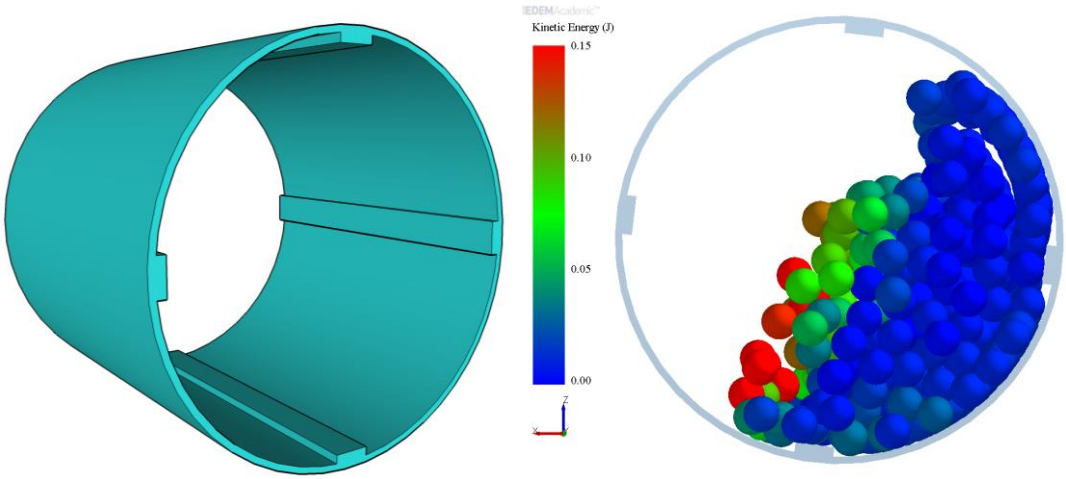

Figure VIII-1 Laboratory scale ball mill model and its simulation on DEM (30% filling, 67% of critical speed, ball size of 25 mm)

For more complex DEM simulations, such as those of autogenous and semi-autogenous mills and ball mills containing grinding media of several size classes, the treatment should take into account the different types of collisions that may happen inside the mill. As proposed by Carvalho (2009), the total number of collision classes may be estimated from a simple combinatory relationship,

$$N_k = (N_{balls} + N_{ore})\left[\frac{(N_{balls} + N_{ore} - 1)}{2} + (1 + N_{rev})\right] \qquad \text{VIII-1}$$

where N_k is the total number of collision pairs, N_{balls} is the number of ball size classes and N_{ore} is the number of ore size classes, N_{rev} is the number of materials in liner, which is considered to be unitary.

The number of classes concept is used directly in the currently version of the UFRJ ball mill model as presented on section VI.2 and also in the mechanistic model for AG and SAG mills developed as part of this Thesis.

In order to limit the volume of data that needs storing, collision energies with values lower than 10^{-8} J are neglected as they are considered just numerical residues from the model as stated by Weerasekara and Powell (2011). The collision energy histogram is created by distributing each collision into 1000 energy equally-spaced energy levels in log-scale bins. This number was chosen in a trade-off between the poorer resolution of the collision energy spectrum achieved with fewer bins and the large need for computer

memory to store the data that would be generated by using more bins, besides the greater computing effort required when simulating using UFRJ breakage model. Each individual energy spectra, from the different collision pairs, can also be combined to give an overall spectrum, being this the original approach used when simulating ball mills using the UFRJ model (Tavares and Carvalho, 2009), as showed on section VI.2. At that time, that was justified on the basis that the particle interaction model was described in a simplified manner, not taking into account the geometry of the contact, requiring information only about the magnitude and frequency of the collisions in the mill (Figure VIII-2).

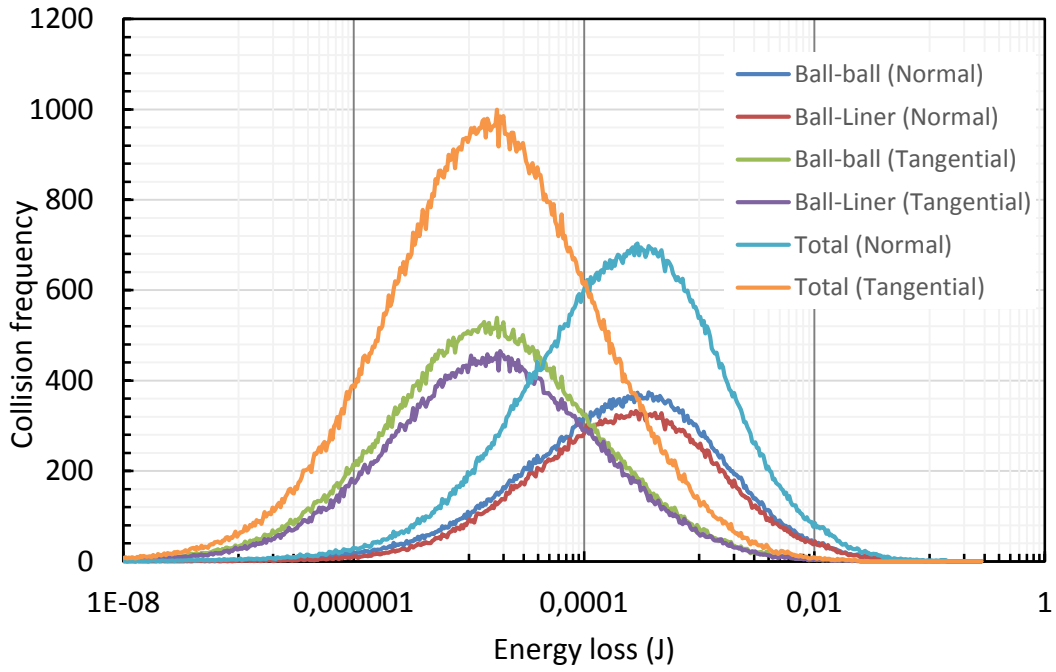

Figure VIII-2 Collision energy spectra (normal and tangential) for a 30.5 cm ball mill, with 30 % filling, 25 mm balls and operating at 70 % of critical speed.

Another analysis that was carried out to post process DEM collision information was to calculate the collision energy spectra by particle type in the simulation. The procedure used to build the collision energy spectra on the basis on the particle type is similar to the one used in UCM (Weerasekara and Powell, 2011). The difference lies in the fact that in UCM the energy losses are calculated indirectly from particle velocities before and after the collision and not from the energy loss given by the Hertz-Mindlin contact model. The method proposed in this work considers not only the collision energy loss registered by DEM but also the split of the energy loss between both elements

involved on the collision. This will make the values of the collision energies per particle compatible to the breakage models, which are based on tests of hitting ore particles sitting on a steel surface with steel strikers. For instance, if both elements involved in collisions are ore particles or steel balls the fraction of the energy that goes into each element is 0.5. However, in the case of SAG mills, which ore particles collide against balls the energy fraction that goes into each element must be calculated. Given particles 1 and 2, their fractions of the collision energy are respectively $e_1$and e_2:

$$e_1 = \frac{k_2}{k_1 + k_2} \qquad \text{VIII-2}$$

and

$$e_2 = \frac{k_1}{k_1 + k_2} \qquad \text{VIII-3}$$

being k_1 and k_2 the stiffness coefficient for elements p_1 and p_2 in the collision. If $p_1$is an ore particle and $p_2$is a steel ball, the ore particle would receive approximately 98 % of the collision energy, while the steel ball would receive only 2 %, given the values of k_1= 5 GPa and k_2= 230 GPa.

For the mill simulation (Figure VIII-1) the normal collision energy spectra by particle type is displayed on Figure VIII-3. As in this case all elements in the simulation are steel balls the energy transferred to each element is half of that collision energy loss.

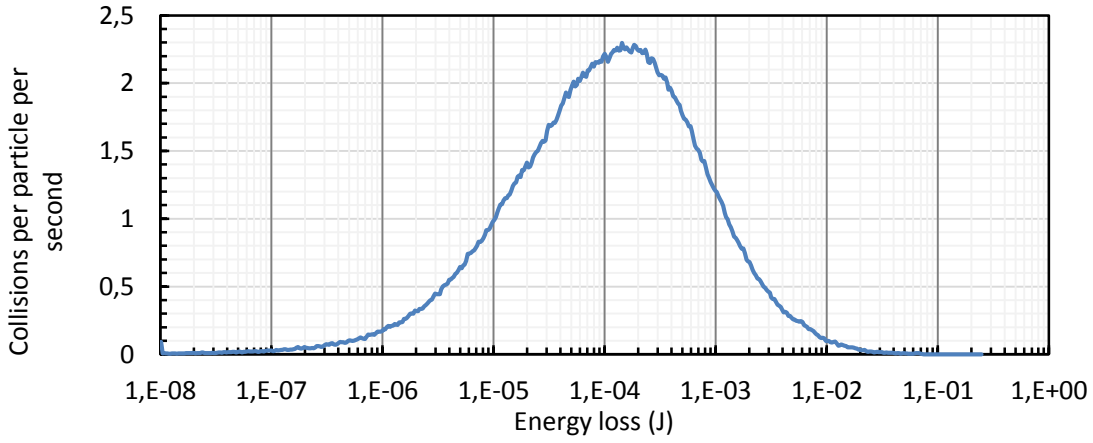

Figure VIII-3 Collision energy spectrum by particle type for the same mill simulation of Figure VIII-2

In order to calculate the mill power, the contribution of the mass of each element in the simulation in a certain time frame was taken into account. The horizontal center of mass of the mill is given by,

$$x_{COM} = \frac{\sum_i x_i m_{p,i}}{\sum_i m_{p,i}} \qquad \text{VIII-4}$$

where x_i is the horizontal position coordinate of the particle i and $m_{p,i}$ is the mass of the particle i. The power is then calculated by multiplying the center of mass by the mill speed, the total mass of the particles and acceleration due to gravity:

$$P_{DEM} = x_{COM}\omega_m g \sum_i m_{pi} \qquad \text{VIII-5}$$

where ω_m is the rotation speed of the mill in rad/s.

Figure VIII-4 shows the power draw calculated from Equation VIII-5 for the DEM simulation of the laboratory mill showed in Figure VIII-1. The power draw is calculated on each saved timeframe from which particle positions are extracted from the DEM simulation.

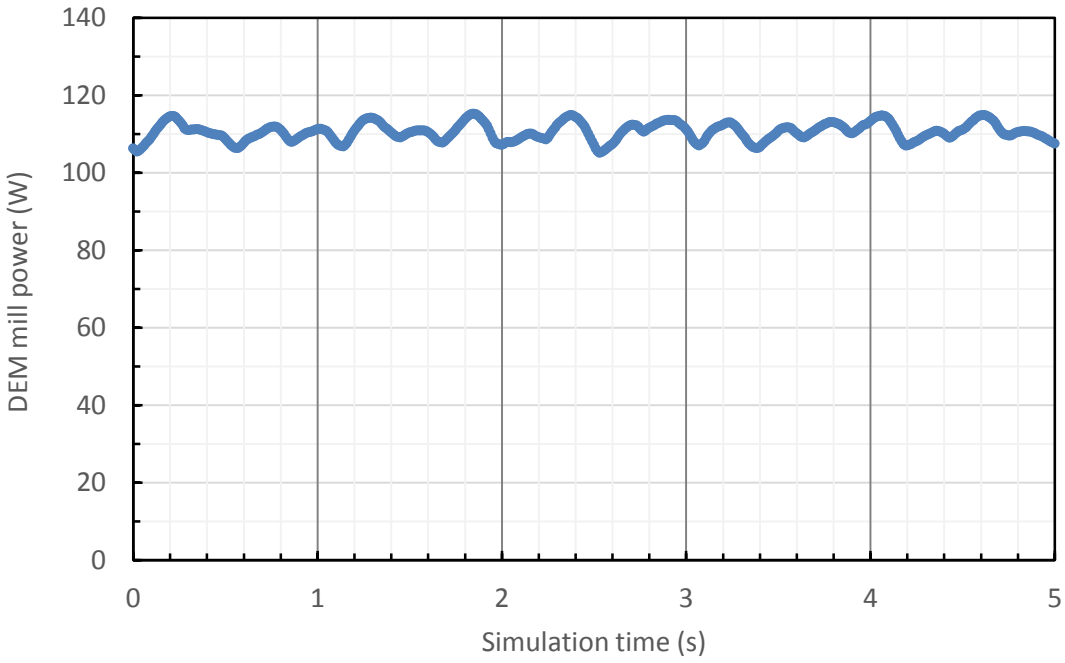

Figure VIII-4 Mill power calculated from the simulation of the mill depicted on Figure VIII-1. The dots show the time on which particle data was saved

Post processing the data required the development of computational routines in Matlab R2012® (Mathworks, 2012) to analyze the charge motion. The mass density distribution among the charge is analyzed by concatenating the axial dimension of the mill into a single coordinate. Then the horizontal and vertical axes of the mill were divided into a 100 by 100 bin matrix. An example is displayed in Figure VIII-5 (left), for a 30 cm ball mill. For each save time frame of the DEM simulations, the coordinates of the center of the particles are registered and allocated in their corresponding bin. Finally, the sum of the mass of all particles are divided by the total time of the duration of the DEM data sampling for each bin. The color scale indicates the mass per unit of time per mill length (kg/s/m).

The second analysis corresponds to the velocity profile within the mill (Figure VIII-5). The mill section is divided in bins and the average particle velocities for each bin are displayed. The colors represent the resultant velocity of the particles in horizontal and vertical axes, expressed in logarithmic scale. The blue region in the middle of the charge is the region of near zero velocity, also defined as the eye of the charge.

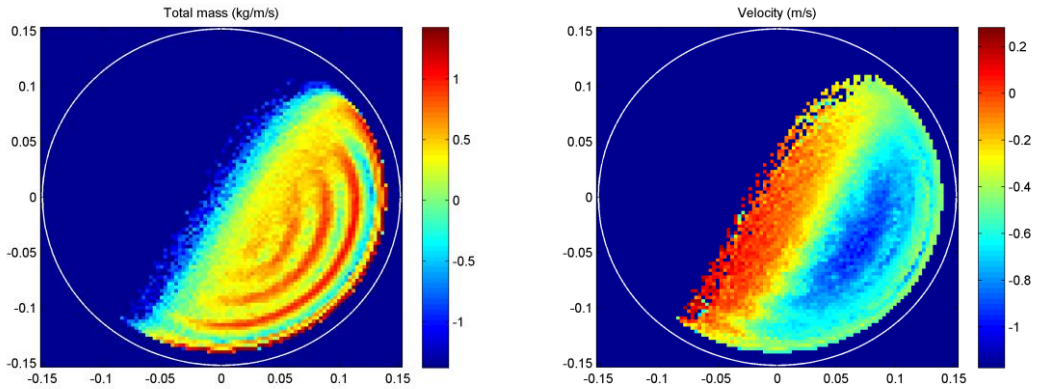

Figure VIII-5 Mass distribution plot (left) and velocity profile (right) for the mill depicted in Figure VIII-1

The post-processing routines also generates the spatial distribution of the collisions in the mill. Figure VIII-6 and Figure VIII-7 displays the two analyses that are conducted: first, the average energy loss (along simulation time and mill length) and the total energy loss frequency (total collision energy loss per second of the simulation). These graphs assist in better understanding where the energy is dissipated in collisions

inside the mill. The magnitude of the dissipated energies is represented by colors in log-scale.

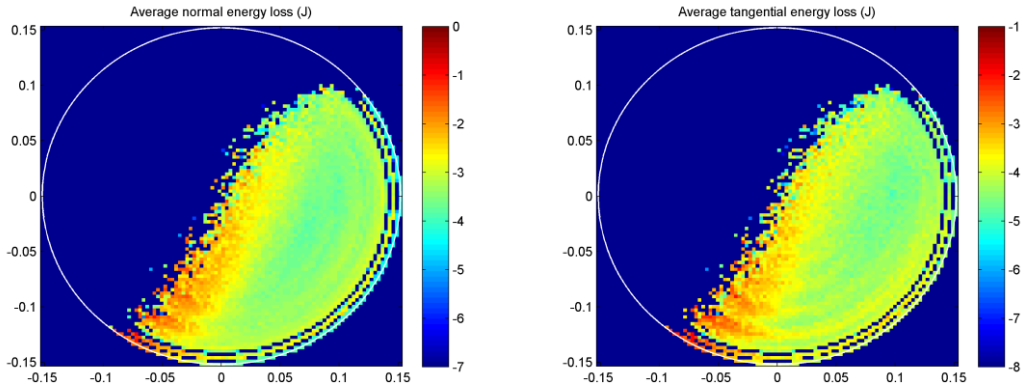

Figure VIII-6 Spatial distribution of the average normal energy loss (left) and tangential energy loss in the mill (right)

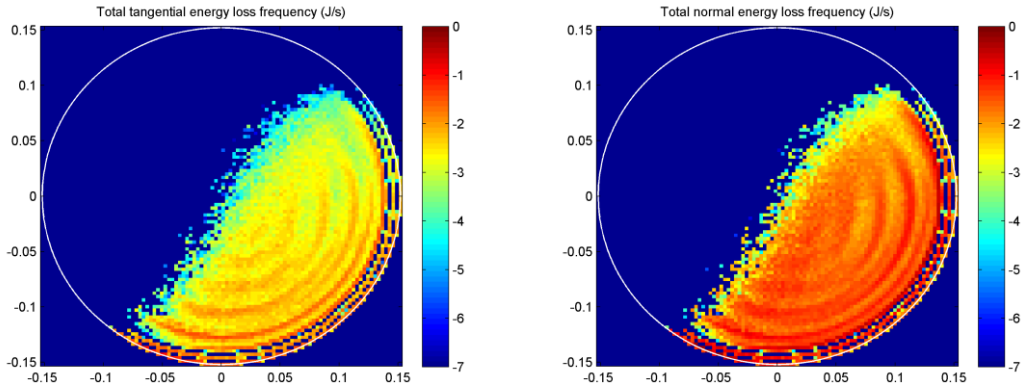

Figure VIII-7 Spatial distribution of the total normal and tangential energy loss in the mill

VIII.2 Mill simulations

In order to provide information for the UFRJ mechanistic model development, several DEM simulations of tumbling mills were conducted. A number of different ball mills and SAG mills were simulated and their data was post-processed, generating the

information from the routines described on section VIII.1. The mills simulated in this thesis are divided in three categories:

- laboratory scale: up to 0.9 meters in diameter
- pilot scale: from 0.9 to 1.8 meters in diameter
- industrial scale: larger than 1.8 meters in diameter

An extensive simulation work was conducted in order to first understand qualitatively how the main grinding variables affected batch grinding. Then, simulations of the pilot scale SAG mill are presented, representing conditions applied in real life pilot scale tests. It is then demonstrated how detailed post-processing on DEM can be useful to give rapid and useful insights about the operation of industrial SAG mills.

VIII.2.1 Laboratory mills

Bench scale mills simulations covered a range of design and operation parameters, which are listed below. The batch mill geometries are presented on Figure VIII-8, Figure VIII-9, Figure VIII-10 and Figure VIII-11. For each mill, two liner configurations were used, a regular rectangular shaped and a smooth wave format.

- Mill diameter (0.2 m to 1.8 m)
- Liner profile (wave versus rectangular bars)
- Mill speed (20 % to 110 % of critical speed)
- Grinding media size (15 mm to 60 mm)
- Mill filling (10 % to 50 %)

Batch ball mills

The batch ball mill test has been conducted on LTM for several years as it provides data to the back fitting of selection and breakage function of ores. This data is used on circuit simulations using the traditional PBM approach. This mill was chosen as the starting point for the simulations and the preliminary applications of the mechanistic model approach on LTM. The base case is the 30.5 cm ball mill, equipped with four lifter

bars that has been described in sections VIII.1 and VI.2, whose geometry is displayed on the left side of Figure VIII-9.

The first set of simulations was carried out varying the mill speed on the 30.5 cm mill that is equipped with rectangular lifters (Figure VIII-9 left). The power calculation results from using the center of mass of the charge are presented in Figure VIII-12. The figure shows, for a simulation interval of 5 seconds, that at the regular mill speed (67.5 % and 70 %) the oscillation of the power is consistent with the mill speed. The value obtained is close to the measured power on the real mill at these operational conditions. As expected, lower speeds resulted in lower power draws, whereas at higher speeds the oscillation of the power values is higher, due to the influence of the erratic motion of the cataracting balls. Figure VIII-13 presents the average power values as function of mill speed for a ball mill operating with 30% filling and equipped with rectangular lifter bars.

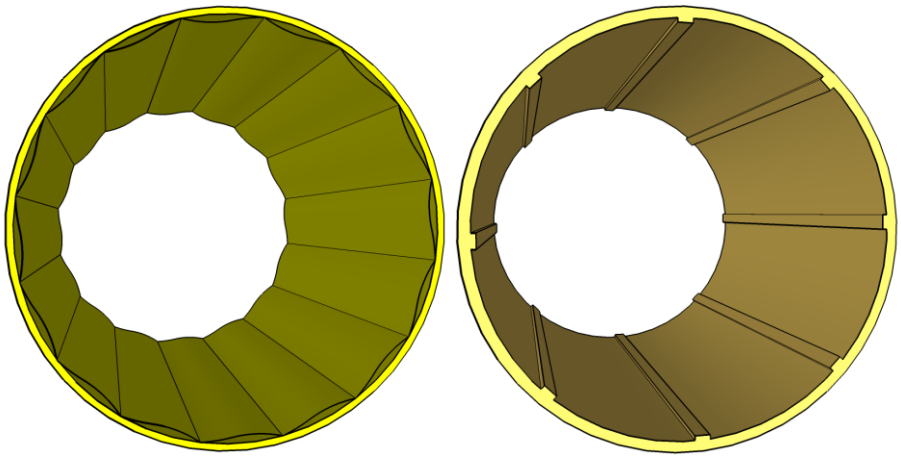

Figure VIII-8 Internal configuration of 0.2 m of diameter and 0.3 m in length batch mills simulated

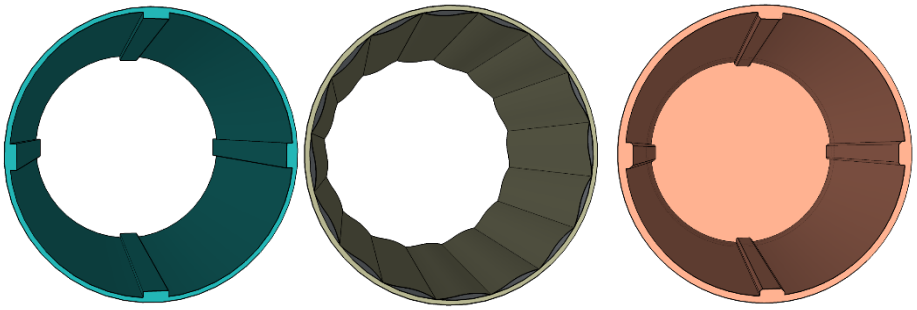

Figure VIII-9 Internal configuration of 0.3 m of diameter and 0.3 m in length batch mills simulated

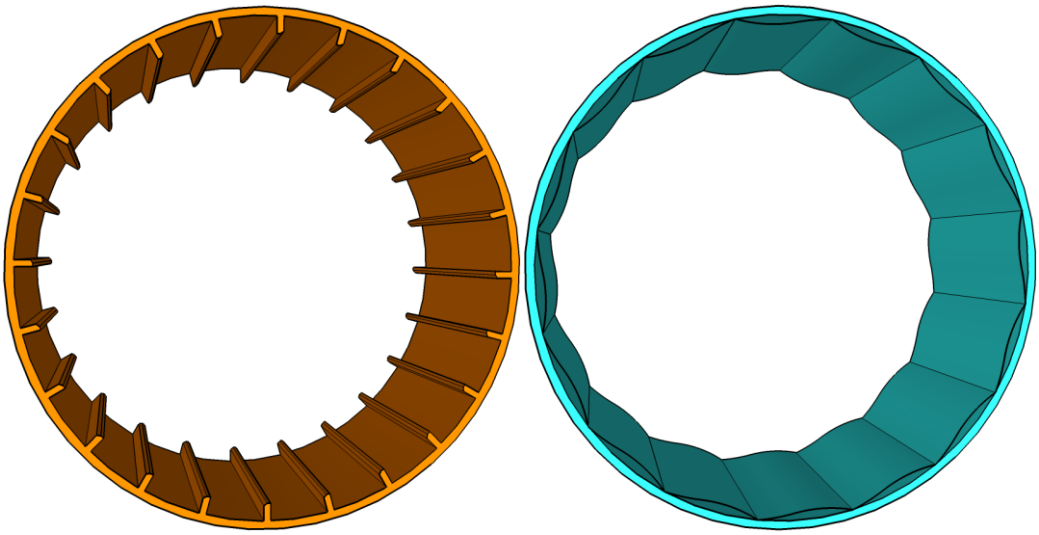

Figure VIII-10 Internal configuration of 0.6 m of diameter and 0.3 m in length batch mills simulated

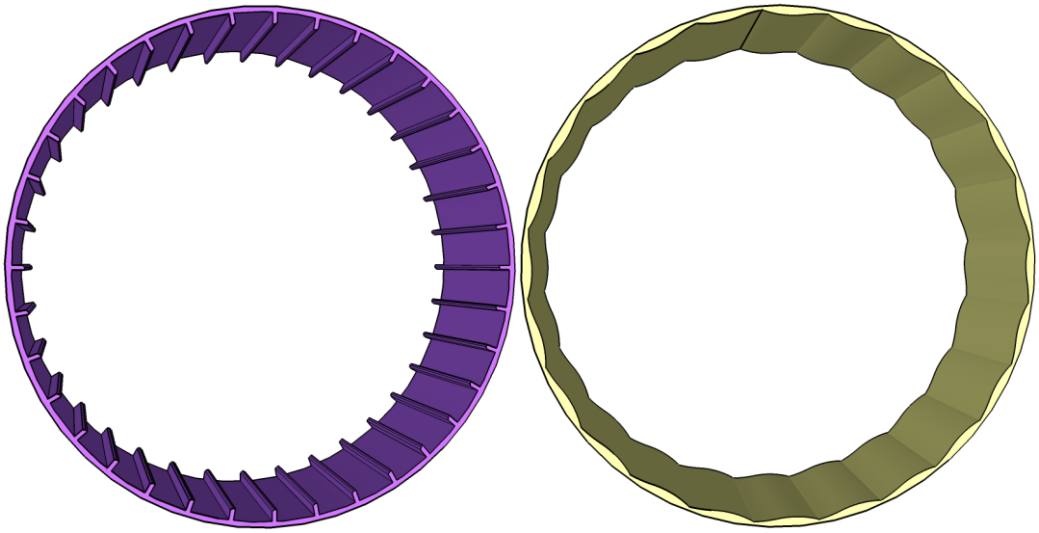

Figure VIII-11 Internal configuration of 0.9 m of diameter and 0.3 m in length batch mills simulated

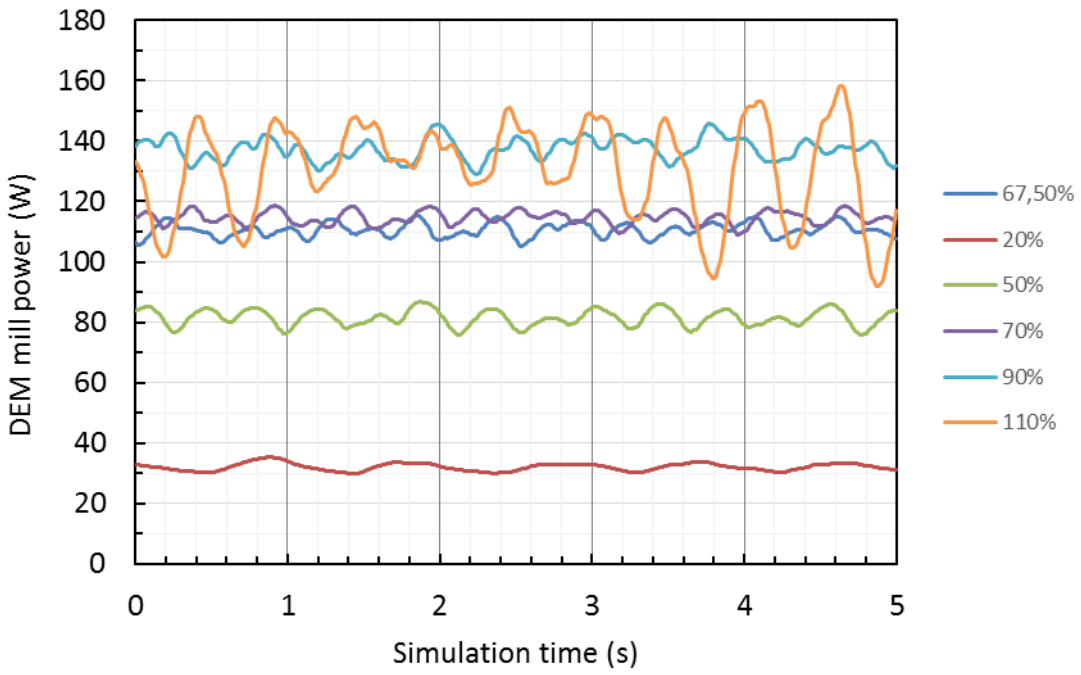

Figure VIII-12 Effect of mill speed (% of critical speed) on the simulated power draw of a 30.5 cm ball mill

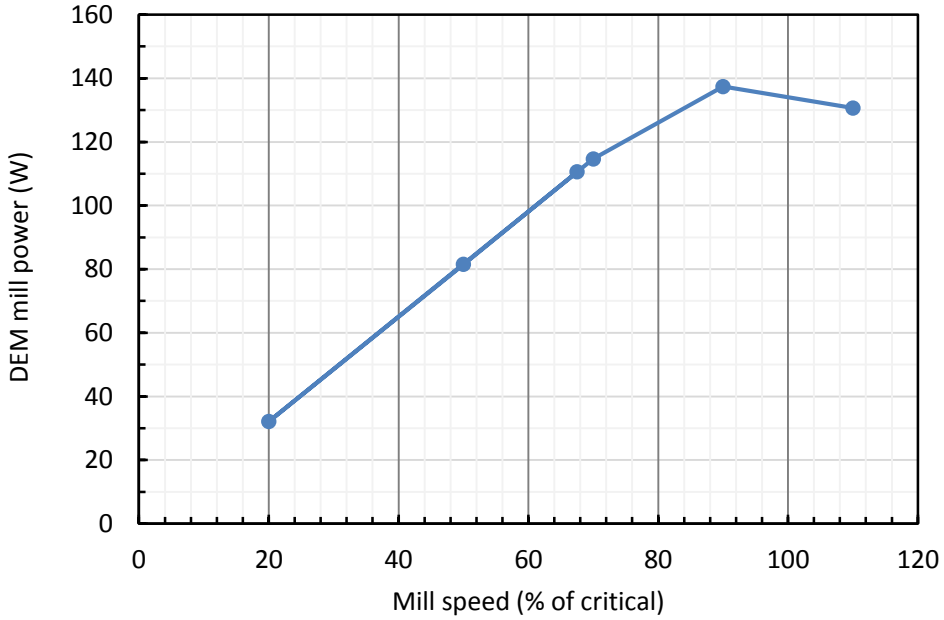

Figure VIII-13 Simulated mill power as function of mill speed for the 30.5 cm batch ball mill equipped with square lifter bars running at 30 % filling with 25 mm balls

Another analysis that can be done is the effect of the ball size. The evolution of the power with time in the base case (30 cm mill) is presented on Figure VIII-14. Though the power oscillation shows a limited variation on the simulations when balls of smaller diameter are used, for 60 mm balls, the erratic motion of the balls becomes noticeable on the estimated power. The fact that a very small number of balls were used in the simulations to reach the 30 % mill filling explains this effect. The power draw becomes less sensitive to the ball size as the ratio between the ball size and mill diameter is reduced, and this translates into the power draw of industrial mills being less affected by the top size of the grinding media. Though the power values are similar, the effect on the breakage rates is expected to appear. This is a subject that will be investigated in section IX.4 and is of great relevance in the application of UFRJ mechanistic modelling approach.

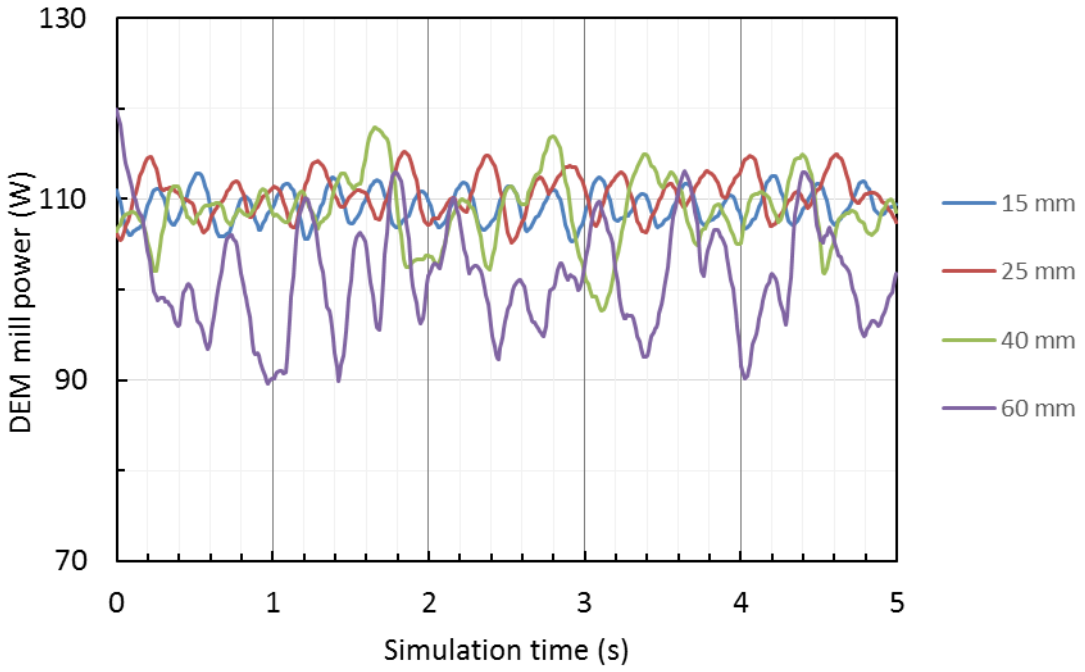

Figure VIII-14 Effect of ball size on the simulated power draw of a 30.5 cm ball mill running at 67.5 % of critical speed with a ball filling of 30 %

Another set of simulations covered the effect of mill filling. Figure VIII-15 presents the evolution of the power for the base case at different filling levels that ranged from 10 % to 50 %. Simulation results show that power increases with the filling level to a

maximum value, which ranges from 40 % and 50 %. The frequency and magnitude of the oscillation in the power indicates that the charge dynamics does not change significantly with mill filling.

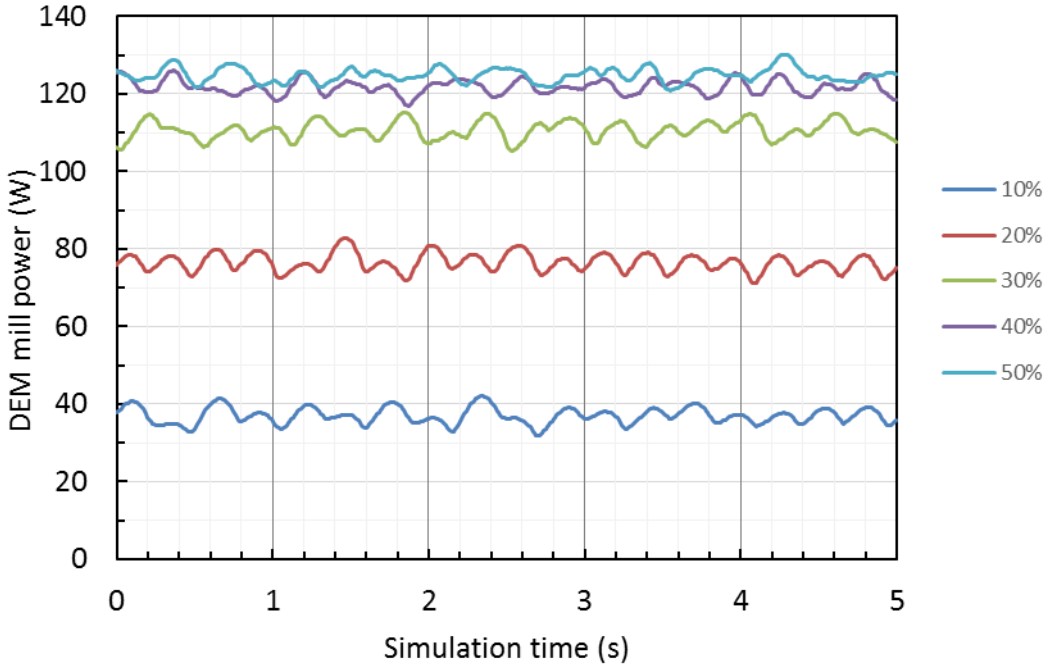

Figure VIII-15 Effect of mill filling on the power draw of a 30.5 cm ball mill

Figure VIII-16 to Figure VIII-19 show simulated velocity profiles as a function of selected design and operating variables. In the case of Figure VIII-16 the effect of the shift from cascading to cataracting and then to partial centrifugal motion becomes evident. Figure VIII-17 shows that the motion of balls is influenced by size, with smaller balls being lifted higher up in the charge than larger ones, thus demonstrating the risk of testing large balls in smaller diameter mills. Figure VIII-18 shows the effect of mill filling, which shows the effect of appearance and motion of the eye of the charge. Finally, Figure VIII-19 shows simulations on the effect of mill diameter, which demonstrates the increase in the maximum magnitudes of the collision velocities with mill size.

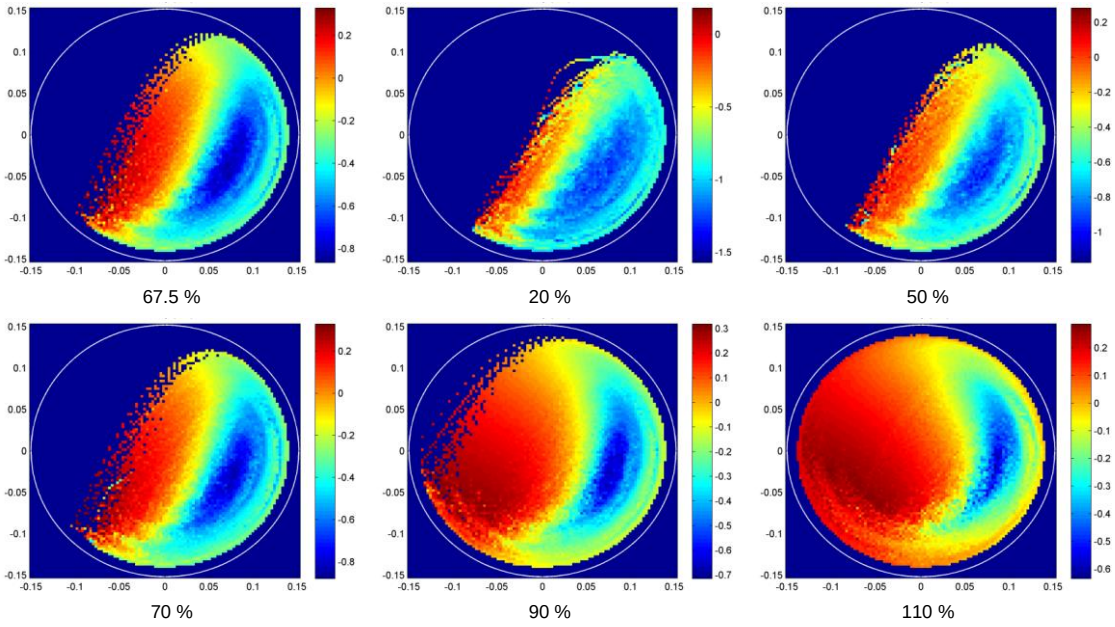

Figure VIII-16 Velocity profiles showing the effect of % of critical speed (30 cm mill, 30 % filling, ball size 25 mm) – velocity expressed as log (m/s)

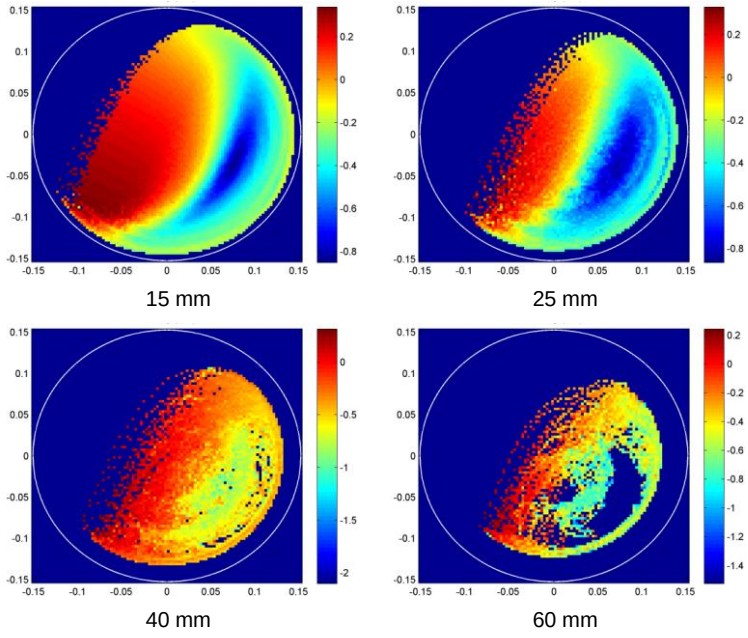

Figure VIII-17 Velocity profiles showing the effect of ball size (30 cm mill, 30 % filling, 67.5 % of critical speed) – velocity expressed as log(m/s)

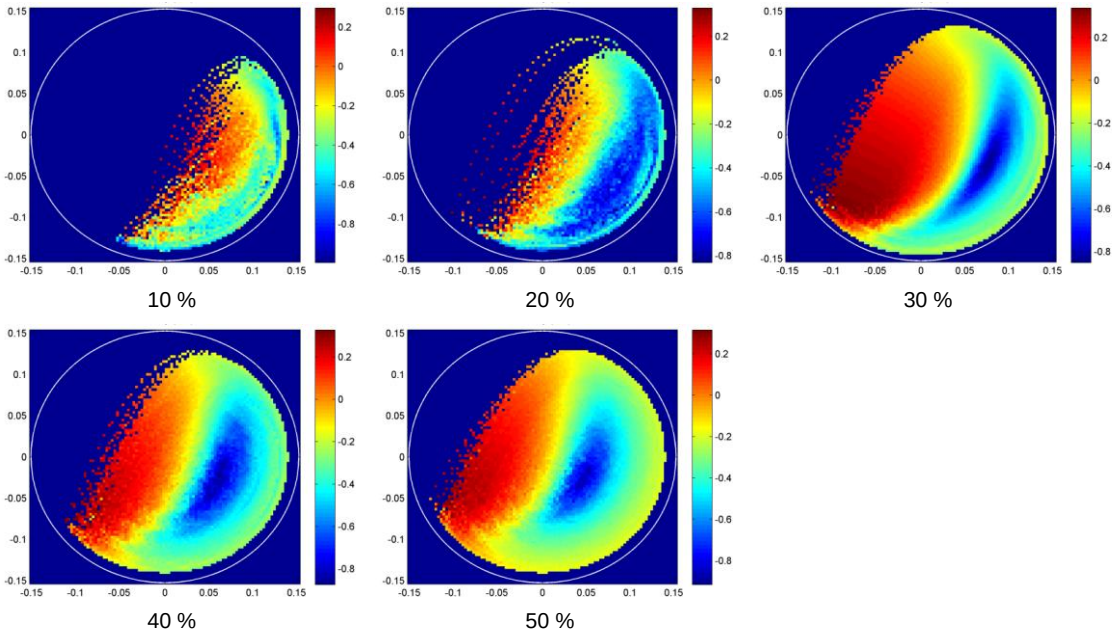

Figure VIII-18 Velocity profiles showing the effect of mill filling (30 cm mill, ball size 25 mm, 67.5 % of critical speed) – velocity expressed as log (m/s)

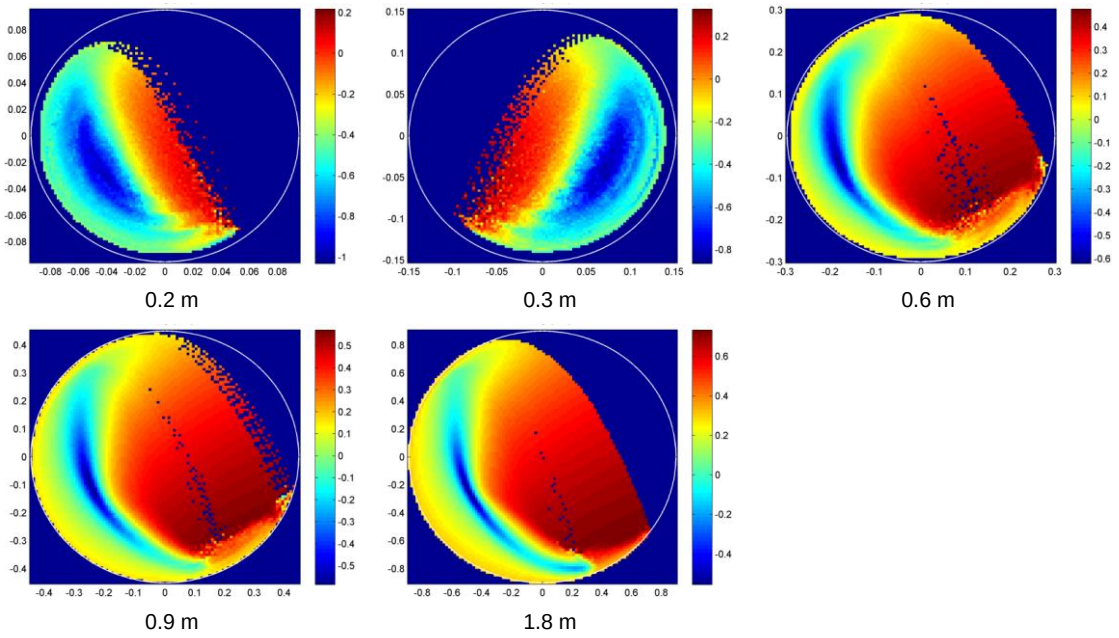

Figure VIII-19 Velocity profiles showing the effect of mill diameter for rectangular lifters (ball size 25 mm, 67.5 % of critical speed, mill filling 30 %) – velocity expressed as log (m/s)

Batch SAG mill

The batch laboratory scale SAG mill measuring 0.6 m in diameter, 0.3 m in length and described in section VII.1 was simulated. Each mono-size range resulted into a DEM simulation for the initial conditions, which means that the simulation contains the balls and the exactly amount of particles contained in each mono-size. For the coarsest initial material, an additional DEM simulation was made. In order to minimize stochastic effects due to the small number of particles of 63 mm in the mill a new mill was designed, but in this case it is 1.5 m in length, while with the same length. The amount of particles in the simulation was increased by a factor of 5. The power draw from this simulation is compared to the regular (in a 0.3 m long mill) in Figure VIII-20.

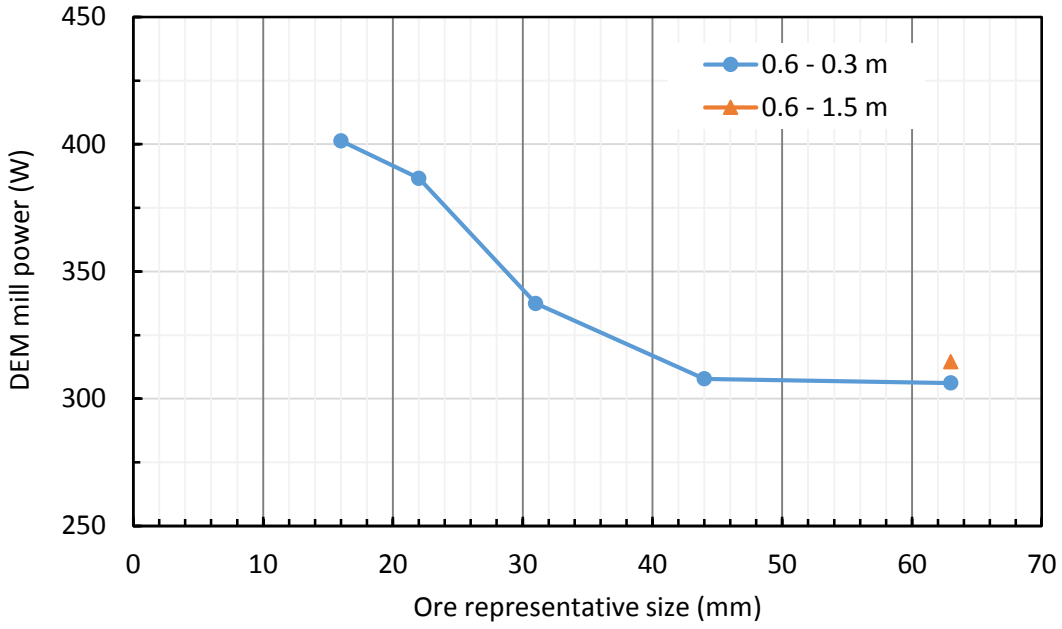

Figure VIII-20 Comparison of the mill power as function of the mono-size initial material. The triangle represents a DEM simulation made in an artificial built mill with 1.5 in length.

VIII.2.2 Pilot scale SAG

The DEM simulations of the 1.8 meters pilot scale SAG mill were performed first only considering just the cylindrical section of the mill. The ore and ball contents were inputted into each simulation as discussed previously. The net power draw calculated from the center of mass of the DEM simulations reproduced quite well the values

measured on the pilot scale tests. A comparison also shows the predictions obtained using Morrell's power equation (Morrell, 1996), which in general agreed with the experimental and DEM data (Figure VIII-21).

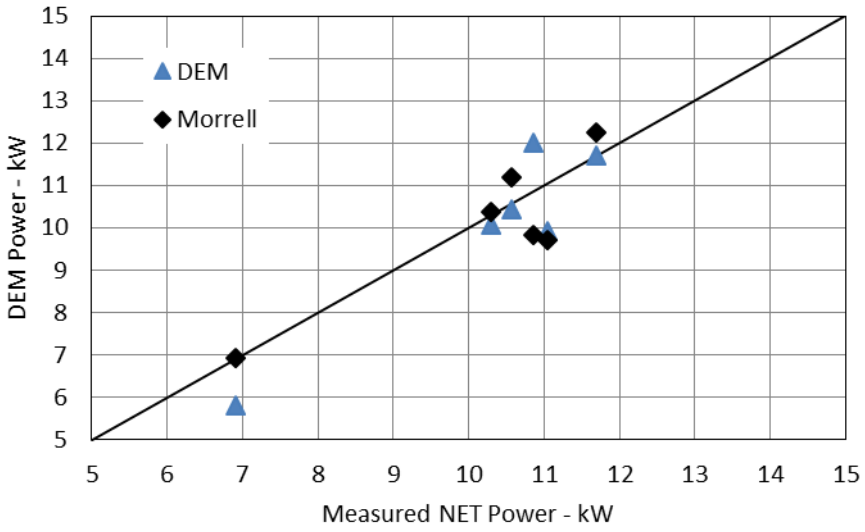

Figure VIII-21 Comparison between measured power to DEM power (Equation VIII-5) and the prediction using Morrell's power model (Equation IV-6) for the pilot-scale SAG mill

In order to assess the effect of size distribution of the particles, two case studies were chosen: cases 01 (SAG mode) and 03 (AG mode). In both cases the mill operated at the same mill speed (24.5 rpm) and presented different charge levels and hold-up distributions as depicted on Figure VII-12, with case 03 being the autogenous mill test.

Figure VIII-22 shows a comparison of the overall collision energy spectra as a function of collisions per particle per second between cases 01 and 03. As expected, the presence of steel grinding media on case 01 resulted on a more aggressive energy environment (Figure VIII-23). Case 03, related to the autogenous grinding test shows maximum collision energies that are half of the maximum values obtained from the SAG operation (Figure VIII-24). The presence and survival of particles larger than 150 mm on case 03, however, contribute to reducing the difference on the energy spectrum. The simulation showed that these particles provide impacts that are equivalent to those from 90 mm steel balls in this mill.

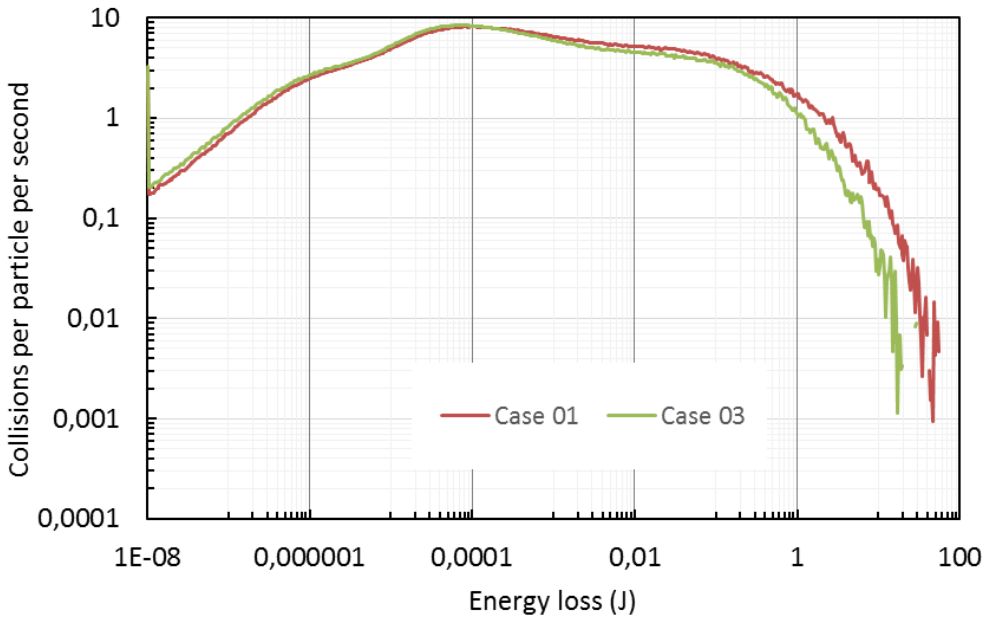

Figure VIII-22 Energy spectra comparison for pilot-scale SAG mill – total energy transferred to particles

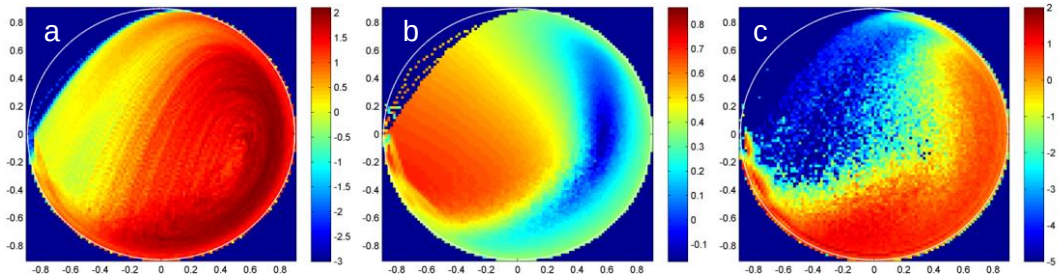

Figure VIII-23 (a) Charge motion - log(kg/m/s); (b) velocity profiles - log(m/s); and (c) total normal collision energies distribution - log(1/s). The simulations are based on the measured hold-up of the case 01

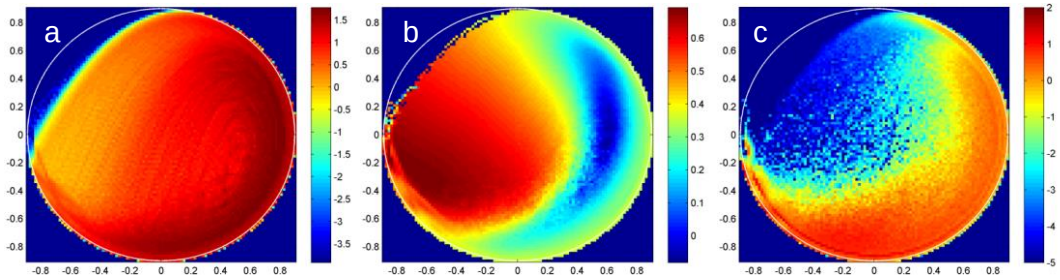

Figure VIII-24 (a) Charge motion - log(kg/m/s); (b) velocity profiles - log(m/s); and (c) total normal collision energies distribution - log(1/s). The simulations are based on the measured hold-up of the case 03

VIII.2.3 Industrial SAG mill

The DEM simulations of an industrial scale SAG mill allowed the development of a simplified approach to provide engineers with a tool to evaluate and compare the performance of different SAG mill designs. The approach requires the combination of the data processing technique presented in section VIII.1, to the application of a simplified breakage model based on some characteristics of the ore of interest regarding its fracture energies, damage amenability, appearance function and abrasion, previously presented in section III.3.

The selected mill has 12 meters in diameter and 8 meters in length, being equipped with 36 lifters. The mill speed is set to 9.3 rpm, the total charge level is 30 % with a ball filling of 16.5 %. Figure VIII-25 shows the ball size distribution used in the simulations, being specified as a suitable one for grinding a tough copper ore. The DEM simulation of this mill was built considering a periodic cylindrical slice of 500 mm of length. This assumption is regarded as valid following earlier studies that compared full size mill simulation and simulations of slices of the mill (Cleary, 2010). However, a limitation present on mill slice simulations is the lack of information on the effect of the conical ends and their lifters on the charge motion. In spite of that, the slice simulation was adopted since it represents a much more convenient and quicker alternative when performing comparisons among operational conditions or mill geometries.

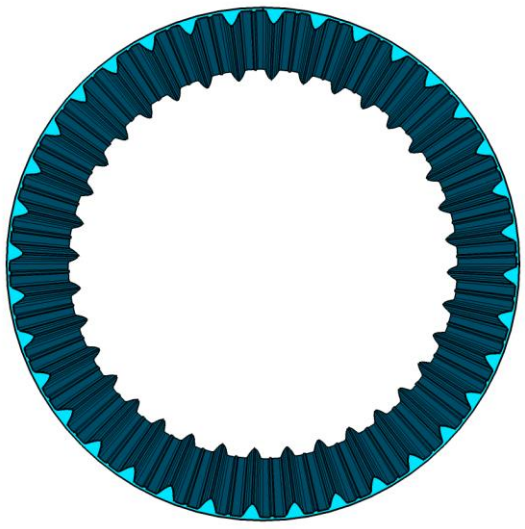

Figure VIII-25 Cylindrical section of the simulated 12 meter SAG mill

Table VIII-1 Ball size distribution of the simulated 12 meter SAG mill

Ball size (in)	5.5	5	4.5	4	3.5
%	30.8	23.4	17.5	12.9	15.4

The size distribution of the hold-up of SAG or AG mills is very seldom available, since there are only a few cases reported in the literature when all the charge of such mills operating at industrial scale was fully analyzed (Mwansa, 2011, Bueno *et al*, 2011). Most DEM simulations performed on industrial SAG mills use the fresh feed size distribution, which is incorrect since part of the ore particles contained in the feed may break immediately upon entering the mill, whereas other survive longer. Unfortunately, the fresh feed particle size distribution is the only data available if DEM simulations are performed in the design stage of a Green Field project. A relationship between fresh feed particle size distribution and the hold-up needed to be established and for pilot scale data was used. One should bear in mind that this is also not rigorously correct, since the relationship that is valid for a pilot scale mill may not be valid for an industrial mill. For instance, the hold-up of pilot scale mills usually possesses a smaller amount of fines due to the fact that the discharge grate is significantly more efficient than that in full-scale mills. In addition to that, the number of particles contained in the coarser size fraction, which markedly influences the mechanical environment inside the grinding mill, is usually very small. Depending on the ore type, a single +200 mm particle that survived on the hold-up could create a bias on the results. With those limitations in mind, a simple mathematical model is proposed to transform the fresh feed particle size distribution on the hold-up for DEM simulations. It is recognized that, in spite of the fact that it does not account for recycle, pebble-crushing and even ore properties, this model will provide a particle size distribution that is more realistic than the one representing the fresh feed to describe the mill hold-up. Details of the model may be found in the Appendix A. An example of application is shown in Figure VIII-26.

In order to match the total mass on the charge, the mass of the sub-DEM, particles, that is, those with sizes below 20.8 mm, mass is distributed among the last three finer DEM size classes according to the following rules:

- The smallest DEM particle diameter is 20 mm
- 10 % of the sub-DEM mass is added to the 20.8 mm size class
- 50 % of the sub-DEM mass is added to the 25.4 mm size class

- 40 % of the sub-DEM mass is added to the 29.2 mm size class

This distribution of sub-DEM particles into coarser sizes in simulations helps keeping the mill volume consistent in the simulation and also reduces the number of particles contained in the simulation.

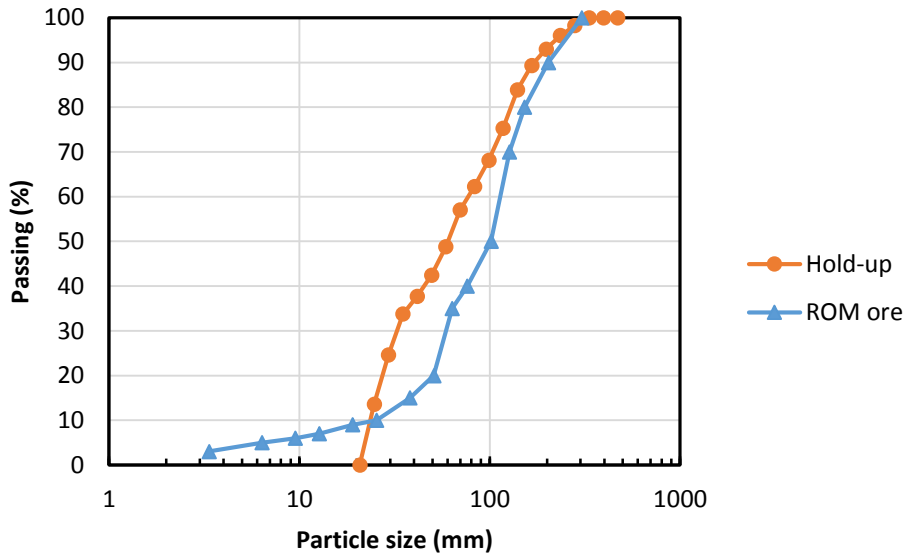

Figure VIII-26 Comparison between the given run-of-mine and the estimated mill charge particle size distribution to be used on DEM simulations

In addition to the extraction of the collision energy spectra, the present work proposes the concept of effective collisions as part of the simplified approach for describing the performance of industrial mills. The average number of effective collisions represents the frequency of collisions that would result in breakage of particles contained in a specific size class, either in a single collision event (catastrophic fracture) or in repeated collision events (accrual of damage).

The model considers that the energy transfer in collision events involving two elements should be high enough to damage the weakest particle according to the fracture energy distribution of the size classes of these elements. If the collision meets this criterion, then it is considered an effective collision event. This allows the logging of the number of effective collisions for the particles present in the EDEM® simulations (DEM particles). If the energy applied to the particle classes in that collision is not high

enough, then it will be available to break the finer particles, such as the fine particle population (sub-DEM), which do not appear explicitly in the DEM simulations.

This calculation is possible using the particle fracture energy distribution for each size class. This model is based on the observation that particles contained in a narrow size range demand different impact energies to cause breakage. The minimum energy chosen is the one identified as capable of breaking even the toughest of the particles of a standard copper ore contained in a specified class when hit a specific number of times. This number is calculated based on the continuum damage model of particle breakage of Tavares and King (2002), which is reviewed in detail in section III.3.3.

The evaluation of effective collisions for the selected size ranges gives a mill signature, which should correlate directly to the mill performance. The greater the frequency of effective collisions in a given class, the greater the breakage rates of particles contained in that class will be. For instance, the larger the number of effective collisions in the medium and medium-fine ranges, the greater the processing capacity of the mill will be. Also, the larger the number of effective collisions in the sub-DEM range, the finer the product of the SAG mill.

The calculation of the effective collision frequency of the ore particles in DEM is the following: first, the elements involved in the collision are identified, then the energy loss on that collision is split among both elements. The coefficient of energy split for each element is calculated using the Equations VIII-2 and VIII-3, which depend on the elastic properties of the bodies in contact, be it an ore particle, a steel ball or a mill liner. If the element in the collision is an ore particle, then the absorbed energy is compared to the distribution of fracture energies of particles of that size class. If the absorbed energy is capable of breaking 99 % of the particles (energy equivalent to the 99^{th} percentile of the particle fracture energy distribution) this collision energy will be tallied as an effective collision. If not, an additional calculation is conducted using the damage model to check if the weakest particles will suffer breakage at an arbitrary large number (taken as 40) of impacts at the selected energy level. If in that case the particle breaks, that collision is also considered as an effective one. If the collision energy is not able to break the particle, it is then used to break the smaller particles in the mill that are not present in DEM simulation (sub-DEM particles). The same assumption is used for the case of steel-steel collisions. Figure VIII-27 shows the decision flowchart of the procedure.

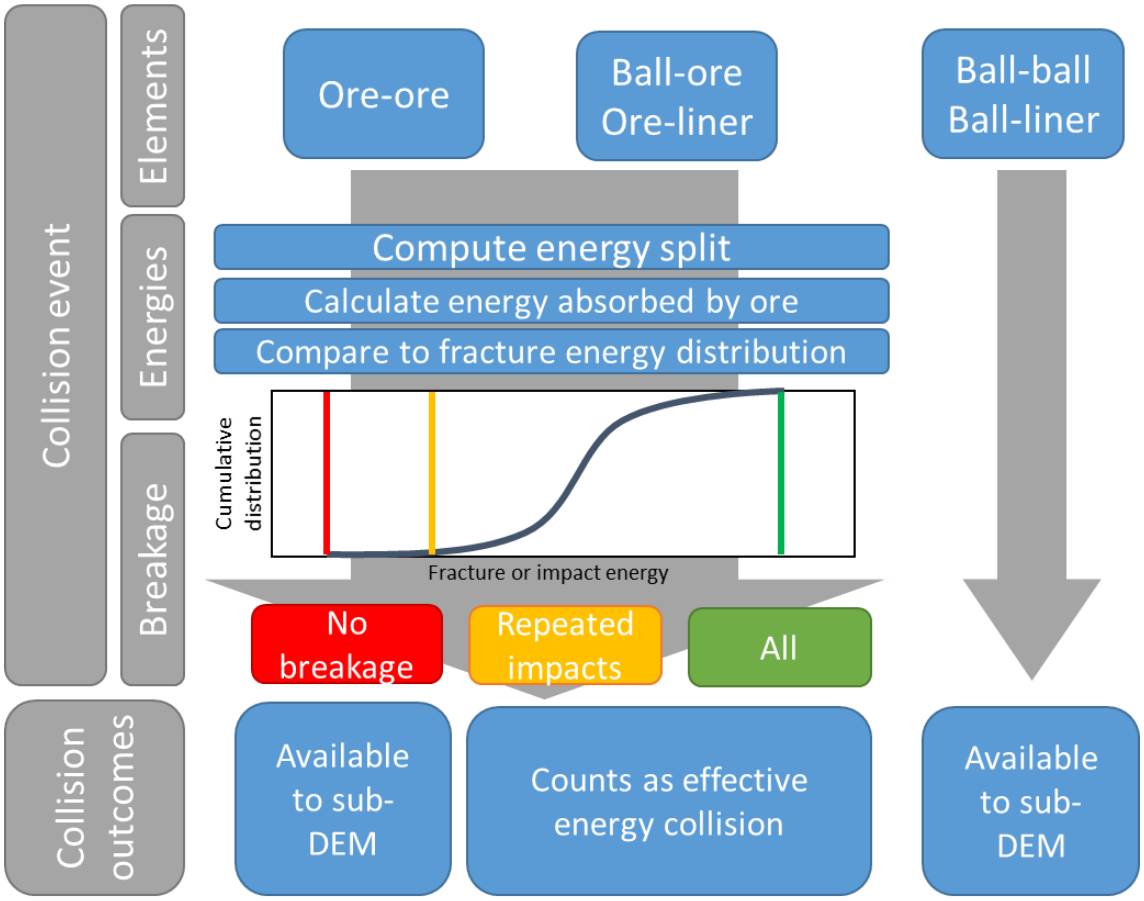

Figure VIII-27 Decision flowchart for the effective collision energy calculations

The effective collision energy calculation for the sub-DEM particles take into account the collisions that were ineffective to break DEM particles, as well as the steel-steel balls or balls-liner collisions. The main difference in the case of sub-DEM particles is the use of the particle interaction model described in section VI.3. Now, each selected collision provides energy input to a hypothetic sub-DEM particles population. For each sub-DEM particle size classes, the number of particles captured is calculated from Equation VI-21, which requires the capture radius to be estimated from Equation VI-22. Then, the collision energy is split equally among the captured particles and a verification is performed on the capability of the collision energy on breaking 99 % of the particle population, as the procedure for the DEM particles. The procedure to compute the effective collisions from repeated impacts is also analogous to the procedure used for DEM particles. Figure VIII-28 shows an example of the application of this technique.

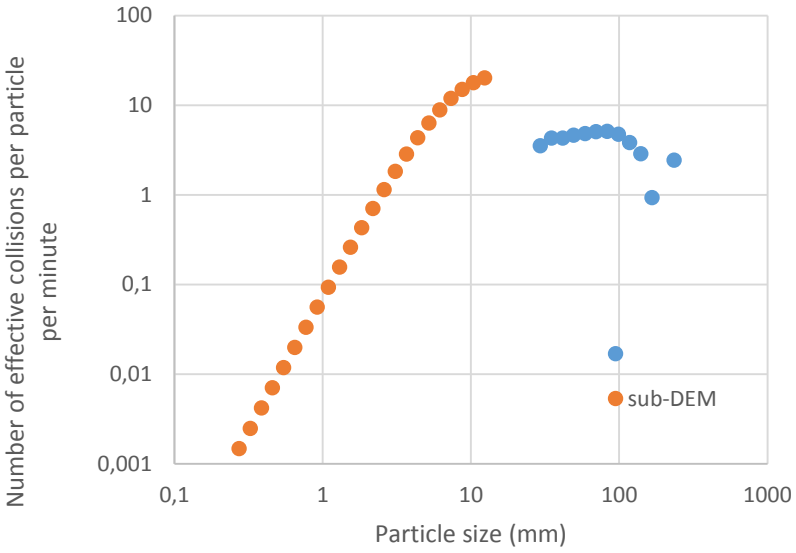

Figure VIII-28 Example of a result from the effective collision energy approach

Another analysis that is conducted is the evaluation of the energy spectra of the collision energies absorbed by the liners. Figure VIII-29 shows an example of the collisions suffered by the liners. The main spectra are separated in three groups: total, ore and balls. Total collisions refers to all collisions suffered by the liners, ore-liner shows only the contribution of collisions of ore particles against the liner, while balls-liners shows the contribution of ball collisions against the liners. These spectra are in their inverse cumulative form, in which each point represents the number of collisions per seconds that have magnitude that is either equal or higher than the given energy.

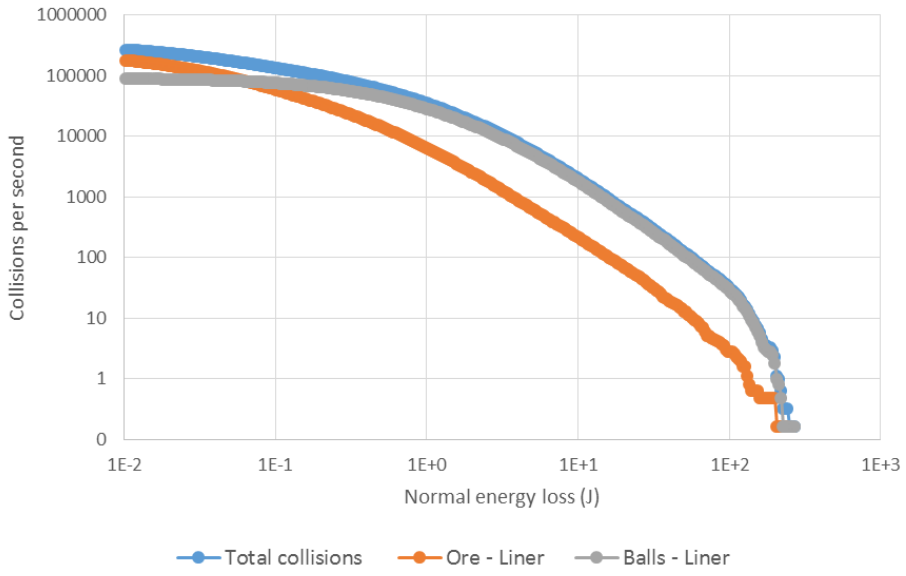

Figure VIII-29 Cumulative collisions per second on the liner

Analysis of the liner design

In order to demonstrate the applicability of the this analysis model a comparison of the performance of two SAG mills operating at the same speed, ball and ore load, but with different liner designs is presented (Figure VIII-30). Liner design A has 36 sections of two peaks, in which one is 300 mm in height while the other has 30 mm. Liner design B also consists of two peaks, but in this case both have approximately 200 mm in height. The design B not only represents a worn out version of the peak present in design A, but also includes a secondary peak. The aim of the secondary peak is to make charge motion more even, reducing the oscillation on power.

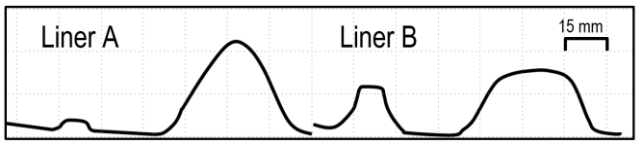

Figure VIII-30 Liner profiles for the selected case studies

It is observed that both mills presented similar maximum values in the velocity distribution of the particles. Figure VIII-31 presents the velocity profiles from snapshots of both DEM simulations at steady conditions. The design A presents a well defined cataracting flow pattern, due to the greater amount of particles that are projected by the

liner while a fraction of that mass falls into the center of the charge in a cascading movement with speeds slightly lower than the values found in the simulation of the mill design B. On design A there is a significant amount of particles hitting the toe of the charge with some of them being projected directly at the mill liners. The liner design B allowed two streams of cataracting particles. In addition to the catacracting particles, there was a more intense downward cascade flow, with particles at a higher speed than those found in the simulation of the design A.

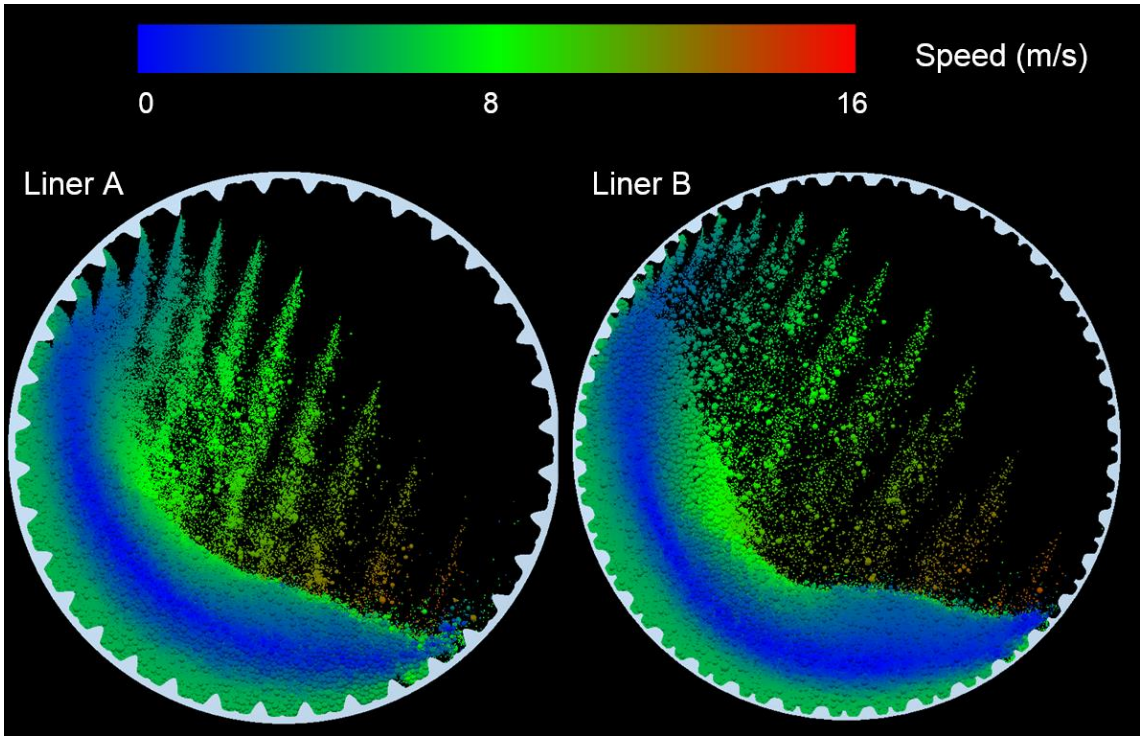

Figure VIII-31 Snapshots of the DEM simulations of mills with different liner types (Figure VIII-30). Particles are colored by their velocity (m/s)

In terms of the energy transferred to the particles which can be used in comminution, liner design A distributes the energy more evenly in the charge while liner design B concentrates the energy transfer next to the toe position and close to the center of the mill in the cascading zone. Figure VIII-32 and Figure VIII-33 presents the collision energy spectra, expressed as energy transferred to particles, in mill design A and B respectively. In the legend, ore class 1 refers to the coarsest ore particle size in the simulations while ore class 15 refers to 20 mm ore particles. The number of impacts of

high energy is significant on mill liner design B for the top three particle size classes, with some collisions reacheing up to 1000 J. This indicates a more efficient breakage of the coarser particles. On the other hand, with the high efficiency breakage of the coarser particles there would be less energy available to break the finer ones.

The effective collision energy analysis proposed in this chapter resulted in the confirmation that the mill design B is more aggressive to the coarser particles in the charge (Figure VIII-34). It also shows a slightly lower number of effective collisions for the intermediate size, between 20 and 50 mm, which corresponds to the critical size range in industrial SAG mills. The grinding media that is able to contribute to breakage of these particles are the steel balls and the coarser ore particles. The effective collisions available to grind the sub-DEM particles showed a similar behavior. A summary of the analysis is presented on Table VIII-2.

Table VIII-2 Summary of the results comparing both liner designs

Liner design	A	B
DEM net power (MW)	19.2	19.8
Particle size range	Effective collision frequency	
+ 1mm – 12.5 mm	23.2	24.6
- 50 mm	3.8	3.6
+ 50 mm – 100 mm	4.9	4.8
100 mm	2.3	5.6
Impact energies on liner	Collision frequency	
> 7 J	3,502	3,380
> 0,03 J	217,730	211,069

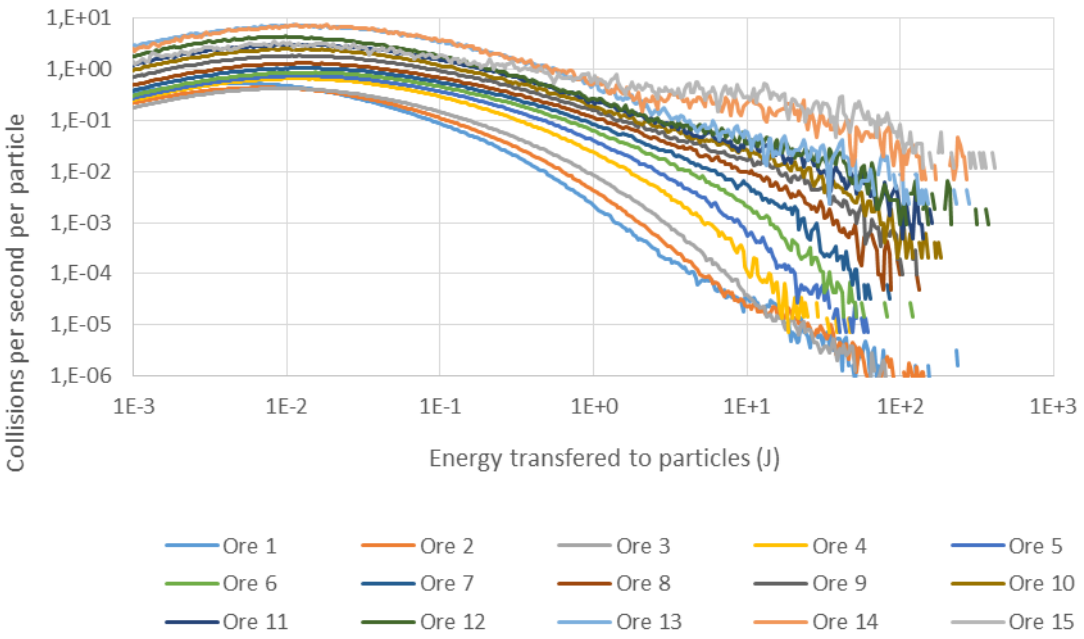

Figure VIII-32 Energy transferred to ore particles due to collisions for each ore class (liner design A)

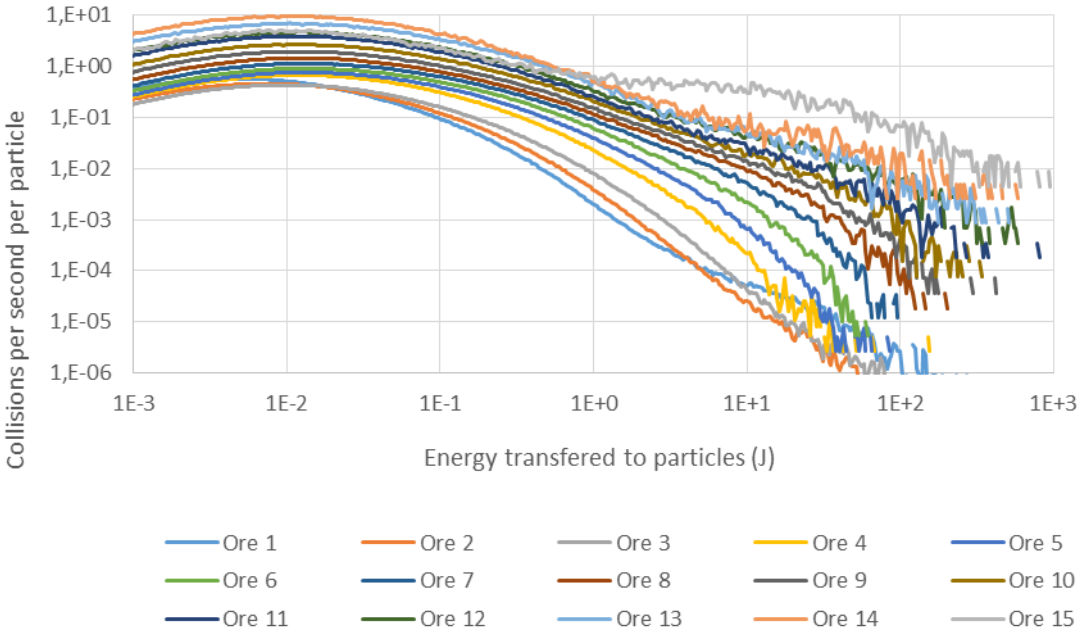

Figure VIII-33 Energy transferred to ore particles due to collisions for each ore class (liner design B)

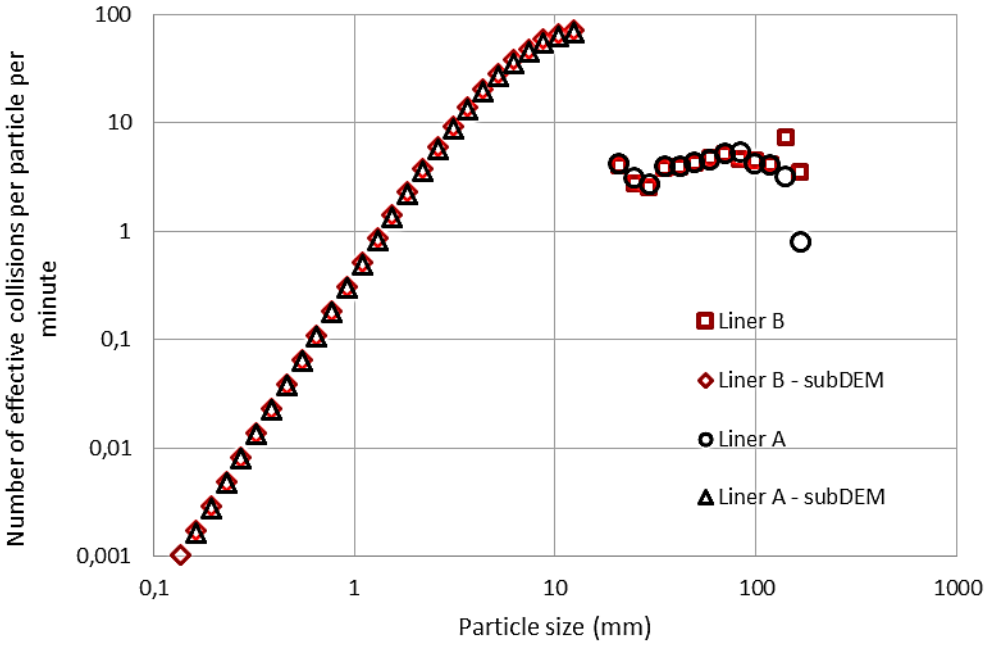

Figure VIII-34 Effective collisions per particle class comparing both liner designs

IX. The mechanistic model of AG/SAG mills

This chapter presents the results of the development of the sub-models that form the foundations of the AG/SAG mill model. First, the conceptual model for the SAG mills is presented, then the improved models of specific mechanisms of particle breakage are commented, including the one describing surface breakage and the revamped particle damage model. In the third section, the breakage of sub-DEM is analyzed for the case of batch ball mill grinding using DEM data from the simulations presented on section VIII.2.1. This includes a sensitivity analysis of the operation parameters in tumbling mills of different sizes, as well as the incorporation of the capture and energy split models in the revised mechanistic mill model. Finally, the concept of the AG/SAG mill model is then demonstrated through simulations of batch grinding tests of coarse particles and pilot scale mill simulations.

IX.1 Conceptual model

As previously mentioned, the conceptual model of the SAG mill is an evolution of the previously proposed mechanistic ball mill model. The general mass balance equation for the grinding zone assumes that AG and SAG mills are perfectly mixed reactors, such that the contents of the mill are the same on each spatial coordinate inside the mill. This assumption is generally justified since most of these mills present high-aspect ratio (diameter/length). The material that leaves the grinding zone is subjected to an internal classification effect due to the grate and pebble ports. The flow sheet of the model is presented in Figure IX-1, which is equivalent to Austin's perfect mixing mill approach (Figure IV-14) (Austin *et al*., 1986).

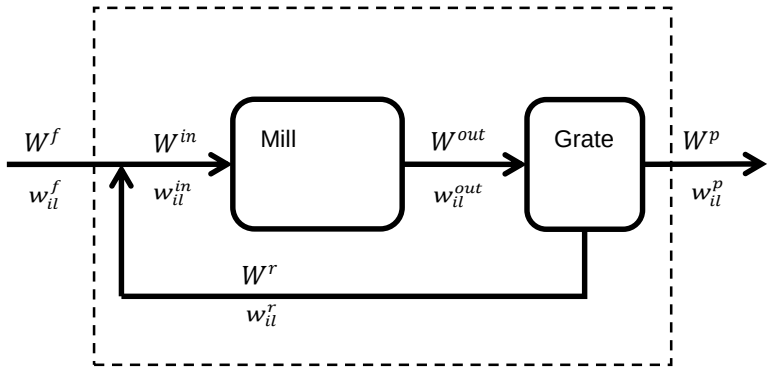

Figure IX-1 Description of the approach used to model AG/SAG mills

As autogenous and semi-autogenous mills typically exhibit significant variations during their continuous operation, in terms of ore characteristics, so that the equation should be time dependent. The continuous dynamic equation for the fraction in size/component class il in the grinding zone can be written as,

$$\frac{d(w_{il}M)}{dt} = w_{il}^{in}W^{in} - w_{il}W^{out} - w_{il}\left[\sum_k \omega_k\left(D_{ilk}^b + D_{ilk}^s\right)\right] + \sum_{j=1}^{i-1} w_{jl}\left[\sum_k \omega_k\left(A_{jlk}^b + A_{jlk}^s\right)\right] \quad \text{IX-1}$$

which is analogous to the expression used to describe the dynamics of continuous mills VI-2, given that the term on the left-hand side represents the change in the mass of particles contained in class il, the first and second terms in the right-hand side the flowrates of material in class il into the grinding zone and out of it, respectively. The following term represents the disappearance of particles in the class il due to breakage (body and surface) and the last term the appearance of material in class il from breakage of particles contained in coarser size fractions. The flowrate of material entering the grinding zone is given by

$$w_{il}^{in}W^{in} = w_{il}^f W_{il}^f + w_{il}^r W^r \quad \text{IX-2}$$

in which w are the size fractions of particles and W the total flowrates. The index f refers to material in the feed stream, r the internal recycle and in the material that actually enters the active zone in the mill. The size distribution of the recycle stream within the mill is given by (Austin *et al.,* 1986)

$$w_{il}^{r} = \frac{c_{il} w_{il}}{\sum_{i=1}^{N_s} \sum_{j=1}^{Nc} c_{ij} w_{il}} \qquad \text{IX-3}$$

where c_{il} is the discharge (classification) function for particles contained in size class il, N_s and N_c are the number of size and composition classes, respectively. The recycle flowrate is given by

$$W^{r} = W^{out} \sum_{i=1}^{N_s} \sum_{j=1}^{Nc} c_{ij} w_{il} \qquad \text{IX-4}$$

whereas the discharge flowrate and the product size distributions are given by

$$W^{p} = W^{out} - W^{r} \qquad \text{IX-5}$$

and

$$w_{il}^{p} = \left(\frac{(1 - c_{ij}) w_{il}}{\sum_{i=1}^{N_s} \sum_{j=1}^{Nc} (1 - c_{ij}) w_{il}} \right) \qquad \text{IX-6}$$

The global mass balance for the mill is then given by

$$\frac{\mathrm{d}M}{dt} = W^{out} \sum_{i=1}^{N_s} \sum_{j=1}^{Nc} c_{ij} w_{il} + W^{in} - W^{out} \qquad \text{IX-7}$$

The disappearance and appearance terms related to particle body breakage in IX-1 are given by

$$D_{ilk}^{b} = \int_{0}^{E_{max}} \int_{0}^{E_{max}} m_{ilk}(E_N, E_T) p_k(E_N, E_T) \int_{0}^{1} [1 - b_{iilk}(e, E_N, E_T)] F_{il}(e, E_N, E_T, t) p_k(e) \mathrm{d}e \, \mathrm{d}E_N \mathrm{d}E_T \qquad \text{IX-8}$$

$$A_{ilk}^{b} = \int_{0}^{E_{max}} \int_{0}^{E_{max}} m_{jlk}(E_N, E_T) p_k(E_N, E_T) \int_{0}^{1} b_{ijlk}(e, E_N, E_T) F_{jl}(e, E_N, E_T, t) p_k(e) \mathrm{d}e \, \mathrm{d}E_N \, \mathrm{d}E_T \qquad \text{IX-9}$$

whereas the corresponding terms for surface breakage are given by

$$D^{S}_{ilk} = \int_{0}^{E_{max}} \int_{0}^{E_{max}} \kappa_{il}(E_N, E_T) m_{ilk}(E_N, E_T) p_k(E_N, E_T) \int_{0}^{1} [1 - F_{il}(e, E_N, E_T, t)] p_k(e) \mathrm{d}e \, \mathrm{d}E_N \mathrm{d}E_T \quad \text{IX-10}$$

$$A^{S}_{ilk} = \int_{0}^{E_{max}} \int_{0}^{E_{max}} \kappa_{jl}(E_N, E_T) m_{jlk}(E_N, E_T) p_k(E_N, E_T) \int_{0}^{1} a_{ijlk}(e, E_N, E_T, t) \left[1 - F_{jl}(e, E_N, E_T, t)\right] p_k(e) \mathrm{d}e \, \mathrm{d}E_N \mathrm{d}E_T \quad \text{IX-11}$$

where $p_k(E_N, E_T)$ represents collision energy spectrum for contact class k, which is composed of both a normal and a tangential (shear) component and the mass fraction lost due to surface breakage is $\kappa_{il}(E_N, E_T) = t_{a10,il}$.

Besides the mass balance, the model also requires expressions to describe how the fracture energies of the particles contained in the charge evolve with time in grinding. These are of key importance, since they can describe the differential breakage of weaker and tougher particles, with the weaker ones breaking more readily, with the toughest ones left in the charge and becoming weaker due to accrual of damage.

In order to convey the information on the collision geometry to the UFRJ model it is necessary to define each of the collision classes. A collision class *k* contains information about the particles involved in that type of collision, in terms of material (ore, balls, liner) and size.

Table IX-1 shows a summary of the collision matrix for a pilot scale SAG mill. The DEM particle class is then defined as p and q, in which “zero” means that the element involved in that collision is a steel ball or the mill liner, whereas values other than zero mean that a real ore particle is involved in the collision within DEM. The indexes *p* and *q* can be made to coincide with the particle size classes (i) in the mechanistic model.

One important part of the model is related to the estimation of the mass captured $m_{il}(E_N, E_T)$ and the energy split among captured particles of class il, $p(e)$, that appear in Equations IX-8 to IX-11. In these the mass of particles captured in a stressing event is given by $m_i = N_{cap,i} m_{p,i}$, where $N_{cap,i}$ is the number of particles captured in the stressing event. In this moment a distinction must be made between particle sizes which are explicitly simulated using DEM and particle sizes which are not sub-DEM sizes.

In the case of particles which are explicitly simulated using DEM three cases are identified: if both ore particles involved in contact *k* are from the same size fraction i ($p = q \neq 0$), then $N_{cap,i}$ = 2; if only one ore particle in contact *k* comes from the size fraction i ($p \neq q \neq 0$), then $N_{cap,i}$ = 1 and if neither particle involved in the collision is from size class i ($p = q = 0$), then $N_{cap,i}$ = 0. The sub-DEM particles are treated as if they were inside a ball mill, in which the mass captured between colliding grinding media can be calculated from the particle interaction model reviewed on section VI.3.

Table IX-1 Example of selected contact class indexes for a pilot SAG mill

Contact class	Elements in contact	DEM particle class		Particle diameter	
k		p	q	d_p (mm)	d_q (mm)
1	Ball-ball	0	0	160	160
4	Ball-particle	0	2	160	140
10	Ball-liner	0	0	160	∞
28	Particle-particle	2	2	140	140
53	Particle-particle	7	7	18	18
54	Particle-liner	7	0	18	∞

IX.2 Simplified approach

A first demonstration of the concept of the SAG model is here presented. The particle interaction approach is the simplified form that uses the same concepts of the ball mill simulations with the mechanistic model developed in 2009 (Tavares and Carvalho, 2009) as presented on section VI.2. In order to estimate the mass captured (Equation VI-19), the equivalent impact energy $E^*$is assumed to be equal to the 80 percentile of the distribution of a given contact type *k*.

The energy split function is considered as being uniform among particles captured in the bed, being described by the Dirac delta function (Tavares and Carvalho, 2009). For the case of DEM particles in which ore particles in contact come either from the same size class ($p = q \neq 0$) or from different size classes ($p \neq q \neq 0$), $p_i(e) = \delta(e - 0.5)$. On the other hand, for sub-DEM particles, the energy split function is given by

$$p_i(e) = \delta\left(e - \frac{1}{N_{cap,i}}\right) \qquad \text{IX-12}$$

In order to demonstrate the potential of the MPBM approach to describe comminution in a SAG mill, a pilot plant mill grinding the copper ore was simulated. The mill has 1.8 m of diameter (6´x 2´) and was operated at 75% of critical speed. Total mill filling was 25%, comprised of 10% of steel balls, with a top size of 150 mm, and 15% of ore. The mill was drawing 13.7 kW of power, and these conditions corresponds to the pilot test case #1 presented in section VIII.2.2.

The mill charge, as measured after a crash-stop (Figure VII-12) in the pilot scale SAG mill has been used to simulate the mechanical environment in the mill using DEM, with a typical image of the charge in motion shown in Figure VIII-23.The collision energy spectrum for selected contacts is illustrated in Figure IX-2. The breakage model parameters for the copper ore are presented in Table VII-1.

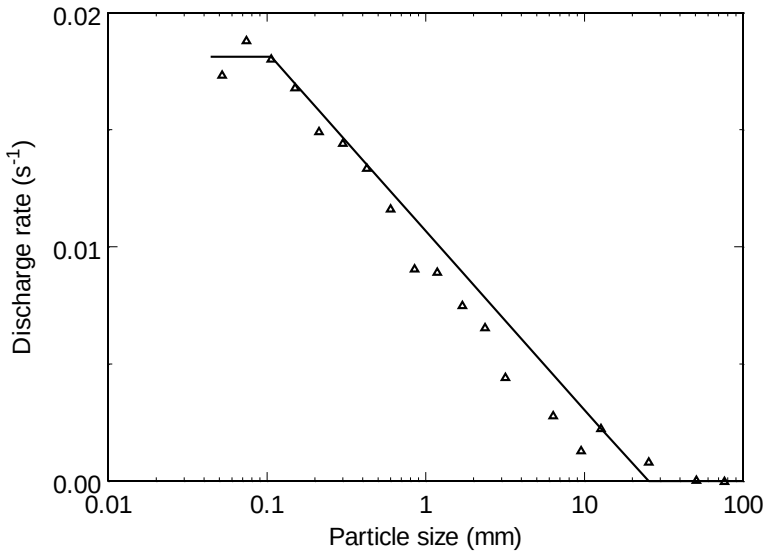

Figure IX-2 Calculated discharge function for the pilot-scale SAG mill

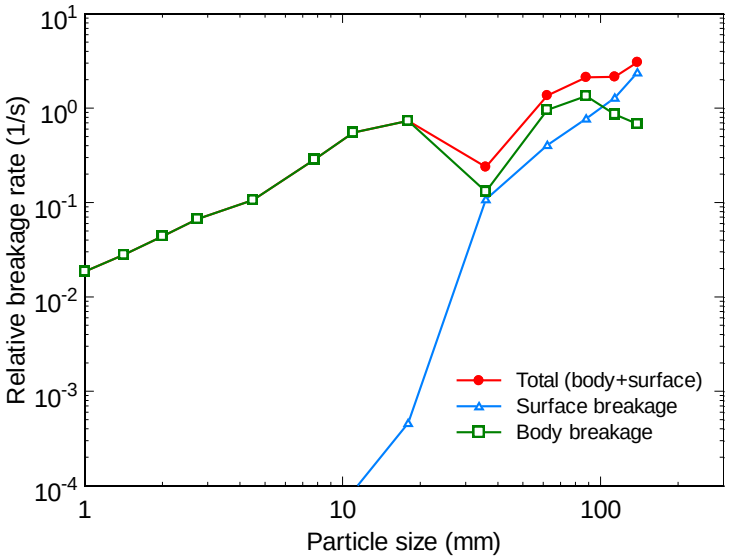

Figure IX-3 Breakage rates for grinding the copper ore in the pilot SAG mill predicted using the simplified SAG mill model

From the DEM simulations of the mill hold-up in motion for the pilot scale mill, collision (normal and shear) energy spectra have been estimated. These data were then fed to the UFRJ mechanistic model equations, solving them numerically for a given lapse of time. In order to illustrate the model response, the apparent breakage rates, estimated from the terms in brackets in Equation IX-1, were estimated. Figure IX-3 shows the apparent breakage rates as a function of particle size, which resemble typical results shown in the literature, in which fine particles have low breakage rates, reaching a maximum at about 10-20 mm, dropping for particles at about 40 mm in size, then raising again for particles with sizes up to 150 mm.

Figure IX-3 also shows the contributions of body and surface breakage on the apparent breakage rates for the different particle sizes. Whereas surface breakage plays a very important role in breakage of the coarsest particles contained in the hold-up, it becomes of limited importance for finer particles contained in the charge. In every case, it is likely that particles are often stressed with insufficient amount of energy to cause breakage in each collision event, so that particles are progressively damaged and, only then, broken.

These simulations showed that the initial application of UFRJ model provides qualitatively sensible results, since it was able to describe that the relationship between breakage rates and particle size follows the same trend as that reported by Austin *et al*. (1986) (Figure IV-15) and Leung *et al*. (1987) (Figure IV-17). Unfortunately, the high complexity of the system of equations required long computing times, demanded several hours just to run 30 seconds of simulation. This was due to a number of reasons. For instance, the way the prototype code was designed to test the model involved several nested calculation loops. This means that particle sizes, fracture energies, collision energies and mass capture model calculations obeyed a hierarchy.

The computational time limitation allowed for simulating only a few seconds of mill operation. As such, based on the DEM simulations from given hold-up size analysis, the simulation allowed to predict the breakage of the ore particles inside the mill, with no feed or discharge of material. It is recognized that this assumption is not robust enough to provide accurate predictions of the mill performance, being the charge stabilization one of the critical requirements to be met by the UFRJ model applied to SAG and AG mills. It is expected that the mill product performance can be predicted if the stabilization of the ore hold-up can be accurately described.

IX.3 Improvements on particle breakage models

As discussed, the development of this thesis required the improvement of some models and procedures. These improvements ranged from a new appearance function model calculation, a surface breakage model refinement and a simplification of the Tavares (2009) damage accumulation model.

IX.3.1 New appearance function model and optimization

An important part of the mechanistic model developed at UFRJ is that it uses some of the breakage characterization parameters from standard tests. Examples are the A and b parameters and the appearance function that come from the standard Drop Weight Tester. This allows, in principle, using parameters that are compatible with databases collected in the past. However, the traditional cubic spline method, used by Whiten (1972), is not identified as the most appropriate description for the wide range of t_{10}

values that are encountered when simulating mills using the mechanistic breakage model. In addition to this, the cubic-spline method requires at least three fitting parameters (spline knots) per t_n curve.

In order to overcome these limitations, the incomplete beta function equation was implemented as an alternative and more appropriate model. It is a continuous function of the type $t_n = \mathrm{f}(t_{10}, \alpha_n, \beta_n)$, whose first attempt to apply in describing drop weight data was in the work by Milin (1994). The advantages of utilizing the incomplete beta function include the fact that it is a continuous function in the [0,1] domain, besides the fact that it requires fitting only two parameters per t_{10} - t_n curve. The functional form of the incomplete beta function in terms of $t_{10}, \alpha_n, \beta_n$ is,

$$t_n(t_{10}, \alpha_n, \beta_n) = \frac{1}{\int_0^1 y^{\alpha_n - 1}\,(1-y)^{\beta_n - 1}\mathrm{d}y} \int_0^{t_{10}} y^{\alpha_n - 1}\,(1-y)^{\beta_n - 1}\mathrm{d}y \qquad \text{IX-13}$$

The incomplete beta function is a monotonic crescent function on the [0,1] domain. It is useful to fit the t_{10} data. The set of α_n e β_n parameters is function of the ore and may be determined from the t_{10} - t_n obtained experimentally from the Drop Weight Test. The objective function may be written as

$$f_{obj}(\alpha, \beta) = \sum_n (t_n - t_n^*)^2 \qquad \text{IX-14}$$

However if the set of α_n e β_n parameters are fitted without constraints, an inappropriate result may appear. An example of this is presented in Figure IX-4. It shows some t_n curves cross each other for t_{10}values below 10 %, which is the low energy range. The impact of this undesirable effect on the particle size distributions is the generation of negative cumulative passing values which are, evidently, not valid.

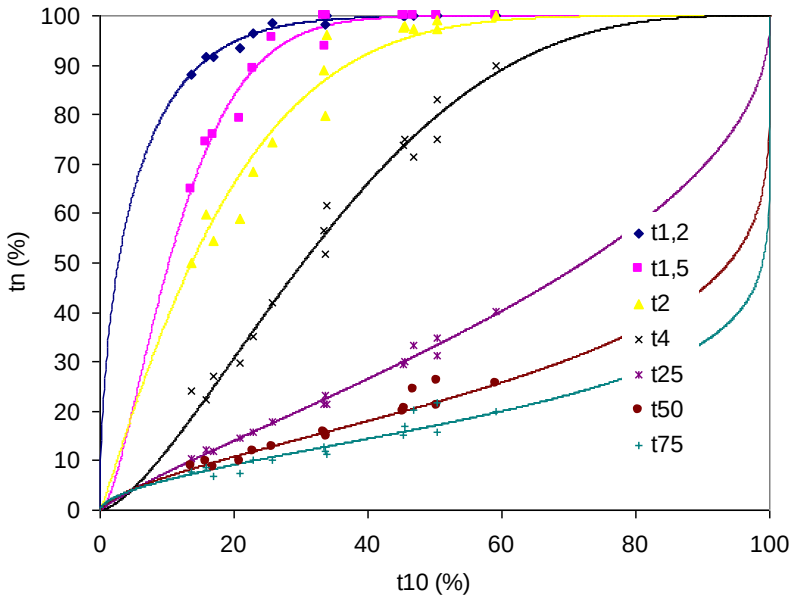

Figure IX-4 Set of $t_{10} - t_n$ data and fitted curves using the incomplete beta function model without constraints

In order to ensure that the curves do not cross each other and, therefore, do not give unrealistic results within the domain of t_{10} values of interest, a constraint optimization strategy was implemented. The constraint considers that t_n values are always equal or greater than t_{n+1} values for the same t_{10} value, that is $t_n(t_{10}) \geq t_{n+1}(t_{10})$. A method that can be used to insert this constraint is to apply a penalty to the objective function by the use of a function that is as large as or larger than the interval that violates the constraints. An appropriate function for this task is of the form,

$$w_n = \int_0^1 \max[t_{n+1}(t_{10}, \alpha_{n+1}, \beta_{n+1}) - t_n(t_{10}, \alpha_n, \beta_n), 0]\mathrm{d}t \qquad \text{IX-15}$$

With the penalty function w_n, the objective function can be rewritten as,

$$f(\alpha, \beta) = \sum_n (t_n - t_n^*)^2 + \sum_n \int_0^1 \max[t_{n+1}(t_{10}, \alpha_{n+1}, \beta_{n+1}) - t_n(t_{10}, \alpha_n, \beta_n), 0]\mathrm{d}t \qquad \text{IX-16}$$

Then, the result from the previous example of optimization is presented in Figure IX-5. For the same data set of Figure IX-4 the optimum fitting does not show any crossing among the t_n curves. The optimization algorithm was the *Active Set* optimization and it was coded in the function fmincon of Matlab 6.5® (Mathworks, 2008).

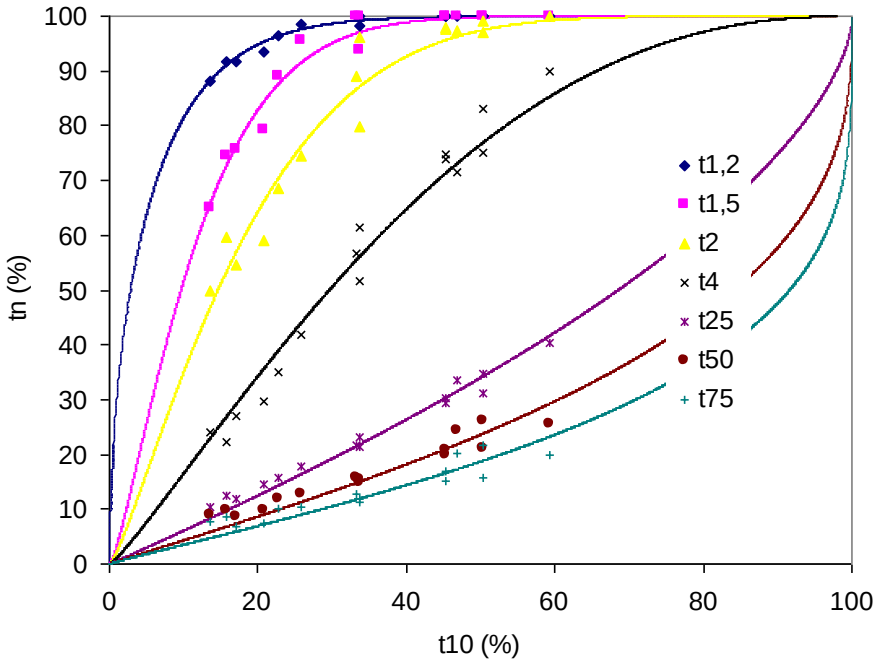

Figure IX-5 Set of $t_{10} - t_n$ data and fitted curves using the incomplete beta function model with the constraint optimization

IX.3.2 Surface breakage modeling

The use of the JKMRC abrasion breakage test (Napier-Munn *et al.,* 1996) result as an input to the original mechanistic mill model presented a series of limitations, particularly because it did not account for the effect of particle size and impact energy on the outcome of each surface breakage event. Although the study of surface breakage is an area of intense research at the moment, there is no widely accepted mathematical description that could be applied in place of it. An improved mathematical description has been proposed that takes into account some of these effects.

The improved model is based on the hypothesis that the amount of surface breakage products generated on a stressing event is affected by the magnitude of the collision energy and on the impact angle. In analogy to the equation proposed to describe

body breakage (Equation III-15), the relationship that describes the amount of surface breakage product follows a power law relationship with the ratio between the collision energy and the median particle fracture energy:

$$t_{a10} = a_a \left(\frac{E_m}{E_{m50u}} \right)^{\upsilon_a} \qquad \text{IX-17}$$

where E_{m50u} is the median specific fracture energy of the particles that did not suffer body breakage and the parameters a_a e υ_a must be fit to experimental data.

IX.3.3 Simplified damage model

The numerical iterative solution of the damage equation (Equation III-28) using Newton's method (Atkinson, 1989) has to be called a large number of times during the mechanistic model simulation, to calculate the damage value. Even though it converges quite quickly this can consume a lot of computational time. The main problem resides on the number of times the damage equation has to be solved in a single simulation time step. In order to circumvent this requirement and thus reduce the time taken to solve the problem, a new analytical equation is proposed to calculate the damage suffered by particles of fracture energy E_m when stressed with an energy input E_k.

First, the solution of the damage model for a range of values was calculated using Newton's method. The solution using Newton's method has proven to be reliable and has always found the root of the damage equation. The iterative method consists on the calculation of the value of function $f(D^k)$ and its first order derivate $f(D^k)$ for the damage value D^k. Then, the damage at the new iteration step D^{k+1} is calculated from the Equation IX-18.

$$D^{k+1} = D^k - \frac{f(D^k)}{f'(D^k)} \qquad \text{IX-18}$$

The procedure is repeated until the convergence criteria is achieved, $(D^{k+1} - D^k) < 10^{-8}$. The function $f(D)$ and its first order derivate form are:

$$f(D) = \left[\frac{2\gamma(1-D)r}{2\gamma - 5D + 5} \right]^{\frac{2\gamma}{5}} - D \qquad \text{IX-19}$$

$$f'(D) = \left\{ \frac{1}{5} \left[\frac{2\gamma(1-D)r}{2\gamma - 5D + 5} \right]^{\frac{2\gamma}{5}} \left[\frac{-2\gamma r}{2\gamma - 5D + 5} + \frac{10\gamma(1-D)r}{(2\gamma - 5D + 5)^2} \right] \frac{(2\gamma - 5D + 5)}{(1-D)r} \right\} - 1 \qquad \text{IX-20}$$

where r is the ratio between the energy applied over the particle fracture energy before damage.

The analytical damage equation that was found to satisfy and reproduce quite well the results from the formal damage solution is given by

$$D(r) = \frac{\emptyset_d}{2} erfc\left[-\frac{\log(r) - \mu_1}{\sigma_1 \sqrt{2}} \right] + \frac{1 - \emptyset_d}{2} erfc\left[-\frac{\log(r) - \mu_2}{\sigma_2 \sqrt{2}} \right] \qquad \text{IX-21}$$

where $D(r_i, \gamma)$ is the damage calculated from Newton's method applied to the original model proposed by Tavares (2009). It is a weighted sum of two complementary error functions and it depends on five fitting parameters ($\emptyset_d$, μ_1, μ_2, σ_1 and σ_2) which were fitted to damage parameter (γ) values from 3.0 to 8.0 in intervals of 0.01 units. Figure IX-6 shows how the fitting parameters vary with γ and also the value of the objective function $f_{obj}(\gamma)$ of the fitting procedure, which has the form represented by Equation IX-22:

$$f_{obj}(\gamma) = \sum_i [D(r_i) - D(r_i, \gamma)]^2 \qquad \text{IX-22}$$

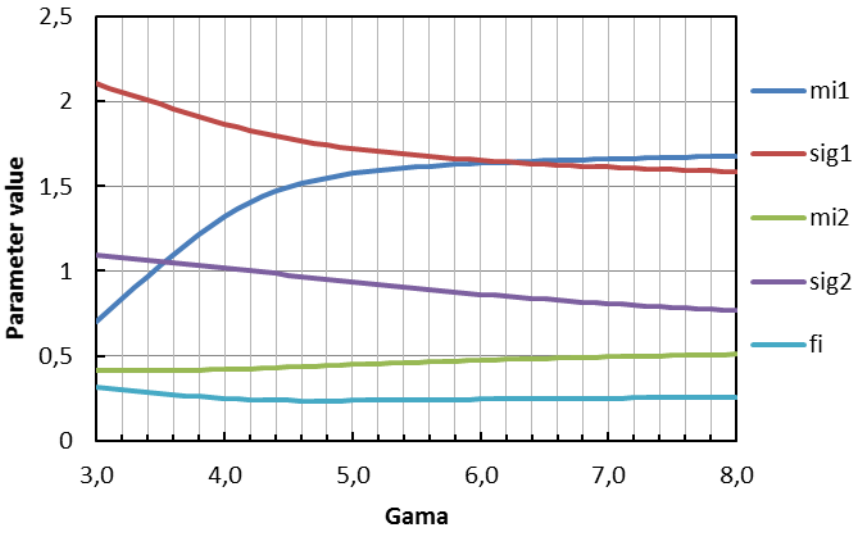

Figure IX-6 Parameters in Equation IX-21 as function of the damage accumulation (γ) value

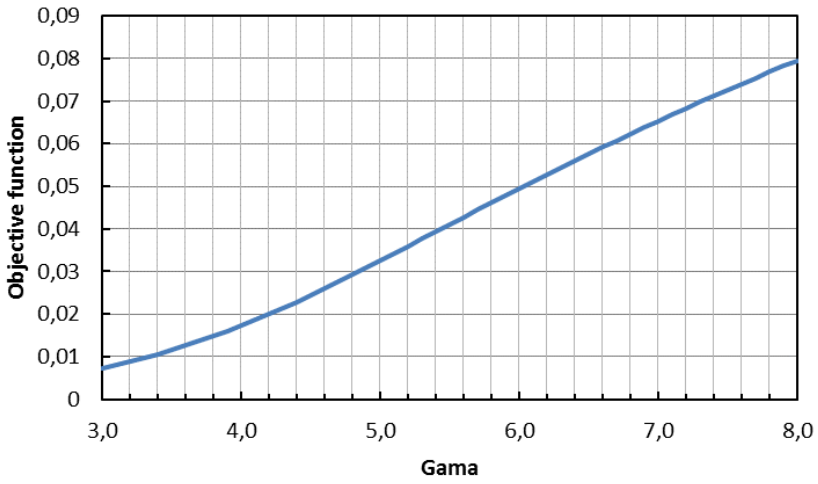

Figure IX-7 Values of the objective function as function of the damage accumulation (γ) value

Once the parameters in Equation IX-21 have been fitted, the value of damage was calculated for a range of values of the damage parameter (γ) using the optimum set of parameters for each γ value. For values that were equal or smaller than 5, the value of the calculated damage corresponds quite well to the one calculated from the original model in a wide range of values for the ratio r. In the case of damage parameter values above 5 the deviation becomes noticeable and the analytical model should be used carefully. This is illustrated in Figure IX-8.

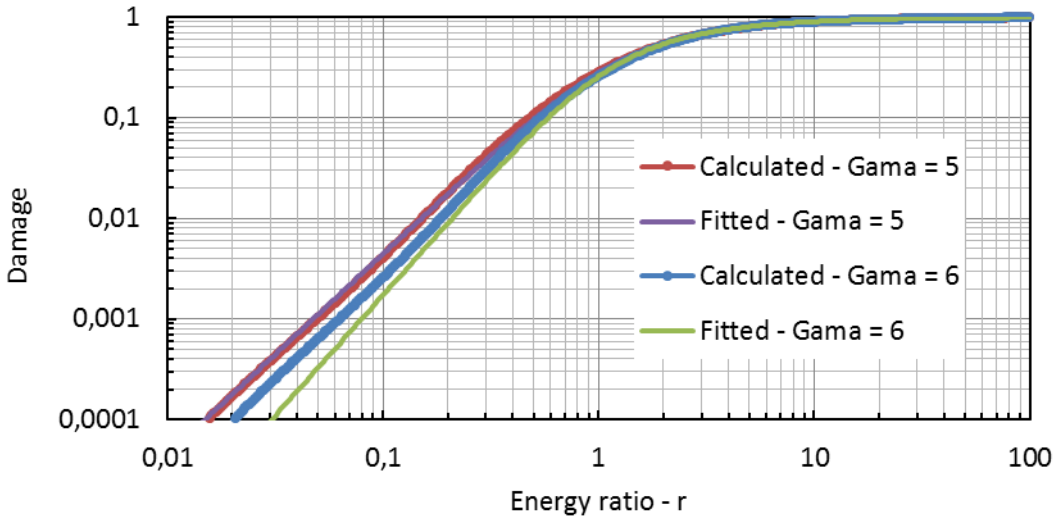

Figure IX-8 Comparison between both method of damage calculation for two sets of damage parameters

IX.4 Breakage of sub-DEM particles

An important stage of development of the SAG mill model was to demonstrate that the mechanistic approach is able to predict the effect of several operating and design parameters when the mill charge is entirely composed of unbreakable elements, that is, grinding balls. This is the case of ball mills. Once the ball mill predictions reach a satisfactory level, the confidence on the application of the model to the more complex SAG mill will increase.

DEM simulation outcomes of ball mills that were presented on section VIII.2.1 fed the mechanistic model to predict grinding of mono-sized feeds. As such, the effect of the following variables was investigated through simulations using the mechanistic model:

- Mill size
- Liner design
- Ball size
- Mill filling
- Mill speed.

Mono-sized feeds ranging from 7.9 mm to 0.105 mm were used in the simulations. The six different listed ores were used in these simulations, and their model parameters are listed in Table III-1. A combination of all DEM simulations, particle sizes and ores resulted in approximately 5050 simulation runs. All simulations using the mechanistic model required about one day to complete.

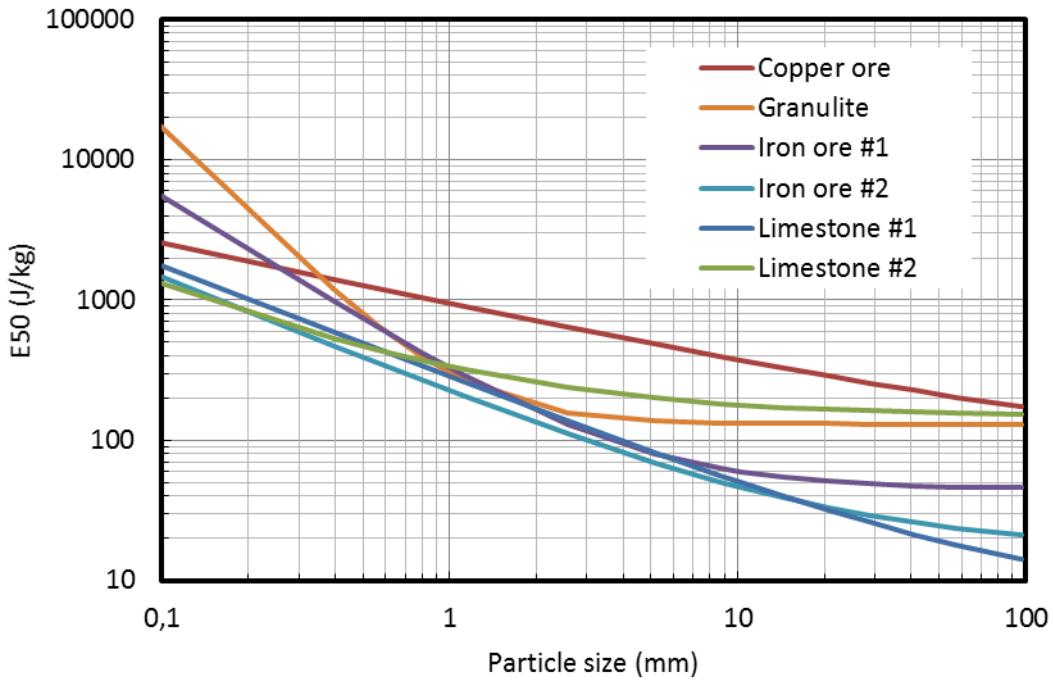

Figure IX-9 Median of the fracture energy distribution as function of the particle size for selected materials

Simulations of grinding using the mechanistic model have been carried out by imitating batch tests with narrow size samples, such as those suggested as part of the scale-up method proposed by Austin *et al.* (1984) to determine breakage distribution and breakage rate functions. Particle sizes tested ranged from 75-106 μm to 5.6-7.9 mm, covering a total of 13 size intervals. Typical results from simulations are shown in Figure IX-9. Previous studies have demonstrated the good agreement between experiments and simulations using the mechanistic ball mill model (Tavares and Carvalho, 2009; Tavares and Carvalho, 2010).

Disappearance plots have been prepared as a function of particle size and results are shown in Figure IX-10. From these plots it is possible, in analogy to the analyses of experimental data from batch grinding tests, to estimate the equivalent first-order breakage rates. These are often estimated assuming the validity of the expression (Austin *et al.,* 1984)

$$\frac{dw_1(t)}{dt} = -k_1 w_1(t) \qquad \text{IX-23}$$

which has the solution

$$\ln\left(\frac{w_1(t)}{w_1(0)}\right) = -k_1 t \qquad \text{IX-24}$$

where k_1 are the specific breakage rates, given by the slope of the best-fit line. The least squares best-fit values of the breakage rates have been estimated from the simulated data up to a grinding time of 30 minutes or until no more than 10% of the original material remains.

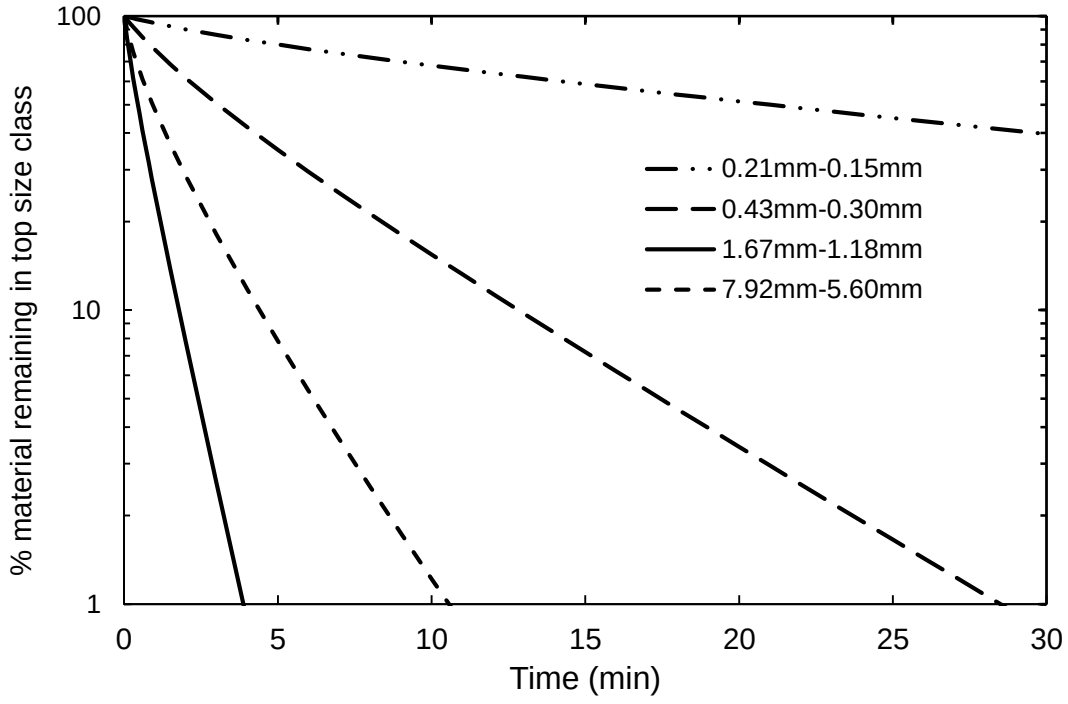

Figure IX-10 Simulated disappearance plots of batch grinding tests for granulite (30% ball load, 25 mm ball size and 68% of critical speed in a 30.5 cm diameter mill)

The effect of particle size on the breakage rates of a number of materials is illustrated in Figure IX-11. It reproduces the well-documented trend of breakage rates with particle size, with an increase in breakage rates up to a maximum, at a particle size of about 1-4 mm, following by a drop at coarser sizes for the different materials. Simulated results, represented using symbols, were used in fitting parameters of the equation proposed by Austin *et al.* (1984):

$$s_i = \frac{S_1 d_i^{\alpha}}{1 + (d_i/\mu)^{\Lambda}} \qquad \text{IX-25}$$

where S_1, α, μ and Λ are model parameters that must be fitted to data, with d_i and μ given in millimeters. Parameter S_1 approaches the specific breakage rate of 1 mm particles as μ increases.

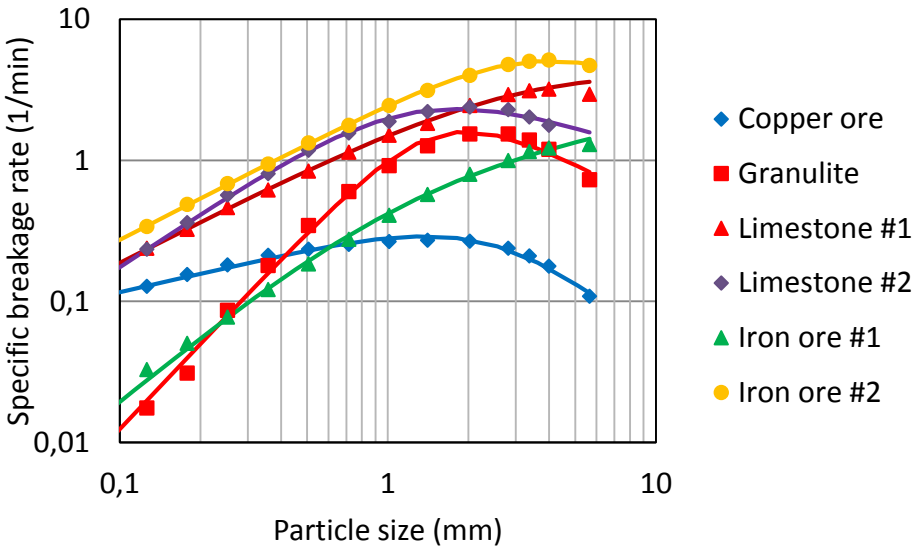

Figure IX-11 Effect of the particle size on the breakage rates for the selected ores. The dots represent the breakage rate at specific particle sizes calculated from the outcomes of the mechanistic model. The lines are the best fit using the selection function (Equation IX-25)

The effect of ball size on specific breakage rates predicted using the mechanistic model is illustrated in Figure IX-12 for selected materials, and shows that the model is capable of accounting for the shift in the size corresponding to the maximum breakage rate with a change in ball size, which has been widely documented in the literature (Austin *et al.,* 1984; Austin and Concha, 1993; Erdem and Ergun, 2009; Katubilwa and Moys, 2009). Smaller ball sizes produce less energetic impacts (Figure VIII-17) and each impact captures fewer particles (Barrios *et al.,* 2011), being also less efficient at nipping coarser particles. Offsetting these effects that tend to decrease the specific rate of breakage as ball size decreases is the increased frequency of impacts that results from the larger number of smaller balls in the mill.

Figure IX-12 also shows that the slope of the line at finer sizes, represented by the fitting parameter α in Equation IX-25, may or may not vary with ball diameter. In several studies reported in the literature it was assumed that this slope remained constant as ball sizes varied, although it is recognized that this assumption was less due to experimental evidence and more because of lack of precise information for finer sizes (Austin *et al.,* 1984; Katubilwa and Moys, 2009). Indeed, variations in the slope of the specific breakage rate functions with ball sizes have been observed by a number of researchers (Herbst and Lo, 1992; Martinovic *et al.,* 1990). The simulated results from Figure IX-12 demonstrate that these two situations can occur, depending on material breakage properties.

It is important to realize that the different scale-up methods recognize the effect of ball size not only on the specific breakage rates, but also on the breakage distribution function. Herbst and Fuerstenau (1980) suggested that batch tests should be conducted with the ball size distribution that would be used in the industrial mill, primarily with the aim of describing the breakage distribution function. On the other hand, Austin *et al*. (1984) suggested conducting batch grinding tests with different ball diameters and then calculating the weighed-average breakage function for the actual ball size distribution that would be used in the full-scale mill. Indeed, these alternatives have been successfully used in the past, but a challenge remains when larger ball sizes are to be used in an industrial mill. Tests in small diameter batch mills should not be conducted using large ball sizes, since the motion of balls of such diameters will bear very limited resemblance to what happens in the operation of an industrial mill (Austin *et al.,* 1984). As such, the mechanistic model has a significant potential benefit over the other scale-up approaches when dealing with predictions of mills that use large ball sizes. This is particularly relevant, given the current trend in the minerals industry of using mills of increasing diameters, which are being progressively used to process even coarser feeds and, thus, requiring larger diameter make-up balls.

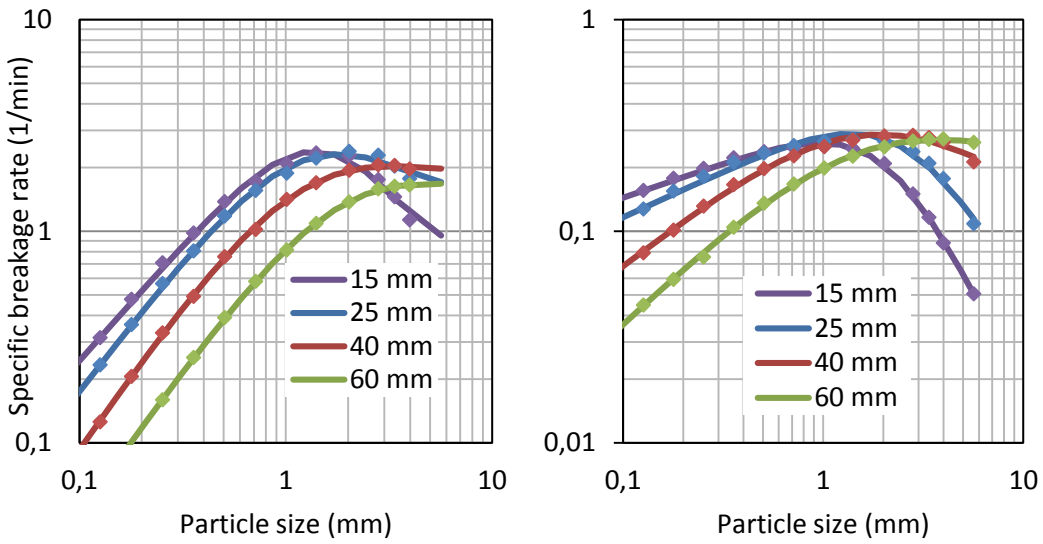

Figure IX-12 Breakage rates obtained from mechanistic model simulations showing the effect of ball size on a 30 cm for the Limestone #2 (left) and Copper ore (right)

The effect of mill speed on the breakage rates is illustrated in Figure IX-13. It shows that breakage rates increase significantly with fraction of critical speed, especially above 20%, dropping above the critical speed. This is associated with the increase in median specific collision energies, and the reduction in their specific frequency (number of collisions divided by ball load) for mill speeds above, about, 50%. It is important to state, however, that the assumption of perfect mixing of balls and powder charge becomes questionable as mill frequencies approach and surpass the critical speed, since, in these conditions, particles are more amenable to centrifuge than the balls, given their finer sizes.

It is now worthwhile to compare the predictions using the mechanistic model to estimates using the scale-up approaches by Austin *et al.* (1984) and Herbst and Fuerstenau (1980). In the approach proposed by Austin and co-workers, mill frequency influences the scale-up parameter S_1 according to the relationship,

$$S_1 \propto (\varphi_c - 0.1)\left(\frac{1}{1+\exp[15.7(\varphi_c-0.94)]}\right) \qquad \text{for } 0.4 < \varphi_c < 0.9 \qquad \text{IX-26}$$

where φ_c is the fraction of critical speed.

Herbst and Fuerstenau (1980) proposed that the specific breakage rates vary in proportion to the ratio between the net mill power and the mill load (P/M). Different

models have been proposed in the literature to describe the variation of mill power with mill design and operating variables (King, 2001) and, thus, predictions will vary with the chosen model. If the expression proposed by Rowland and Kjos (1980) is used, and assuming that the parameter S_1 from Equation IX-23 can be used to describe the variation of the breakage rates with particle size within the Herbst and Fuerstenau (1980) scale-up approach, then

$$S_1 \propto \varphi_c \left(1 - \frac{0.1}{2^{9-10\varphi_c}}\right) \qquad \text{IX-27}$$

In order to conveniently compare values of the parameter S_1 estimated from predictions using the mechanistic model to those predicted by the scale-up rules, results were represented as the ratio between S_1 values estimated for the different percentages of critical speed and a reference value, arbitrarily taken as 68% of critical speed. Figure IX-14 shows that the different approaches provide consistent predictions, although not identical. The mechanistic model predictions were positioned within the range of values estimated using Equations IX-26 and IX-27. It is important to realize, however, that the Herbst and Fuerstenau (1980) and Austin *et al.* (1984) predictions are independent of feed material when plotted in a graph such as the one shown in Figure IX-14, whereas the mechanistic model accounts for material effects. Further, some studies in the literature (Shoji *et al.,* 1982) have shown that the relationship between power and percent of critical speed does not remain invariant with other variables, such as mill diameter, filling and liner configuration, which further limits the validity of Equations IX-26 and IX-27, in particular for small diameter mills.

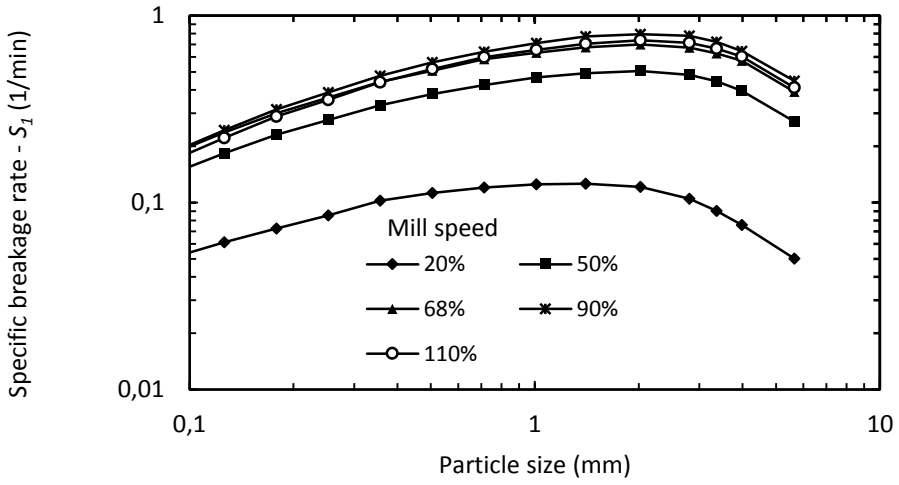

Figure IX-13 Simulations on the effect of mill speed: breakage rates as a function of particle size (left) for Copper ore (30% ball load, 25 mm ball size in a 0.6 m diameter mill).

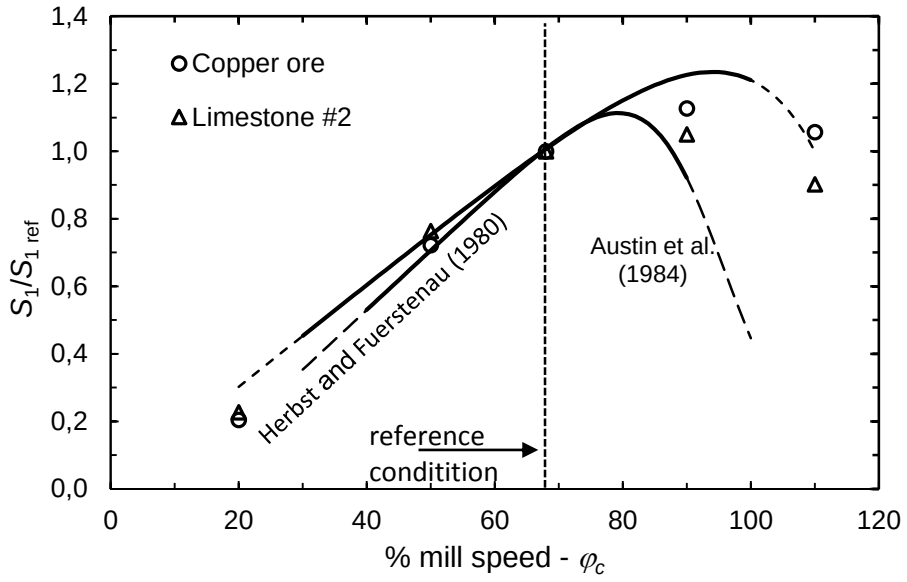

Figure IX-14 Simulated normalized breakage rates predicted by the mechanistic mode for selected materials and predictions using the model by Austin *et al.* (1984) and Herbst and Fuerstenau (1980) (30% ball load, 25 mm ball size in a 0.6 m diameter mill).

Predictions on the effect of mill filling on the breakage rates are illustrated in Figure IX-15. It shows that mill filling has a very limited effect on the breakage rates over a wide range of simulated conditions.

Results such as those from Figure IX-16 can then be compared to predictions using the scale-up relationships proposed by Austin *et al.* (1984) and Herbst and Fuerstenau (1980). Austin *et al.* (1984) proposed that the relationship between parameter S_1 and the fractional mill filling (J) could be described by

$$S_1 \propto \frac{1}{1+6.6J^{2.3}} \qquad \text{for } 0.2 < J < 0.6 \qquad \text{IX-28}$$

whereas in the approach proposed by Herbst and Fuerstenau (1980), considering Rowland and Kjos (1978) mill power model, the relationship would be (Austin and Concha, 1993)

$$S_1 \propto J(1-0.937J) \qquad \text{IX-29}$$

Figure IX-15 compares the results and shows that the mechanistic model is in reasonable agreement with predictions from the scale-up methods within the range of

mill loads from 20 to 50%. The figure once again shows the material-specific effect captured by the mechanistic model, which is not taken into account using either scale-up method.

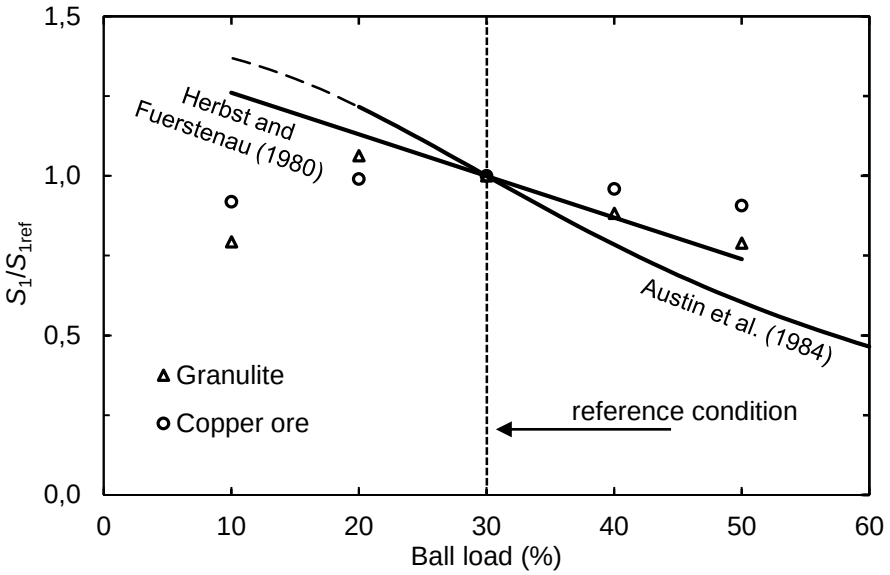

Figure IX-15 Simulated normalized breakage rates predicted by the mechanistic model for selected materials, and predictions using the model by Austin *et al.* (1984) and Herbst and Fuerstenau (1980) (25 mm ball size and 68% of critical speed in a 0.9 m diameter mill)

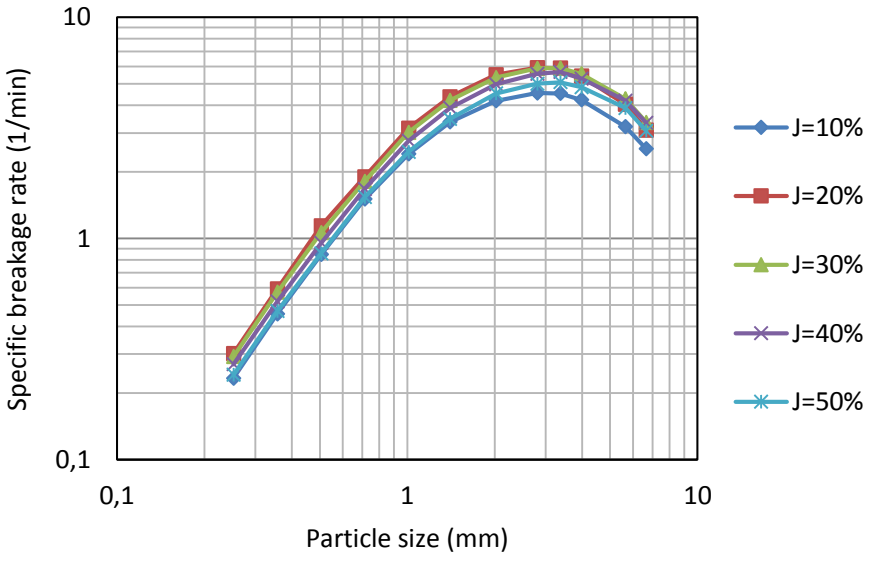

Figure IX-16 Mill filling effect for Granulite

The effect of mill liner on the specific breakage rates predicted using the mechanistic model is illustrated in Figure IX-17, which shows that it has a significant effect in the mills studied. When taller and, thus, more aggressive liners (Figure VIII-9 and Figure VIII-10) are used, the specific breakage rates of particles over the range of sizes also increase when compared to the nearly smooth liners. This is a variable that has not been incorporated in any of the empirical scale-up methods in the literature and its effect in grinding can be assessed using DEM-based scale-up models, such as the mechanistic ball mill model.

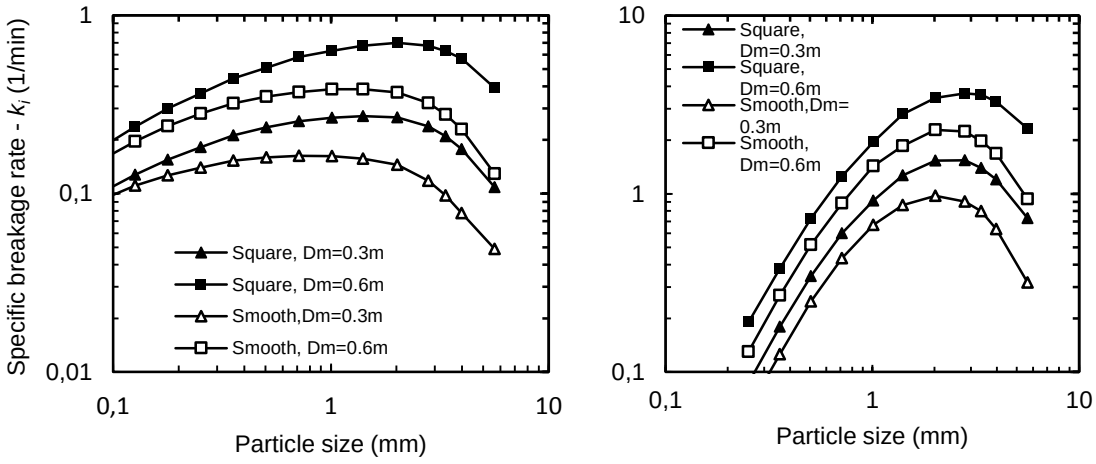

Figure IX-17 Effect of liner profile, depicted in Figure VIII-9 and Figure VIII-10 on breakage rates of Copper ore (left) and Granulite (right) (30 % mill filling and 68% of critical speed)

In the scale-up approach proposed by Herbst and Fuerstenau (1980), specific breakage rates vary directly with specific mill power, that is, the ratio between the net mill power and the mill load. This is in qualitative agreement with Bond's method of designing ball mills, in which the fineness of a ball mill product is dictated primarily by specific energy and ore grindability (Austin and Concha, 1993; King, 2001). Although not explicitly, the scale-up approach proposed by Austin *et al*. (1984) also incorporates the influence of operating and design variables in grinding as they affect mill power through functional forms that are similar to those given, for instance, by Equations IX-26 and IX-28. In the mechanistic ball mill model, the frequency and the distribution of collision energies, rather than the mill power, is used, besides the material breakage properties, as input to the simulations. Since these pieces of information are highly convoluted in

the mechanistic model (Equations IX-8 to IX-11), it is worthwhile analyzing if the predicted specific breakage rates are related to mill power.

Figure IX-18 compares for all materials and grinding conditions simulated the relationship between specific net mill power, given by the ratio of mill power calculated by DEM and mill load, and the specific breakage rate parameter S_1. Condensing a total of over five thousand simulations that included six materials over 13 size classes and conducted with a range of conditions, including mill and ball diameters, liner designs, mill fillings and speeds, Figure IX-18 shows that a material-specific signature appears. Indeed, the approximately linear relationship between S_1 and the net specific mill power is consistent with the scale-up approach proposed by Herbst and Fuerstenau (1980), which is based on the definition of the material and energy-specific breakage rates in ball milling.

It is important to realize, however, that although the mechanistic model recognizes the dominant effect of specific power on breakage rates, the scatter around the trend line suggests that other effects can have a smaller, but important role. This is illustrated in Figure IX-19, which compares predictions from batch grinding at the same specific power for the same mill but operating at different conditions such as mill speed and ball load.

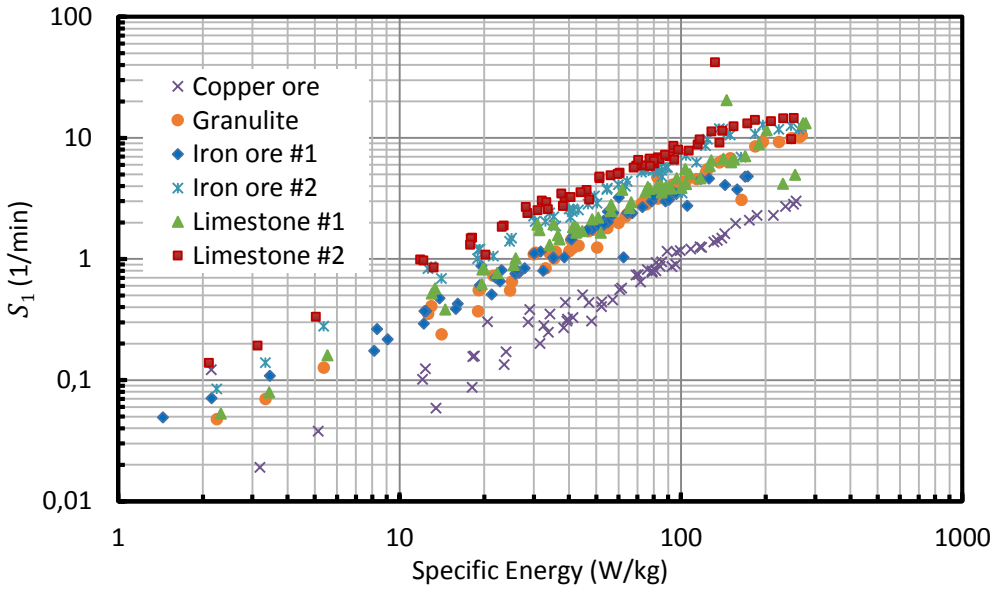

Figure IX-18 Predictions of specific breakage rate parameter S_1 using the mechanistic model as a function of mill specific power

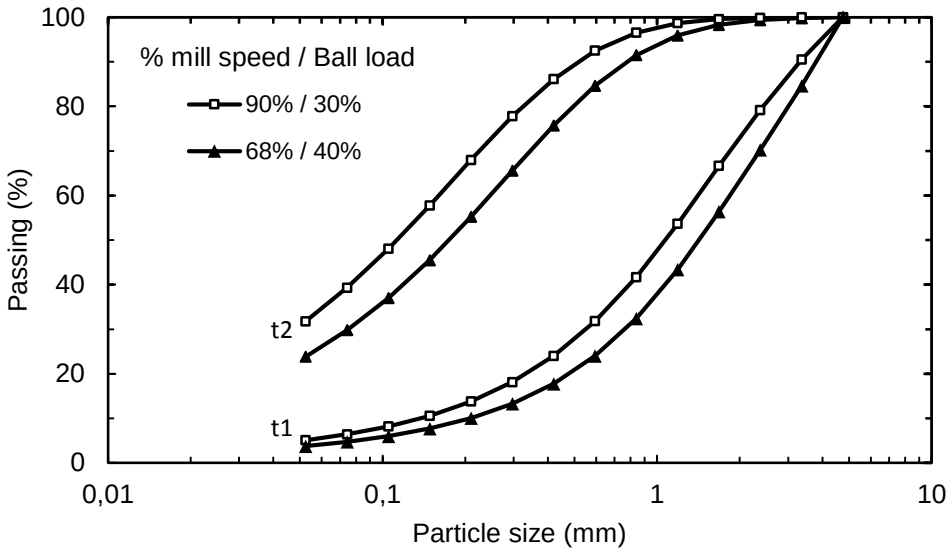

Figure IX-19 Product size distributions predicted using the mechanistic model from grinding the copper ore in a 1.8 m diameter mill operating at two different conditions, which resulted in the same specific power (186 kW/t) but different size distributions in a batch mill from a constant feed size distribution. t1 and t2 represent two different grinding times.

Finally, the full batch grinding simulation results are compared to the experimental measurements for a selected ore at three different initial monosized distributions. The initial size fraction for each test are: 0.600-0.425 mm (Figure IX-20), 1.70-1.18 mm (Figure IX-21) and 2.83-2.00 (Figure IX-22). The mill was rotating at 54 rpm (67.5 % of critical speed), with a ball filling of 30 % of 25 mm steel balls. These results have no sort of back calculation from batch grinding data. All the ore parameters were determined from bench scale breakage tests and yet, the results shows a good correlation, with the finer material presenting a bit of overgrinding effect when comparing the the experimental data to the simulations. The finer material (Figure IX-20) presents first-order breakage rates and in the conditions of the test, the capture model indicates that a number of particles are captured in each collision. This does not happen for the coarser material, above 1.70 mm, in this mill, the capture model indicates that in most of the collisions just a few particles or even a single particle are captured. This evidences the transition of the model from an operation condition where the dominant collisions capture multiple particles to a condition where the balls capture only a single particle per collision.

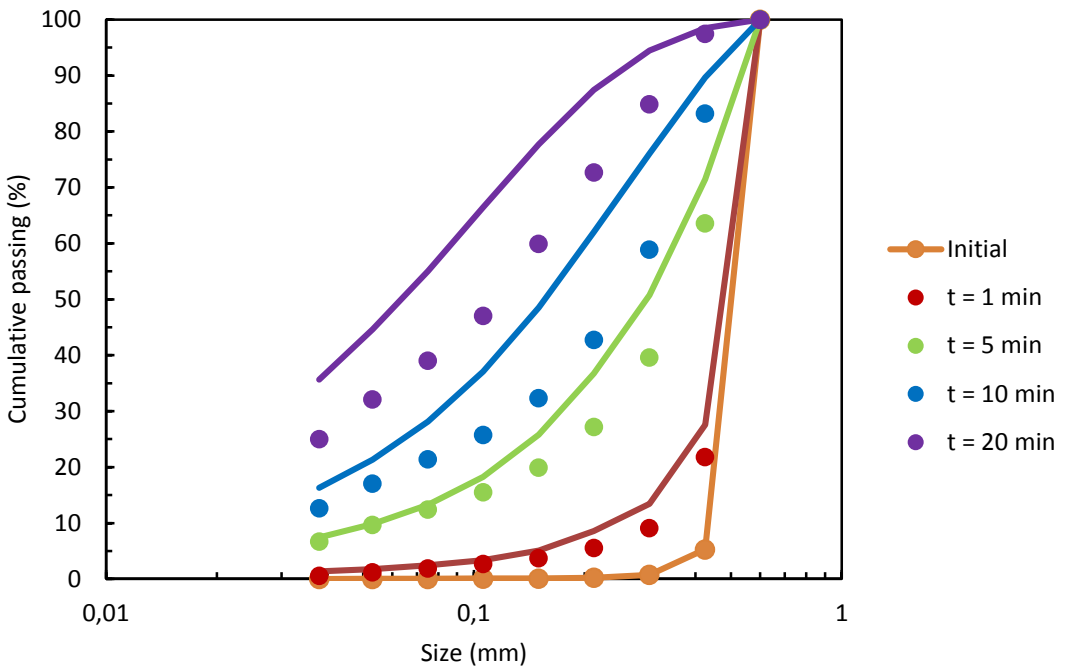

Figure IX-20 Comparison between simulated and experimental batch grinding results for 0.600-0.425 mm copper ore

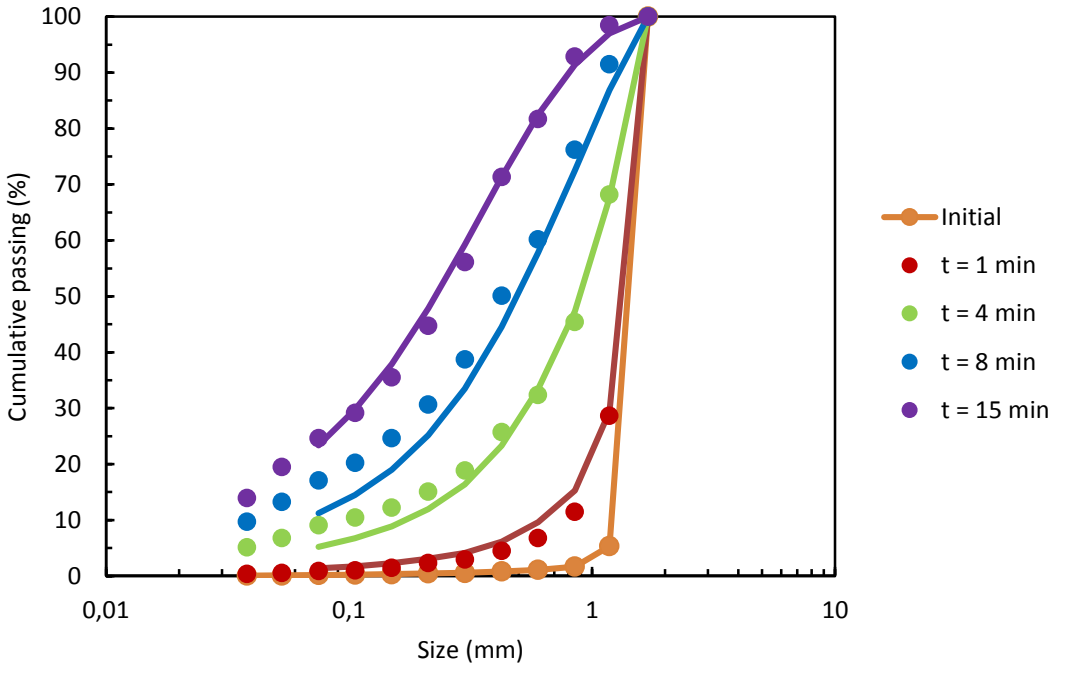

Figure IX-21 Comparison between simulated and experimental batch grinding results for 1.70-1.18 mm copper ore

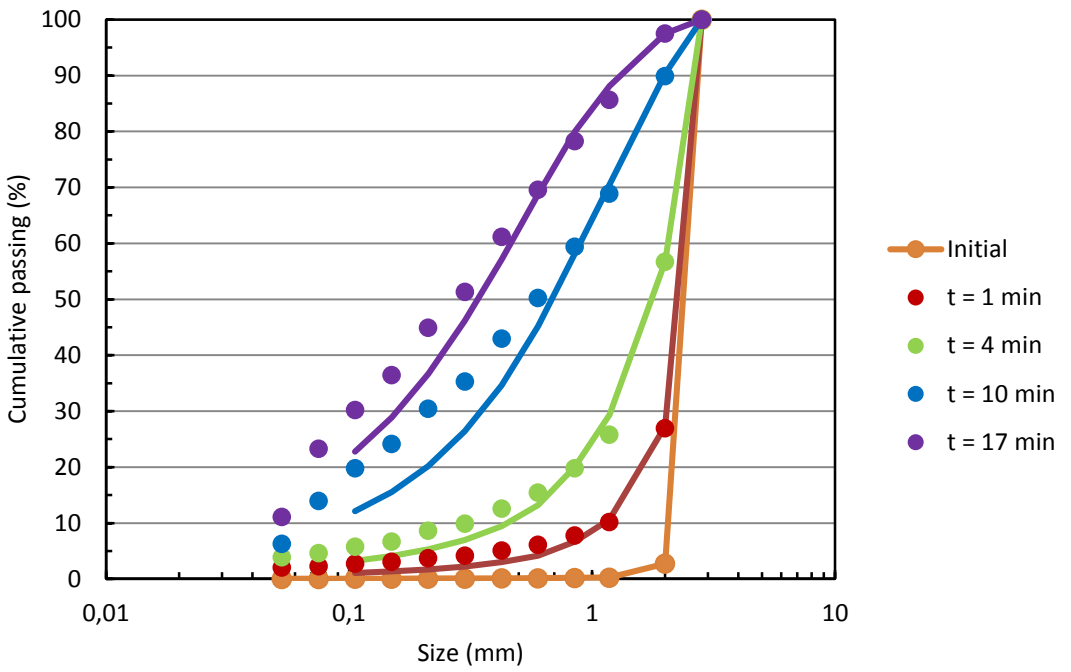

Figure IX-22 Comparison between simulated and experimental batch grinding results for 2.83-2.00 mm copper ore

The updated mechanistic model was able to predict the grinding behavior of mills as a function of several important variables, including ball size, mill filling, particle size, mill geometry and mill speed, for the case when the grinding media is not undergoing breakage. This corroborates the hypothesis that it is possible to predict the outcomes of a mill if the grinding environment is fully known and the ore breakage models are calibrated, provided that no breakage happens of particles contained in the DEM simulations. However, this corresponds to case when the grinding environment is in a pseudo-steady state, such as a ball mill. In this mill, the changes in ball charge are result of ball wear and breakage into scats, which are too slow in comparison to the changes in the charge of SAG and AG mills, which fluctuate as the properties of the ore fed to the mill change.

IX.5 Breakage of DEM particles

Breakage of DEM particles plays an important role on the success of the mechanistic model of AG/SAG mills developed. As such, there is a significant challenge in AG/SAG mill modeling to stabilize the grinding charge during the simulations.

One of the main assumptions in the conceptual model of SAG mills (Equation IX-1) is that grinding environment remains constant during a certain period, allowing the solution of the mass balances. For ball mills this assumption is valid, as the role of the balls is very well defined on the grinding. Thus, the changes on their size distribution due to wear or fracturing the steel balls is very slow when compared to the grinding dynamics. However, for SAG mills and AG mills, the grinding environment is continuously changing, so as to absorb the disturbances in the properties of the ore contained in the feed. As such, one of the key challenges in this case is to identify for each mill simulation the ideal time span during which the collision energy spectra generated from an older hold-up remains valid.

Verifying the validity of the model started with using measured distributions of the hold-up from a pilot scale test, calculating breakage of the sub-DEM particles (-12.5 mm) and comparing the amount of fines generated from breakage to the amount of material leaving the mill, which was measured in the pilot case studies. This approach is equivalent to simulating the ball mill using the mechanistic model, and assumes that the size distribution of the coarse particles remains constant with time.

Based on these assumptions, simulations to test the model for two different pilot scale cases were performed. The improvements performed on the previous SAG model approach (section IX.2), which also include the advances reported on section IX.3 have been incorporated to the SAG model. A summary of the improvements in this case were:

- New computational code
- Inclusion of particle capture model
- Inclusion of radial/monolayer energy split model
- New surface breakage model
- Optimized particle damage calculation

Table IX.2 presents the mechanistic model simulation results for both case 01 and case 03 respectively. The results show for both simulations that the amount of the sub-

DEM particles generated on a short period combined to the amount of fine particles that were fed to the mill were smaller than the mass discharged from the mill. The lack of fine particles generated from breakage indicates, as expected, that the contribution from the breakage of the coarser particles (DEM) plays a major role on the generation of fines, either by fracturing into a distribution of fragments, losing small bits due to chipping effect or continuously losing mass due to abrasion. This effect is even smaller in the case of autogenous grinding. These results indicate that in order to predict breakage, stabilization of the charge its necessary when predicting SAG performance using the mechanistic model.

Table IX-2 Fine discharge: measured versus simulation using the conceptual model

Fines discharge (t/h)	Case 01	Case 03
Measured	1.14	0.69
Prediction	0.92	0.45
Model prediction (% error)	-19%	-36%

The charge stabilization means that both the size distribution and the amount of coarse particles remains slightly constant during the operation of the mill. The proposed simulation procedure starts from an initial guess or from a measured hold-up. For the simulation of a pilot scale mill, the particle size distribution and total mass of the charge is relatively easy to be measured, as the mills are usually crash-stopped. However, for industrial scale mills, there are just a few records of measurements of the entire charge and they are of proprietary use. Fortunately, the laser scan technique is just starting to be applied on the estimation of the contents of the mill. If there are no measurements available, the hold-up distribution could be estimated from an approximation based on the fresh feed particle size distribution or even from estimations generated using phenomenological models such as Leung's model (Leung *et al*., 1986). This comes into play as the mechanistic model takes advantage of a good initial guess of the hold-up.

The proposed solution algorithm is the following:

1. The simulation procedure starts with an initial guess of the hold-up.
2. Proceed DEM simulation using the initial ore charge guess
3. Extract the collision energy spectra and mill power
4. Proceed mechanistic model simulation for short period of time

5. Analyze the breakage and transformation suffered by the particles
6. If there is a significantly change on the size distribution of the autogenous grinding media, perform a new DEM simulation and repeat from step 3. If not, advance time step.

The charge stabilization loop will provide the most probable solution to the mill among the infinity of results possible (Figure IX-23).

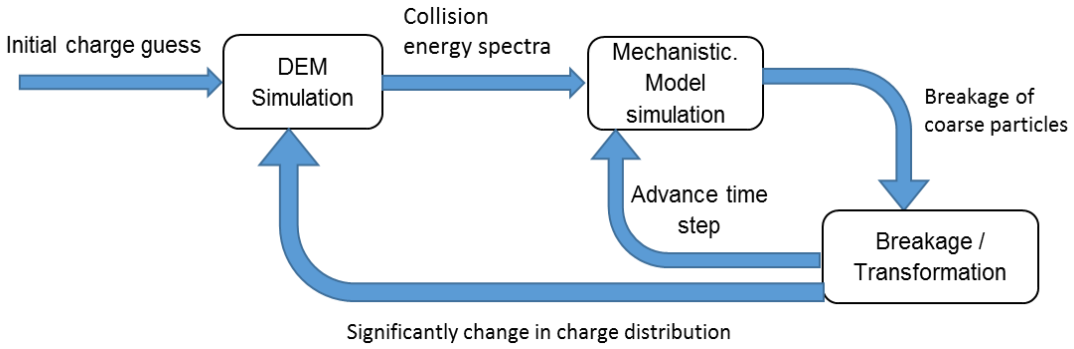

Figure IX-23 Simulation framework of the SAG model

X. Conclusions

The development of a mechanistic model of complex size reduction machines such as SAG and AG mills is a formidable task, requiring very detailed descriptions of a number of microprocesses. It became evident throughout the present work that mathematical models describing several of these microprocesses and appropriate outputs from a DEM simulation software were either not available or were not computationally feasible to incorporate in such complex framework.

For instance, a more efficient solution to the model of weakening due to repeated impacts has been proposed by using an approximate analytical solution, which improved computation efficiency by a factor of 10. Another improvement was the incorporation of a continuous analytical solution for the energy-dependent appearance function. This allowed reducing the number of fitting parameters as well as guaranteeing consistent results even for low t_{10} values. These values cover the interface between surface and volume breakage of particles. Regarding surface breakage, a simplified model has been proposed that accounts for the effect of stressing energy and material variability. Although it represents an advance in comparison to earlier descriptions, it is recognized as the breakage microprocesses that requires the greatest attention in the future.

While, after proper calibration, DEM simulations offered detailed information regarding the mechanical environment inside the various mills simulated, it became evident that proper routines needed to be developed to post-process and compile the enormous amount of data generated, which was object of the present work. These also proved to be useful tools for comparing the effect of a number of design and operation variables in grinding, being applied in a case study of liner design.

The model proposed considers that breakage in SAG/AG mills concern of particles that are contained in the DEM simulations as well as particles that are not explicitly appearing in the DEM simulations, called sub-DEM particles. A simulation study of breakage of sub-DEM particles demonstrated that the model is capable of accounting for the main design and operating variables that influence milling, besides ore characteristics. A preliminary study of breakage of DEM particles, on the other hand, demonstrated that the model could qualitatively describe the effect of particle size on breakage rates.

A framework for describing comminution in the SAG/AG mill has been proposed, and is based on two-way coupling of DEM and the microscale population balance model. Preliminary attempts to apply this model have demonstrated that the successful simulation of SAG/AG mills requires accounting for all breakage contributions, both the fragments from breakage of coarser particles and sub-DEM particles, and also that the charge of ore in the mill has reached stabilization.

XI. Future work

The model framework proposed to model SAG mills opens several fields of applications. There are a number of DEM simulations already concluded but waiting to be further tested with the mechanistic model. This is a continuous evolving topic of research.

Regarding process understanding, several simulations trials can be done such as: the evaluation of having the ore pre-crushed before entering the mill; extend throughput prediction analysis to other pilot plant studies with other ores; evaluate the effect of increasing the ball charge; reproduce public domain locked-cycle test results by the use of simulations.

There is also room for improving the computational code, which may allow a quicker validation of the model framework under different design and operational conditions. This type of improvement showed to be of great relevance in the case of sub-DEM breakage modelling. The use of a more efficient computational code will speed up the parameterization of the model and the search for the validity range of the assumptions

The model framework as proposed, allows the incorporation of better models. There is a need for understanding how particles behave when hit in slurry beds, which is an ongoing study on LTM. The aim is to improve the particle interaction model. Also the full modelling of a SAG mill requires a material transport model to be incorporated into the mechanistic model.

XII. References

Aguiar, K., Barrios, G., Tavares, L. M. (2011). Estudo da quebra de partículas em leitos polidispersos. *XXIV Encontro Nacional de Tratamento de Minérios e Metalurgia Extrativa*, *1*, pp. 376-383. Salvador.

Amestica, R., Gonzalez, G., Menacho, J., Barria, J. (1996). A mechanistic state equation model for semi-autogenous mills. *International Journal of Mineral Processing, 44-45*, pp. 349-360.

Apelt, T., Asprey, S., Thornhill, N. (2001). Inferential measurement of SAG mill parameters. *Minerals Engineering, 14*(6), pp. 575-591.

Atkinson, K. (1989). *An Introduction to Numerical Analysis.* John Wiley & Sons.

Austin , L., Menacho, J., Pearcy, F. (1987). A General Model for Semi-autogenous and Autogenous Milling. *Proceedings of the Twentieth International Symposium on the Application of Computers and Mathematics in the Mineral Industries. 2*, pp. 107-126. Johannesburg: SAIMM.

Austin, L., Concha, F. (1994). *Diseño y Simulación de Circuitos de Molienda y Clasificación* (Vol. 1). Santiago: Universidad Técnica Federico Santa María Ediciones.

Austin, L., Barahona, C., Weymont, N., Suryanarayanan, K. (1986). An Improved Simulation Model for Semi-Autogenous Grinding. *Powder Technology, 47*, pp. 265-283.

Austin, L., Klimpel, R., Luckie, P. (1984). *Process Engineering of Size Reduction: Ball Milling.* Nova Iorque: Society of Mining Engineers of AIME.

Bagherzadeh Kh, A., Mirghasemi, A., Mohammadi, S. (2011). Numerical simulation of particle breakage of angular particles using combined DEM and FEM. *Powder Technology, 205*, pp. 15-29.

Barrios, G., Carvalho , R., Tavares, L. M. (2011). Modeling breakage of monodispersed particles in unconfined beds. *Minerals Engineering, 24*, pp. 308-318.

Barrios, G., Carvalho, R. M., Tavares, L. M. (2011). Extending breakage characterisation to fine sizes by impact on particle beds. *Transactions of the Institute of Mining and Metallurgy. Section C., 120*, pp. 37-44.

Bbosa, L. S., Govender, I., Mainza, A. N., Powell, A. (2010). Power draw estimations in experimental tumbling mills using PEPT. *Minerals Engineering*, pp. xxx-xxx.

Bergerman, M., Delboni, H., Nankran, M. (2009, Janeiro-Março). Optimization of the Sossego SAG mill grinding circuit. *REM: Revista da Escola de Minas, 62*(1), 93-97.

Bourgeois, F. (1993). *Single particle fracture as a basis for microscale modeling of comminution processes.* Ph. D. Thesis, University of Utah, Salt Lake City.

Bueno, M., Shi, F., Kojovic, T., Powell, M. (2010, September 6-10). Invetigation on multicomponent semi-autogenous grinding. *XXV International Mineral Processing Congress (IMPC) 2010*, 611-618.

Carvalho, R. M. (2009). *Desenvolvimento de modelo matemático generalisado da cominuição.* Dissertação de Mestrado, Universidade Federal do Rio de Janeiro, Departamento de Engenharia Metalúrgica e de Materiais, Rio de Janeiro.

Carvalho, R. M., Tavares, L. M. (2009). Dynamic Modeling of Comminution Using a General Microscale Breakage Model. *Computer Aided Chemical Engineering, 27*, pp. 519-524.

Carvalho, R. M., Tavares, L. M. (2009). Modelagem generalizada da cominuição. *XXIII Encontro Nacional de Tratamento de Minérios e Metalurgia Extrativa*, *1*, pp. 185-192. Gramado.

Carvalho, R. M., Tavares, L. M. (2011). Leaping foward in SAG and AG mill simulation using a mechanistic model framework. *International Autogenous Grinding, Semi-Autogenous Grinding and High Pressure Grinding Roll Technology 2011*, (pp. 1-26). Vancouver.

Carvalho, R. M., Tavares, L. M. (2011). Modelagem mecanicista da moagem. *XXIV Encontro Nacional de Tratamento de Minérios e Metalurgia Extrativa*, *1*, pp. 765-775. Salvador.

Carvalho, R. M., Tavares, L. M. (2013, April). Predicting the effect of operating and design variables on breakage rates using the mechanistic ball mill model. *Minerals Engineering, 43-44*, pp. 91-101.

Carvalho, R. M., Tavares , L., Secchi, A. (2012). Modeling the appearace function using incomplete beta function. *Minerals Engineering*.

Chandramohan, R., Holtham, P., Powell, M. (2010). The Influence of Particle Shape in Rock Fracture. *XXV International Mineral Processing Congress (2010)*, (pp. 3164-3171). Brisbane.

Cho, K. (1987). *Breakage mechanisms in size reduction.* Ph. D. Thesis, University of Utah, Salt Lake City.

Cleary , P. (2001). Recent advances in DEM modelling of tumbling mills. *Minerals Engineering, 14*(10), pp. 1295-1319.

Cleary, P. W., Morrison, R., Morrel, S. (2003). Comparison of DEM and experiment for a scale model SAG mill. *International Journal of Mineral Processing, 68*, pp. 129-165.

Cleary, P., Hoyer, D. (2000). Centrifugal mill charge motion and power draw: comparison of DEM predictions with experiment. *International Journal of Mineral Processing, 59*, pp. 131-148.

Cleary, P., Sinnot, M., Morrison, R. (2006). Predictionj of slurry transport in SAG mills using SPH fluid flow in a dynamic DEM based porous media. *Minerals Engineering, 19*(15), 1517-1527.

Coetzee, C., Els, D. (2009, March). Calibration of discrete element parameters and the modelling of silo discharge and bucket filling. *Computers and electronics in agriculture, 65*(2), pp. 198-212.

Cogency. (2009). ASG Software.

Condori, P., Powell, M. (2006). A proposed mechanistic slurry discharge model for AG/SAG mills. *SAG Conference*, *III*, pp. 421-435. Vancouver.

Cundall, P., Strack, O. (1979). A discrete numerical model for granular assemblies. *Geotechnique, 29*, p. 517.

Delboni Jr, H., Morrell, S. (2002). A Load-Interactive Model for Predicting the Performance of Autogenous and Semi-Autogenous Mills. *KONA, 20*, pp. 208-222.

Delboni Jr, H., Chieregati, A., Bergerman, M. (2010). Development and Validation of Ore Characterisation Test and Use in Variability Campaigns of Comminution Circuits. *XXV International Mineral Processing Congress (IMPC) 2010 Procedings*, (pp. 667-675). Brisbane.

Delboni Jr., H. (2000, Janeiro/Fevereiro). Moagem autógena: Método de dimensionamento e otimização da operação. *BRASIL MINERAL*(180), 28-39.

Delboni Jr., H., Morrell, S. (1996). The Modelling of Autogenous and Semi-Autogenous Mills. *SAG 1996*, *2*, pp. 713-728. Vancouver.

Dem Solutions Ltd. (2010). *EDEM.* Edimburgh.

Digre, M. (1989). Testing for SAG/AG circuits. In A. Mular, G. Agar, *Advances in Autogenous and Semi-autogenous Grinding Technology* (pp. 9-23). Vancouver: UBC.

Djordjevic, N. (2005). Influence of charge size distribution on net-power draw of tumbling mill based on DEM modelling. *Minerals Engineering, 18*, pp. 375-378.

Djordjevic, N., Morrison, R., Loveday, B., Cleary, P. (2006). Modelling comminution patterns within a pilot scale AG/SAG mill. *Minerals Engineering, 19*, pp. 1505-1516.

Dong, H., Moys, M. (2002). Assessment of discrete element method for bouncing in a grinding mill. *International Journal of Mineral Processing, 65*, pp. 213-226.

Fuerstenau, D. W., Abouzeid, A. M. (2002). The energy efficiency of ball milling in comminution. *International Journal of Mineral Processing, 67*, pp. 161-185.

Fuerstenau, M., Han, K. (2003). *Principles of Mineral Processing.* Colorado: Society for Mining, Metallurgy, and Exploration (SME).

Galán, O., Barton, G., Romagnoli, J. (2002). Robust control of a SAG mill. *Powder Technology, 124*, pp. 264-271.

Govender, I., Powell, M. (2006). Validation of DEM using an empirical power model dreived from 3D particle tracking experiments. *Minerals Engineering, 19*(10), pp. 1005-1012.

Govender, I., Morrison, A., Mainza, A., Van Der Westuizen, A., Franzidis, J.-P., Powell, M. (2010). Using Positron Emission Particle Tracking (PEPT) to Investigate Industrial Systems. *XXV International Mineral Processing Congress (IMPC) 2010 Procedings*, (pp. 2483-2853). Brisbane.

Gupta, A., Yan, D. (2006). *Mineral processing design and operation: an introduction.* Amsterdã: Elsevier.

Gupta, A., Yan, D. (2006). *Mineral Processing Design and Operation: An Introduction* (Vol. 1). Amsterdan, Holanda: Elsevier Science.

Guzmán, L., García, D. (2010). Media Type Effect on Grinding Efficiency. *XXV International Mineral Processing Congress (IMPC) 2010 Procedings*, (pp. 3207-3215). Brisbane.

Hassanpour, A., Tan, H., Bayly, A., Gopalkrishnan, P., Ng, B., Ghadiri, M. (2011). Analysis of particle motion in a paddle mixer using Discrete Element Method (DEM). *Powder Technology, 206*, pp. 189-194.

Herbst, J. (2004). A microscale look at tumbling mill scale-up using high fidelity simulation. *International Journal of Mineral Processing, 74*, pp. S299-S306.

Höfler, A., Herbst, J. (1990). Ball mill modeling through micro-scale fragmentation studies: fully monitored particle bed comminution versus particle impact tests. *Proceedings of the 7th European Symposium on Comminution*, (pp. 1-17). Ljubljana, Slovenia.

Itasca Consulting Group Inc. (1999). *PFC3D Particle Flow Code in 3 Dimensions.* Minneapolis, Minnesota.

Jayasundara, C., Yang, R., Guo , B., Yu, A., Govender, I., Mainza, A., . . . Rubenstein, J. (2010). CFD-DEM modelling of particle flow in IsaMills - Comparison between simulations and PEPT measurements. *Minerals Engineering*, pp. xxx-xxx.

Jayasundara, C., Yang, R., Yu, A., Rubenstein, J. (2010). Discrete Element Method - Computational Fluid Dynamics Modelling of Flow Behavior in a Stirred Mill - Effect of Operation Conditions. *XXV International Mineral Processing Congress (IMPC) 2010 Procedings*, (pp. 3247-3256). Brisbane.

JKSimMet. (2003). *JKSimMet Manual v5.1.* Brisbane.

Johnson, K. (1985). *Contact Mechanics.* Cambridge: Cambridge University PRess.

Jones Jr, S. M., Fresko, M. (2011). Autogenous and Semi-autogenous mills 2010 update. *SAG Conference 2011*, (pp. 1-24). Vancouver.

Jones Jr., S. (2006). Autogenous and Semi-autogenous Mills 2005 update. *SAG 2006*, *I398-I495.* Vancouver.

Kallon, D., Govender, I., Mainza, A. (2010). Circulation rate modelling of mill charge using position emission particle tracking. *Minerals Engineering*, pp. xxx-xxx.

Khanal , M., Schubert, W., Tomas, J. (2007). Discrete element method simulation of bed comminution. *Minerals Engineering, 20*, pp. 179-187.

King, R. (2001). *Modeling and Simulation of Mineral Processing Systems.* Oxford, Reino Unido: Butterworth-Heinemann.

King, R., Bourgeois, F. (1993). Measurement of fracture energy during single particle fracture. *Minerals Engineering, 6*, pp. 353-367.

Klymowsky, I., Rijkers, A. (1996). The use of data from small-scale mills and computer simulation techniques for scale-up and design of SAG mill circuits. *International Journal of Mineral Processing, 44-45*, pp. 273-287.

Ko, Y., Shang, H. (2011). Time delay neural network modeling for particle size in SAG mills. *Powder Technology, 205*, pp. 250-262.

Koivistoinen, P., Levanaho, J. (2006). The role of critical-sized material in AG and SAG grinding. *International Autogenous and Semi-autogenous grinding Technology*, *II*, pp. 246-257. Vancouver.

Kojovic, T. (2005). Influence of aggregate stemming in blasting on the SAG mill performance. *Minerals Engineering, 18*, pp. 1398-1404.

Kojovic, T., Shi, F., Larbi-Bram, S., Manlapig, E. (2010). Validation of the JKMRC Rotary Breakage Tester (JKRBT) ore breakage characterisation device. *XXV International Mineral Processing Congress (IMPC) Proceedings*, (pp. 901-915). Brisbane.

La Nauze, R. D., Temos, J. (2002). Technologies for sustainable operation. *CMMI Congress 2002* (pp. 27-34). Cairns, Queensland: AusIMM.

Larbi-Bram, S., Shi, F., Kojovic, T. (2010). Experimental Study of Ore Characterisation Methods for AG/SAG Mills. *XXV International Mineral Processing Congress (IMPC) 2010 Procedings*, (pp. 929-941). Bribane.

Latchireddi, S., Morrell, S. (2003). Slurry flow in mills: grate-only discharge mechanism (Part I). *Minerals Engineering, 16*, pp. 625-633.

Latchireddi, S., Morrell, S. (2006). Slurry flow in mills with TCPL - An efficient pulp lifter for ag/sag mills. *International Journal of Mineral Processing, 79*, pp. 174-187.

Leung, K., Morrison, R., Whiten, W. (1987). An Energy Based Ore Specific Model for Autogenous and Semi-autogenous Grinding. *Proceedings of Copper 1987*, (pp. 71-85). Santiago, Chile.

Lichter, J., Lim, K., Potapov, A., Kaj, D. (2009). New developments in cone crusher permormance optimization. *Minerals Engineering, 22*, 613-617.

Loveday, B. (2004). The use of fag and sag batch tests for measurement of abrasion raters of full-size rocks. *Minerals Engineering, 17*, pp. 1093-1098.

Loveday, B., Naidoo, D. (1997). Rock abrasion in autogenous milling. *Minerals Engineering, 10*(6), pp. 603-612.

MacPherson, A., Turner, R. (1980). Mineral Processing Plant Design. In A. I. Mular, R. B. Bhappu, A. Mular, R. Bhappu (Eds.), *Mineral Processing Plant Design* (pp. 279-305). Nova Iorque: SME-AIME.

Mao, K., Wang, M., Xu, Z., Chen, T. (2004). DEM simulation of particle damping. *Powder Technology, 142*, pp. 154-165.

Martins, S., Li, W., Radziszewski, P., Caron, S., Aguanno, M., Bakhos, M., Petch, E. (2008). Validating the instrumented ball outputs with simple trajectories. *Minerals Engineering, 21*, pp. 782-788.

Milin, L. (1994). *Modeling the t10 x tn relationship by the incomplete beta function.* Relatório de pesquisa, University of Utah.

Mindlin, R. (1949). Compliance of elastic bodies in contact. *Journal of Applied Mechanics, 71*, pp. 259-268.

Mishra, B. (2003). A review of computer simulation of tumbling mills by the discrete element method: Part II - Practical applications. *International Journal of Mineral Processing, 71*, pp. 95-112.

Mishra, B., Rajamani, R. (1992). The discrete element method for the simulation of ball mills. *Applied Mathematical Modelling, 16*, pp. 598-604.

Morrell, S. (1996). Power draw of wet tumbling mills and its relationship to charge dynamics - Part 1: a continuum approach to modelling of mill power draw. *Transactions of the Institute of Mining and Metallurgy, 105*, pp. C43-C53.

Morrell, S. (2004). A new autogenous and semi-autogenous mill model for scale-up, design and optimisation. *Minerals Engineering, 17*, pp. 437-445.

Morrell, S., Finch, W., Kojovic, T., Delboni Jr, H. (1996). Modellling and simulation of large diameter autogeneous and semi-autogeneous mills. *International Journal of Mineral Processing, 44-45*, pp. 289-300.

Morrison, R. D., Cleary, P. W. (2008). Towards a virtual comminution machine. *Minerals Engineering, 21*, pp. 770-781.

Morrison, R., Cleary, P. (2004). Using DEM to model ore breakage within a pilot scale SAG mill. *Minerals Engineering, 17*, pp. 1117-1124.

Morrison, R., Cleary, P. (2010). Estimating Breakage of Fine Ore Particles by Media in a Small Ball Mill Using DEM. *XXV International Mineral Processing Congress (IMPC) 2010*, (pp. 3287-3297). Brisbane.

Morrison, R., Morrell, S. (1997). In R. Kawatra, *Comminution Practices* (pp. 139-146). Colorado: SME.

Morrison, R., Shi, F., Whyte, R. (2007). Modelling of incremental rock breakage by impact - For use in DEM models. *Minerals Engineering, 20*, pp. 303-309.

Mular, A. L., Agar, G. E. (1989). The use of 60 cm pilot plant for scale-up of semi-autogenous grinding mills. In A. Mular, G. Agar, *Advances in Autogenous and Semi-autogenous Grinding Technology* (pp. 137-153). Vancouver: UBC.

Napier-Munn, T. (1996). *Mineral comminution circuits: their operation and optimisation.* Indooroopilly, Australia/Queensland: Julius Kruttschnitt Mineral Resarch Centre / University of Queensland.

Narayanan, S., Whiten, W. (1988). Determination of comminution characteristics from single particle breakage tests and its application to ball mill scale-up. *Transactions of the Institute of Mining and Metallurgy, 97*, pp. C115-C124.

Pontt, J. (2004). MONSAG: A new monitoring system for measuring the load filling of a SAG mill. *Minerals Engineering, 17*, pp. 1143-1148.

Pontt, J., Rodriguez, J., Valderrama, W., Sepúlveda, G., Alzamora, G. (2004). Resonance effects, power quality and reliability issues of high-power converters-fed drivers employed in modern SAG circuits. *Minerals Engineering, 17*, pp. 1125-1134.

Potapov, A., Herbst, J., Song, M., Pate, W. (2007). A DEM-PBM fast breakage model for simulation of comminution processes. *Proceedings of the MEI Discrete Element Methods (DEM) 07 Conference.*

Powell, M. (2006). The unified comminution model - a conceptually new model. *Proceedings of the XXIII IMPC*, (pp. 1783-1788). Istanbul.

Powell, M., Mainza, A. (2006). Extended grinding curves are essential to the comparison of milling performance. *Minerals Engineering, 19*, pp. 1487-1494.

Powell, M., Morrison, R. (2006). A new look at Breakage testing. *11th European Symposium on Comminution* (p. 6). Budapest: European Federation of Chemical Engineers.

Powell, M., Morrison, R. (2007,). The future of comminution modeling. *International Journal of Mineral Processing, 84*, pp. 228-239.

Powell, M., Nurick, G. (1996). A study of charge motion in rotary mills: Part I - extension of the theory. *Minerals Engineering, 9*(2), pp. 259-268.

Powell, M., Valery, W. (2006). Slurry pooling and transport issues in SAG mills. *SAG Conference 2006*, *I*, pp. I133-I152. Vancouver.

Powell, M., Weerasekara, N. (2010). Building the Unified Comminution Model. *XXV International Mineral Processing Congress (IMPC) 2010*, (pp. 1133-1141). Brisbane.

Powell, M., Benzer , H., Mainza, A., Evertsson, M., Tavares, L. M., Potgieter, M., . . . Rule, C. (2011). Transforming the effectiveness of HPGR circuit at Anglo Platinum Mogalakwena. *International Autogenous Grinding, Semi-Autogenous Grinding and High-Pressure Grinding Roll Technology 2011,*, (pp. 1-23). Vancouver.

Powell, M., Govender, I., McBride, A. (2008). Applying DEM outputs to the unified comminution model. *Minerals Engineering, 21*, pp. 744-750.

Powell, M., Morrell, S., Latchireddi, S. (2001). Developments in the understanding of south african style SAG mills. *Minerals Engineering, 14*(10), pp. 1143-1153.

Powell, M., van der Westhuizen, A., Mainza, A. (2009). Applying grindcurves to mill operation and optimisation. *Minerals Engineering, 22*, pp. 625-632.

Powell, M., Weerasekara, N., Cole, S., LaRoche, R., Favier, J. (2011). DEM modelling of liner evolution and its influence on grinding rate in ball mills. *Minerals Engineering, 24*, pp. 341-351.

Quist , J., Evertsson, E. (2010). Application of Discrete Elementh Method for Simulating Feeding Conditions and Size Reduction in Cone Crushers. *XXV International Mineral Processing Congress (IMPC) 2010 Procedings*, (pp. 3337-3347). Brisbane.

Rajamani, R., Mishra, B., Venugopal, R., Datta, A. (2000). Discrete element analysis of tumbling mills. *Powder Technology, 109*, pp. 105-xxx.

Ramos, E., Carvalho, R. M., Tavares, L. M. (2011). Simulação do movimento da carga em moinhos de bolas utilizando o método dos elementos discretos. *XXIV Encontro Nacional de Tratamento de Minérios e Metalurgia Extrativa*, *1*, pp. 440-447. Salvador.

Rezaeizadeh, M., Fooladi, M., Powell, M., Mansouri, S. (2010). Experimental observations of lifter parameters and mill operation on power draw and liner impact loading. *Minerals Engineering, 23*, pp. 1182-1191.

Rosario, P. (2010). *Comminution Circuit Design and Simulation for Development of a Novel High Pressure Grinding Roll Circuit.* Tese de Doutorado, University of British Columbia, Vancouver.

Salazar, J., Magne, L., Acuña, G., Cubillos, F. (2009). Dynamic modelling and simulation of semi-autogenous mills. *Minerals Engineering, 22*, pp. 70-77.

Sato, A., Kano, J., Saito, F. (2010). Analysis of abrasion mechanism of grinding media in a planetary mill with DEM simulation. *Advanced Powder Technology, 21*, pp. 212-216.

Schoenert, K. (1986). On the limitation of energy saving in milling. *World Congress Particle Technology, Part II Comminution*, (p. 1). Nurnberg.

Sepulveda, J. (2008). The theoretical rationale behind current trends in operating practice of semi-autogenous grinding operations. *V International Mineral Processing Seminar - Procemin.* Santiago, Chile.

Sinnott, M., Cleary, P., Morrison, R. (2011). Is media shape important for grinding performance in stirred mills? *Minerals Engineering, 24*, pp. 138-151.

Tavares, L. M. (1997). *Microscale investigation of particle breakage applied to the study of thermal and mechanical predamage.* Ph. D. Thesis, University of Utah, Salt Lake City.

Tavares, L. M. (1999). Energy absorbed in breakage of single particles in drop weight testing. *Minerals Engineering, 12*(1), pp. 43-50.

Tavares, L. M. (2004). Optimum routes for particle breakage by impact. *Powder Technology, 142*(2-3), pp. 81-91.

Tavares, L. M. (2005). Particle weakening in high-pressure roll grinding. *Minerals Engineering, 18*, pp. 651-657.

Tavares, L. M. (2007). Breakage of particles: Quasi-static. In M. Ghadiri, M. Hounslow, *Handbook of Powder Technology: Particle Breakage* (Vol. 12, pp. 3-68). Amsterdã: Elsevier B. V.

Tavares, L. M. (2009). Analysis of particle fracture by repeated stressing as damage accumulation. *Powder Technology, 190*, pp. 327-339.

Tavares, L. M., Carvalho, R. M. (2007). Impact work index prediction from continuum damage model of particle fracture. *Minerals Engineering, 20*, pp. 1368-1375.

Tavares, L. M., Carvalho, R. M. (2009). Modeling breakage rates of coarse particles in ball mills. *Minerals Engineering, 22*(7-8), pp. 650-659.

Tavares, L. M., Carvalho, R. M. (2009). Modeling iron ore degradation during handling. *2nd International Symposium on Iron Ore*, *v1*, pp. 69-80. São Luís.

Tavares, L. M., Carvalho, R. M. (2010). A mechanistic model of batch grinding in ball mills. *XXV International Mineral Processing Congress (IMPC) 2010 Procedings*, (pp. 1287-1297). Brisbane.

Tavares, L. M., Carvalho, R. M. (2011). Aplicações do método dos elementos discretos. *11o Simpósio do Minério de Ferro. 1*, pp. 293-303. Vitória: ABM.

Tavares, L. M., Carvalho, R. M. (2011, Novembro). Modeling ore degradation during handling using continuum damage mechanics. *International Journal of Mineral Processing, 101*(1-4), pp. 21-27.

Tavares, L. M., King, R. (1998). Single particle fracture under impact loading. *Inernational Journal of Mineral Processing, 54*, pp. 1-28.

Tavares, L. M., King, R. (2002). Modeling of particle fracture by repeated impacts using continuum damage mechanics. *Powder Technology, 123*(2-3), pp. 138-146.

Tavares, L. M., King, R. (2004). Modeling of the load-deformation response from impact-breakage of particles. *International Journal of Mineral Processing, 74*, pp. s267-s277.

Trimble Navigation Limited. (2012). Sketchup 8.0.16846.

Tuzcu, E., Rajamani, R. (2010). Modeling breakage rates in mills with impact energy spectra and ultra fast load cell data. *Minerals Engineering*, 24, pp. 252-260.

van der Westhuizen, A., Govender, I., Mainza, A., Rubenstein, J. (2011). Tracking the motion of media particles inside an IsaMill™ using PEPT. *Minerals Engineering*, pp. 195-204.

van Nierop, M., Glover, G., Hinde, A., Moys, M. (2001). A discrete element method investigation of the charge motion and power draw of an experimental two-dimensional mill. *International Journal of Mineral Processing, 61*, pp. 77-92.

Verret, F., Chiasson, G., McKen, A. (2011). Sag mill testing - an overview of the test procedures available to characterize ore grindability. *International Autogenous Grinding and Semi-autogenous Grinding and High Pressure Grinding Roll Technology 2011*, *1*, pp. 1-14. Vancouver.

Vervoorn, P., Austin, L. (1990). The analysis of repeated breakage events as an equivalent rate process. *Powder Technology, 63*, pp. 141-147.

Wang, X., Rhodes, M. (2005). Pulsed fluidization - a DEM study of a fascinating phenomenon. *Powder Technology, 159*, pp. 142-149.

Weerasekara, N., Powell, M. (2010). Exploring the Breakage Enviroment in Mills with Discrete Element Methods. *XXV International Mineral Processing Congress (IMPC) 2010 Proceedings*, (pp. 1357-1365). Brisbane.

Weichert, R., Herbst, J. (1986). An ultra fast load cell for measuring particle breakage. *Proceedings of World Congress Particle Technology: Part II. Comminution*, (pp. 3-15).

Whiten, W. (1972). The use of periodic spline functions for regression and smoothing. *Australian Computer Journal, 4*, pp. 31-34.

Wills, B., Napier-Munn, T. (2006). *Mineral Processing Technology: An Introduction to the Practical Aspects of Ore Treatment and Mineral Recovery* (7ª ed.). Butterworth-Heinemann.

Yahyaei, M., Banisi, S. (2010). Spreadsheet-based modeling of liner wear impact on charge motion in tumbling mills. *Minerals Engineering, 23*, pp. 1213-1219.

Zhou, Y. D., Wright, B. D., Yang, R. Y., Xu, B. H., Yu, A. B. (1999). Rolling friction in the dynamic simulation of sandpile formation. *Physica, 269*, pp. 536-553.

Appendix A - Austin model fitting

The model fits data available from Austin's work (Austin and Concha, 1993). Austin have published the particle size distribution of the hold-up based on the fitting of his SAG model. The proposed model consists on the use of batch grinding equation to convert Austin's reported fresh feed into the hold-up particle size distribution. The model is based on Austin's phenomenological model solution for the batch grinding equation (Equation A.1), which must be solved for a total grinding time of 0.05 seconds.

$$\frac{dw_i}{dt} = -s_i w_i + \sum_{j=1}^{i-1} b_{ij} s_j w_j \qquad \text{A.1}$$

The breakage function and selection function with their fitted parameters are presented on Equations A.2 e A.3.

$$B_{ij} = 0.5\left(\frac{D_i}{D_j}\right)^{0.5} + 0.5\left(\frac{D_i}{D_j}\right)^{4} \qquad \text{A.2}$$

$$s_i = \frac{0.02 dp_i^2}{1 + \left(\frac{dp_i}{30}\right)^2} \qquad \text{A.3}$$

Appendix B – List of publications

BARRIOS, G. K., CARVALHO, R. M. de, Kwade, A., TAVARES, L. M.. Contact parameter estimation for DEM simulation of iron ore pellet handling. Powder Technology (Print). (2012), v.248, p.84 - 93, 2013.

CARVALHO, R. M. de, TAVARES, L. M.. Predicting the effect of operating and design variables on breakage rates using the mechanistic ball mill model. Minerals Engineering. (2012), v.43-44, p.91 - 101, 2013.

CUNHA, E. R., CARVALHO, R. M. de, TAVARES, Luis Marcelo Marques. Simulation of solids flow and energy transfer in a vertical shaft impact crusher using DEM. Minerals Engineering. (2012), v.43-44, p.85 - 90, 2013.

Weerasekara N., S., Powell M., W., Cleary P., M., Tavares L., M., Evertsson, D., Morrison R., J., Quist, CARVALHO, R. M. de.The contribution of DEM to the science of comminution. Powder Technology (Print). (2012), v.248, p.3 - 24, 2013.

TAVARES, L. M., CARVALHO, R. M. de. Modeling ore degradation during handling using continuum damage mechanics. International Journal of Mineral Processing (Print). (2012), v.112-113, p.1 - 6, 2012.

BARRIOS, G. K. P., CARVALHO, R. M. de, TAVARES, L. M.. Extending breakage characterisation to fine sizes by impact on particle beds. Transactions - Institution of Mining and Metallurgy. Section C. Mineral Processing & Extractive Metallurgy. (2012), v.102, p.37 - 44, 2011.

BARRIOS, G. K., CARVALHO, R. M. de, TAVARES, L. M.. Modeling breakage of monodispersed particles in unconfined beds. Minerals Engineering. (2012), v.24, p.308 - 318, 2010.

TAVARES, L. M., CARVALHO, R. M. de. Modeling ore degradation during handling using continuum damage mechanics. International Journal of Mineral Processing. (2012), v.101, p.21 - 27, 2010.

BARRIOS, G. K., CARVALHO, R. M. de, TAVARES, L. M. . Breakage of particles by impact in unconfined beds with multiple layers In: 13th European Symposium on Comminution and Classification, 2013, Braunschweig.Proceedings of the 13th European Symposium on Comminution and Classification. Sierke Verlag, 2013. v.1.

CARVALHO, R. M., TAVARES, L. M.. DEM-based simulation framework as a tool to predict grinding in AG/SAG mills In: Anais do 13th Brazilian Symposium on Iron Ore, 2012, Rio de Janeiro. Anais do 13th Brazilian Symposium on Iron Ore, 2012. p.753 – 763

CARVALHO, R. M., TAVARES, L. M.. Predicting effect of media size in ball milling using the mechanistic grinding model In: PROCEMIN 2012, 2012, SANTIAGO. Proceedings of the 9th International Mineral Processing Conference. , 2012. p.114 – 123

CARVALHO, R. M. de, Tavares, L. M.. Fifth International Conference On Autogenous And Semiautogenous Grinding Technology In: Fifth International Conference On Autogenous And Semiautogenous Grinding Technology, 2011, Vancouver. FIFTH INTERNATIONAL CONFERENCE ON AUTOGENOUS AND SEMIAUTOGENOUS GRINDING TECHNOLOGY. 2011.

CARVALHO, R. M., TAVARES, L. M. Modelagem Mecanicista da Moagem In: XXIV Encontro Nacional de Tratamento de Minérios e Metalurgia Extrativa, 2011, Salvador. XXIV Encontro Nacional de Tratamento de Minérios, 2011. p.765 – 775

RAMOS, E. S., CARVALHO, R. M. de, TAVARES, L. M. Marques. Simulação do Movimento da Carga em Moinho de Bolas Utilizando o Método dos Elementos Discretos In: XXIV Encontro Nacional de Tratamento de Minérios e Metalurgia Extrativa, 2011, Salvador. XXIV Encontro Nacional de Tratamento de Minérios, 2011. p.440 – 447

TAVARES, L. M., CARVALHO, R. M. de. A mechanistic model of batch grinding in ball mills In: XXV International Mineral Processing Congress, 2010, Brisbane. Proceedings of the XXV IMPC. Melbourne. Melbourne: AUSIMM, 2010. v.1. p.1 - 11

Cunha, E. R, CARVALHO, R. M. de, TAVARES, L. M.. Mechanistic model of the vertical shaft impact crusher In: 13th European Symposium on Comminution and Classification, 2013, Braunschweig. Proceedings of the 13th European Symposium on Comminution and Classification. , 2013. v.1. p.343 – 343

CARVALHO, R. M. de, TAVARES, L. M. Marques. DEM-PBM coupling to predict breakage in comminution processes In: EDEM Conference, 2011, Edinburgh. Abstracts of the EDEM Conference. Edinburgh, 2011. p.39 - 44